A Pharmacometrics Approach to Understanding Drug Disposition and Drug Interactions in Healthy Individuals and Patients Undergoing Roux-en-Y Gastric Bypass

Kuan-Fu Chen

A dissertation

submitted in partial fulfillment of the

requirements for the degree of

Doctor of Philosophy

University of Washington

2020

Reading Committee:

Yvonne Lin, Chair

Edward Kelly

Julia Cui

Program Authorized to Offer Degree:

Pharmaceutics

University of Washington

Abstract

A Pharmacometrics Approach to Understanding Drug Disposition and Drug Interactions in Healthy Individuals and Patients Undergoing Roux-en-Y Gastric Bypass

Kuan-Fu Chen

Chair of the Supervisory Committee:
Yvonne Lin
Department of Pharmaceutics

In this dissertation, pharmacometric approaches were used to better understand drug disposition and predict drug interactions in morbidly obese individuals undergoing Roux-en-Y gastric bypass surgery (RYGBS) and to determine the kinetic characteristics of theoretical endogenous biomarkers that would permit the detection of potential drug interactions. Chapter 2 examined how RYGBS affected drug absorption and intestinal and hepatic metabolism *in vivo* by ascertaining the pharmacokinetics of acetaminophen in patients at three timepoints (e.g., pre-RYGBS and 3- and 12-months post-RYGBS). Following RYGBS, peak APAP concentrations at the 3-month and 12-month visits increased by 2-fold compared to baseline ($p < 0.01$) and the median time to peak concentration decreased from 35 min to 10 min. The apparent oral clearance of APAP decreased 34% after RYGBS ($p < 0.01$). The decrease in metabolite-to-parent AUC ratios of all four metabolites at 3-months and 12-months is possibly indicative of a decline in the activities of CYP2E1, UGT1A1, UGT1A9, and SULT1A1 following RYGBS. As drug-drug interaction (DDI) studies have not been conducted in patients undergoing RYGBS, we used an in

silico approach to predict DDIs in this patient population (Chapter 3). Using physiologically-based pharmacokinetic (PBPK) modeling, we simulated the impact of RYGBS on the absorption and metabolism of midazolam, acetaminophen, digoxin, and their major metabolites. Secondly, we built PBPK models for verapamil, a highly soluble inhibitor, and posaconazole, a poorly soluble inhibitor, to evaluate CYP3A- and P-gp-mediated DDIs pre- and post-RYGBS. For verapamil inhibition, RYGBS did not affect the fold-change of the inhibited AUC ratio or inhibited peak concentration ratio for either midazolam or digoxin. For posaconazole inhibition, the inhibited midazolam AUC increased by 2.0-fold pre-RYGBS, but only increased by 1.6-fold post-RYGBS due to decreased absorption. For DDI assessment, the use of endogenous biomarkers is a relatively non-invasive approach to provide early detection of potential DDIs during first-in-human clinical trials. Chapter 4 describes a simulation study to investigate how the sensitivity of a theoretical biomarker is affected by metabolite half-life, fraction of the endogenous parent that is metabolized to the metabolite of interest ($f_{m,metabolite}$), and fraction of the endogenous parent that is metabolized by CYP3A4 ($f_{m,CYP3A4}$). Several sensitivity indices, including the metabolite concentration (C_m), the metabolite-to-parent concentration ratio (C_m/Cp), the metabolite AUC (AUC_m), and the metabolite-to-parent AUC ratio (AUC_m/AUC_p), were explored in different DDI scenarios. A 20% change in the sensitivity indices was set as the detection threshold for single dose inhibition, mechanism-based inhibition, and induction. Our simulation results demonstrated that the sensitivity of the hypothetical endogenous biomarker was reduced by increasing metabolite half-life. As $f_{m,metabolite}$ was decreased, the change in C_m and AUC_m increased, but the change in C_m/C_p and AUC_m/AUC_p decreased. As $f_{m,CYP3A4}$ was decreased, the change in all indices decreased. The predicted magnitude of change based on our simulations was comparable to the clinically observed magnitude of change for putative

CYP3A4 endogenous biomarkers. In summary, pharmacometrics was used in this dissertation to understand the impacts of RYGBS on drug disposition, predict CYP3A4 and P-gp DDIs in RYGBS patients, and investigate the kinetic characteristics of endogenous CYP3A4 biomarkers.

Dedication

To my family,

who have given me a lifetime of love and support and always believe in me,

and to my partner, Justin,

whose encouragement and companionship made it possible for me to complete this work.

Table of Contents

CHAPTER 1

INTRODUCTION

1.1 Background

Genetic and environmental factors are known to contribute to the interindividual variability in drug absorption and disposition (Visscher et al. 2008). For example, using a classical twin model, Penno et al. estimated that heritability accounted for 85% of the interindividual variability in antipyrine 4-hydroxylation formation via cytochrome P450 3A (CYP3A) (Penno et al. 1981). A recent twin study by Rahmioglu et al. estimated that heritability accounted for 66% of the interindividual variability in CYP3A induction (Rahmioglu et al. 2011). The remaining interindividual variability in baseline and induced CYP3A activities could be due to inherent variables (e.g., epigenetics) or other intrinsic and extrinsic patient factors. These intrinsic factors (e.g., age, gender, diseases) and extrinsic factors (e.g., diet, smoking, drug-drug interactions, and other environmental factors) can cause pronounced effects on the pharmacokinetics of drugs (Reyner et al. 2019). Although some of the factors such as age, gender, diseases, and drug-drug interactions have been extensively studied, many of these factors remain understudied. To further understand how intestinal-associated factors contribute to pharmacokinetic variability, we studied the impact of alterations to the intestinal anatomical structure in Chapters 2 and 3.

Traditionally, evaluating and predicting the effects of an aforementioned factor on pharmacokinetics requires administration of a probe drug. Recently, there is increased interest in using endogenous compounds as biomarkers of drug metabolizing enzyme and transporter activity to enable findings of dose-related efficacy or toxicity in early drug development (Mariappan et al. 2017, Chu et al. 2018, Rodrigues et al. 2018). However, currently proposed endogenous biomarkers have major limitations, especially in cases of enzyme inhibition, due to sensitivity-related issues resulted from long elimination half-lives (Yang and Rodrigues 2010,

Mao et al. 2017, Mariappan et al. 2017). To further understand how the kinetic characteristics of an endogenous biomarker affect its utility, we conducted a theoretical study to evaluate the sensitivity and selectivity of a simulated endogenous biomarker under various drug interaction scenarios in Chapter 4.

1.2 Intestinal- Factors Associated with Pharmacokinetic Variability

The small intestine is the primary site for drug absorption. Most marketed drugs are designed to be orally administered due to convenience and cost-effectiveness (Lipinski 2000). Administering drug via this route, however, introduces higher interindividual variability from drug absorption and pre-systemic metabolism. For example, the rate and extent of drug absorbed by passive diffusion can be affected by gastrointestinal transit time, villi density, intestinal diameter, and concentration gradient across the gut wall (Vertzoni et al. 2019). In many instances, the process of drug absorption is further complicated by active transport, where drug can be brought into or out of the enterocytes by influx or efflux transporters. For example, fexofenadine is actively transported by organic anion transporting polypeptide 1A2 (OATP1A2) from the gut lumen into enterocytes, leading to higher oral bioavailability (Bailey et al. 2007, Glaeser et al. 2007). In contrast, some chemotherapeutic drugs (e.g. paclitaxel, methotrexate, and topotecan) are effluxed by P-glycoprotein (P-gp), multidrug resistance associated proteins (MRPs), and breast cancer resistance protein (BCRP) from enterocytes back to the lumen, leading to lower oral bioavailability (Breedveld et al. 2006, Ross and Nakanishi 2010, Estudante et al. 2013).

After being absorbed, drugs inside the enterocytes can encounter intestinal drug metabolizing enzymes. Multiple cytochromes P450 (CYPs), including CYP3A4, 3A5, 2C9,

2C19 and 2D6, are known to be expressed in the intestine (Paine et al. 2006, Xie et al. 2016, Drozdzik et al. 2018, Fritz et al. 2019). CYP3A4 and CYP3A5 are the most abundant intestinal drug-metabolizing enzymes (Figures 1.1A and B) (Paine et al. 2006, Groer et al. 2014, Peters et al. 2016, Xie et al. 2016). In addition to CYPs, the Phase II enzymes, glucuronosyltransferases (UGTs) and sulfotransferases (SULTs), can participate in intestinal metabolism. UGT2B17 is the most abundant UGT isoforms in the intestine, followed by UGT1A1and UGT1A10 (Figure 1.1C) (Harbourt et al. 2012, Sato et al. 2014). The small intestine has the highest abundance of SULTs compared to other tissues (Riches et al. 2009). SULT1B1 and 1A3 are the major intestinal isoforms, followed by SULT1A1 and more minor SULT isoforms (Figure 1.1D) (Riches et al. 2009).

Many of these drug metabolizing enzymes and transporters have distinct patterns of regional expression along the intestine. The intra-subject mRNA and protein levels in different intestinal regions were quantified and compared (Drozdzik et al. 2014, Drozdzik et al. 2018, Fritz et al. 2019). CYP3A4 protein expression was the highest in the jejunum and decreased in the ileum and was undetectable in the colon (Figure 1.2) (Drozdzik et al. 2018, Fritz et al. 2019). CYP3A5, CYP2C9, 2C19 and CYP2D6 demonstrated similar expression patterns to CYP3A4, but had substantially lower protein levels (Figure 1.2) (Drozdzik et al. 2018, Fritz et al. 2019). SULT1A, UGT1A, and UGT2B7 also were highest in the jejunum (Figure 1.3) (Drozdzik et al. 2018, Fritz et al. 2019). In contrast, P-gp expression increased along the length of the small intestine and peaked at the distal ileum, but decreased in the colon (Figure 1.4) (Mouly and Paine 2003, Drozdzik et al. 2014). BCRP also exhibited an increasing trend but less dramatic compared to P-gp (Figure 1.4) (Drozdzik et al. 2014). MRP2 and MRP3 was more uniformly expressed along the length of the small intestine, but MRP3 was significantly elevated in the colon (Figure

1.4) (Drozdzik et al. 2014). Common intestinal uptake transporters, such as OATP2B1, OCT1, and OCT3, were uniformly expressed along the length of the small intestine (Figure 1.4) (Drozdzik et al. 2014). Because intestinal drug metabolizing enzymes and transporters are differentially expressed along the intestinal tract, the degree to which drug substrates are metabolized or transported will depend in part upon the absorption site and absorption window in the intestine.

1.3 Altering Pharmacokinetics by Roux-en-Y Gastric Bypass Surgery

In adults, obesity is defined as having a body mass index (BMI) greater than 30 kg/m^2. Obesity is a global epidemic (Mitchell et al. 2011, Zobel et al. 2016). The World Health Organization reported that in 2016, 650 million adults worldwide were obese and the Centers for Disease Control and Prevention reported that in 2015-2016, 93.3 million individuals in the United States population were obese (prevalence of 39.8%) (Hales et al. 2017). Obesity can alter drug distribution and elimination. For example, the increased volume of distribution of lipophilic drugs, such as thiopental, can lead to a longer drug half-life in obese patients (De Baerdemaeker and Margarson 2016). Additionally, a higher hepatic blood flow in obese patients results in increased hepatic elimination of high extraction ratio drugs (e.g., propofol and fentanyl) (Shibutani et al. 2004, Cortínez et al. 2010, van Kralingen et al. 2011). Similarly, for drugs primarily eliminated by renal filtration, such as vancomycin, clearance increases due to higher glomerular filtration rates in obese patients (Bauer et al. 1998). However, for drugs that are low or moderate extraction ratio drugs, hepatic clearance may depend on obesity-specific changes in CYP expression. Studies consistently report decreased hepatic CYP3A4 activity and increased hepatic CYP2E1 and UGT activity in obese individuals (Abernethy et al. 1982, Abernethy et al.

1983, Abernethy et al. 1984, Greenblatt et al. 1984, O'Shea et al. 1994, Caraco et al. 1995, Lucas et al. 1998, Emery et al. 2003).

Among possible treatments for obesity, bariatric surgery is one of the most effective interventions (Benaiges et al. 2015). Roux-en-Y gastric bypass surgery (RYGBS) is the most popular bariatric procedure, accounting for approximately 45% of the total number of bariatric surgeries performed globally (Angrisani et al. 2015). As illustrated in Figure 1.5, the RYGB procedure creates a small gastric pouch (~20 mL) and connects the jejunum with a gastrojejuno-anastomosis (i.e., Roux limb), bypassing most of the stomach and duodenum (Schauer et al. 2000). The anatomical alteration leads to postoperative physiological changes, including weight-loss, decreased adipose tissue mass, reduced gastric emptying time, increased gastrointestinal pH, and decreased inflammation (Savassi-Rocha et al. 2014, Hachon et al. 2017). These alterations can impact drug absorption and disposition.

Following RYGBS, for some drugs, the rate and extent of absorption can be affected through decreased solubility and a decreased absorption window, whereas the extent of absorption of other drugs may not be altered. Moreover, due to the anatomical alterations after RYGB surgery, substrates will bypass efflux/uptake intestinal transporters located in the proximal region of intestine, and a higher concentration of drugs may reach efflux/uptake intestinal transporters located at the distal region of the intestine (illustrated in Figure 1.6A for efflux and Figure 1.6B for uptake). A higher fraction of drugs may escape intestinal metabolism if drug absorption occurs later along the intestinal tract, especially for the enzymes that have a decreasing gradient along the intestine (illustrated in Figure 1.6C). Furthermore, the expression of the intestinal drug metabolizing enzymes and/or uptake/efflux transporters may be altered following the surgery, however knowledge regarding the post-RYGBS regulation of intestinal

enzymes and transporters is lacking.

Changes to the bioavailability of drugs post-RYGBS are difficult to predict. Absorption may be impacted based on the physicochemical properties of the drug and interactions with transporters. Intestinal metabolism can be decreased due to bypassing intestinal enzymes. Hepatic metabolism may be upregulated or downregulated post-RYGBS as surgery can reverse enzyme expression changes due to obesity. Compared to healthy subjects, obese patients have higher hepatic CYP2E1, UGTs, and SULTs activities, but reduced CYP3A4 activity (Abernethy et al. 1983, Emery et al. 2003, Hardwick et al. 2013, Brill et al. 2015). Following gastric bypass surgery, the liver size decreases, in part due to reduction in liver fat content (Lewis et al. 2006) and a reduction in the number of hepatocytes (Sun and Karin 2012). These changes can result in an overall decrease in the total enzyme abundance. Besides surgery-related anatomical alterations, the post-RYGBS pharmacokinetics can be further influenced by the restricted diet and calorie intake in patients. *In vivo* and *in vitro* studies showed decreased CYP activity and reduced levels of microsomal proteins, CYPs, and P450 reductase in malnourished rats on low protein and low fat diets (Mgbodile and Campbell 1972, Campbell and Hayes 1974, Yang et al. 1992, Mao et al. 2006). Interestingly, reducing caloric intake while keeping protein constant also decreased the metabolite formation from aminophenazone in men (Krishnaswamy et al. 1984). Therefore, protein malabsorption, low fat diets, and the calorie deficit following RYGBS could retard the synthesis of enzymes and proteins essential for CYP-mediated drug metabolism.

The mechanisms by which RYGBS impact drug absorption and metabolism are complicated, and drugs may be impacted differently depending on the enzymes and transporters responsible for their disposition. Table 1.1 qualitatively summarizes the current knowledge of the physiological changes following RYGBS and their possible impacts on drug pharmacokinetics

(Padwal et al. 2010, Brocks et al. 2012, Darwich et al. 2012, De Smet et al. 2013, Stein et al. 2014, Greenblatt and Greenblatt 2015, Hachon et al. 2017). However, there exists limited literature regarding quantitative understanding of the impact of RYGBS on pharmacokinetics in a mechanistic manner. Furthermore, there is an urgent need to study the post-RYGBS changes in metabolite kinetics and the risks of drug-drug interactions, for toxic metabolites and drug-drug interactions are common sources of clinical drug-induced toxicity (Attia 2010, Rekic et al. 2017).

The first part of this dissertation focuses on the pharmacokinetic consequences of bariatric surgery in morbidly obese patients. Specifically, we would like to investigate how bypassing gastrointestinal segments affects the rate and extent of drug absorption and intestinal and hepatic metabolism.

1.4 Detection of Drug-Drug Interactions

A typical drug-drug interaction (DDI) can occur when drugs are concomitantly administered and a precipitant drug acts as an inducer or inhibitor of a drug metabolizing enzyme or transporter for an object drug. The resultant changes in the object drug concentration can lead to a higher risk of toxicity or loss of effectiveness. Multi-drug administration is common in many diseases and populations, such as obese patients, HIV patients, and geriatric patients (Linjakumpu et al. 2002, Gibbs et al. 2005, Courlet et al. 2019) and therefore, highly prevalent. In the United States, it is estimated that 20% of all adverse drug events are attributed to DDIs (Magro et al. 2012). A meta-analysis revealed that DDIs occur in 33% of general patients and 67% of intensive care patients during a hospital stay (Zheng et al. 2018).

To prevent DDIs, the U.S. Food and Drug Administration (FDA) and its international counterparts recommend pharmaceutical companies conduct a clinical DDI study when a new

chemical entity (NCE) is flagged as an inhibitor or inducer during *in vitro* screening as per prediction criteria in the published guidelines (summarized in Table 1.2). Conventionally, a single probe drug is administered with the NCE at a therapeutic dose in a prospective crossover study. The change in the area under plasma concentration-time curve (AUC) or peak concentration of the probe drug is used as a sensitive index (Rodrigues et al. 2018, Tornio et al. 2019). Due to advancements in mass spectrometry, the microdosing cocktail approach has become increasingly popular (Figure 1.7), in which several substrates that are metabolized and transported with high specificity and selectivity are administered concomitantly at subtherapeutic doses to measure the activity of multiple drug metabolizing enzymes or transporters simultaneously (Prueksaritanont et al. 2017, Tornio et al. 2019).

Although the use of *in vitro* prediction criteria for DDI screening is convenient, it often leads to a high rate of false predictions, causing tremendous loss in money and time. In a retrospective analysis including 107 clinical studies, Vaidyanathan et al. reported that ~30% of *in vitro-in vivo* DDI extrapolations were falsely predicted (15% false positive and 14% false negative) (Vaidyanathan et al. 2016). The discrepancy between *in vitro* predictions and *in vivo* DDI outcomes could be the result of inaccurate protein binding measures, inconsistent experimentally derived IC_{50} values using different probe substrates, and variability in expression systems or incubation conditions (Vaidyanathan et al. 2016, Choi et al. 2019). But given the *in vitro* potential of the NCE to cause DDIs, dedicated *in vivo* studies would have to be conducted to verify the predictions.

To avoid the need for dedicated DDI clinical studies, thereby saving considerable time and financial resources, a less invasive or noninvasive DDI assessment as early as First-In-Human clinical studies would be advantageous. The false positive and negative DDI predictions

based on *in vitro* screening data could be minimized by using endogenous biomarkers that reflect *in vivo* enzyme or transporter activity. Using endogenous substrates as a surrogate probe has been proposed (Figure 1.7) and several endogenous compounds have been evaluated for their ability to assess DDIs (Mariappan et al. 2017, Chu et al. 2018, Rodrigues et al. 2018, Tornio et al. 2019). For example, these compounds include: 4β-hydroxycholesterol for CYP3A4, *N*-methylnicotinamide for MATE1/2K and OCT2, and coproporphyrins I/III for OATP1B1 and 1B3 (Mariappan et al. 2017, Chu et al. 2018, Rodrigues et al. 2018, Tornio et al. 2019). The usefulness and limitation of proposed endogenous CYP3A biomarkers is summarized in the following section.

1.5 Endogenous CYP3A Biomarkers

CYP3A, the most abundant drug metabolizing enzyme in the liver and intestine, is responsible for metabolizing more than 50% of current medications (Paine et al. 2006, Liu et al. 2007, Achour et al. 2014). As CYP3A plays a significant role in the metabolism of many drugs, the enzyme is frequently a target of DDIs, and detection of these DDIs would be desirable with sensitive and specific CYP3A endogenous biomarkers. A wide range of endogenous compounds, such as steroids and bile acids, are also metabolized by CYP3A (Watkins 1994, Mariappan et al. 2017). Currently, four hepatic CYP3A endogenous biomarkers, including urinary 6β-hydroxycortisol/cortisol (and 6β-hydroxycortisone/cortisone), plasma 4β-hydroxycholesterol, urinary 7β-hydroxydehydroepiandrosterone/dehydroepiandrosterone, and urinary 1β-hydroxydeoxycholic acid, have been proposed and validated by *in vitro* experiments or *in vivo* studies (Bienvenu et al. 1991, Joellenbeck et al. 1992, Peng et al. 2011, Shin et al. 2013, Hayes et al. 2016).

6β-hydroxycortisol and 6β-hydroxycortisone are formed by 6β-hydroxylation of cortisol and cortisone, respectively. Several studies published in the 1980s and 1990s proposed using the urinary 6β-hydroxycortisol/cortisol ratio as a hepatic CYP3A biomarker (Saenger et al. 1981, Ged et al. 1989, Bienvenu et al. 1991, Joellenbeck et al. 1992). However, large intra-individual variability (54-57%) in the urinary ratio often rendered the CYP3A4 activity assessment inaccurate (Tran et al. 1999). Peng et al. (2011) confirmed the role of CYP3A4 in 6β-hydroxylation by inhibiting the reaction with itraconazole and ketoconazole in human liver microsomes (HLMs), followed by a clinical study showing an itraconazole dose-dependent decrease in the formation of 6β-hydroxycortisol and 6β-hydroxycortisone. Although the formation clearance, defined by the authors as the ratio of the amount of metabolite excreted in urine to the parent AUC, of 6β-hydroxycortisone was more sensitive to CYP3A4 inhibition compared to 6β-hydroxycortisol, a combined formation clearance was recommended because cortisol and 6β-hydroxycortisol can be reversibly converted to cortisone and 6β-hydroxycortisone (Peng et al. 2011). In addition to the interconversion, the active secretion of 6β-hydroxycortisol by OAT3 in kidney proximal tubules could further confound CYP3A4 assessment (Imamura et al. 2014).

4β-hydroxycholesterol is a minor metabolite of cholesterol metabolism (0.002% of total cholesterol) (Mao et al. 2017). The major role of CYP3A4 in 4β-hydroxycholesterol formation was confirmed *in vitro* and *in vivo* (Bodin et al. 2001, Bodin et al. 2002). However, clinical studies reported that baseline plasma 4β-hydroxycholesterol were only weakly correlated with IV and oral midazolam clearance (Tomalik-Scharte et al. 2009, Bjorkhem-Bergman et al. 2013). In contrast, 4β-hydroxycholesterol is highly responsive to CYP3A4 induction in DDI studies. Shin et al. (2013) found that the plasma 4β-hydroxycholesterol/cholesterol ratio and IV midazolam

clearance increased by 242% and 212%, respectively, following 10 days of rifampin administration. Similarly, Kasichayanula et al. (2014) reported comparable increases in 4β-hydroxycholesterol and IV midazolam clearance after 15 days of repeated rifampin dosing (228% and 204%, respectively). Compared to the urinary 6β-hydroxycortisol/cortisol ratio, plasma 4β-hydroxycholesterol is more promising for assessing CYP3A4 induction due to lower intra-individual variability (4.8 to 13.2%) and the absence of the confounding effects of interconversion and active secretion (Figure 1.8) (Diczfalusy et al. 2009, Dutreix et al. 2014). Unfortunately, given its long half-life (~60 hours), 4β-hydroxycholesterol is not useful in assessing CYP3A4 inhibition, as the precipitant inhibitors are given for relatively short durations in typical DDI studies (Bodin et al. 2002, Yang and Rodrigues 2010, Mao et al. 2017). Plasma 4β-hydroxycholesterol was unchanged after 4 days of ketoconazole administration and were only decreased by ~25% following two weeks of ketoconazole administration (Figure 1.9) (Shin et al. 2013, Kasichayanula et al. 2014).

7β-hydroxydehydroepiandrosterone (7β-OH-DHEA) is one of the oxidative metabolites of dehydroepiandrosterone (DHEA), the most abundant endogenous steroid hormone circulating in humans (Klinge et al. 2018). In a metabolomics study comparing inhibited-to-control and induced-to-control fold-change in urinary metabolic ratios, 7β-OH-DHEA/DHEA was identified as significant along with 6β-hydroxycortisol/cortisol and 6β-hydroxycortisone/cortisone during feature selection (Shin et al. 2013). When regressed against midazolam IV clearance, 7β-OH-DHEA/DHEA was moderately correlated ($p < 0.001$, $r^2 = 0.407$) as were the other biomarkers tested (Figures 1.10A-E). Shin et al. (2013) proposed an empirical equation combining 7β-OH-DHEA/DHEA and 6β-hydroxycortisone/cortisone to predict midazolam clearance. Their metric was able to predict 70.5% variability in log-transformed midazolam systemic clearance (Figure

1.10F) (2013). Despite being a promising alternative, 7β-OH-DHEA/DHEA has not yet been validated *in vitro*.

Most recently, urinary 1β-hydroxydeoxycholic acid (1β-OH-DCA), a bile acid metabolite, was proposed to be a novel CYP3A biomarker (Hayes et al. 2016). In DCA incubations, the formation of 1β-OH-DCA was strongly inhibited by ketoconazole in HLMs and was catalyzed by CYP3A4 and CYP3A7 with high specificity among a panel of 21 recombinant human cytochromes tested (Figures 1.11A and B). The urinary 1β-OH-DCA/DCA ratio in a patient treated with the CYP3A inducer carbamazepine was 7-fold higher than the urinary 1β-OH-DCA/DCA ratio in a pooled sample from healthy subjects (Figures 1.11C and D). Both DCA and 1β-OH-DCA were rapidly metabolized in HLMs. In 1β-OH-DCA incubations (4 μM in 10^6 hepatocytes/ml), 56% of the starting sample was metabolized after 40 minutes (Hayes et al. 2016). Although clinical studies need to be conducted to validate urinary 1β-OH-DCA/DCA ratio as a CYP3A4 biomarker, the short *in vitro* half-life may be indicative of a more sensitive biomarker for CYP3A4 inhibition.

Given the structural diversity of endogenous compounds and variability in both the formation and elimination of potential CYP3A4 biomarkers, there is a need to refine our understanding of the key features of a sensitive and specific CYP3A4 biomarker. The second part of this dissertation focuses on identifying kinetic characteristics of a potential hepatic CYP3A4 biomarker. Specifically, we investigated how the sensitivity and selectivity of a theoretical endogenous biomarker are affected by metabolite half-life, fraction of the endogenous parent that is metabolized to the metabolite of interest, and fraction of the endogenous parent that is metabolized by CYP3A4.

1.6 Dissertation Rationales and Aims

This dissertation consists of three body chapters. In Chapter 2, we investigated the impact of RYGBS on acetaminophen (APAP) absorption and metabolism. APAP is a commonly used over-the-counter analgesic drug, which is generally safe, but has the potential to cause liver failure when overdosed (Reid et al. 2005). APAP is a commonly used probe for UGTs and SULTs (Bairam et al. 2018, Lv et al. 2019) and its metabolic pathways are shown in Figure 1.12 (Cook et al. 2015). Major metabolites of APAP, APAP-glucuronide (APAP-gluc) and APAP-sulfate (APAP-sulf), are inactive (Abernethy et al. 1983, Mazaleuskaya et al. 2015). However, APAP toxicity results from a minor pathway (5–10% of the total dose), where CYP2E1 produces a toxic intermediate metabolite which is detoxified by glutathione conjugation and sequentially metabolized to APAP-cysteine (APAP-cys) and APAP-N-acetylcysteine (APAP-nac) (McGill and Jaeschke 2013, Mazaleuskaya et al. 2015). A recent study reported a 1.5-fold increase in APAP exposure following RYGBS (Goday Arno et al. 2017). Higher exposure to APAP after RYGB surgery may increase the exposure to the toxic metabolite. Therefore, using samples obtained from a RYGBS clinical study, our goal was to compare the pre- and post-RYGBS pharmacokinetics of APAP and its metabolites (i.e., APAP-gluc, APAP-sulf, APAP-cys, and APAP-nac). Quantifying APAP and these metabolites allowed us to elucidate post-RYGBS changes in the APAP metabolic fate by glucuronidation, sulfation, or the toxic pathway. We hypothesized that the APAP absorption rate increases and APAP metabolism decreases in morbidly obese patients following RYGBS.

In Chapter 3, we simulated potential CYP3A4 and P-gp drug-drug interactions (DDIs) in patients undergoing RYGBS. Physiologically-based pharmacokinetic (PBPK) modeling was used to elucidate the mechanisms by which RYGBS changes drug absorption and disposition.

Post-RYGBS anatomical and physiological conditions were emulated by adjusting the parameters in the absorption model so that drugs bypassed duodenum and jejunum I *in silico*. Midazolam and digoxin from a previous publication in patients undergoing RYGBS (Chan et al. 2015) were used as CYP3A4 and P-gp probe drugs, respectively. Following RYGBS, the rates of midazolam and digoxin absorption were increased without a change in midazolam and digoxin exposure. To predict CYP3A4- and P-gp-mediated DDIs in patients undergoing RYGBS, we selected verapamil and posaconazole as CYP3A4 and P-gp inhibitors. Both compounds have high permeability, but verapamil is a Biopharmaceutics Classification System (BCS) Class I compound (high solubility) and posaconazole is a BCS Class II compound (low solubility). After RYGBS, drugs that are weak bases and have pH-dependent solubility are likely to be subject to decreased disintegration and increased precipitation, leading to low bioavailability (Malone 2003, Padwal et al. 2010, Angeles et al. 2019). Therefore, we hypothesized that following RGYBS, midazolam, acetaminophen and digoxin drug-interactions would be stronger with high solubility inhibitors than low solubility inhibitors.

In Chapter 4, we performed a simulation study to quantify changes of a theoretical hepatic CYP3A4 biomarker in response to theoretical precipitants. The pharmacokinetic constants for the theoretical precipitants were based on those for rifampin, ketoconazole, itraconazole, and clarithromycin for induction, moderate competitive inhibition, strong competitive inhibition, and mechanism-based inhibition, respectively. Multiple biomarker sensitivity indices were compared, including the metabolite concentration (C_m), the metabolite-to-parent concentration ratio (C_m/C_p), the metabolite AUC (AUC_m), and the metabolite-to-parent AUC ratio (AUC_m/AUC_p). In theory, the most sensitive indices reflecting the largest changes from baseline would be the peak C_m or maximum C_m/C_p for induction and the trough C_m or

minimum C_m/C_p for inhibition. However, sampling at the exact peak or trough of the endogenous biomarker is often not achievable as it is hard to predict when these maximal or minimal values would occur. Therefore, we also explored more practical alternatives by sampling at the time to reach the precipitant drug's peak concentration or substituting AUC for spot sampling. We hypothesized that the ability of an endogenous biomarker to detect DDIs with a threshold of at least a 20% change, would increase with a shorter metabolite half-life, a higher fraction of the endogenous parent compound metabolized to the metabolite of interest, and a higher fraction of the endogenous parent compound metabolized by CYP3A4.

1.7 References

Abernethy, D. R., M. Divoll, D. J. Greenblatt and B. Ameer (1982). "Obesity, sex, and acetaminophen disposition." Clin Pharmacol Ther **31**(6): 783-790.

Abernethy, D. R., D. J. Greenblatt, M. Divoll and R. I. Shader (1983). "Enhanced glucuronide conjugation of drugs in obesity: studies of lorazepam, oxazepam, and acetaminophen." J Lab Clin Med **101**(6): 873-880.

Abernethy, D. R., D. J. Greenblatt, M. Divoll, R. B. Smith and R. I. Shader (1984). "The influence of obesity on the pharmacokinetics of oral alprazolam and triazolam." Clin Pharmacokinet **9**(2): 177-183.

Achour, B., J. Barber and A. Rostami-Hodjegan (2014). "Expression of hepatic drug-metabolizing cytochrome p450 enzymes and their intercorrelations: a meta-analysis." Drug Metab Dispos **42**(8): 1349-1356.

Angeles, P. C., I. Robertsen, L. T. Seeberg, V. Krogstad, J. Skattebu, R. Sandbu, A. Asberg and J. Hjelmesaeth (2019). "The influence of bariatric surgery on oral drug bioavailability in patients with obesity: A systematic review." Obes Rev **20**(9): 1299-1311.

Angrisani, L., A. Santonicola, P. Iovino, G. Formisano, H. Buchwald and N. Scopinaro (2015). "Bariatric Surgery Worldwide 2013." Obes Surg **25**(10): 1822-1832.

Attia, S. M. (2010). "Deleterious effects of reactive metabolites." Oxid Med Cell Longev **3**(4): 238-253.

Bailey, D. G., G. K. Dresser, B. F. Leake and R. B. Kim (2007). "Naringin is a major and selective clinical inhibitor of organic anion-transporting polypeptide 1A2 (OATP1A2) in grapefruit juice." Clin Pharmacol Ther **81**(4): 495-502.

Bairam, A. F., M. I. Rasool, F. A. Alherz, M. S. Abunnaja, A. A. El Daibani, K. Kurogi and M. C. Liu (2018). "Effects of human SULT1A3/SULT1A4 genetic polymorphisms on the sulfation of acetaminophen and opioid drugs by the cytosolic sulfotransferase SULT1A3." Arch Biochem Biophys **648**: 44-52.

Bauer, L. A., D. J. Black and J. S. Lill (1998). "Vancomycin dosing in morbidly obese patients." Eur J Clin Pharmacol **54**(8): 621-625.

Benaiges, D., A. Goday, J. Pedro-Botet, A. Mas, J. J. Chillaron and J. A. Flores-Le Roux (2015). "Bariatric surgery: to whom and when?" Minerva Endocrinol **40**(2): 119-128.

Bienvenu, T., E. Rey, G. Pons, P. d'Athis and G. Olive (1991). "A simple non-invasive procedure for the investigation of cytochrome P-450 IIIA dependent enzymes in humans." Int J Clin Pharmacol Ther Toxicol **29**(11): 441-445.

Bjorkhem-Bergman, L., T. Backstrom, H. Nylen, Y. Ronquist-Nii, E. Bredberg, T. B. Andersson, L. Bertilsson and U. Diczfalusy (2013). "Comparison of endogenous 4beta-hydroxycholesterol with midazolam as markers for CYP3A4 induction by rifampicin." Drug Metab Dispos **41**(8): 1488-1493.

Bodin, K., U. Andersson, E. Rystedt, E. Ellis, M. Norlin, I. Pikuleva, G. Eggertsen, I. Bjorkhem and U. Diczfalusy (2002). "Metabolism of 4 beta -hydroxycholesterol in humans." J Biol Chem **277**(35): 31534-31540.

Bodin, K., L. Bretillon, Y. Aden, L. Bertilsson, U. Broome, C. Einarsson and U. Diczfalusy (2001). "Antiepileptic drugs increase plasma levels of 4beta-hydroxycholesterol in humans: evidence for involvement of cytochrome p450 3A4." J Biol Chem **276**(42): 38685-38689.

Breedveld, P., J. H. Beijnen and J. H. Schellens (2006). "Use of P-glycoprotein and BCRP inhibitors to improve oral bioavailability and CNS penetration of anticancer drugs." Trends Pharmacol Sci **27**(1): 17-24.

Brill, M. J., A. van Rongen, E. P. van Dongen, B. van Ramshorst, E. J. Hazebroek, A. S. Darwich, A. Rostami-Hodjegan and C. A. Knibbe (2015). "The Pharmacokinetics of the CYP3A Substrate Midazolam in Morbidly Obese Patients Before and One Year After Bariatric Surgery." Pharm Res **32**(12): 3927-3936.

Brocks, D. R., M. Ben-Eltriki, R. Q. Gabr and R. S. Padwal (2012). "The effects of gastric bypass surgery on drug absorption and pharmacokinetics." Expert Opin Drug Metab Toxicol **8**(12): 1505-1519.

Campbell, T. C. and J. R. Hayes (1974). "Role of nutrition in the drug-metabolizing enzyme system." Pharmacol Rev **26**(3): 171-197.

Caraco, Y., E. Zylber-Katz, E. M. Berry and M. Levy (1995). "Carbamazepine pharmacokinetics in obese and lean subjects." Ann Pharmacother **29**(9): 843-847.

Chan, L. N., Y. S. Lin, J. C. Tay-Sontheimer, D. Trawick, B. K. Oelschlager, D. R. Flum, K. K. Patton, D. D. Shen and J. R. Horn (2015). "Proximal Roux-en-Y gastric bypass alters drug absorption pattern but not systemic exposure of CYP3A4 and P-glycoprotein substrates." Pharmacotherapy **35**(4): 361-369.

Choi, G. W., Y. B. Lee and H. Y. Cho (2019). "Interpretation of Non-Clinical Data for Prediction of Human Pharmacokinetic Parameters: In Vitro-In Vivo Extrapolation and Allometric Scaling." Pharmaceutics **11**(4).

Chu, X., M. Liao, H. Shen, K. Yoshida, A. A. Zur, V. Arya, A. Galetin, K. M. Giacomini, I. Hanna, H. Kusuhara, Y. Lai, D. Rodrigues, Y. Sugiyama, M. J. Zamek-Gliszczynski and

L. Zhang (2018). "Clinical Probes and Endogenous Biomarkers as Substrates for Transporter Drug-Drug Interaction Evaluation: Perspectives From the International Transporter Consortium." Clin Pharmacol Ther **104**(5): 836-864.

Cook, S. F., A. D. King, J. N. van den Anker and D. G. Wilkins (2015). "Simultaneous quantification of acetaminophen and five acetaminophen metabolites in human plasma and urine by high-performance liquid chromatography-electrospray ionization-tandem mass spectrometry: Method validation and application to a neonatal pharmacokinetic study." J Chromatogr B Analyt Technol Biomed Life Sci **1007**: 30-42.

Cortínez, L. I., B. J. Anderson, A. Penna, L. Olivares, H. R. Muñoz, N. H. Holford, M. M. Struys and P. Sepulveda (2010). "Influence of obesity on propofol pharmacokinetics: derivation of a pharmacokinetic model." Br J Anaesth **105**(4): 448-456.

Courlet, P., F. Livio, M. Guidi, M. Cavassini, M. Battegay, M. Stoeckle, T. Buclin, S. Alves Saldanha, C. Csajka, C. Marzolini and L. Decosterd (2019). "Polypharmacy, Drug-Drug Interactions, and Inappropriate Drugs: New Challenges in the Aging Population With HIV." Open Forum Infect Dis **6**(12): ofz531.

Darwich, A. S., D. Pade, B. J. Ammori, M. Jamei, D. M. Ashcroft and A. Rostami-Hodjegan (2012). "A mechanistic pharmacokinetic model to assess modified oral drug bioavailability post bariatric surgery in morbidly obese patients: interplay between CYP3A gut wall metabolism, permeability and dissolution." J Pharm Pharmacol **64**(7): 1008-1024.

De Baerdemaeker, L. and M. Margarson (2016). "Best anaesthetic drug strategy for morbidly obese patients." Curr Opin Anaesthesiol **29**(1): 119-128.

De Smet, J., J. Van Bocxlaer and K. Boussery (2013). "The influence of bypass procedures and other anatomical changes in the gastrointestinal tract on the oral bioavailability of drugs." J Clin Pharmacol **53**(4): 361-376.

Diczfalusy, U., K. P. Kanebratt, E. Bredberg, T. B. Andersson, Y. Bottiger and L. Bertilsson (2009). "4beta-hydroxycholesterol as an endogenous marker for CYP3A4/5 activity. Stability and half-life of elimination after induction with rifampicin." Br J Clin Pharmacol **67**(1): 38-43.

Drozdzik, M., D. Busch, J. Lapczuk, J. Muller, M. Ostrowski, M. Kurzawski and S. Oswald (2018). "Protein Abundance of Clinically Relevant Drug-Metabolizing Enzymes in the Human Liver and Intestine: A Comparative Analysis in Paired Tissue Specimens." Clin Pharmacol Ther **104**(3): 515-524.

Drozdzik, M., C. Groer, J. Penski, J. Lapczuk, M. Ostrowski, Y. Lai, B. Prasad, J. D. Unadkat, W. Siegmund and S. Oswald (2014). "Protein abundance of clinically relevant multidrug transporters along the entire length of the human intestine." Mol Pharm **11**(10): 3547-3555.

Dutreix, C., S. Lorenzo and Y. Wang (2014). "Comparison of two endogenous biomarkers of CYP3A4 activity in a drug-drug interaction study between midostaurin and rifampicin." Eur J Clin Pharmacol **70**(8): 915-920.

Emery, M. G., J. M. Fisher, J. Y. Chien, E. D. Kharasch, E. P. Dellinger, K. V. Kowdley and K. E. Thummel (2003). "CYP2E1 activity before and after weight loss in morbidly obese subjects with nonalcoholic fatty liver disease." Hepatology **38**(2): 428-435.

Estudante, M., J. G. Morais, G. Soveral and L. Z. Benet (2013). "Intestinal drug transporters: an overview." Adv Drug Deliv Rev **65**(10): 1340-1356.

Fritz, A., D. Busch, J. Lapczuk, M. Ostrowski, M. Drozdzik and S. Oswald (2019). "Expression of clinically relevant drug-metabolizing enzymes along the human intestine and their correlation to drug transporters and nuclear receptors: An intra-subject analysis." Basic Clin Pharmacol Toxicol **124**(3): 245-255.

Ged, C., J. M. Rouillon, L. Pichard, J. Combalbert, N. Bressot, P. Bories, H. Michel, P. Beaune and P. Maurel (1989). "The increase in urinary excretion of 6 beta-hydroxycortisol as a marker of human hepatic cytochrome P450IIIA induction." Br J Clin Pharmacol **28**(4): 373-387.

Gibbs, H., J. Broom, J. Brown, R. Laws, J. Reckless, P. Noble, S. Kumar, L. McCombie and M. Lean (2005). "The impact of obesity on drug prescribing in primary care." Br J Gen Pract **55**(519): 743-749.

Glaeser, H., D. G. Bailey, G. K. Dresser, J. C. Gregor, U. I. Schwarz, J. S. McGrath, E. Jolicoeur, W. Lee, B. F. Leake, R. G. Tirona and R. B. Kim (2007). "Intestinal drug transporter expression and the impact of grapefruit juice in humans." Clin Pharmacol Ther **81**(3): 362-370.

Goday Arno, A., M. Farre, J. Rodriguez-Morato, J. M. Ramon, C. Perez-Mana, E. Papaseit, E. Civit, K. Langohr, M. Li Carbo, D. B. Boix, O. C. Nino, J. A. F. Le Roux, M. Pera, L. Grande and R. de la Torre (2017). "Pharmacokinetics in Morbid Obesity: Influence of Two Bariatric Surgery Techniques on Paracetamol and Caffeine Metabolism." Obes Surg **27**(12): 3194-3201.

Greenblatt, D. J., D. R. Abernethy, A. Locniskar, J. S. Harmatz, R. A. Limjuco and R. I. Shader (1984). "Effect of age, gender, and obesity on midazolam kinetics." Anesthesiology **61**(1): 27-35.

Greenblatt, H. K. and D. J. Greenblatt (2015). "Altered drug disposition following bariatric surgery: a research challenge." Clin Pharmacokinet **54**(6): 573-579.

Groer, C., D. Busch, M. Patrzyk, K. Beyer, A. Busemann, C. D. Heidecke, M. Drozdzik, W. Siegmund and S. Oswald (2014). "Absolute protein quantification of clinically relevant cytochrome P450 enzymes and UDP-glucuronosyltransferases by mass spectrometry-based targeted proteomics." J Pharm Biomed Anal **100**: 393-401.

Hachon, L., X. Decleves, P. Faucher, C. Carette and C. Lloret-Linares (2017). "RYGB and Drug Disposition: How to Do Better? Analysis of Pharmacokinetic Studies and Recommendations for Clinical Practice." Obes Surg **27**(4): 1076-1090.

Hales, C. M., M. D. Carroll, C. D. Fryar and C. L. Ogden (2017). "Prevalence of Obesity Among Adults and Youth: United States, 2015-2016." NCHS Data Brief(288): 1-8.

Harbourt, D. E., J. K. Fallon, S. Ito, T. Baba, J. K. Ritter, G. L. Glish and P. C. Smith (2012). "Quantification of human uridine-diphosphate glucuronosyl transferase 1A isoforms in liver, intestine, and kidney using nanobore liquid chromatography-tandem mass spectrometry." Anal Chem **84**(1): 98-105.

Hardwick, R. N., D. W. Ferreira, V. R. More, A. D. Lake, Z. Lu, J. E. Manautou, A. L. Slitt and N. J. Cherrington (2013). "Altered UDP-glucuronosyltransferase and sulfotransferase expression and function during progressive stages of human nonalcoholic fatty liver disease." Drug Metab Dispos **41**(3): 554-561.

Hayes, M. A., X. Q. Li, G. Gronberg, U. Diczfalusy and T. B. Andersson (2016). "CYP3A Specifically Catalyzes 1beta-Hydroxylation of Deoxycholic Acid: Characterization and Enzymatic Synthesis of a Potential Novel Urinary Biomarker for CYP3A Activity." Drug Metab Dispos **44**(9): 1480-1489.

Imamura, Y., Y. Tsuruya, K. Damme, D. Heer, Y. Kumagai, K. Maeda, N. Murayama, N. Okudaira, A. Kurihara, T. Izumi, Y. Sugiyama and H. Kusuhara (2014). "6beta-Hydroxycortisol is an endogenous probe for evaluation of drug-drug interactions involving a multispecific renal organic anion transporter, OAT3/SLC22A8, in healthy subjects." Drug Metab Dispos **42**(4): 685-694.

Joellenbeck, L., Z. Qian, A. Zarba and J. D. Groopman (1992). "Urinary 6 beta-hydroxycortisol/cortisol ratios measured by high-performance liquid chromatography for use as a biomarker for the human cytochrome P-450 3A4." Cancer Epidemiol Biomarkers Prev **1**(7): 567-572.

Kasichayanula, S., D. W. Boulton, W. L. Luo, A. D. Rodrigues, Z. Yang, A. Goodenough, M. Lee, M. Jemal and F. LaCreta (2014). "Validation of 4beta-hydroxycholesterol and evaluation of other endogenous biomarkers for the assessment of CYP3A activity in healthy subjects." Br J Clin Pharmacol **78**(5): 1122-1134.

Klinge, C. M., B. J. Clark and R. A. Prough (2018). "Dehydroepiandrosterone Research: Past, Current, and Future." Vitam Horm **108**: 1-28.

Krishnaswamy, K., R. Kalamegham and N. A. Naidu (1984). "Dietary influences on the kinetics of antipyrine and aminopyrine in human subjects." Br J Clin Pharmacol **17**(2): 139-146.

Lewis, M. C., M. L. Phillips, J. P. Slavotinek, L. Kow, C. H. Thompson and J. Toouli (2006). "Change in liver size and fat content after treatment with Optifast very low calorie diet." Obes Surg **16**(6): 697-701.

Linjakumpu, T., S. Hartikainen, T. Klaukka, J. Veijola, S. L. Kivela and R. Isoaho (2002). "Use of medications and polypharmacy are increasing among the elderly." J Clin Epidemiol **55**(8): 809-817.

Lipinski, C. A. (2000). "Drug-like properties and the causes of poor solubility and poor permeability." J Pharmacol Toxicol Methods **44**(1): 235-249.

Liu, Y. T., H. P. Hao, C. X. Liu, G. J. Wang and H. G. Xie (2007). "Drugs as CYP3A probes, inducers, and inhibitors." Drug Metab Rev **39**(4): 699-721.

Lucas, D., C. Farez, L. G. Bardou, J. Vaisse, J. R. Attali and P. Valensi (1998). "Cytochrome P450 2E1 activity in diabetic and obese patients as assessed by chlorzoxazone hydroxylation." Fundam Clin Pharmacol **12**(5): 553-558.

Lv, X., J. B. Zhang, J. Hou, T. Y. Dou, G. B. Ge, W. Z. Hu and L. Yang (2019). "Chemical Probes for Human UDP-Glucuronosyltransferases: A Comprehensive Review." Biotechnol J **14**(1): e1800002.

Magro, L., U. Moretti and R. Leone (2012). "Epidemiology and characteristics of adverse drug reactions caused by drug-drug interactions." Expert Opin Drug Saf **11**(1): 83-94.

Malone, M. (2003). "Altered drug disposition in obesity and after bariatric surgery." Nutr Clin Pract **18**(2): 131-135.

Mao, J., I. Martin, J. McLeod, G. Nolan, R. van Horn, M. Vourvahis and Y. S. Lin (2017). "Perspective: 4beta-hydroxycholesterol as an emerging endogenous biomarker of hepatic CYP3A." Drug Metab Rev **49**(1): 18-34.

Mao, Z. L., Y. K. Tam and R. T. Coutts (2006). "Effect of protein and calorie malnutrition on drug metabolism in rat - in vitro." J Pharm Pharm Sci **9**(1): 60-70.

Mariappan, T. T., H. Shen and P. Marathe (2017). "Endogenous Biomarkers to Assess Drug-Drug Interactions by Drug Transporters and Enzymes." Curr Drug Metab **18**(8): 757-768.

Mazaleuskaya, L. L., K. Sangkuhl, C. F. Thorn, G. A. FitzGerald, R. B. Altman and T. E. Klein (2015). "PharmGKB summary: pathways of acetaminophen metabolism at the therapeutic versus toxic doses." Pharmacogenet Genomics **25**(8): 416-426.

McGill, M. R. and H. Jaeschke (2013). "Metabolism and disposition of acetaminophen: recent advances in relation to hepatotoxicity and diagnosis." Pharm Res **30**(9): 2174-2187.

Mgbodile, M. U. and T. C. Campbell (1972). "Effect of protein deprivation of male weanling rats on the kinetics of hepatic microsomal enzyme activity." J Nutr **102**(1): 53-60.

Mitchell, N. S., V. A. Catenacci, H. R. Wyatt and J. O. Hill (2011). "Obesity: overview of an epidemic." Psychiatr Clin North Am **34**(4): 717-732.

Mouly, S. and M. F. Paine (2003). "P-glycoprotein increases from proximal to distal regions of human small intestine." Pharm Res **20**(10): 1595-1599.

O'Shea, D., S. N. Davis, R. B. Kim and G. R. Wilkinson (1994). "Effect of fasting and obesity in humans on the 6-hydroxylation of chlorzoxazone: a putative probe of CYP2E1 activity." Clin Pharmacol Ther **56**(4): 359-367.

Padwal, R., D. Brocks and A. M. Sharma (2010). "A systematic review of drug absorption following bariatric surgery and its theoretical implications." Obes Rev **11**(1): 41-50.

Paine, M. F., H. L. Hart, S. S. Ludington, R. L. Haining, A. E. Rettie and D. C. Zeldin (2006). "The human intestinal cytochrome P450 "pie"." Drug Metab Dispos **34**(5): 880-886.

Peng, C. C., I. Templeton, K. E. Thummel, C. Davis, K. L. Kunze and N. Isoherranen (2011). "Evaluation of 6beta-hydroxycortisol, 6beta-hydroxycortisone, and a combination of the two as endogenous probes for inhibition of CYP3A4 in vivo." Clin Pharmacol Ther **89**(6): 888-895.

Penno, M. B., B. H. Dvorchik and E. S. Vesell (1981). "Genetic variation in rates of antipyrine metabolite formation: a study in uninduced twins." Proc Natl Acad Sci U S A **78**(8): 5193-5196.

Peters, S. A., C. R. Jones, A. L. Ungell and O. J. Hatley (2016). "Predicting Drug Extraction in the Human Gut Wall: Assessing Contributions from Drug Metabolizing Enzymes and Transporter Proteins using Preclinical Models." Clin Pharmacokinet **55**(6): 673-696.

Prueksaritanont, T., D. A. Tatosian, X. Chu, R. Railkar, R. Evers, C. Chavez-Eng, R. Lutz, W. Zeng, J. Yabut, G. H. Chan, X. Cai, A. H. Latham, J. Hehman, D. Stypinski, J. Brejda, C. Zhou, B. Thornton, K. P. Bateman, I. Fraser and S. A. Stoch (2017). "Validation of a microdose probe drug cocktail for clinical drug interaction assessments for drug transporters and CYP3A." Clin Pharmacol Ther **101**(4): 519-530.

Rahmioglu, N., J. Heaton, G. Clement, R. Gill, G. Surdulescu, K. Zlobecka, D. Hodgkiss, Y. Ma, R. C. Hider, N. W. Smith and K. R. Ahmadi (2011). "Genetic epidemiology of induced CYP3A4 activity." Pharmacogenet Genomics **21**(10): 642-651.

Reid, A. B., R. C. Kurten, S. S. McCullough, R. W. Brock and J. A. Hinson (2005). "Mechanisms of acetaminophen-induced hepatotoxicity: role of oxidative stress and mitochondrial permeability transition in freshly isolated mouse hepatocytes." J Pharmacol Exp Ther **312**(2): 509-516.

Rekic, D., K. S. Reynolds, P. Zhao, L. Zhang, K. Yoshida, M. Sachar, M. Piquette Miller, S. M. Huang and I. Zineh (2017). "Clinical Drug-Drug Interaction Evaluations to Inform Drug Use and Enable Drug Access." J Pharm Sci **106**(9): 2214-2218.

Reyner, E., B. Lum, J. Jing, M. Kagedal, J. A. Ware and L. J. Dickmann (2019). "Intrinsic and Extrinsic Pharmacokinetic Variability of Small Molecule Targeted Cancer Therapy." Clin Transl Sci.

Riches, Z., E. L. Stanley, J. C. Bloomer and M. W. Coughtrie (2009). "Quantitative evaluation of the expression and activity of five major sulfotransferases (SULTs) in human tissues: the SULT "pie"." Drug Metab Dispos **37**(11): 2255-2261.

Rodrigues, A. D., K. S. Taskar, H. Kusuhara and Y. Sugiyama (2018). "Endogenous Probes for Drug Transporters: Balancing Vision With Reality." Clin Pharmacol Ther **103**(3): 434-448.

Ross, D. D. and T. Nakanishi (2010). "Impact of breast cancer resistance protein on cancer treatment outcomes." Methods Mol Biol **596**: 251-290.

Saenger, P., E. Forster and J. Kream (1981). "6 beta-Hydroxycortisol: a noninvasive indicator of enzyme induction." J Clin Endocrinol Metab **52**(3): 381-384.

Sato, Y., M. Nagata, K. Tetsuka, K. Tamura, A. Miyashita, A. Kawamura and T. Usui (2014). "Optimized methods for targeted peptide-based quantification of human uridine 5'-diphosphate-glucuronosyltransferases in biological specimens using liquid chromatography-tandem mass spectrometry." Drug Metab Dispos **42**(5): 885-889.

Savassi-Rocha, A. L., M. T. Diniz, E. G. Vilela, F. Diniz Mde, S. R. Sanches, A. S. da Cunha, L. Ferrari Mde, H. O. Torres, B. A. Maciente, G. S. Ataliba, P. M. Araujo, T. B. Guerra and I. K. Balbino (2014). "Changes in intestinal permeability after Roux-en-Y gastric bypass." Obes Surg **24**(2): 184-190.

Schauer, P. R., S. Ikramuddin, W. Gourash, R. Ramanathan and J. Luketich (2000). "Outcomes after laparoscopic Roux-en-Y gastric bypass for morbid obesity." Ann Surg **232**(4): 515-529.

Shibutani, K., M. A. Inchiosa, Jr., K. Sawada and M. Bairamian (2004). "Accuracy of pharmacokinetic models for predicting plasma fentanyl concentrations in lean and obese surgical patients: derivation of dosing weight ("pharmacokinetic mass")." Anesthesiology **101**(3): 603-613.

Shin, K. H., M. H. Choi, K. S. Lim, K. S. Yu, I. J. Jang and J. Y. Cho (2013). "Evaluation of endogenous metabolic markers of hepatic CYP3A activity using metabolic profiling and midazolam clearance." Clin Pharmacol Ther **94**(5): 601-609.

Stein, J., C. Stier, H. Raab and R. Weiner (2014). "Review article: The nutritional and pharmacological consequences of obesity surgery." Aliment Pharmacol Ther **40**(6): 582-609.

Sun, B. and M. Karin (2012). "Obesity, inflammation, and liver cancer." J Hepatol **56**(3): 704-713.

Tomalik-Scharte, D., D. Lutjohann, O. Doroshyenko, D. Frank, A. Jetter and U. Fuhr (2009). "Plasma 4beta-hydroxycholesterol: an endogenous CYP3A metric?" Clin Pharmacol Ther **86**(2): 147-153.

Tornio, A., A. M. Filppula, M. Niemi and J. T. Backman (2019). "Clinical Studies on Drug-Drug Interactions Involving Metabolism and Transport: Methodology, Pitfalls, and Interpretation." Clin Pharmacol Ther **105**(6): 1345-1361.

Tran, J. Q., S. J. Kovacs, T. S. McIntosh, H. M. Davis and D. E. Martin (1999). "Morning spot and 24-hour urinary 6 beta-hydroxycortisol to cortisol ratios: intraindividual variability

and correlation under basal conditions and conditions of CYP 3A4 induction." J Clin Pharmacol **39**(5): 487-494.

Vaidyanathan, J., K. Yoshida, V. Arya and L. Zhang (2016). "Comparing Various In Vitro Prediction Criteria to Assess the Potential of a New Molecular Entity to Inhibit Organic Anion Transporting Polypeptide 1B1." J Clin Pharmacol **56 Suppl 7**: S59-72.

van Kralingen, S., J. Diepstraten, M. Y. Peeters, V. H. Deneer, B. van Ramshorst, R. J. Wiezer, E. P. van Dongen, M. Danhof and C. A. Knibbe (2011). "Population pharmacokinetics and pharmacodynamics of propofol in morbidly obese patients." Clin Pharmacokinet **50**(11): 739-750.

Vertzoni, M., P. Augustijns, M. Grimm, M. Koziolek, G. Lemmens, N. Parrott, C. Pentafragka, C. Reppas, J. Rubbens, J. Van Den Alphabeele, T. Vanuytsel, W. Weitschies and C. G. Wilson (2019). "Impact of regional differences along the gastrointestinal tract of healthy adults on oral drug absorption: An UNGAP review." Eur J Pharm Sci **134**: 153-175.

Visscher, P. M., W. G. Hill and N. R. Wray (2008). "Heritability in the genomics era--concepts and misconceptions." Nat Rev Genet **9**(4): 255-266.

Watkins, P. B. (1994). "Noninvasive tests of CYP3A enzymes." Pharmacogenetics **4**(4): 171-184.

Xie, F., X. Ding and Q. Y. Zhang (2016). "An update on the role of intestinal cytochrome P450 enzymes in drug disposition." Acta Pharm Sin B **6**(5): 374-383.

Yang, C. S., J. F. Brady and J. Y. Hong (1992). "Dietary effects on cytochromes P450, xenobiotic metabolism, and toxicity." Faseb j **6**(2): 737-744.

Yang, Z. and A. D. Rodrigues (2010). "Does the long plasma half-life of 4beta-hydroxycholesterol impact its utility as a cytochrome P450 3A (CYP3A) metric?" J Clin Pharmacol **50**(11): 1330-1338.

Zheng, W. Y., L. C. Richardson, L. Li, R. O. Day, J. I. Westbrook and M. T. Baysari (2018). "Drug-drug interactions and their harmful effects in hospitalised patients: a systematic review and meta-analysis." Eur J Clin Pharmacol **74**(1): 15-27.

Zobel, E. H., T. W. Hansen, P. Rossing and B. J. von Scholten (2016). "Global Changes in Food Supply and the Obesity Epidemic." Curr Obes Rep **5**(4): 449-455.

1.8 Figures and Tables

Table 1.1. Possible impacts of anatomical and physiological changes following RYGBS on pharmacokinetics of drugs (from Hachon et al., 2017).

Anatomical changes	Physiological changes	Possible impact on pharmacokinetics
Reduced gastric volume	Alteration of gastric emptying time	Change in the rate of oral absorption
	Increased gastric pH	Change in the extent of oral absorption
	Increased gastrointestinal tract pH	Change in the rate and extent of oral absorption
Bypass of the duodenum	Reduced surface of absorption	Change in the rate and extent of oral absorption
	Reduced intestinal first-pass metabolism (Mainly CYP3A4, CYP3A5)	Change in the extent of oral absorption
	Reduced intestinal first-pass efflux: P-gp	Change in the extent of oral absorption
	Decreased intestinal transit time	Change in the rate of oral absorption
Dissociation of bile salt delivery	Decreased or delayed absorption of drugs requiring pancreatic secretions or solubilization with bile salts	Change in the extent of oral absorption
	Reduced enterohepatic circulation	Change in the extent of oral absorption
Weight loss	Decreased low-grade inflammation	Change in drug metabolism
	Decreased steatohepatitis and insulin resistance	Change in the extent of oral absorption
	Decreased fat and lean mass	Change in drug distribution

Table 1.2. Summary of equations proposed by FDA to calculate the predicted ratio of the object drug's area under the concentration-time curve (AUC).

Interaction	Equations	Criteria
Reversible inhibition	$R_1 = 1 + (I_{max,u} / K_i)$ $R_{1,gut} = 1 + (I_{gut} / K_i)$	$R_1 \geq 1.2$ $R_{1,gut} \geq 11$
Time dependent inhibition (TDI)	$R_2 = (k_{obs} + k_{deg}) / k_{deg}$ $k_{obs} = (k_{inact} \times 50 \times I_{max,u}) / (K_I + 50 \times I_{max,u})$	$R_2 \geq 1.25$
Induction	$R_3 = 1 / [1 + (d \times E_{max} \times 10 \times I_{max,u}) / (EC_{50} + (10 \times I_{max,u}))]$	$R_3 \leq 0.8$

Abbreviations: R_1 or $R_{1,gut}$ = the predicted ratio of the object drug's AUC in the presence and absence of an inhibitor for basic models of reversible inhibition; $I_{max,u}$ = the maximal unbound plasma concentration of the interacting drug; I_{gut} = the intestinal luminal concentration of the interacting drug calculated as the dose/250 mL; K_i = the unbound inhibition constant determined *in vitro*; R_2 = the predicted ratio of the object drug's AUC in the presence and absence of an inhibitor for basic models of enzyme TDI; k_{obs} = the observed (apparent first order) inactivation rate constant of the affected enzyme; k_{deg} = the apparent first-order degradation rate constant of the affected enzyme; K_I = the inhibitor concentration causing half-maximal inactivation; R_3 = the predicted ratio of the object drug's AUC in the presence and absence of an inducer for basic models of enzyme induction; d = the scaling factor and is assumed to be 1 unless supported by prior experience with the system used; E_{max} = the maximum induction effect determined *in vitro*; EC_{50} = the concentration causing half-maximal effect determined *in vitro*.

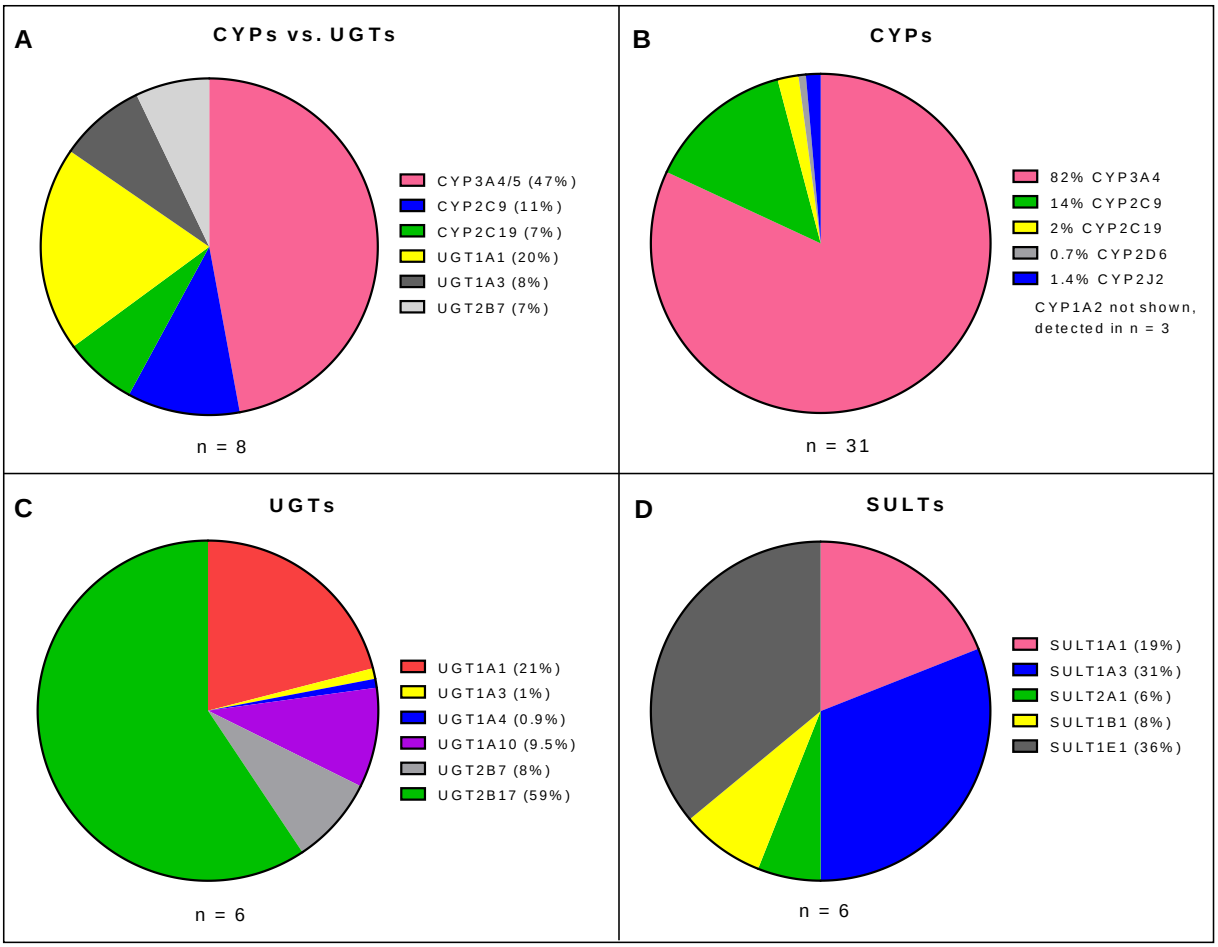

Figure 1.1. The relative abundance of intestinal CYPs, UGTs, and SULTs. Pie charts comparing A) major CYP and UGT isoforms quantified by mass spectrometry (n = 8, Gröer et al., 2014); B) CYPs quantified by immunoblotting (n = 31, Paine et al., 2006); C) UGTs quantified by mass spectrometry (n=6, Sato et al., 2014); D) SULTs quantified by immunoblotting (n = 6, adapted from Riches et al., 2009)

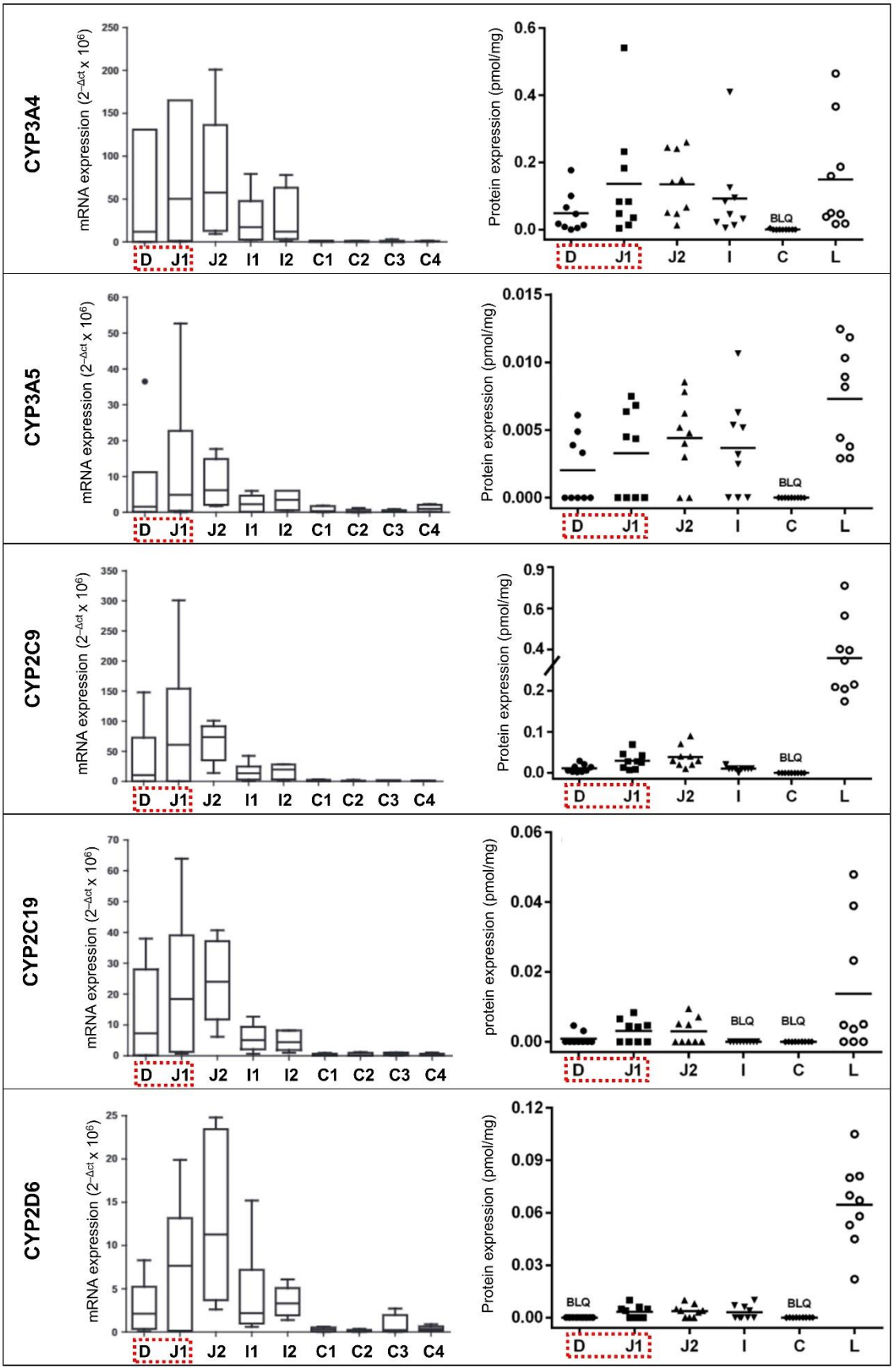
CYP3A4
mRNA expression (2^-Δct x 10^6)
Protein expression (pmol/mg)
CYP3A5
mRNA expression (2^-Δct x 10^6)
Protein expression (pmol/mg)
CYP2C9
mRNA expression (2^-Δct x 10^6)
Protein expression (pmol/mg)
CYP2C19
mRNA expression (2^-Δct x 10^6)
protein expression (pmol/mg)
CYP2D6
mRNA expression (2^-Δct x 10^6)
Protein expression (pmol/mg)
D J1 J2 I1 I2 C1 C2 C3 C4
D J1 J2 I C L
BLQ

Figure 1.2. Intestinal and hepatic CYP mRNA expression (left, n = 6; adapted from Fritz et al., 2019) and protein abundance (right, n = 9; adapted from Drozdzik et al., 2018). Sample means are indicated by horizontal bars. The red boxes indicate bypassed regions after Roux-en-Y surgery. D = duodenum; J1 = proximal jejunum; J2 = distal jejunum; I1 = proximal ileum; I2 = distal ileum; C1 = proximal colon; C2 = upper middle colon; C3 = lower middle colon; C4 = distal colon; L = liver.

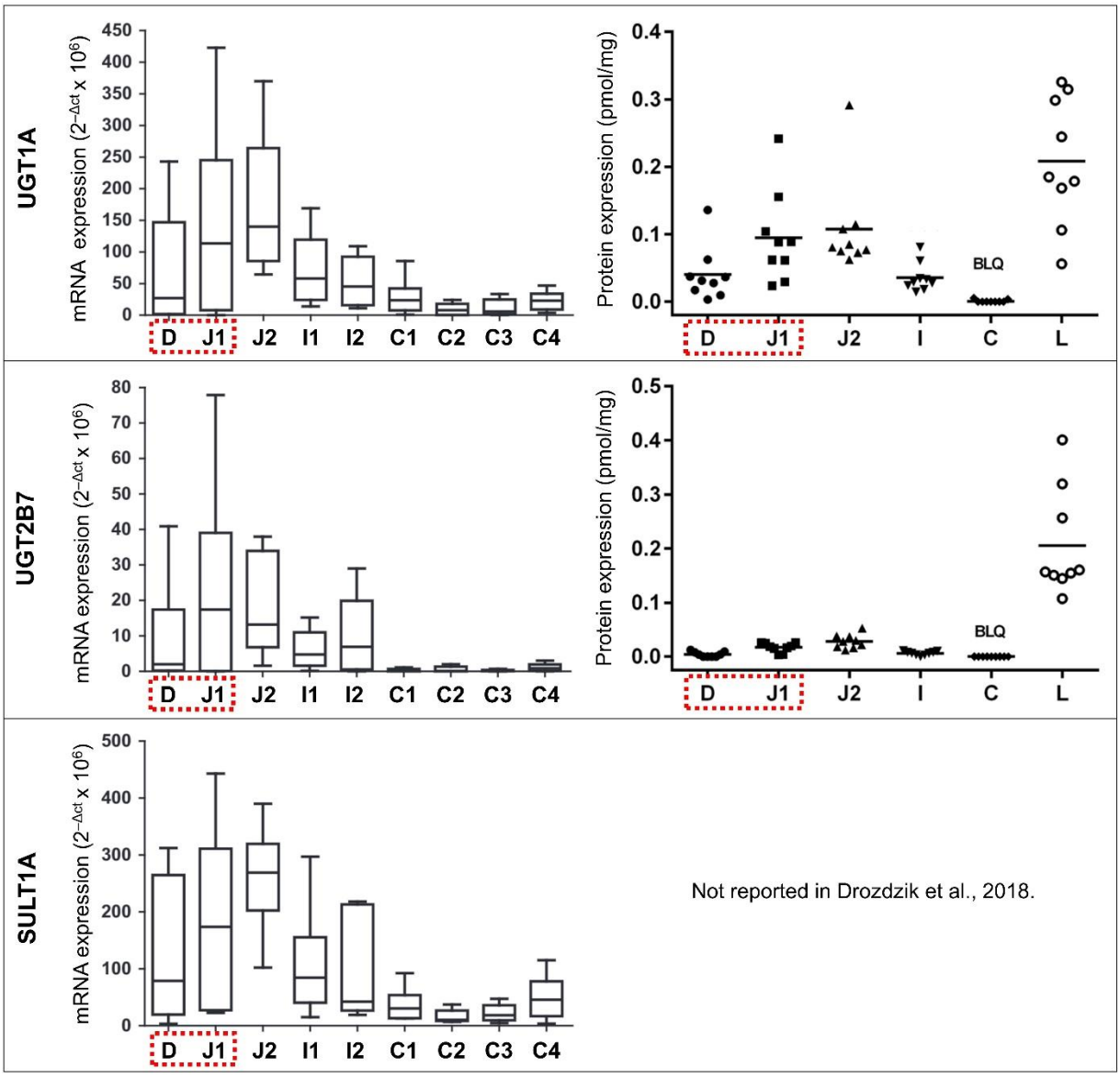

Figure 1.3 Intestinal and hepatic UGT1A, UGT2B7, and SULT1A mRNA expression (left panels, n = 6; adapted from Fritz et al., 2019) and protein abundance (right panels, n = 9; adapted from Drozdzik et al., 2018). Sample means are indicated by horizontal bars. The red boxes indicate bypassed regions after Roux-en-Y surgery. D = duodenum; J1 = proximal jejunum; J2 = distal jejunum; I1 = proximal ileum; I2 = distal ileum; C1 = proximal colon; C2 = upper middle colon; C3 = lower middle colon; C4 = distal colon; L = liver.

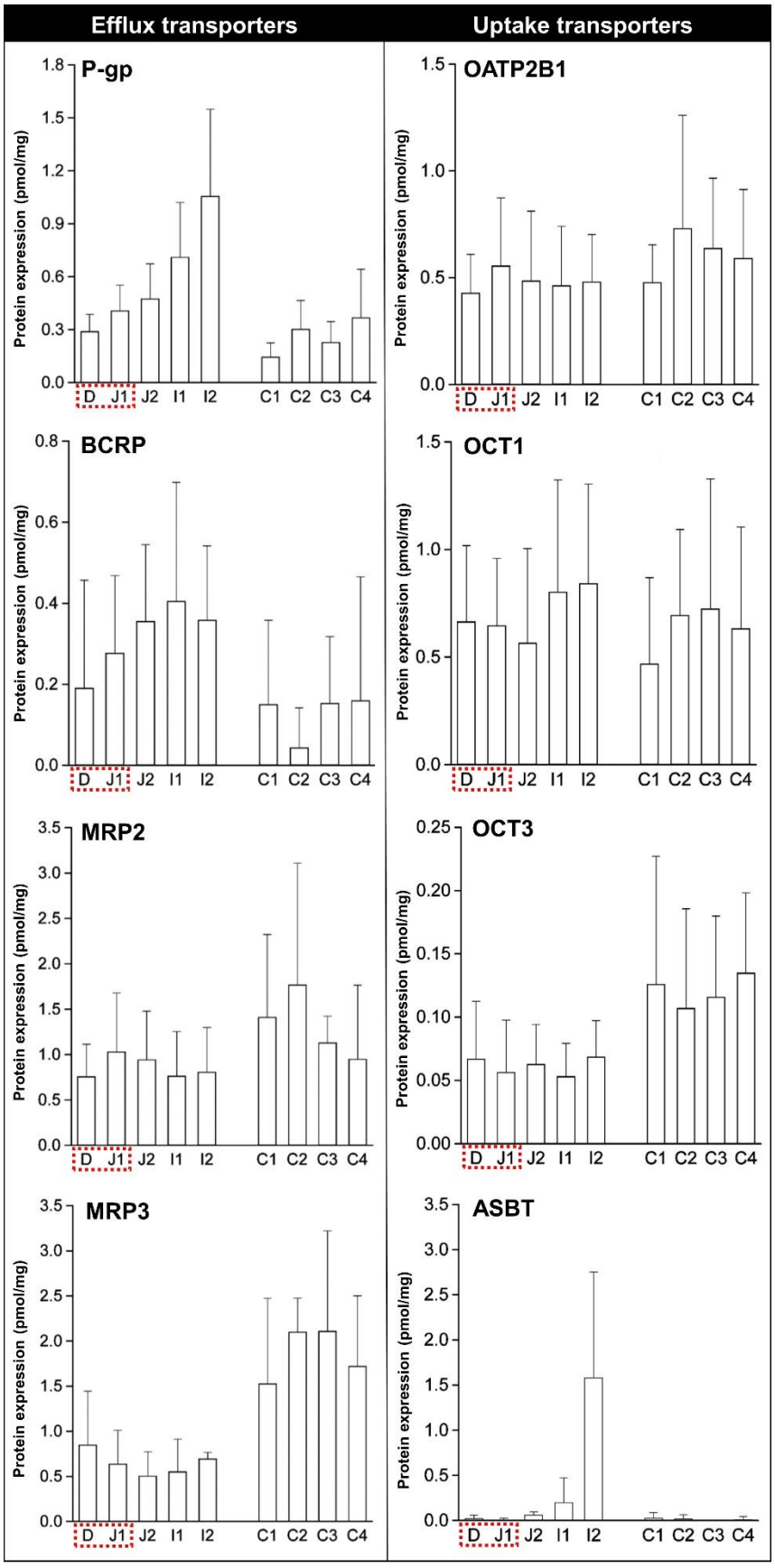
Efflux transporters
Uptake transporters
P-gp
OATP2B1
BCRP
OCT1
MRP2
OCT3
MRP3
ASBT
Protein expression (pmol/mg)
D J1 J2 I1 I2 C1 C2 C3 C4

Figure 1.4. Intestinal protein expression of uptake and efflux transporters (n = 6; adapted from Drozdzik et al., 2014). The red boxes indicate bypassed regions after Roux-en-Y surgery. D = duodenum; J1 = proximal jejunum; J2 = distal jejunum; I1 = proximal ileum; I2 = distal ileum; C1 = proximal colon; C2 = upper middle colon; C3 = lower middle colon; C4 = distal colon; L = liver.

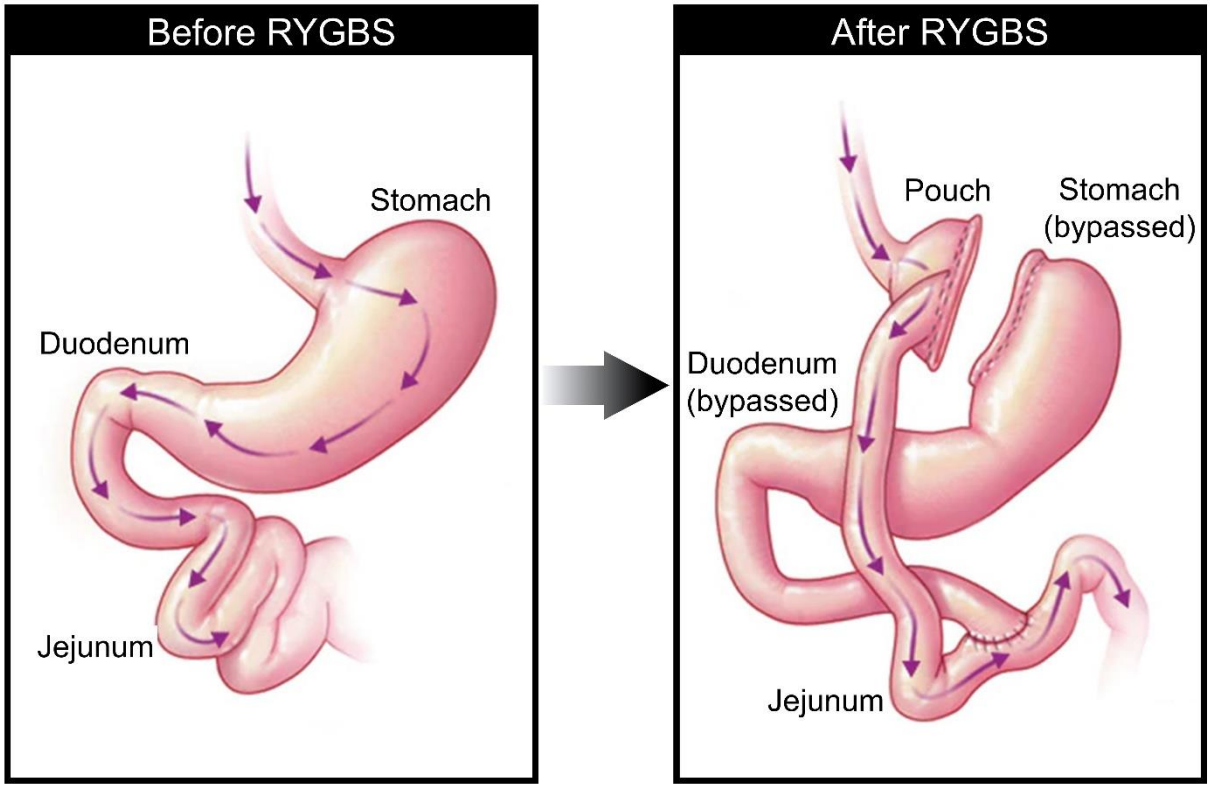

Figure 1.5. Roux-en-Y gastric bypass procedure adapted from Mayo Foundation for Medical Education and Research., 2017.

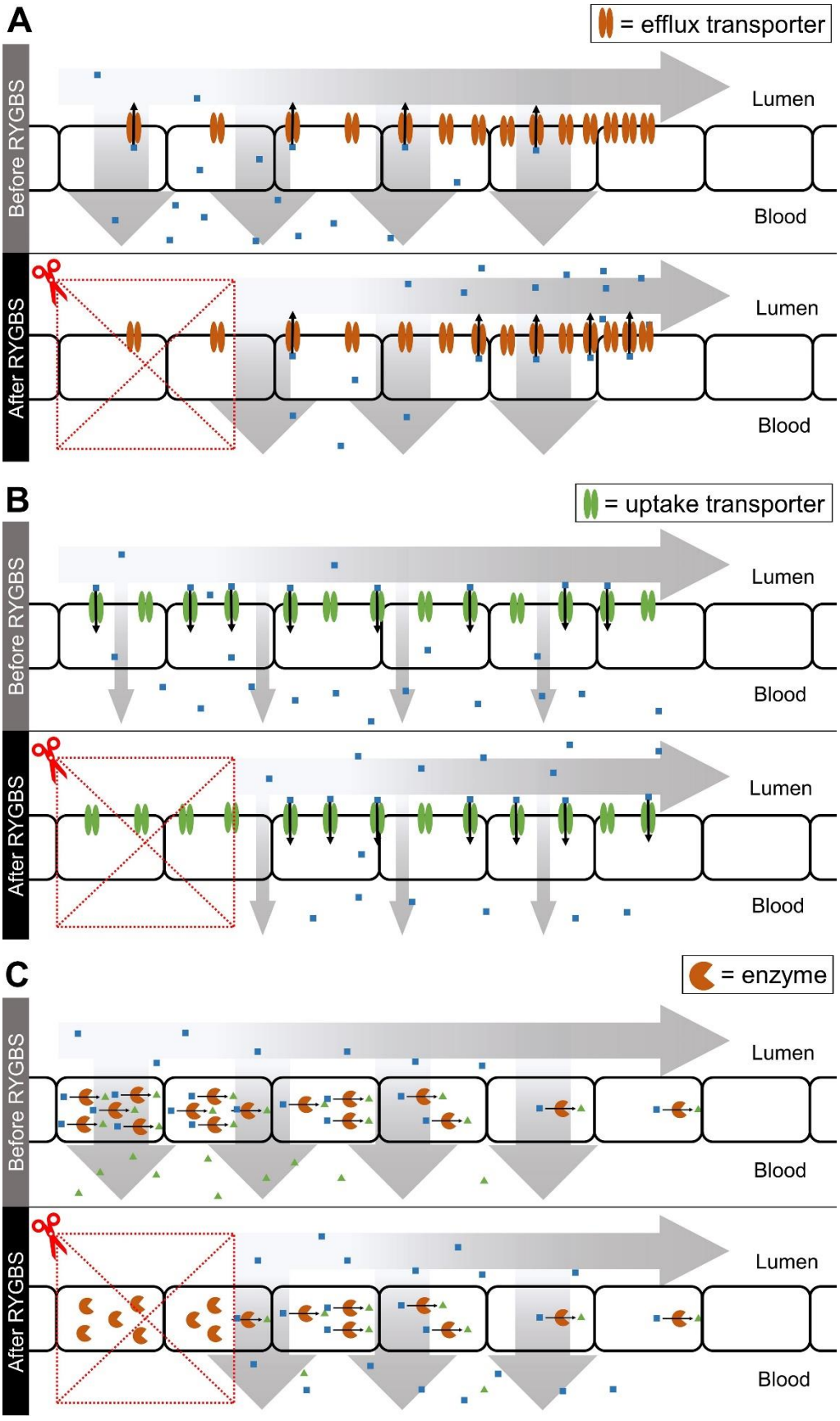
A
= efflux transporter
Before RYGBS
Lumen
Blood
After RYGBS
Lumen
Blood
B
= uptake transporter
Before RYGBS
Lumen
Blood
After RYGBS
Lumen
Blood
C
= enzyme
Before RYGBS
Lumen
Blood
After RYGBS
Lumen
Blood

Figure 1.6 Comparisons of hypothesized changes in intestinal efflux transport (A), uptake transport (B), and metabolism (C) before and after Roux-en-Y gastric bypass surgery. Blue squares represent drug and green triangles represent metabolite. Bypassed regions due to RYGBS are indicated by red boxes.

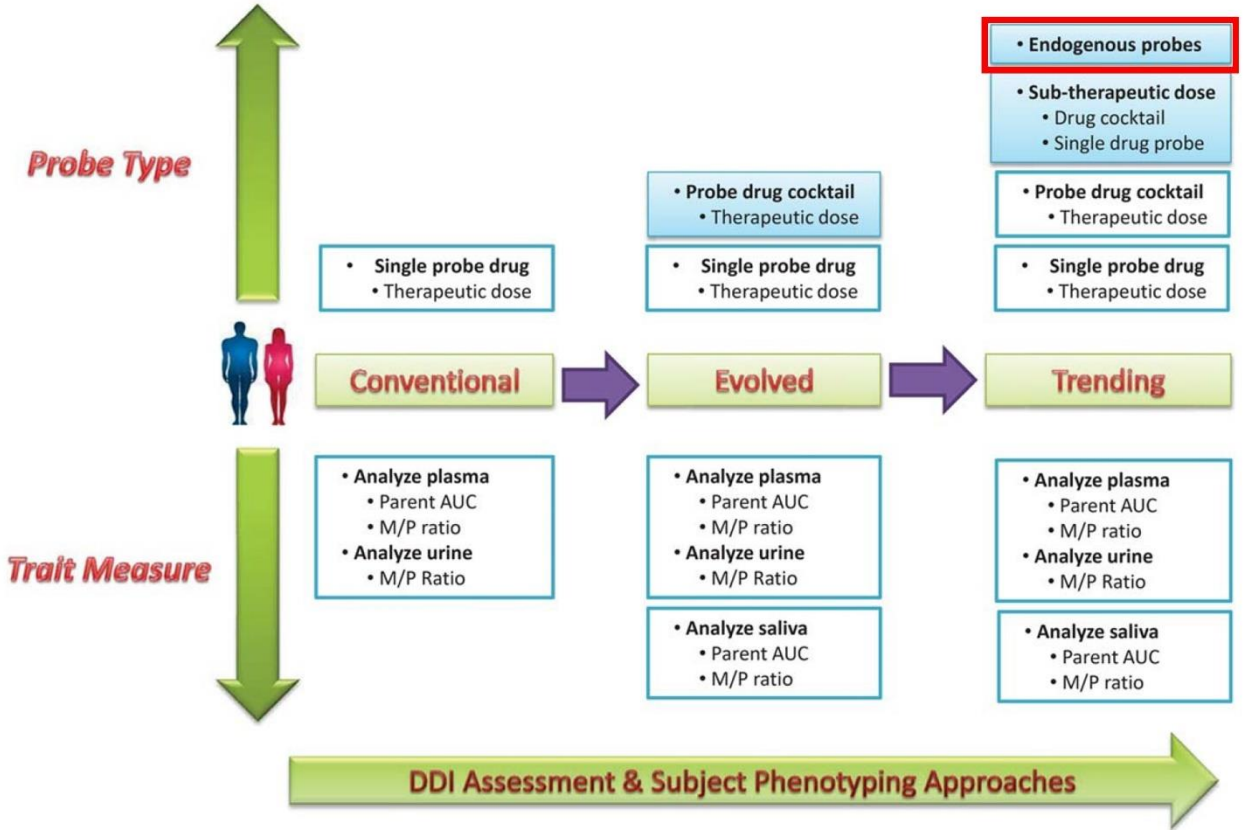

Figure 1.7. The evolution of drug-drug interaction assessment in clinical studies from Rodrigues et al., 2018. M/P ratio = metabolite-to-parent ratio; AUC = area under the plasma concentration-time curve.

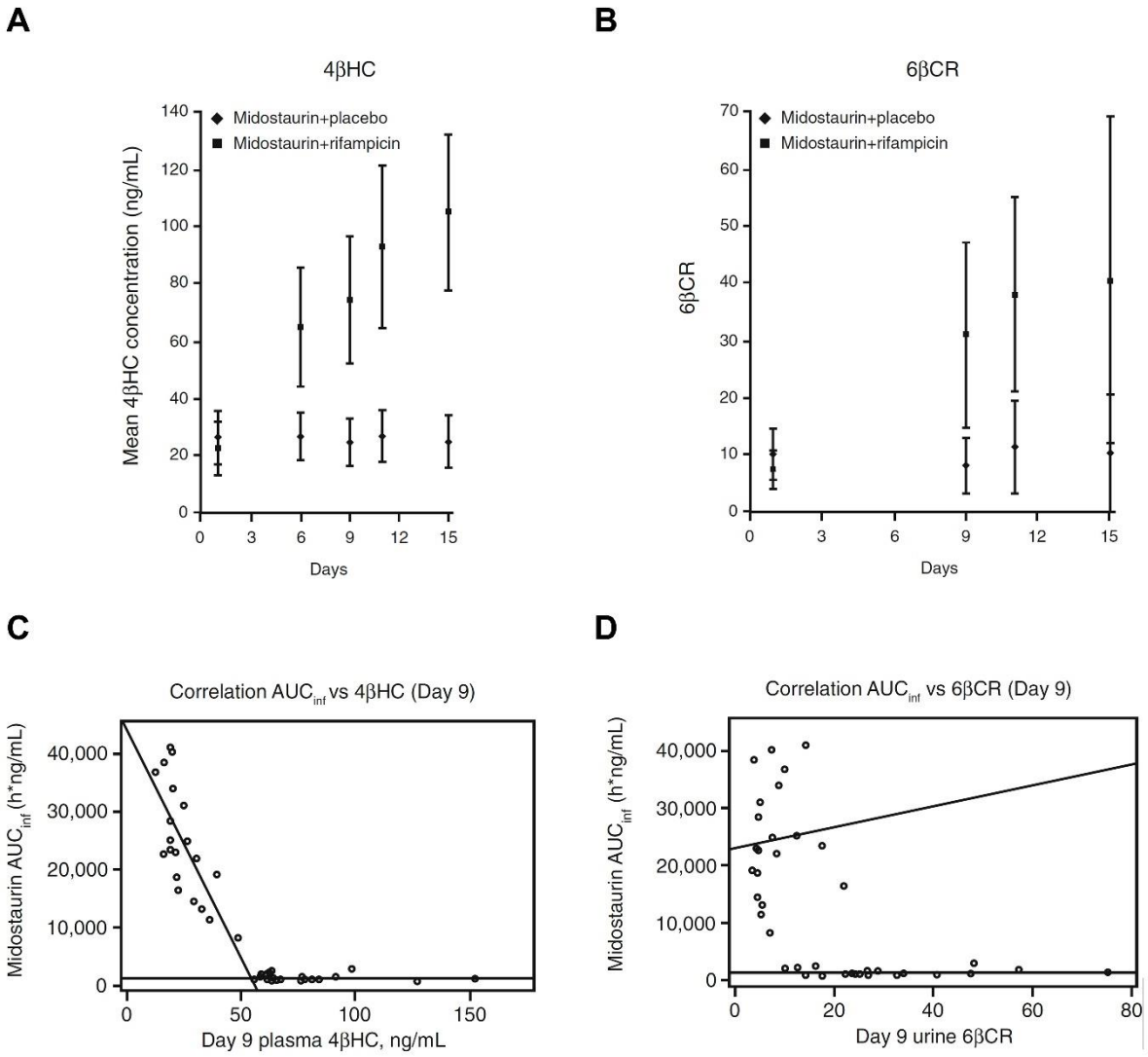

Figure 1.8. Comparison of 4β-hydroxycholesterol (4βHC) and 6β-hydroxycortisol/cortisol (6βCR) as a CYP3A4 biomarker (from Dutreix et al., 2014). Subjects received placebo or 600 mg rifampin daily. On day 9, subjects received 50 mg midostaurin, a protein kinase inhibitor metabolized primarily by CYP3A4. Plasma 4βHC levels (A) and urinary 6βCR (B) over time in both the control (midostaurin + placebo) and treatment (midostaurin + rifampin) groups (arithmetic mean ± SD). Correlation between midostaurin AUC_{inf} and 4βHC levels (C) or 6βCR (D). 4βHC = plasma 4β-hydroxycholesterol; 6βCR = urinary 6β-hydroxycortisol/cortisol ratio.

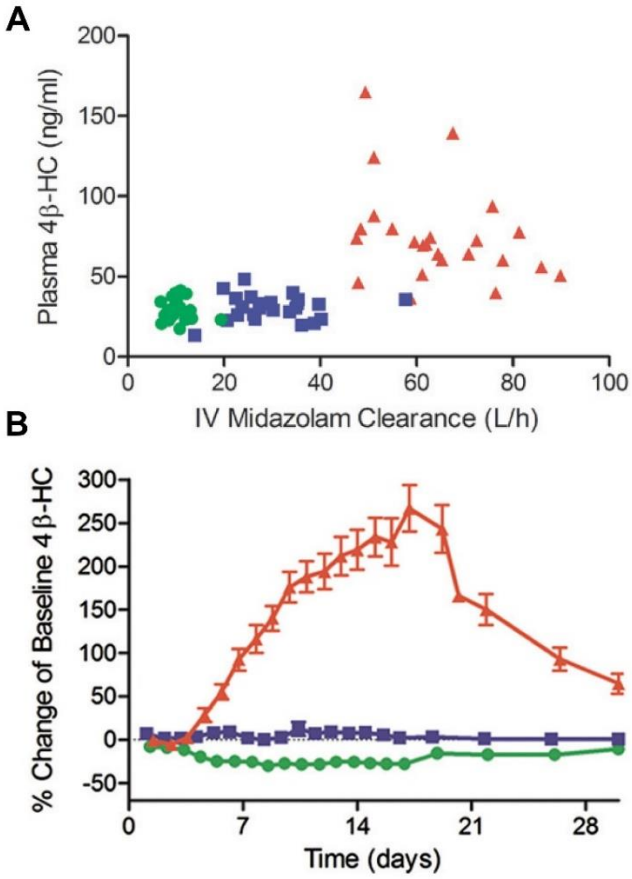

Figure 1.9. Comparison of 4β-hydroxycholesterol (4β-HC) at baseline (blue squares), under CYP3A4 inhibition (green circles), and under CYP3A4 induction (red triangles) from Mao et al., 2017. (A) Correlation between plasma 4β-HC and IV midazolam clearance in subjects at baseline and following inhibition with 400 mg ketoconazole for 4 days and induction with 600 mg rifampin for 10 days (n = 24 healthy volunteers from Shin et al., 2013; $R^2 = 0.381$; $p < 0.001$) (B) Time course of mean plasma 4β-HC concentrations following treatment with placebo, ketoconazole or rifampin for two weeks (n = 10 placebo; n = 12 for ketoconazole or rifampin from Kasichayanula et al., 2014).

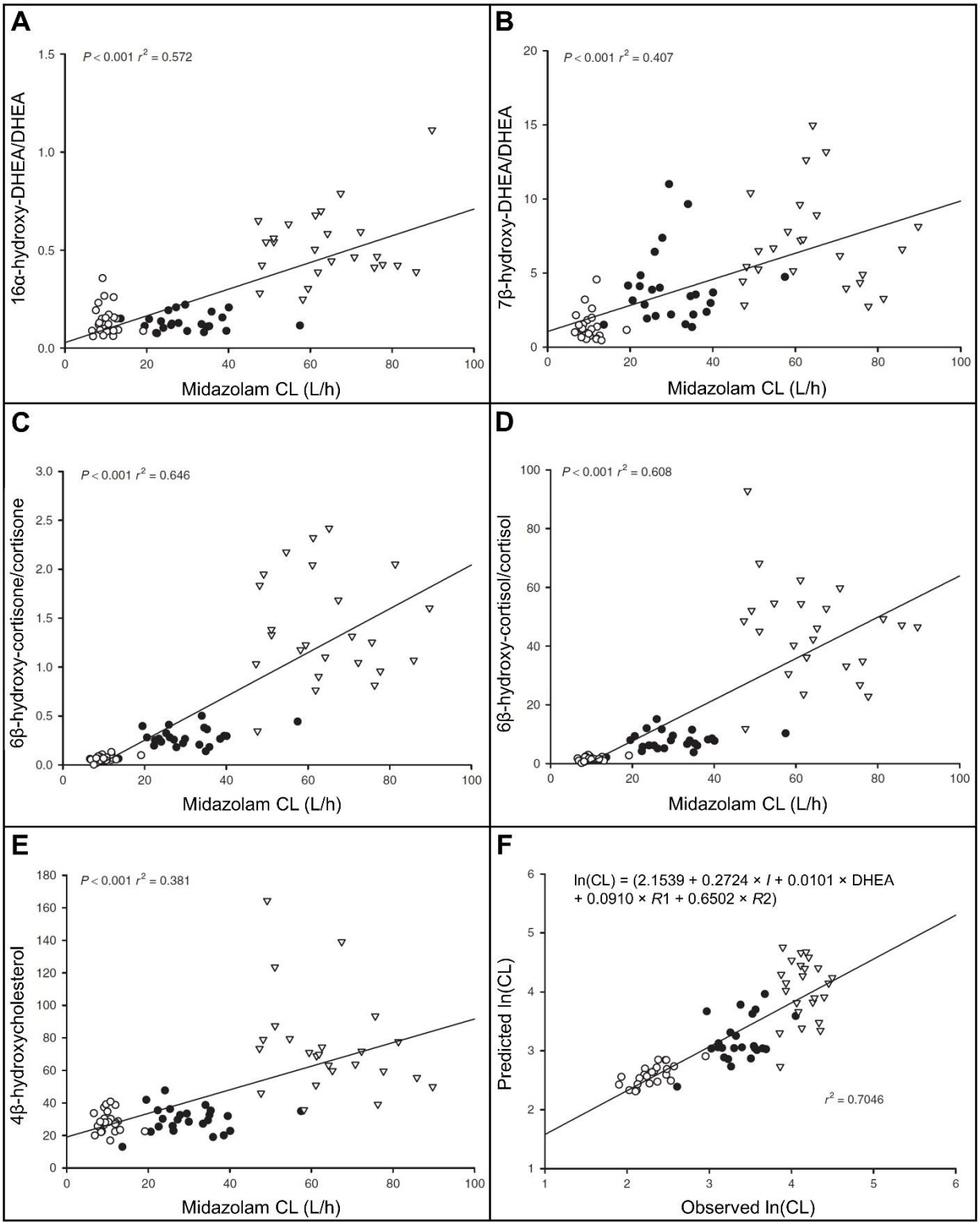

Figure 1.10 Correlations with hepatic CYP3A activity for different endogenous biomarkers from Shin et al., 2013. (A-E) Endogenous biomarkers vs. midazolam clearance. (F) Observed vs. predicted log-transformed midazolam clearance calculated using the empirical equation shown,

where I = 1 for CYP3A5*1/*3 and I = 0 for CYP3A5*3/*3; R1 = 7β-hydroxy-DHEA/DHEA; R2 = 6β-hydroxycortisone/cortisone. Solid circles = control phase; open circles = CYP3A-inhibited phase; open triangles = CYP3A-induced phase; DHEA = dehydroepiandrosterone.

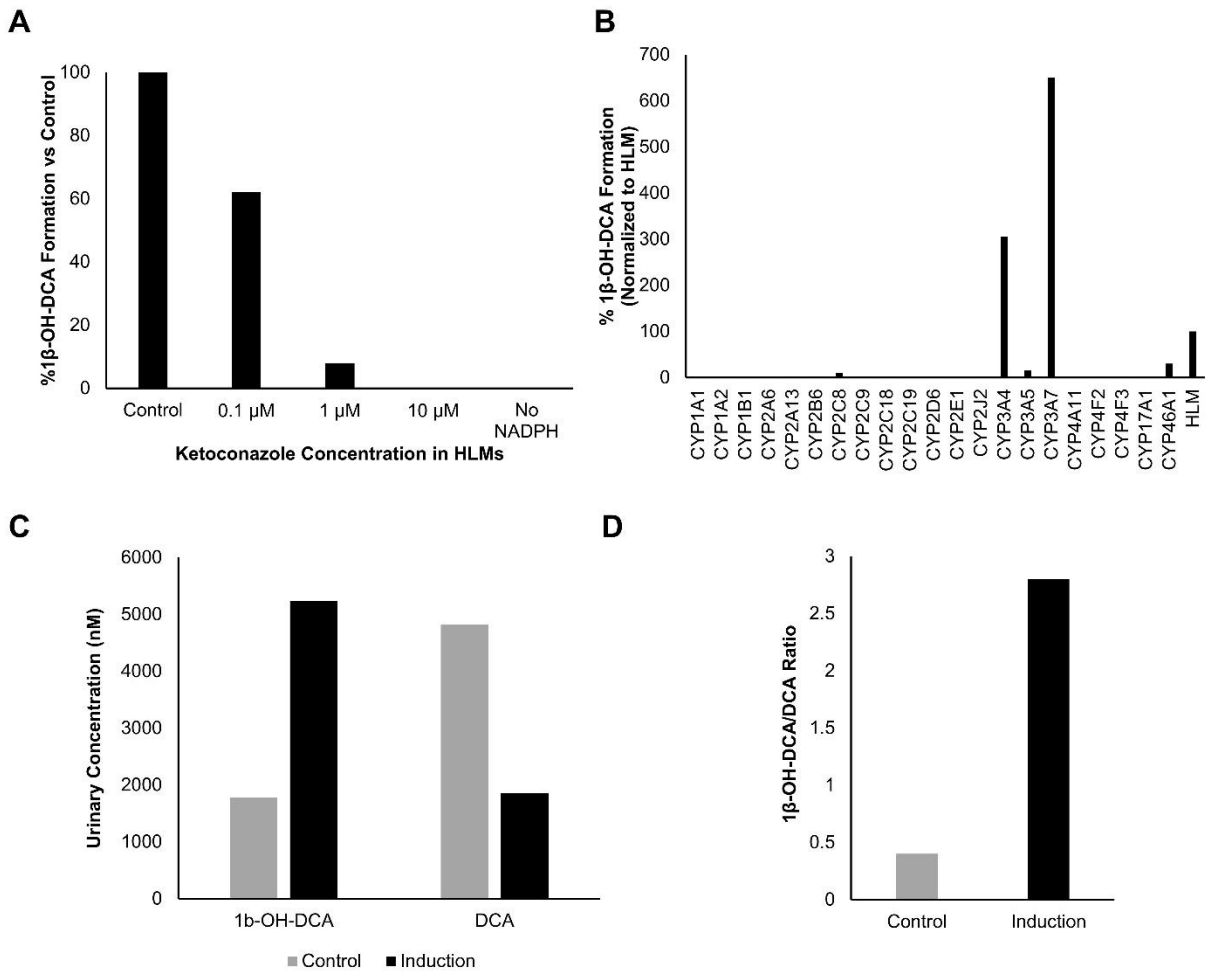

Figure 1.11 Metabolite profiles of deoxycholic acid (DCA) and 1β-hydroxy-deoxycholic acid (1β-OH-DCA) adapted from Hayes et al., 2016. (A) Inhibition by ketoconazole of 1β-OH-DCA formation in human liver microsomes (2 mM DCA for 60 minutes). (B) DCA 1β-hydroxylation activities of 21 recombinant human cytochromes (2 or 20 μM DCA in 100 pmol protein/ml for 60 minutes). (C) and (D) Concentrations and ratios of 1β-OH-DCA and DCA in pooled urine from healthy subjects vs. from a patient treated with carbamazepine.

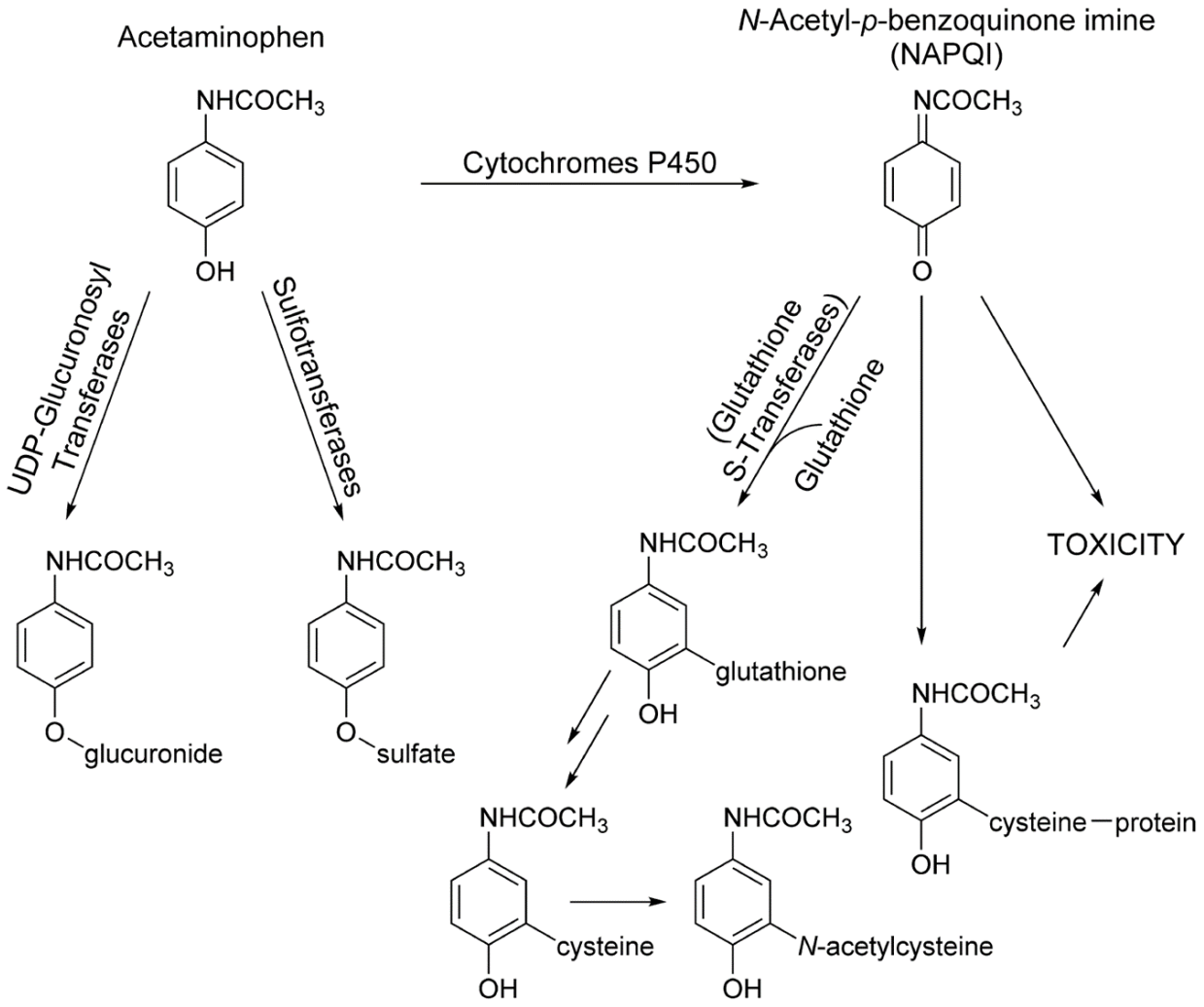

Figure 1.12. Acetaminophen metabolic pathways from Cook et al., 2015.

CHAPTER 2

The Impact of Proximal Roux-en-Y Gastric Bypass Surgery on Acetaminophen Absorption and Metabolism

Chapter 2 is published

In

Pharmacotherapy. 2020 Mar;40(3):191-203

2.1 Introduction

Obesity is a global epidemic and as reported by the Centers for Disease Control and Prevention (CDC), the United States has the greatest number of adults with body mass index (BMI) greater than 30 kg/m^2 (93.3 million; population prevalence of 39.8%) (Hales et al. 2017). Bariatric surgery is one of the most effective interventions (Benaiges et al. 2015). Following bariatric surgery, patients typically lose a substantial proportion of their body weight in one year (Wee et al. 2017) and experience improvements in Type 2 diabetes mellitus symptoms (Fruhbeck 2015).

The most popular bariatric procedure is Roux-en-Y gastric bypass surgery (RYGBS), which accounts for approximately 45% of the total number of bariatric surgeries performed globally (Angrisani et al. 2015). In the RYGB procedure, a new pouch is created by using a small part of the stomach and it is attached directly to the jejunum, resulting in anatomical pathway that bypasses most of the stomach and duodenum (Schauer et al. 2000). The anatomical change and consequential reduction in body weight can lead to alterations in food absorption and blood flow, as well as in metabolic function, such as metabolism of glucose, pancreatic lipid, and vitamin D (Honka et al. 2015, Thakkar and Michalsky 2015, Peterson et al. 2016). Not surprisingly, drug pharmacokinetics, from the perspective of absorption, distribution, metabolism, and excretion, can also be altered following surgery.

The metabolism of drugs can be affected by RYGBS due to differential exposure to intestinal enzymes or by upregulation or downregulation of hepatic enzymes following RYGBS surgery. Moreover, some drug metabolizing enzymes have regional expression in the intestine and RYGBS changes where drug enters the small intestine. For example, cytochrome P450 (CYP) 3A expression is the highest in the upper portion of the small intestine and decreases

along the intestinal tract, whereas CYP2C9, glucuronosyltransferase (UGT) 1A1, and UGT2B7 levels are higher in jejunum compared to other intestinal segments (Drozdzik et al. 2018). Additionally, hepatic enzyme expression can be altered by obesity. For instance, CYP2E1, UGTs, sulfotransferases (SULTs) are induced in obese subjects (Abernethy et al. 1983, Kotlyar and Carson 1999). Therefore, the impact of weight-loss following RYGBS on intestinal and hepatic metabolism may be isozyme- and tissue-specific.

Acetaminophen (APAP) is a commonly used over-the-counter analgesic drug, which is generally safe, but has the potential to cause liver failure when overdosed. More than 30,000 patients are hospitalized for APAP-induced hepatic toxicity each year in the US (Blieden 2014). As illustrated in Figure 2.1, the main metabolites of APAP are APAP-glucuronide (APAP-glu; 52–57% of the total dose) formed by UGT1A1 and UGT1A6, and APAP-sulfate (APAP-sulf; 30–44% of the total dose) formed by SULT1A1, SULT1A3/4, and SULT1E1 (Abernethy et al. 1982, Mazaleuskaya et al. 2015). APAP-glu and APAP-sulf are inactive metabolites. APAP toxicity results from a minor pathway (5–10% of the total dose), in which CYP2E1 produces *N*-acetyl-p-benzoquinone imine (NAPQI), an active intermediate metabolite that can bind to cellular proteins, leading to oxidative stress and mitochondrial damage (McGill et al. 2013, Mazaleuskaya et al. 2015). NAPQI is detoxified by glutathione conjugation, and the glutathione-conjugate metabolite is sequentially metabolized to APAP-cysteine (APAP-cys) and APAP-*N*-acetylcysteine (APAP-nac). Previous studies have shown increased CYP2E1-mediated oxidation of APAP in morbidly obese patients (Kotlyar and Carson 1999, van Rongen et al. 2016). However, no studies have addressed potential changes in APAP metabolism following RYGBS. In this longitudinal study, our goal was to investigate the effects of RYGBS on absorption and metabolism of APAP in morbidly obese patients.

2.2 Patients & Methods

Study patients.

Morbidly obese patients undergoing RYGBS were enrolled in a prospective, non-blinded, longitudinal study of the pharmacokinetics of acetaminophen, midazolam and digoxin. Participants recruited had to meet the practice standard, including requirements regarding BMI along with obesity-related comorbidities, established by the Center for Bariatric Surgery at the University of Washington Medical Center for RYGB. Participants with documented liver or kidney disease, or heart failure were excluded. Participants with contradictions to midazolam or digoxin were also excluded.

Study Procedures.

The study protocol was approved by the Institutional Review Board at the University of Washington. The study procedures consisted of a total of three study visits: presurgical baseline, 3-month and 12-month postsurgical visits. On each study visit, the participants received 1,500 mg of acetaminophen oral liquid after an overnight fast. Plasma samples were collected at predose, 10, 20, 30, 40, 50, and 60 min, 75, 90, 120, 180, 240, 360, 720, and 1440 hrs after dose administration. Plasma samples were stored at -80°C until analyzed.

Acetaminophen and Metabolite Assay.

Reagents and chemicals. APAP was purchased from Sigma-Aldrich (St Louis, MO, USA). 4-acetamidophenyl β-D-glucuronide sodium salt, 4-acetaminophen sulfate potassium salt, 3-(*N*-acetyl-L-cystein-S-yl) acetaminophen sodium salt, and 3-cysteinylacetaminophen trifluoroacetic acid salt were purchased from Toronto Research Chemicals (Toronto, ON, Canada). Deuterated analogues were used as internal standards. Acetaminophen-d4 (APAP-d4),

4-acetamidophenyl β-D-glucuronide-d3 sodium salt (APAP-gluc-d3), 4-acetaminophen-d3 sulfate (APAP-sulf-d3), 3-(*N*-Acetyl-L-cystein-S-yl) acetaminophen-d5 sodium salt (APAP-nac-d5), and 3-cysteinylacetaminophen-d5 trifluoroacetic acid salt (APAP-cys-d5) were also purchased from Toronto Research Chemicals.

Sample preparation. Samples were prepared based on a previously published analytical method (Cook 2015) with modifications. All deuterated chemicals were combined and diluted to make an internal standard mix (IS). To prepare the PK plasma samples for analysis, 30 μL of plasma was mixed with 20 μL of IS and 50 μL of 50:50 methanol:water and vortexed. Protein precipitation was performed by adding 600 μL of acetonitrile to the plasma mix and samples were centrifuged at 1100xg for 15 min. The supernatant was transferred to a new tube, dried under nitrogen gas, and reconstituted with 100 μL of 1% formic acid. The calibration curve samples were prepared using the same procedures, except that PK plasma sample was replaced with blank plasma and that 50:50 methanol:water was replaced with diluted calibration stock solutions. The final concentrations of calibration curve samples ranged from 0.05 to 50 μg/mL for APAP, APAP-gluc, and APAP-sulf and ranged from 0.05 to 5 μg/mL for APAP-cys and APAP-nac. The low and high quality control samples contained 20 μg/mL and 400 ng/mL of APAP, APAP-gluc, and APAP-sulf and 2 μg/mL and 40 μg/mL of APAP-cys and APAP-nac, respectively.

Liquid chromatography-tandem mass spectrometry (LC-MS/MS). The separation and quantification of APAP and its metabolites were conducted on an Agilent 1290 infinity HPLC system coupled with an Agilent 6460 triple quadrupole mass spectrometer (Agilent Technologies, Santa Clara, CA). Instrument control, assay optimization, and data acquisition were performed using MassHunter Workstation software (Agilent Technologies, Santa Clara,

CA). Separation was achieved using an Acquity HSS PFP column (2.1 × 100 mm, 1.8 μm, Waters, USA). The mobile phases were composed of 95:5 acetonitrile:formic acid in water (v/v) (A) and 5:95 acetonitrile:formic acid in water (B). The final concentration of formic acid was 0.1% for both mobile phases. The column was maintained at 40°C and 10 μL of each sample was injected. The flow rate was fixed at 0.3 mL/min and the elution gradient was set as follows: starting at 0% B, increasing to 25% B from 0 to 6 min, increasing to 100% B from 6 to 6.5 min, holding 100% B from 6.5 to 9 min, decreasing to 0% B from 9.5 to 10 min, and re-equilibrating with 100% A from 10 to 13 min. Mass transitions used for quantification were: APAP *m/z* 152.1 → 110.1, APAP-d4 *m/z* 156.1 → 114.1, APAP-gluc *m/z* 328.1 → 152, APAP-gluc-d3 *m/z* 331.1 → 155, APAP-sulf *m/z* 230 → 150.1, APAP-sulf-d3 *m/z* 233 → 153.1, APAP-cys *m/z* 271.1 → 140, APAP-cys-d5 *m/z* 276.1 → 142.9, APAP-nac *m/z* 313.1 → 208, APAP-nac-d5 *m/z* 318.1 → 213. All analytes were monitored in positive electrospray ionization mode (ESI+) except for APAP-sulf and APAP-sulf-d3, which were monitored in negative electrospray ionization mode (ESI-). The gas temperature and pressure were fixed at 350°C and 45 psi for both ionization modes, and the ion spray voltage was set at +4500V and -3500V for positive and negative modes, respectively.

Data Analysis.

LC-MS/MS data analysis. Peak integration was performed using MassHunter Quantitative Analysis (version B.04.00, Agilent Technologies). Standard curves were calculated using a weighting factor of 1/X and sample concentrations were interpolated using GraphPad Prism (version 6.07, GraphPad Software, San Diego, CA). Peak area ratios of analytes to corresponding internal standards were used for calculation and interpolation. The acceptable

error range for the low and high QCs was 15% for the difference between expected and calculated values.

Pharmacokinetics analysis. Noncompartmental analysis (NCA) of APAP, APAP-gluc, APAP-sulf, APAP-cys, and APAP-nac was performed using Phoenix WinNonlin (version 7.0, Pharsight, Mountain View, CA). The elimination rate constant (λ_z) was estimated as the slope of terminal log-linear concentration versus time points for each patient, and terminal half-life ($t_{1/2}$) was calculated as $t_{1/2} = \ln 2/\lambda_z$. The area under the plasma concentration-time curve from time 0 to infinity ($AUC_{0\text{-}inf}$) was estimated by the linear trapezoidal rule to the last observable concentration and adding the extrapolated AUC (C_{last}/λ_z). The area under the plasma concentration-time curve from time 0 to 30 min ($AUC_{0\text{-}30}$) was estimated by the linear trapezoidal rule to the 30 min timepoint. The apparent oral clearance (CL/F) was calculated using dose/$AUC_{0\text{-}inf}$, and apparent volume of distribution (V_z/F) was calculated using equation $V_z/F = CL/(F \cdot \lambda_z)$. CL/F and V_z/F of metabolites were not calculated. Simulations of a multiple dosing regimen (1,500 mg every 4 hrs) were performed using the average of the estimated compartmental parameters from pre- and post-RYGBS data from this study.

Statistical analysis. Descriptive statistics were determined and expressed as mean ± standard deviation. Lean body weight was calculated using the Boer Formula (Boer 1984). The Wilcoxon signed rank test was used to compare paired data from the 3-month or the 12-month post-RYGBS visit to the presurgical baseline visit. P-values less than 0.05 were considered significant.

2.3 Results

Study patients.

Demographics and weight-loss. Twelve patients undergoing RYGBS were enrolled in this study. Pharmacokinetics of midazolam and digoxin were summarized in a previous publication (Chan 2015). Due to limited sample volumes, APAP and metabolite data were only determined for ten of the twelve patients. One subject did not complete the 3-month postsurgical visit and one subject did not complete the 12-month postsurgical visit. Thus, there were a total of eight subjects for whom we have data for all three visits. The demographics of the study subjects are summarized in Table 2.1. The median age was 43.5 years and the majority of the patients were white females. Prior to surgery, the patients had a mean baseline weight of 138 ± 29 kg. The patients lost 18.1 ± 3.62% of their body weight in first 3 months and a total of 27.4 ± 9.2% of their weight by the end of the study. In general, most patients continued to lose weight between the 3-month and 12-month visits, however, two subjects gained weight between those visits. The mean BMI was 51 kg/m^2, 42 kg/m^2, and 39 kg/m^2 for the baseline, 3-month, and 12-month visits, respectively.

Acetaminophen and Metabolite Pharmacokinetics.

Acetaminophen. At the baseline visit, the peak concentration (C_{max}) of APAP was 18.5 ± 7.2 μg/mL and was observed at 35 min (Table 2.2, Figure 2.2A). Compared to baseline, the peak concentrations of APAP increased by two-fold at 3-months and 12-months ($p = 0.0039$ and $p = 0.0078$, respectively). Following RYGBS, the time to peak concentration (T_{max}) occurred at the first measured timepoint at 10 min (Figure 2.2B). The apparent volume of distribution was 97.3

± 32.1 L, 82.4 ± 27.3 L, and 76.0 ± 29.6 L at pre-RYGBS and 3-month and 12-month post-RYGB, respectively.

The apparent oral clearance of APAP was 30.3 ± 8.1 L/hr at baseline and markedly decreased by 34.6 % and 31.7% at 3-months and 12-months ($p = 0.0039$ and $p = 0.0078$, respectively; Table 2.2). The terminal half-life was comparable at baseline (2.2 ± 0.4 hrs) and the 3- and 12-months post-RYGBS visits (2.9 ± 0.4 hrs and 2.6 ± 0.7 hrs, respectively; Table 2.2, Figure 2.2A). The $AUC_{0\text{-}inf}$ was 53.0 ± 15.2 µg·hr/mL at baseline and increased by 1.6-fold at 3-months and 1.5-fold at 12-months ($p = 0.0039$ and $p = 0.0078$, respectively) post-RYGBS (Table 2.2, Figure 2.2A). In addition, we calculated $AUC_{0\text{-}30}$ to evaluate the change in early-phase exposure resulting from the impact of RYGBS on absorption. Compared to the baseline $AUC_{0\text{-}30}$ (4.7 ± 3.1 µg·hr/mL), $AUC_{0\text{-}30}$ was 2.6-fold higher at 3-months (12.1 ± 1.3 µg·hr/mL, $p = 0.0039$) and 12-months (12.4 ± 3.7 µg·hr/mL, $p = 0.0039$; Table 2.2, Figure 2.2B). Normalized by total exposure, the ratio of $AUC_{0\text{-}30}$ to $AUC_{0\text{-}inf}$ ($AUC_{0\text{-}30}/AUC_{0\text{-}inf}$) was used to evaluate the shift in the fraction of total exposure that had occurred in first 30 min. $AUC_{0\text{-}30}/AUC_{0\text{-}inf}$ increased from 9% at baseline to 16% after the surgery ($p = 0.012$ and $p = 0.0039$ for 3- and 12-months post-RYGBS, respectively) (Table 2.2).

Acetaminophen-glucuronide. At the presurgical baseline, the peak APAP-gluc (26.3 ± 7.2 µg/mL) occurred at 4 hrs. RYGBS did not alter the APAP-gluc peak concentrations, nor the time to peak concentrations in patients (Table 2.2, Figure 2.2C). Exposure to APAP-gluc was slightly higher at 3-months post-RYGBS compared to baseline (253 ± 105 µg·hr/mL vs. 211 ± 68 µg·hr/mL, $p = 0.012$) and unchanged at 12-months post-RYGBS (224 ± 64 µg·hr. The AUC ratio of the APAP-gluc metabolite to APAP parent (AUC_m/AUC_p) was 22.0% and 32.5% lower at 3- and 12-months post-RYGBS ($p = 0.0039$ and $p = 0.012$), respectively.

Acetaminophen-sulfate. At baseline, the peak concentration of APAP-sulf was 8.9 ± 2.1 μg/mL which occurred at 2 hrs, and the half-life was estimated to be 3.3 ± 0.5 hrs (Table 2.2). Following RYGBS, APAP-sulf peak concentrations and time to peak concentrations were comparable to those at presurgical baseline (Table 2.2 and Figure 2.2D). Exposure to APAP-sulf increased at 3-months post-RYGBS compared to baseline (72.0 ± 18.8 μg·hr/mL vs. 57.2 ± 12 μg·hr/mL, p = 0.020). The 12-month post-RYGBS exposure to APAP-sulf was elevated, but not significant. compared to baseline. In contrast, the AUC_m/AUC_p ratios decreased by 17.4% and 22.6% at 3- and 12-months post-RYGBS, respectively (p = 0.020 and p = 0.027, Figure 2.3B).

Acetaminophen-cystein. At baseline, the APAP-cys peak concentration was 1.1 ± 0.3 μg/mL and occurred at 4 hrs. Overall, APAP-cys peak concentrations were not affected by RYGBS (Table 2.2 and Figure 2.2E). Compared to the baseline $AUC_{0\text{-}inf}$ (9.3 ± 2.9 μg·hr/mL), exposure to APAP-cys was unchanged at 3-months and decreased by 15% at 12-months (7.9 ± 2.7 μg·hr/mL, p = 0.037, Table 2.2). Larger decreases in the AUC_m/AUC_p ratios were observed at 3- and 12-months post-RYGBS (26.3%, p = 0.016, and 47.4%, p = 0.016, respectively, Table 2.2) compared to the baseline AUC_m/AUC_p ratio.

Acetaminophen-N-acetylcystein. APAP-nac peak concentration was 0.43 ± 0.2 μg/mL at baseline and was comparable post-RYGBS (Table 2.2). The time to peak concentration (4 hrs) was not altered following RYGBS. Exposure to APAP-nac before and after the surgery was comparable. The AUC_m/AUC_p ratio of APAP-nac decreased by 25.0% and 38.2% at 3- and 12-months, respectively (p = 0.012 and p = 0.0039) (Figure 2.3D).

Association with body weight. Total body weight was moderately correlated with APAP apparent oral clearance ($p < 0.0001$, $R^2 = 0.51$, Fig. 4A), apparent volume of distribution (p <

0.0001, $R^2 = 0.42$; Fig. 4B) and peak concentration ($p < 0.0001$, $R^2 = 0.49$, Fig. 4C). Compared to baseline, APAP weight-normalized apparent oral clearance at 3-months RYGBS was lower (0.22 L/hr/kg vs. 0.18 L/hr/kg, $p = 0.0039$), though no difference was observed at 12-months (data not shown). APAP weight-normalized apparent volume of distribution was 0.7 L/kg in all visits (data not shown). APAP weight-normalized peak concentration was 0.15 µg/mL/kg at baseline and increased by 2.3-fold and 2.6-fold ($p = 0.0039$ and $p = 0.0039$), respectively (data not shown). The correlation of APAP-gluc AUC_m/AUC_p and the total body weight was not significant (Figure 2.4D). APAP-gluc weight-normalized peak concentration was 0.20 µg/mL/kg at baseline and increased by 1.3- and 1.5-fold at 3-month and 12-month postsurgical visits ($p = 0.020$ and $p = 0.0039$), whereas the other metabolites were unchanged. The total body weight was weakly correlated with the AUC_m/AUC_p ratios of APAP-sulf ($p = 0.007$, $R^2 = 0.25$, Fig. 4E), APAP-cys ($p < 0.0001$, $R^2 = 0.48$, Fig. 4F), and APAP-nac ($p = 0.0019$, $R^2 = 0.31$, Fig. 4G).

Simulations. In general, the estimated half-life of APAP and its metabolites was not altered following RYGBS, except for a minor transient increase in the half-life of APAP-gluc, APAP-sulf and APAP-cys at 3-months post-RYGBS (Figure 2.5). We performed simulations of multiple APAP dosing (650 mg every 4 hrs) to ascertain differences in the exposures in morbidly obese patients pre- and post-RYGBS (Figure 2.6). Steady-state peak and trough APAP fluctuations were comparable in morbidly obese patients pre- and post-RYGBS (6.2- and 6.9-fold, respectively). Simulated peak concentrations were substantially higher post-RYGBS compared to pre-RYGBS (8.8 vs. 21.7 ug/mL). Similarly, post-RYGBS patients had 1.7-fold higher APAP exposure at steady-state compared to pre-RYGBS patients.

2.4 Discussion

In our study, we observed alterations in APAP absorption and metabolism after RYGBS. The rate of absorption increased considerably after RYGB surgery, resulting in markedly higher peak APAP concentrations and shortened time to peak concentrations. Compared with the baseline, the ratio of 30-min AUC to total AUC ($AUC_{0\text{-}30}/AUC_{inf}$) increased by approximately two-fold at 3- and 12-months post-RYGBS. APAP, which is rapidly absorbed by passive diffusion (Raffa et al. 2014), can be used as a biomarker to evaluate gastric emptying and intestinal transit time (Srinivas 2015). These data indicate that bypassing most of the stomach and duodenum led to more rapid absorption which significantly increased early-phase exposure.

We did not observe changes in the apparent volume of distribution of APAP pre- and post-surgery in our study. In contrast, Goday et al. (2017) reported a decrease in the volume of distribution. Both studies are in agreement that the weight-normalized volume of distribution for APAP was unchanged pre- and post-surgery.

Though the apparent oral clearance of APAP decreased post-RYGB surgery and was correlated with the total body weight, the weight-normalized apparent oral clearance of APAP also was decreased 3-months post-surgery, suggesting that other factors, in addition to weight, contribute to the difference in the apparent oral clearance of APAP. The change in apparent oral clearance could be due to downregulation of drug metabolizing enzymes involved in the metabolism of APAP, increased bioavailability of APAP, or a combination of both reasons. Enzyme regulation and intestinal permeability have been shown to be related to obesity and body weight (Ghose et al. 2011, Damms-Machado et al. 2017). In contrast, we did not observe a difference in the weight-normalized apparent oral clearance of APAP at 12-months compared to baseline. It is possible that the lack of difference might be due to increased variation in enzyme

expression caused by disparate weight-loss outcomes as some subjects continued to lose weight, while others had started to regain weight. Interestingly, our findings agree with results from Arno et al., (2017) where the weight-normalized apparent oral clearance of APAP decreased at the earlier postsurgical visit (1-month) but was comparable to baseline at the later postsurgical visit (6-months).

For all metabolites, the ratio of metabolite AUC-to-APAP AUC (AUC_m/AUC_p) was decreased following surgery and was correlated with the total body weight. As APAP is primarily cleared hepatically (Mazaleuskaya et al. 2015), the decreased AUC_m/AUC_p ratios may reflect reduced activity of sulfotransferases (SULTs), glucuronosyltransferase (UGTs), and cytochrome P450 2E1 (CYP2E1) following surgery. However, the decreased AUC_m/AUC_p could also be due to increased metabolite clearance, in addition to decreased formation clearance of the metabolite.

Our pre-surgery findings are consistent with previous studies demonstrating elevated APAP sulfation, glucuronidation and oxidation in obese patients (Abernethy et al. 1982, van Rongen et al. 2016). Although there is speculation that various factors (e.g., glucagon, insulin, sex hormones, growth factors, and pro-inflammatory cytokines) can modulate enzyme expression via nuclear receptors and transcription factors in obesity (Kim and Novak 2007, Klein et al. 2015), the mechanisms responsible for down-regulation of these enzymes following RYGBS are still unknown, but may be due to decreased inflammation or decreased levels of glucagon.

In addition, factors affecting intestinal metabolism could alter APAP pharmacokinetics following the RYGB surgery. For example, UGT and SULT enzymes are expressed in the intestine. UGT1A1 is more abundant in the upper intestine (Xie et al. 2016), whereas the

localization of SULT1A1 is currently unclear (Riches et al. 2009). Bypassing the upper intestine from RYGBS may lead to decreased intestinal metabolism of APAP to APAP-gluc and APAP-sulf.

Finally, the gut microbiome is likely to change after surgery (Osto et al. 2013, Tremaroli et al. 2015). The microbiome can impact APAP metabolism through enzyme induction, enzyme inhibition, and enterohepatic circulation (Wilson and Nicholson 2017). Studies have shown that the gut microbiome can regulate the expression of intestinal SULTs, UGTs, and CYPs, as well as their hepatic counterparts in mice and rats (Meinl et al. 2009, Selwyn et al. 2016). Additionally, *p*-cresol, an endogenous microbial metabolite, undergoes sulfation and can diminish APAP sulfation by competitive inhibition (Clayton et al. 2009). Finally, Hendrickson et al., (2010) reported that APAP can undergo enterohepatic circulation, whereby APAP-gluc is deconjugated by microbial-expressed β-glucuronidase prior to reabsorption (Noh et al. 2017, Pollet et al. 2017). Disrupting enterohepatic circulation can lead to decreases in APAP half-life, resulting in lower APAP exposure.

There are some limitations to our study. Since urine samples were not collected, we were unable to estimate the fraction metabolized for each pathway (f_m). Performing mass balance studies may be necessary to fully understand metabolic changes post-RYGBS and to shed light on extent of oral absorption. Future studies could be designed to administer APAP intravenously and collect all urinary metabolites to estimate the formation clearances and corroborate downregulation of metabolizing enzymes. As the inter-individual variability is high in patients undergoing RYGBS, a larger sample size may be necessary to detect the changes in the apparent volume of distribution or half-life of APAP and its metabolites. In addition, to better capture the

post-RYGBS APAP absorption, future clinical studies should collect multiple plasma samples earlier than the first timepoint in our study (10 min).

Alterations in drug absorption and disposition following RYGBS may necessitate dose adjustment of drugs commonly administered to the morbidly obese to maintain efficacy or prevent toxicity. For example, doses of certain antibiotics (e.g., azithromycin and erythromycin) and selective serotonin reuptake inhibitors (e.g., sertraline and duloxetine) need to be increased due to decreased absorption (Prince et al. 1984, Padwal et al. 2010, Hamad et al. 2012). In contrast, metformin and atorvastatin doses need to be decreased due to higher bioavailability and lower clearance post-surgery (Skottheim et al. 2009, Padwal et al. 2011). The effect of RYGBS on pharmacokinetics may be drug-specific depending on the physiochemical properties, metabolic pathways and transport of the drug. In our simulation of a multiple dosing regimen (Figure 2.6), APAP was predicted to accumulate and fluctuate significantly during a dosing interval in post-RYGBS individuals. Although, the fraction of APAP metabolized by the CYP2E1 pathway decreases post-RYGBS, the higher APAP concentrations may deplete glutathione stores and shunt the metabolism toward the toxic metabolite (NAPQI). Further work will need to explore whether dose adjustment is necessary following multiple APAP dosing post-RYGBS. Moreover, as we only studied the liquid formulation of APAP, the impact of RYGBS on absorption and bioavailability may differ depending on the formulation of APAP (e.g., liquid vs. tablets or sustained-release).

In conclusion, this longitudinal study demonstrates that pharmacokinetics of APAP significantly changed at 3-months and 12-months in patients who underwent RYGBS. The increased rate of absorption of APAP, decreased apparent oral clearance of APAP, and decreased metabolite-to-parent AUC ratios may be due to decreased gastric emptying time and reduced

metabolizing enzyme activities (i.e., CYP2E1, SULTs, and UGTs) following RYGB. Our simulations suggest that morbidly obese patients post-RYGBS will have higher exposure to APAP upon multiple dosing and further work will need to clarify the extent to which detoxification pathways are affected.

2.5 Acknowledgements

This research was supported by ACCP Research Institute Frontiers Research Award; NIH National Center for Research Resources grants UL1 RR025014, KL2 RR025015 and M01-RR-00037 of the University of Washington General Clinical Research Center and the University of Washington School of Pharmacy DMTPR funding.

2.6 References

Abernethy, D. R., M. Divoll, D. J. Greenblatt and B. Ameer (1982). "Obesity, sex, and acetaminophen disposition." Clin Pharmacol Ther **31**(6): 783-790.

Abernethy, D. R., D. J. Greenblatt, M. Divoll and R. I. Shader (1983). "Enhanced glucuronide conjugation of drugs in obesity: studies of lorazepam, oxazepam, and acetaminophen." J Lab Clin Med **101**(6): 873-880.

Angrisani, L., A. Santonicola, P. Iovino, G. Formisano, H. Buchwald and N. Scopinaro (2015). "Bariatric Surgery Worldwide 2013." Obes Surg **25**(10): 1822-1832.

Benaiges, D., A. Goday, J. Pedro-Botet, A. Mas, J. J. Chillaron and J. A. Flores-Le Roux (2015). "Bariatric surgery: to whom and when?" Minerva Endocrinol **40**(2): 119-128.

Clayton, T. A., D. Baker, J. C. Lindon, J. R. Everett and J. K. Nicholson (2009). "Pharmacometabonomic identification of a significant host-microbiome metabolic interaction affecting human drug metabolism." Proc Natl Acad Sci U S A **106**(34): 14728-14733.

Damms-Machado, A., S. Louis, A. Schnitzer, V. Volynets, A. Rings, M. Basrai and S. C. Bischoff (2017). "Gut permeability is related to body weight, fatty liver disease, and insulin resistance in obese individuals undergoing weight reduction." Am J Clin Nutr **105**(1): 127-135.

Drozdzik, M., D. Busch, J. Lapczuk, J. Muller, M. Ostrowski, M. Kurzawski and S. Oswald (2018). "Protein Abundance of Clinically Relevant Drug-Metabolizing Enzymes in the Human Liver and Intestine: A Comparative Analysis in Paired Tissue Specimens." Clin Pharmacol Ther **104**(3): 515-524.

Fruhbeck, G. (2015). "Bariatric and metabolic surgery: a shift in eligibility and success criteria." Nat Rev Endocrinol **11**(8): 465-477.

Ghose, R., O. Omoluabi, A. Gandhi, P. Shah, K. Strohacker, K. C. Carpenter, B. McFarlin and T. Guo (2011). "Role of high-fat diet in regulation of gene expression of drug metabolizing enzymes and transporters." Life Sci **89**(1-2): 57-64.

Goday Arno, A., M. Farre, J. Rodriguez-Morato, J. M. Ramon, C. Perez-Mana, E. Papaseit, E. Civit, K. Langohr, M. Li Carbo, D. B. Boix, O. C. Nino, J. A. F. Le Roux, M. Pera, L. Grande and R. de la Torre (2017). "Pharmacokinetics in Morbid Obesity: Influence of Two Bariatric Surgery Techniques on Paracetamol and Caffeine Metabolism." Obes Surg **27**(12): 3194-3201.

Hales, C. M., M. D. Carroll, C. D. Fryar and C. L. Ogden (2017). "Prevalence of Obesity Among Adults and Youth: United States, 2015-2016." NCHS Data Brief(288): 1-8.

Hamad, G. G., J. C. Helsel, J. M. Perel, G. M. Kozak, M. C. McShea, C. Hughes, A. L. Confer, D. K. Sit, C. A. McCloskey and K. L. Wisner (2012). "The effect of gastric bypass on the pharmacokinetics of serotonin reuptake inhibitors." Am J Psychiatry **169**(3): 256-263.

Hendrickson, R. G., N. J. McKeown, P. L. West and C. R. Burke (2010). "Bactrian ("double hump") acetaminophen pharmacokinetics: a case series and review of the literature." J Med Toxicol **6**(3): 337-344.

Honka, H., J. Koffert, J. C. Hannukainen, J. J. Tuulari, H. K. Karlsson, H. Immonen, V. Oikonen, T. Tolvanen, M. Soinio, P. Salminen, N. Kudomi, A. Mari, P. Iozzo and P. Nuutila (2015). "The effects of bariatric surgery on pancreatic lipid metabolism and blood flow." J Clin Endocrinol Metab **100**(5): 2015-2023.

Kim, S. K. and R. F. Novak (2007). "The role of intracellular signaling in insulin-mediated regulation of drug metabolizing enzyme gene and protein expression." Pharmacol Ther **113**(1): 88-120.

Klein, M., M. Thomas, U. Hofmann, D. Seehofer, G. Damm and U. M. Zanger (2015). "A systematic comparison of the impact of inflammatory signaling on absorption, distribution, metabolism, and excretion gene expression and activity in primary human hepatocytes and HepaRG cells." Drug Metab Dispos **43**(2): 273-283.

Kotlyar, M. and S. W. Carson (1999). "Effects of obesity on the cytochrome P450 enzyme system." Int J Clin Pharmacol Ther **37**(1): 8-19.

Mazaleuskaya, L. L., K. Sangkuhl, C. F. Thorn, G. A. FitzGerald, R. B. Altman and T. E. Klein (2015). "PharmGKB summary: pathways of acetaminophen metabolism at the therapeutic versus toxic doses." Pharmacogenet Genomics **25**(8): 416-426.

McGill, M. R., M. Lebofsky, H. R. Norris, M. H. Slawson, M. L. Bajt, Y. Xie, C. D. Williams, D. G. Wilkins, D. E. Rollins and H. Jaeschke (2013). "Plasma and liver acetaminophen-protein adduct levels in mice after acetaminophen treatment: dose-response, mechanisms, and clinical implications." Toxicol Appl Pharmacol **269**(3): 240-249.

Meinl, W., S. Sczesny, R. Brigelius-Flohe, M. Blaut and H. Glatt (2009). "Impact of gut microbiota on intestinal and hepatic levels of phase 2 xenobiotic-metabolizing enzymes in the rat." Drug Metab Dispos **37**(6): 1179-1186.

Noh, K., Y. R. Kang, M. R. Nepal, R. Shakya, M. J. Kang, W. Kang, S. Lee, H. G. Jeong and T. C. Jeong (2017). "Impact of gut microbiota on drug metabolism: an update for safe and effective use of drugs." Arch Pharm Res **40**(12): 1345-1355.

Osto, M., K. Abegg, M. Bueter, C. W. le Roux, P. D. Cani and T. A. Lutz (2013). "Roux-en-Y gastric bypass surgery in rats alters gut microbiota profile along the intestine." Physiol Behav **119**: 92-96.

Padwal, R., D. Brocks and A. M. Sharma (2010). "A systematic review of drug absorption following bariatric surgery and its theoretical implications." Obes Rev **11**(1): 41-50.

Padwal, R. S., R. Q. Gabr, A. M. Sharma, L. A. Langkaas, D. W. Birch, S. Karmali and D. R. Brocks (2011). "Effect of gastric bypass surgery on the absorption and bioavailability of metformin." Diabetes Care **34**(6): 1295-1300.

Peterson, L. A., X. Zeng, C. P. Caufield-Noll, M. A. Schweitzer, T. H. Magnuson and K. E. Steele (2016). "Vitamin D status and supplementation before and after bariatric surgery: a comprehensive literature review." Surg Obes Relat Dis **12**(3): 693-702.

Pollet, R. M., E. H. D'Agostino, W. G. Walton, Y. Xu, M. S. Little, K. A. Biernat, S. J. Pellock, L. M. Patterson, B. C. Creekmore, H. N. Isenberg, R. R. Bahethi, A. P. Bhatt, J. Liu, R. Z. Gharaibeh and M. R. Redinbo (2017). "An Atlas of beta-Glucuronidases in the Human Intestinal Microbiome." Structure **25**(7): 967-977.e965.

Prince, R. A., J. C. Pincheira, E. E. Mason and K. J. Printen (1984). "Influence of bariatric surgery on erythromycin absorption." J Clin Pharmacol **24**(11-12): 523-527.

Raffa, R. B., J. V. Pergolizzi, Jr., R. Taylor, Jr., J. F. Decker and J. T. Patrick (2014). "Acetaminophen (paracetamol) oral absorption and clinical influences." Pain Pract **14**(7): 668-677.

Riches, Z., E. L. Stanley, J. C. Bloomer and M. W. Coughtrie (2009). "Quantitative evaluation of the expression and activity of five major sulfotransferases (SULTs) in human tissues: the SULT "pie"." Drug Metab Dispos **37**(11): 2255-2261.

Schauer, P. R., S. Ikramuddin, W. Gourash, R. Ramanathan and J. Luketich (2000). "Outcomes after laparoscopic Roux-en-Y gastric bypass for morbid obesity." Ann Surg **232**(4): 515-529.

Selwyn, F. P., S. L. Cheng, C. D. Klaassen and J. Y. Cui (2016). "Regulation of Hepatic Drug-Metabolizing Enzymes in Germ-Free Mice by Conventionalization and Probiotics." Drug Metab Dispos **44**(2): 262-274.

Skottheim, I. B., K. Stormark, H. Christensen, G. S. Jakobsen, J. Hjelmesaeth, T. Jenssen, J. L. Reubsaet, R. Sandbu and A. Asberg (2009). "Significantly altered systemic exposure to atorvastatin acid following gastric bypass surgery in morbidly obese patients." Clin Pharmacol Ther **86**(3): 311-318.

Srinivas, N. R. (2015). "Acetaminophen absorption kinetics in altered gastric emptying: establishing a relevant pharmacokinetic surrogate using published data." J Pain Palliat Care Pharmacother **29**(2): 115-119.

Thakkar, R. K. and M. P. Michalsky (2015). "Update on bariatric surgery in adolescence." Curr Opin Pediatr **27**(3): 370-376.

Tremaroli, V., F. Karlsson, M. Werling, M. Stahlman, P. Kovatcheva-Datchary, T. Olbers, L. Fandriks, C. W. le Roux, J. Nielsen and F. Backhed (2015). "Roux-en-Y Gastric Bypass and Vertical Banded Gastroplasty Induce Long-Term Changes on the Human Gut Microbiome Contributing to Fat Mass Regulation." Cell Metab **22**(2): 228-238.

van Rongen, A., P. A. J. Valitalo, M. Y. M. Peeters, D. Boerma, F. W. Huisman, B. van Ramshorst, E. P. A. van Dongen, J. N. van den Anker and C. A. J. Knibbe (2016). "Morbidly Obese Patients Exhibit Increased CYP2E1-Mediated Oxidation of Acetaminophen." Clin Pharmacokinet **55**(7): 833-847.

Wee, C. C., D. B. Jones, C. Apovian, D. T. Hess, S. N. Chiodi, A. C. Bourland, R. B. Davis, B. Schneider, G. L. Blackburn, E. R. Marcantonio and M. B. Hamel (2017). "Weight Loss After Bariatric Surgery: Do Clinical and Behavioral Factors Explain Racial Differences?" Obes Surg **27**(11): 2873-2884.

Wilson, I. D. and J. K. Nicholson (2017). "Gut microbiome interactions with drug metabolism, efficacy, and toxicity." Transl Res **179**: 204-222.

Xie, F., X. Ding and Q. Y. Zhang (2016). "An update on the role of intestinal cytochrome P450 enzymes in drug disposition." Acta Pharm Sin B **6**(5): 374-383.

2.7 Figures and Tables

Table 2.1. Demographics of the study population.

	Presurgical baseline (n=10)	3-month post-surgery (n=9)	12-month post-surgery (n=9)
Female, n	9	8	8
Race			
White, n	9	8	8
Native American, n	1	1	1
Total body weight, kg	137.7 ± 29.0 (98.0 – 198.3)	113.6 ± 27.1 (75.9 – 170.7)	107.5 ± 27.1 (76.8 – 145.9)
Lean body weight, kg	67.9 ± 10.3 (55.7 – 88.5)	61.6 ± 9.0 (50.1 – 77.0)	56.8 ± 12.5 (31.0 – 72.4)
Body mass index, kg/m2	50.3 ± 12.2 (37.1 – 77.4)	40.8 ± 11.4 (28.7 – 66.7)	38.9 ± 11.0 (27.6 – 57.0)
Weight loss from baseline			
Absolute weight, kg		24.8 ± 6.3 (14.6 – 34.0)	39.2 ± 11.8 (21.3 – 55.2)
Percentage weight, %		18.1 ± 3.62 (12.8 – 22.6)	27.4 ± 9.2 (14.0 – 41.8)

Data are expressed as mean ± SD.

Table 2.2. Overall summary of acetaminophen and metabolite pharmacokinetics before and after Roux-en-Y Gastric bypass in all study subjects.

	Presurgical baseline (n=10)	3-months post-RYGBS (n=9)	12-months post-RYGBS (n=9)
APAP			
$C_{max,}$ μg/mL	18.5 ± 7.2	36.5 ± 6.9 **	36.6 ± 11.9 **
$T_{max,}$ min	35	10 *	10 **
V_z/F, L	97.3 ± 32.1	82.4 ± 27.3	76.0 ± 29.6
CL/F, L/hr	30.3 ± 8.1	19.8 ± 6.3 **	20.7 ± 7.8 **
$t_{1/2,}$ hr	2.2 ± 0.4	2.9 ± 0.4	2.6 ± 0.7
$AUC_{0\text{-}inf}$, μg·hr/mL	53.0 ± 15.2	82.4 ± 24.9 **	81.3 ± 28.0 **
$AUC_{0\text{-}30min}$, μg·hr/mL	4.7 ± 3.1	12.1 ± 1.3 **	12.4 ± 3.7 **
$AUC_{0\text{-}30min}/AUC_{0\text{-}inf}$	0.085 ± 0.04	0.16 ± 0.05 *	0.16 ± 0.05 **
APAP-gluc			
$C_{max,}$ μg/mL	26.3 ± 5.8	28.5 ± 10.8	27.9 ± 9.0
$T_{max,}$ min	240	240	240
$t_{1/2,}$ hr	3.0 ± 0.5	3.7 ± 0.9 *	3.0 ± 0.5
$AUC_{0\text{-}inf}$, μg·hr/mL	211 ± 68	253 ± 105 *	224 ± 64
AUC_m/AUC_p	4.3 ± 2.0	3.4 ± 1.7 **	3.0 ± 1.0 *
APAP-sulf			
$C_{max,}$ μg/mL	8.9 ± 2.1	9.1 ± 2.5	9.3 ± 2.6
$T_{max,}$ min	120	120	120
$t_{1/2,}$ hr	3.3 ± 0.5	3.9 ± 0.5 *	3.0 ± 0.5
$AUC_{0\text{-}inf}$, μg·hr/mL	57.2 ± 12	72.0 ± 18.8 *	67.4 ± 20.6
AUC_m/AUC_p	1.2 ± 0.4	1.0 ± 0.3 *	0.89 ± 0.3 *
APAP-cys			
$C_{max,}$ μg/mL	1.1 ± 0.3	1.0 ± 0.4	0.92 ± 0.3

$T_{max,}$ min	240	240 *	360 *
$t_{1/2,}$ hr	3.2 ± 0.3	4.3 ± 1.1 **	3.3 ± 0.5
$AUC_{0\text{-}inf}$, μg·hr/mL	9.3 ± 2.9	10.1 ± 2.9	7.9 ± 2.7 *
AUC_m/AUC_p	0.19 ± 0.09	0.14 ± 0.06 *	0.10 ± 0.03 **
APAP-nac			
$C_{max,}$ μg/mL	0.43 ± 0.2	0.41 ± 0.2	0.36 ± 0.1
$T_{max,}$ min	240	240	240
$t_{1/2,}$ hr	3.9 ± 1.1	4.5 ± 0.9	4.3 ± 1.7
$AUC_{0\text{-}inf}$, μg·hr/mL	3.5 ± 1.0	3.8 ± 1.6	3.2 ± 1.2
AUC_m/AUC_p	0.068 ± 0.02	0.051 ± 0.03 *	0.042 ± 0.02 **

Data were expressed as mean ± SD, except for T_{max}, which was given as the median. *P < 0.05, **P < 0.01, and ***P < 0.001 compared with baseline. Abbreviations: C_{max}, peak concentration; T_{max}, time to peak concentration; V_z/F, apparent volume of distribution; CL/F, apparent oral clearance; $t_{1/2}$, half-life; $AUC_{0\text{-}inf}$, AUC from time = 0 to infinity; $AUC_{0\text{-}30min}$, AUC from 0 to 30 min; AUC_m/AUC_p, metabolite-to-acetaminophen AUC ratio.

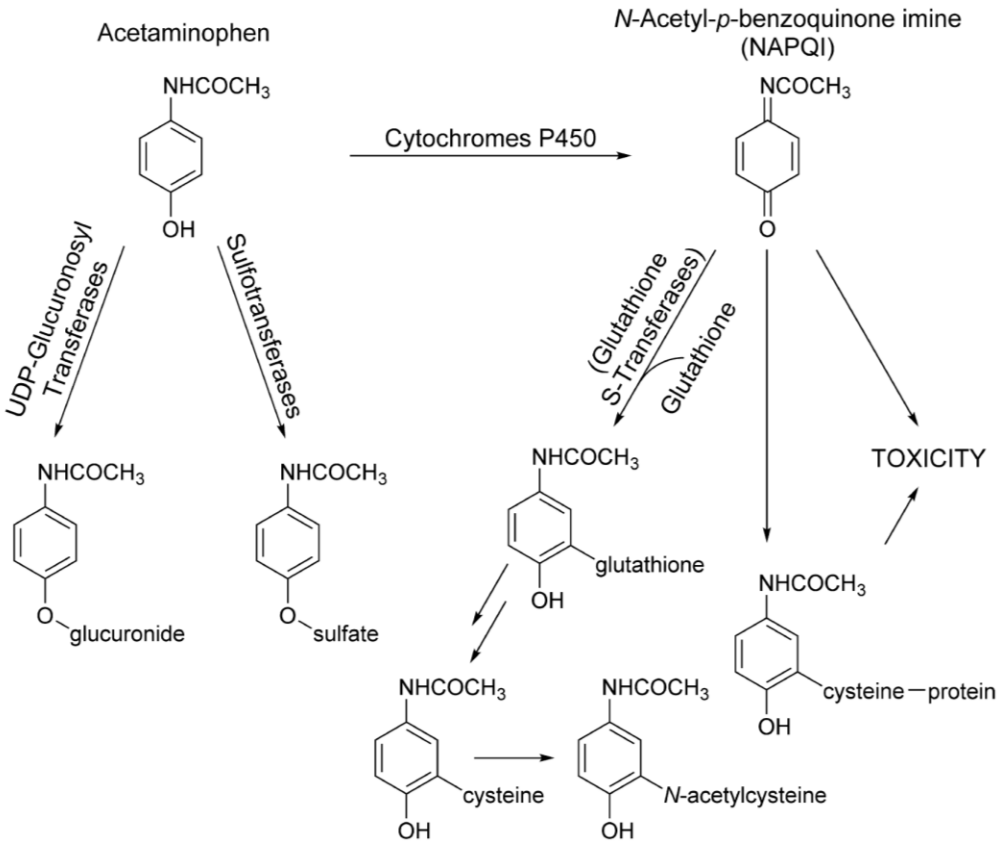

Figure 2.1. Major acetaminophen metabolic pathways. Permission from Cook et al. J. Chromatogr. (2015).

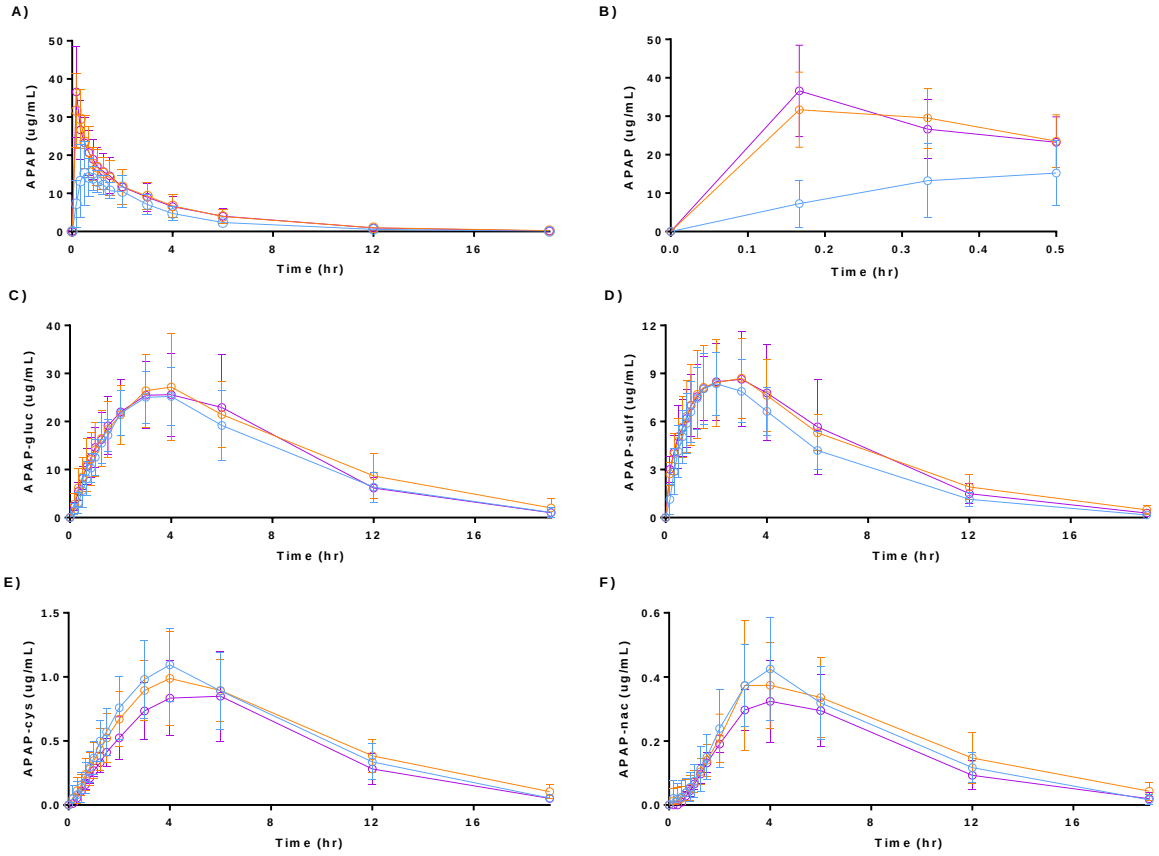

Figure 2.2. Plasma acetaminophen or metabolite concentration-time profiles in morbidly obese patients following 1,500 mg oral liquid acetaminophen (mean ± SD). Study visits: presurgical baseline (blue), 3-month postoperative visit (orange) and 12-month postoperative visit (purple).

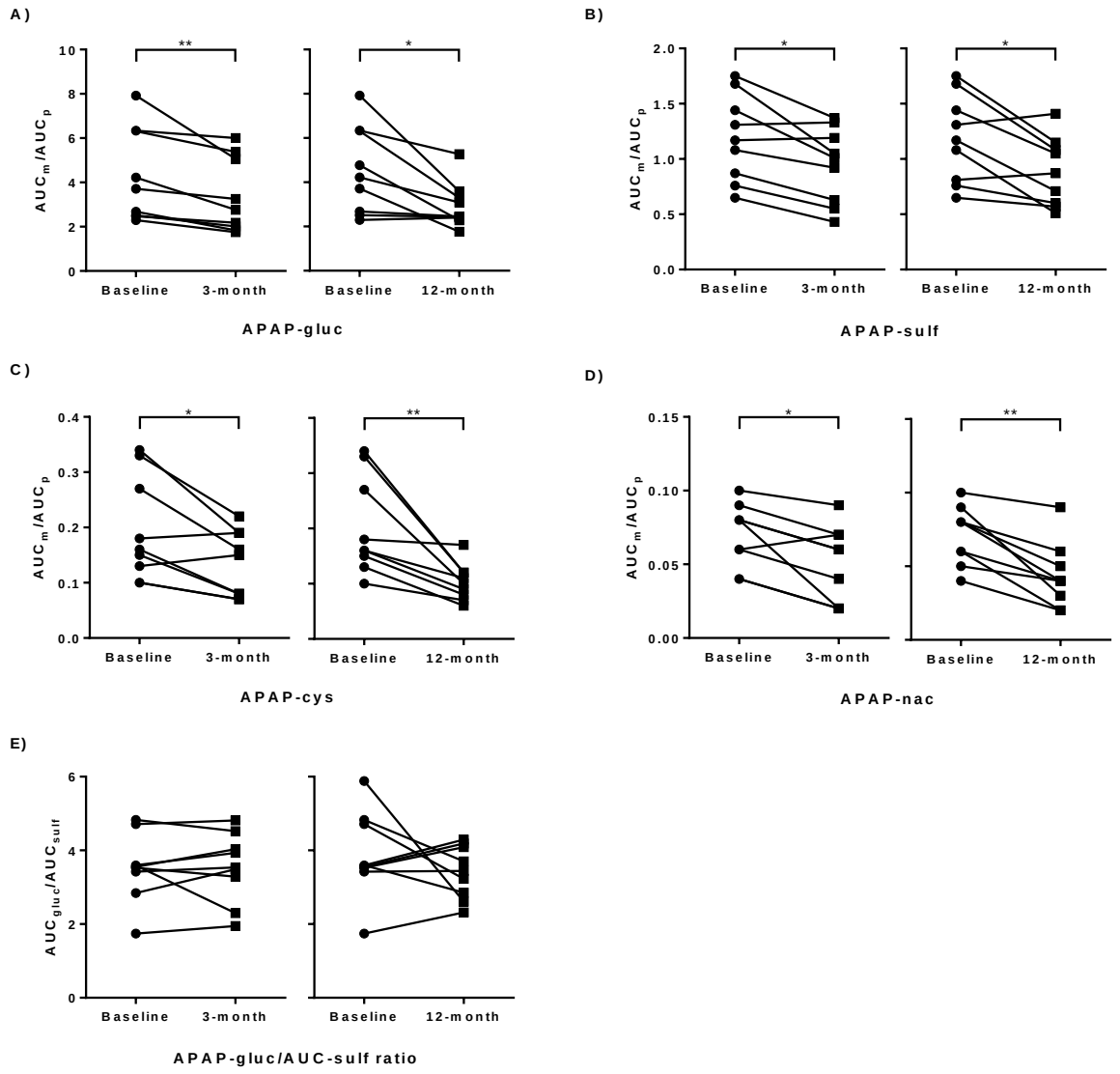

Figure 2.3. Comparison of area under the plasma concentration-time curve from 0 to infinity ($AUC_{0\text{-inf}}$) metabolite-to-acetaminophen ratios between presurgical baseline and 3-month postoperative visit or between presurgical baseline and 12-month postoperative visit. 9 subjects completing each set of visits were included. *$P < 0.05$ and **$P < 0.01$ compared to baseline.

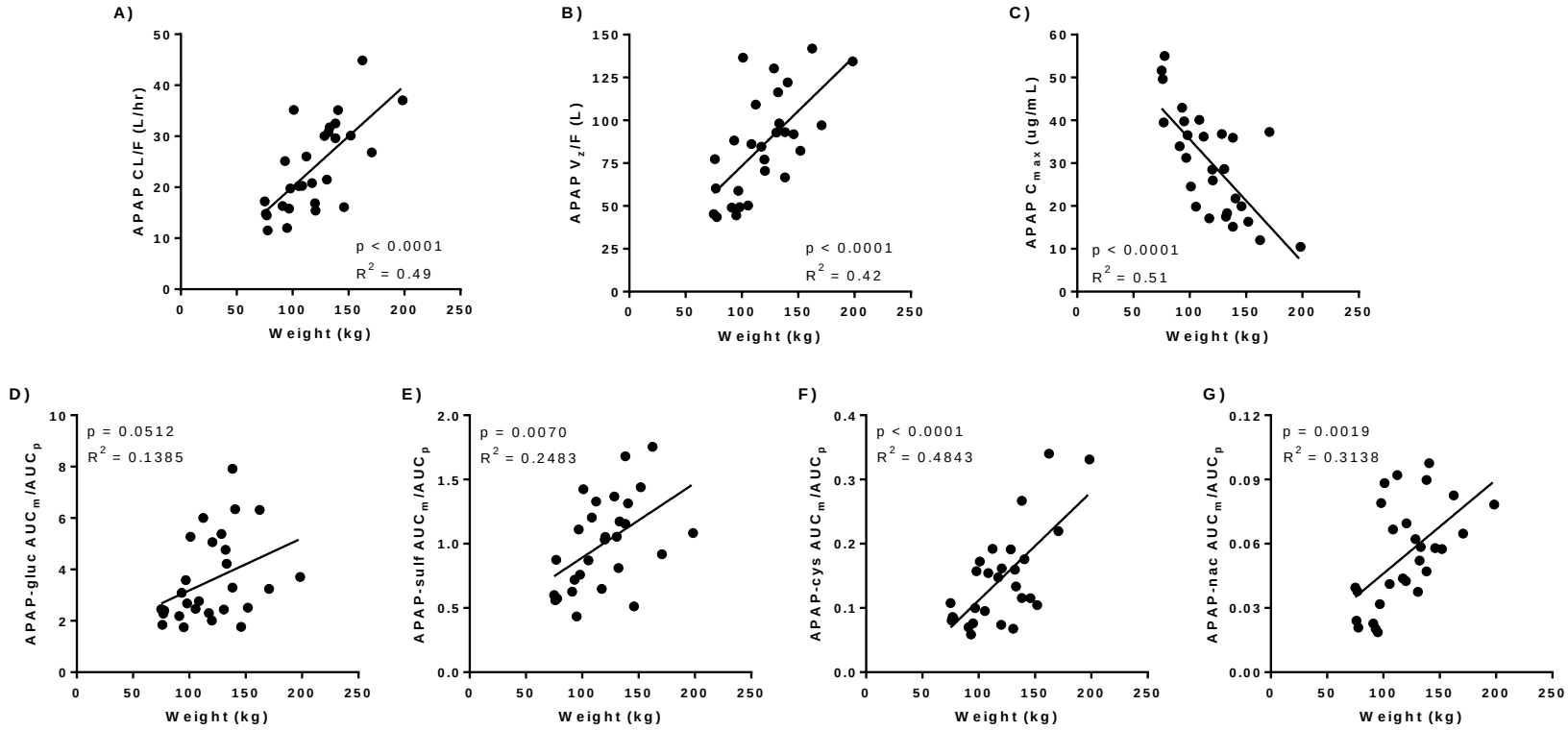

Figure 2.4. Correlations of APAP apparent oral clearance, APAP apparent volume of distribution, APAP peak concentration, and metabolite-to-parent AUC ratios with total body weight.

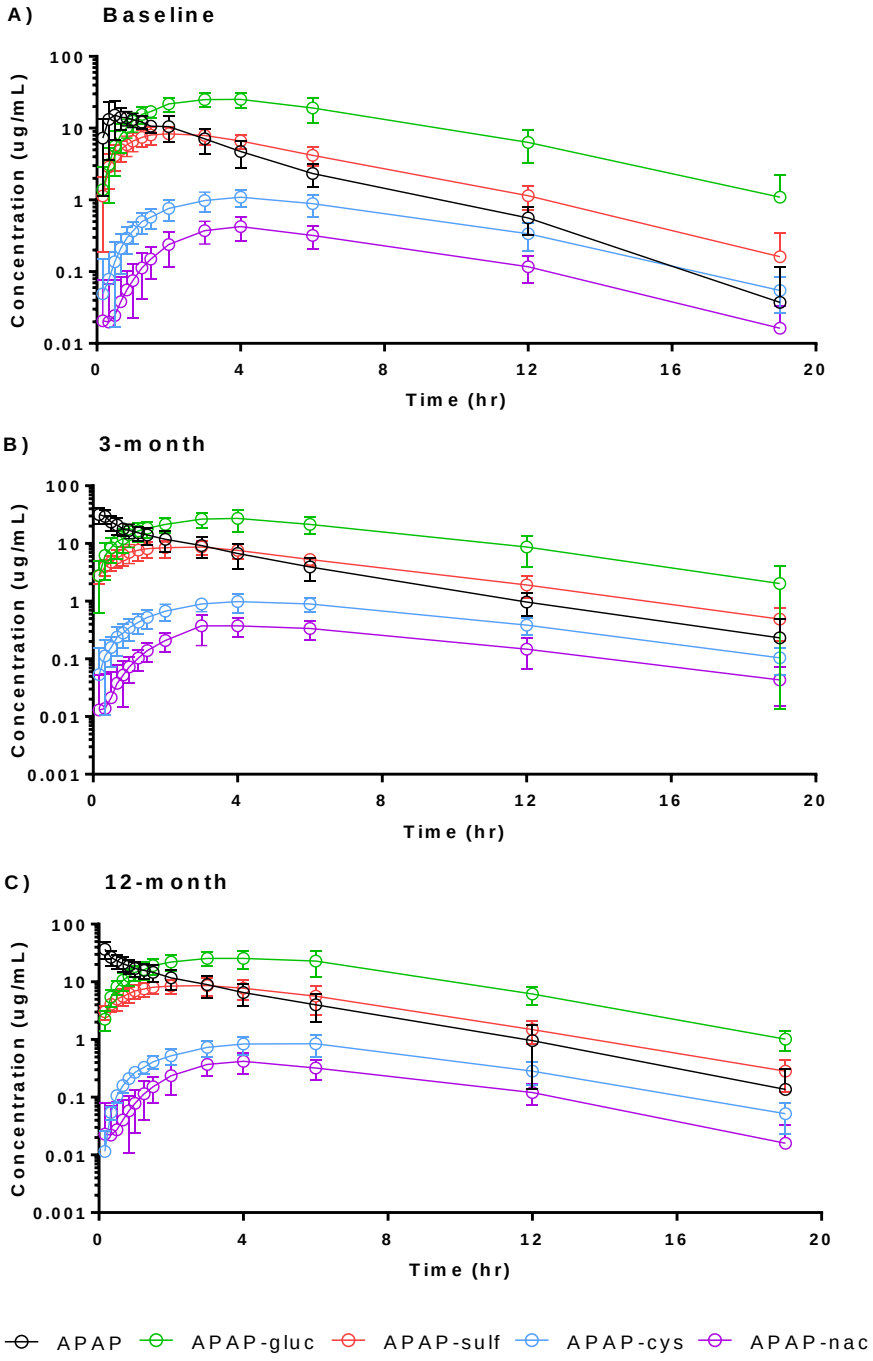

Figure 2.5. Log-scaled concentration-time profiles of acetaminophen and its metabolites in presurgical, 3-month, and 6-month visits (mean ± SD).

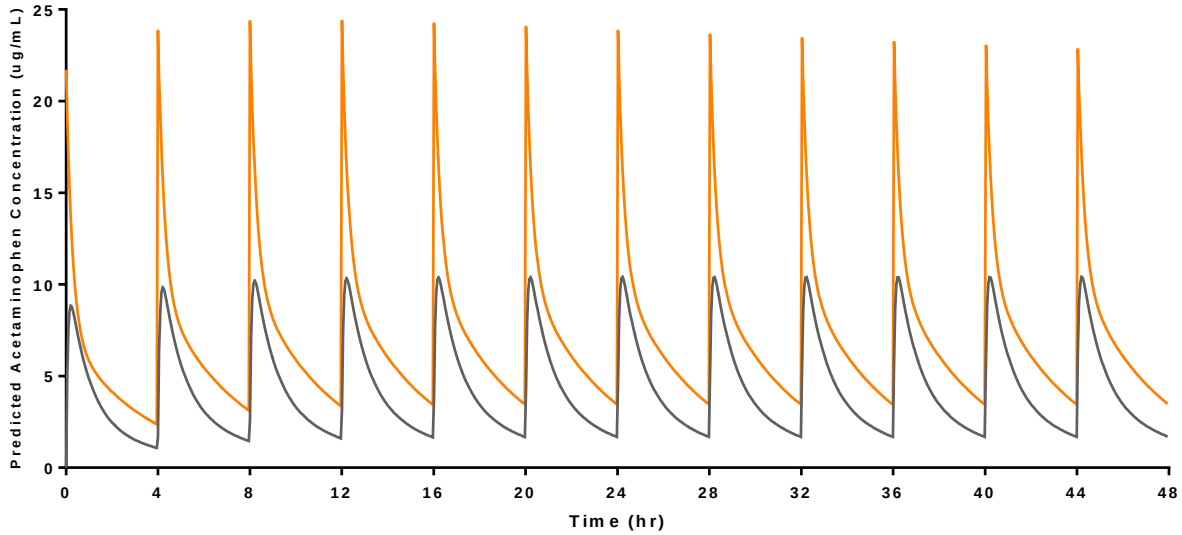

Figure 2.6. Simulations of multiple oral dosing of 650 mg acetaminophen every 4 hours in presurgical patients (gray), and postsurgical patients (orange).

CHAPTER 3

PBPK Modeling of CYP3A and P-gp Substrates to Predict Drug-Drug Interactions in Patients Undergoing Roux-en-Y Gastric Bypass Surgery

Chapter 3 is currently in review

In

Journal of Pharmacokinetics and Pharmacodynamics

3.1 Introduction

Obesity is a serious global epidemic and the prevalence is projected to reach 20% of the adult population worldwide by 2030 (Kelly et al. 2008). Morbid obesity is one of the leading causes of death in the United States with more than 400,000 associated deaths each year (Mokdad et al. 2004). Bariatric surgery is the most effective medical intervention that reduces all-cause mortality rate of morbid obesity by almost half (1.3% in surgical patients vs. 2.3% in non-surgical patients) (Miras and le Roux 2018). Roux-en-Y gastric bypass surgery (RYGBS) accounts for 46.6% of bariatric procedures globally (Arterburn and Courcoulas 2014). The RYGBS procedure creates a small gastric pouch (~20 mL) and connects the jejunum with a gastrojejuno-anastomosis (i.e., Roux limb), bypassing most of the stomach and duodenum. The anatomical alterations and subsequent physiological changes, including weight-loss, increased gastrointestinal pH, decreased plasma alpha-1-acid glycoprotein, altered bile acid levels and microbiome composition, can substantially impact drug absorption and disposition by affecting the drug dissolution rate and modulating the expression of drug metabolizing enzymes and transporters (DMETs) (Liou et al. 2013, Karimi et al. 2018, Duboc et al. 2019).

The bioavailability of an oral drug is determined by three factors: the fraction absorbed (fa), the fraction escaping intestinal first pass metabolism (Fg), and the fraction escaping hepatic first pass metabolism (Fh) before entering the system. Post-operative changes in fa result from a decreased absorption window, enhanced intestinal permeability (Savassi-Rocha et al. 2014), and increased or decreased dissolution and ionization depending on the pKa of the drug (Albaugh et al. 2017, Risstad et al. 2017). In addition, DMETs, such as cytochrome P450 (CYP) 3A, glucuronosyltransferases (UGTs), sulfotransferases (SULTs), and P-glycoprotein (P-gp), are differentially expressed along the intestinal tract. For example, the expression of CYP3A is

higher in the proximal region and lower in the distal region of the small intestine, whereas the expression of P-gp increases along the small intestine (Vaessen et al. 2017). Thus, fa and Fg may change because of altered exposure to DMET as a result of RYGB surgery. Moreover, Fh may change because hepatic DMETs can be upregulated or downregulated in response to weight-loss and abatement of obesity-induced inflammation (Hachon et al. 2017).

As post-RYGBS changes are multifaceted, physiologically based pharmacokinetic (PBPK) modeling can be helpful in understanding the mechanisms by which RYGBS changes drug absorption and disposition. The advanced dissolution, absorption and metabolism (ADAM) model enables simulation of the processes determining drug bioavailability, including dissolution, permeability, regional absorption, transport and metabolism (Jamei M. 2007). The ADAM model divides the small intestine into seven compartments (duodenum, jejunum I - II, and ileum I - IV) and accounts for physiological factors, such as gastrointestinal transit, intestinal surface area and blood flow, pH effects, and distribution of multiple DMETs (Jamei M. 2007). Using this model, Darwich et al. successfully simulated atorvastatin and cyclosporine oral bioavailability by emulating post-RYGBS physiological conditions by altering compartments representing the stomach, duodenum and jejunum I (Darwich et al. 2013). However, there are few PBPK modeling/simulation studies addressing the impact of RYGBS on the rate and extent of drug absorption and potentially altered metabolite kinetics, and no clinical drug interaction studies assessing the risks of drug-drug interactions (DDIs) in morbidly obese patients.

To begin to address these gaps, PBPK models for morbidly obese patients undergoing RYGBS were built using Simcyp for the parent drug and linked with their major metabolites when appropriate (i.e., midazolam and 1’-hydroxymidazolam; acetaminophen, acetaminophen-glucuronide and acetaminophen-sulfate; and digoxin). Midazolam, acetaminophen, and digoxin

can be used as *in vivo* probes for CYP3A4/5 (Phase I), UGTs and SULTs (Phase II), and P-gp (Phase III), respectively. The clinical data used for model verification were previously published by our group and showed marked post-RYGBS changes in the rate of midazolam, digoxin, and acetaminophen absorption (Chan et al. 2015, Chen K. 2020) and in the acetaminophen metabolite-to-parent plasma area under the concentration-time curve ratios (AUC_m/AUC_p) for the glucuronide, sulfate, and cysteine metabolites (Chen K. 2020).

The second aim was to predict CYP3A- and P-gp-mediated DDIs by simulating co-administration with verapamil, an antihypertensive agent, and posaconazole, an antifungal agent, before and after RYGBS using Simcyp. Verapamil and posaconazole are used to treat hypertension and candidiasis, respectively, which afflict obese individuals (Scheinfeld 2004, Jiang et al. 2016). Verapamil and posaconazole are classified as Class I and Class II compounds in the Biopharmaceutics Classification System (BCS), respectively (Benet et al. 2011). BCS Class I compounds have high permeability and solubility, while BCS Class II compounds have high permeability, but low solubility. The goal of this study was to understand mechanistically the absorption and metabolism of CYP3A, UGT and SULT, and P-gp substrates, and predict CYP3A4- and P-gp-mediated DDIs with verapamil and posaconazole following RYGBS using PBPK modeling.

3.2 Methods

Modeling Workflow.

The overall modeling workflow is illustrated in Figure 3.1. Simcyp software was used for the PBPK modeling (version 17, Certara, Princeton, NJ). To begin, the object drugs (midazolam, acetaminophen, and digoxin) and precipitants (verapamil and posaconazole) were modeled following a single IV dose in a healthy population. After ensuring the disposition was well-described, data following a single oral dose of midazolam, acetaminophen, digoxin, verapamil and posaconazole in a healthy population were modeled to focus on absorption. The simulations of single IV and PO dose were verified using observed data from healthy volunteers (Santostasi et al. 1987, Abernethy and Schwartz 1988, Rodin et al. 1988, Backman et al. 1994, Sawicki 2002, Link et al. 2008, Chiew et al. 2010, Krishna et al. 2012, Kersemaekers et al. 2015, Raffa et al. 2018). Once the drugs were verified in a healthy population, pre- and post-RYGBS conditions were emulated by altering population-specific parameters. The drugs were modeled in RYGBS patients given a single IV and PO dose. The simulations of single IV and PO dose were verified using observed data from RYGBS patients (Abernethy and Schwartz 1988, Chan et al. 2015, Gesquiere et al. 2016, Chen K. 2020). In parallel, DDIs (midazolam-verapamil; midazolam-posaconazole; digoxin-verapamil) were modeled and verified using observed data from a healthy population (Rodin et al. 1988, Backman et al. 1994, Krishna et al. 2009). Using the simulations in RYGBS patients, pre- and post-RYGBS absorption and metabolism were compared. Due to lack of precipitants for pharmacokinetic interactions with acetaminophen in RYGBS patients, no acetaminophen-drug interaction was predicted. However, the acetaminophen simulations allowed us to predict the post-RYGBS changes in the fraction metabolized through the toxic pathway. Finally, CYP3A- and P-gp-mediated DDIs in morbidly obese patients were predicted pre- and

post-RYGBS and the extent of inhibition caused by verapamil and posaconazole were compared. The following describes how population- and compound-specific parameters were determined.

Simcyp Population Input.

Three population files were used for the simulations: healthy volunteer population (Simcyp file), morbidly obese population (for pre-RYGBS and adapted as described below) and post-RYGBS morbidly obese population (created as described below). Details of parameters for the pre-RYGBS and post-RYGBS populations are summarized in Table 3.1. The reference Simcyp healthy volunteer population file was used as provided and no modifications were made to the file. The reference Simcyp morbidly obese population file was selected as a template for pre- and post-RYGBS patients. Default values for the physiological parameters in the GI tract and ADAM model were used for pre-RYGBS conditions, while values from Darwich et al. (Darwich et al. 2013) were used to simulate the post-RYGBS conditions. In summary, the post-RYGBS changes included: reducing the stomach volume and mean residence time to 9.9 mL and 0.1 hours, respectively; adjusting the luminal pH of the stomach, duodenum, and jejunum I to 6.5; setting blood flow, intestinal length, bile salts concentration, and other morphological and enzymatic parameters of the bypassed regions to minimal values; and setting fluid velocity to a maximal value to emulate zero residence in bypassed regions after RYGBS.

The impact of morbid obesity on intestinal enzyme abundance and surgical changes resulting in decreased intestinal enzyme abundance was considered. The impact of obesity on the regulation and abundance of intestinal CYPs, UGTs, and SULTs have not been reported, thus intestinal CYPs, UGTs, and SULTs pre-RYGBS abundances were assumed to be equal to the healthy population. The post-RYGBS intestinal CYP3A4 and CYP3A5 abundances were

decreased to 48.3 and 18.0 nmol/small intestine, respectively (Darwich et al. 2013), with RYGBS mimicked by alterations to compartments representing the stomach, duodenum and jejunum I. The intestinal UGT abundances were not adjusted because information regarding the regional expression of UGT isoforms in duodenum and proximal jejunum is not available and acetaminophen is primarily metabolized in the liver.

Post-RYGBS hepatic metabolism is impacted by changes to the overall liver size and regulation of hepatic drug metabolizing enzymes. Weights from our published study were used; the total body weight of RYGBS patients dropped from 137.6 kg pre-RYGBS to 113.7 post-RYGBS kg (Chen K. 2020). Correspondingly, the Simcyp calculated liver weight (LW) decreased from 2.67 kg pre-RYGBS to 2.43 kg post-RYGBS. Given the paucity of quantitative hepatic enzyme expression data in obese individuals and post-RYGBS patients, hepatic enzyme abundances were adjusted based on changes in liver weight-normalized clearances and metabolite-to-parent AUC ratios (AUC_m/AUC_p). For CYP3A4, Brill et al. reported that the post-RYGBS systemic clearance of midazolam was 1.67-fold higher (Brill et al. 2015). This value was normalized by the liver weight to 2.02-fold and used to estimate the fold-change in post-RYGBS hepatic CYP3A4 abundance. The hepatic UGT, SULT and CYP2E1 abundances for Simcyp were adjusted assuming only hepatic elimination and using the equations below.

Based on the well-stirred model, hepatic clearance is:

$$CL = \frac{Q_h f_u CL_{int}}{Q_h + f_u CL_{int}} \qquad \text{Equation 1}$$

where Q_h is hepatic blood flow, fu is the fraction unbound and CLint is the intrinsic clearance. To compare the clearances pre- and post-RYGBS, equation 1 can be rearranged to:

$$\frac{\mathrm{CL_{post}}}{\mathrm{CL_{pre}}} = \frac{Q_{\mathrm{h,post}}\, \mathrm{f_{u,post}}\, CL_{int,post}}{Q_{h,post} + f_{u,post}\, CL_{int,post}} \times \frac{Q_{h,pre} + f_{u,pre}\, CL_{int,pre}}{Q_{\mathrm{h,pre}}\, \mathrm{f_{u,pre}}\, CL_{int,pre}} \qquad \text{Equation 2}$$

For the apparent oral clearance, the well-stirred model can be reduced to:

$$CL/F = f_u\, CL_{int} \qquad \text{Equation 3}$$

The relationship for the metabolite-to-parent AUC ratio is:

$$\frac{\mathrm{AUC_m}}{\mathrm{AUC_p}} = \frac{\mathrm{f_m\ CL}}{\mathrm{CL_m}} \qquad \text{Equation 4}$$

where fm is the fraction cleared through a particular pathway, CL is the clearance of the parent and CL_m is the clearance of the metabolite. The equation can be rearranged to calculate the ratio of fm pre- and post-RYGBS:

$$\frac{\mathrm{f_{m,post}}}{\mathrm{f_{m,pre}}} = \frac{\mathrm{AUC_{m,post}}/\mathrm{AUC_{p,post}}}{\mathrm{AUC_{m,pre}}/\mathrm{AUC_{p,pre}}} \times \frac{\mathrm{CL_{m,post}}}{\mathrm{CL_{post}}} \times \frac{\mathrm{CL_{pre}}}{\mathrm{CL_{m,pre}}} \qquad \text{Equation 5}$$

Finally, assuming no change in pre- and post-RYGBS enzyme kinetics, the ratio of enzyme abundance for a specific pathway (Ei) is related to the intrinsic clearance of that pathway:

$$\frac{\mathrm{Abundance_{Ei,post}}}{\mathrm{Abundance_{Ei,pre}}} = \frac{\mathrm{CL_{int,Ei,post}}}{\mathrm{CL_{int,Ei,pre}}} \qquad \text{Equation 6}$$

where

$$\frac{\mathrm{CL_{int,Ei,post}}}{\mathrm{CL_{int,Ei,pre}}} = \frac{\mathrm{f_{m,Ei,post}\ CL_{int,post}}}{\mathrm{f_{m,Ei,pre}\ CL_{int,pre}}} \qquad \text{Equation 7}$$

Upon substituting Equations 3 and 5 into Equation 7, and rearranging:

$$\frac{\mathrm{CL_{int,Ei,post}}}{\mathrm{CL_{int,Ei,pre}}} = \frac{\mathrm{AUC_{m,post}}/\mathrm{AUC_{p,post}}}{\mathrm{AUC_{m,pre}}/\mathrm{AUC_{p,pre}}} \times \frac{\mathrm{CL_{m,post}}}{\mathrm{CL_{m,pre}}} \times \frac{\mathrm{CL_{pre}}}{\mathrm{CL_{post}}} \times \frac{\mathrm{CL_{int,post}}}{\mathrm{CL_{int,pre}}} \qquad \text{Equation 8}$$

Substituting Equation 2 into Equation 8 and rearranging:

$$\frac{\mathrm{CL_{int,Ei,post}}}{\mathrm{CL_{int,Ei,pre}}} = \frac{\mathrm{AUC_{m,post}}/\mathrm{AUC_{p,post}}}{\mathrm{AUC_{m,pre}}/\mathrm{AUC_{p,pre}}} \cdot \frac{\mathrm{CL_{m,post}}}{\mathrm{CL_{m,pre}}} \cdot \frac{\mathrm{Q_{h,pre}\ f_{u,pre}\ CL_{int,pre}}}{\mathrm{Q_{h,post}\ f_{u,post}\ CL_{int,post}}} \cdot \frac{\mathrm{Q_{h,post}} + \mathrm{f_{u,post}\ CL_{int,post}}}{\mathrm{Q_{h,pre}} + \mathrm{f_{u,pre}\ CL_{int,pre}}} \cdot \frac{\mathrm{CL_{int,post}}}{\mathrm{CL_{int,pre}}} \qquad \text{Equation 9}$$

All drugs simulated in this paper are predominantly bound to albumin in plasma (Gazzard et al. 1973, Iisalo 1977, Tillement et al. 1980, Abernethy and Schwartz 1988, Vree et al. 1989, Milligan et al. 1994, Li et al. 2010, Ohmori et al. 2011). Since the albumin levels were found comparable pre- and post-RYGBS (Cheymol 1988, Ritz et al. 2009, Oliveira Cda et al. 2015,

Antoniewicz et al. 2019), the fraction unbound (fu) is similar pre- and post-RYGBS. Assuming metabolite clearance (CL_m) is similar pre- and post-RYGBS, upon simplifying, the relative abundance of a pathway pre- and post-RYGBS can be calculated using Equation 10.

$$\frac{\text{Abundance}_{\text{Ei,post}}}{\text{Abundance}_{\text{Ei,pre}}} = \frac{{AUC_{m,post}}/{AUC_{p,post}}}{{AUC_{m,pre}}/{AUC_{p,pre}}} \cdot \frac{Q_{\text{h,pre}}}{Q_{\text{h,post}}} \cdot \frac{Q_{h,post} + f_{u,post}\, CL_{int,post}}{Q_{h,pre} + f_{u,pre}\, CL_{int,pre}} \qquad \text{Equation 10}$$

Using the baseline and 3-month post-RYGBS data from Chen et al. (Chen K. 2020), the acetaminophen AUC_m/AUC_p ratios were used in Equation 10 to calculate pathway specific abundances for UGTs, CYP2E1 and SULTs. The 3-month timepoint was used to predict the maximal changes post-RYGBS. The presurgical intrinsic clearance ($CL_{int,pre}$) was calculated using the intravenous clearance and hepatic blood flow reported by von Rongen et al. (van Rongen et al. 2016), and the postsurgical intrinsic clearance ($CL_{int,post}$) was calculated using $CL_{int,pre}$ and the pre- to post-RYGBS oral clearance (CL/F) ratio (Chen K. 2020). The pre- and post-RYGBS hepatic blood flow ($Q_{h,pre}$ and $Q_{h,post}$) were calculated using the Simcyp-predicted cardiac output and % flow to liver. Finally, for each pathway, the liver weight-normalized post-RYGBS to pre-RYGBS enzyme abundance was calculated using:

$$\frac{\text{LW-normalized Abundance}_{\text{Ei,pre}}}{\text{LW-normalized Abundance}_{\text{Ei,post}}} = \frac{\text{Abundance}_{\text{Ei,pre}}/\text{LW}_{\text{pre}}}{\text{Abundance}_{\text{Ei,post}}/\text{LW}_{\text{post}}} \qquad \text{Equation 11}$$

In Simcyp, the default UGT abundances were the same in healthy and morbidly obese populations due to a lack of published studies to inform better estimates. Thus, the post-RYGBS abundances were set to the default values and the pre-RYGBS values were adjusted using on the equations above. Although the regulation of UGT isoforms in obese patients is unclear, the mRNA levels of UGT1A1, 1A4, 1A6, and 1A9 were reported to be correlated (Izukawa et al. 2009), thus the fold-change in enzyme abundance were assumed to be comparable. Since SULTs were not included in Simcyp, SULTs were manually created as a "user-UGT" to model

formation of sulfate metabolites. The SULT enzyme abundances at baseline and 3-months were adjusted proportionally according to the relative enzyme levels. The SULT abundance post-RYGBS was predicted based on the ratio of relative mRNA levels of UGT1A1, SULT1A1 and SULT2A1 reported in healthy adults (Hardwick et al. 2013). The abundances at 3-months were used to develop the post-RYGBS population. Calculated using Equation 11, the fold-changes in enzyme levels from baseline to post-RYGBS were 0.56, 0.44, and 0.65 for UGTs, CYP2E1, and SULTs, respectively.

Compound Input.

The complete list of parameter inputs of parent compounds is listed in Table 3.2 for parent compounds, Table 3.3 for metabolites, and Table 3.4 for inhibitors. The simplified metabolic scheme of object drugs and inhibitors are illustrated in Figure 3.2.

Parent compounds. The Simcyp compound files for midazolam and digoxin were used. A compound file was created for acetaminophen and the values for parameters were drawn from the literature (Mutlib et al. 2006, Laine et al. 2009, Riches et al. 2009, Jiang et al. 2013). The ADAM model and full PBPK model were selected to describe absorption and distribution. Post-RYGBS, the permeability and absorption scalar of duodenum and jejunum I were set to the minimal values to mimic the anatomical changes due to surgery. For midazolam and acetaminophen, the permeability of the remaining intestinal segments was assumed to be equal, since these drugs are highly permeable and are not substrates for transporters. For digoxin, permeability decreased in distal intestinal regions due to increasing efflux. As per the dose administration in our clinical study, midazolam and acetaminophen were given in liquid formulation, and digoxin was given as an immediate-release tablet formulation. Since the

digoxin tablet is highly soluble (Benet et al. 2011), the solubility of digoxin in different intestinal segments was assumed to be the same. Because the absolute volume of distribution (V_d) of digoxin was comparable in obese patients and healthy individuals, the pre-determined adipose- and muscle-partitioning of digoxin were scaled down so that the weight-normalized V_d decreased, consistent with the literature (Abernethy et al. 1981).

Metabolites. The physiochemical properties of 1'-hydroxymidazolam were drawn from the literature (Nguyen et al. 2016) and linked to the CYP3A pathway in midazolam metabolism. The total hepatic clearance of 1'-hydroxymidazolam was extrapolated from the sum of *O*- and *N*-glucuronidation in microsomal incubations (Seo et al. 2010). The physiochemical properties of acetaminophen metabolites were based on online databases and Simcyp predictions and linked to the UGT and SULT pathways in acetaminophen metabolism. The *in vivo* clearances of acetaminophen-glucuronide and acetaminophen-sulfate were calculated by dividing the "theoretical dose" of a metabolite with the observed AUC from our clinical data. The theoretical dose of the metabolite was estimated using the oral bioavailability of acetaminophen and the simulated fraction metabolized via the linked UGT or SULT pathway. Table 3.3 summarizes the parameter details of the metabolites.

Inhibitors. The Simcyp verapamil drug file was used as a template in which the default enzyme inhibitory constants were retained. Norverapamil, a verapamil metabolite, was linked to CYP3A and CYP2C8 pathways to account for norverapamil's contribution to inhibition. The posaconazole drug file was built using literature data. Verapamil was formulated as an immediate release tablet, while posaconazole was formulated as oral suspension due to its low solubility (0.98 mg/L). The formulation-related parameters of posaconazole were studied *in vivo* and *in silico* by Hens et al (Hens et al. 2017). The pre-RYGBS and post-RYGBS solubility of the

inhibitors were calculated based on pH=1.8 and pH=6.5 for stomach, respectively. The precipitation rate constants for posaconazole were fit to observed clinical data.

For the DDI simulation trials, subjects were dosed orally with 240 mg verapamil twice a day for 3 days or 400 mg posaconazole twice a day for 7 days prior to administration of 20 mg midazolam or 0.5 mg digoxin. The doses were determined based on the maximum dose in FDA labels. Additional inhibitor parameters are listed in Table 3.4.

Simulation and Data Analysis.

All simulations were performed in Simcyp and the ADAM model was used for oral administration under fasted conditions. The predictive performance of the model was assessed by comparing the predicted pharmacokinetic profiles and parameters with the observed data from published clinical studies (Table 3.5). The 5^{th} and 95^{th} percentile confidence intervals of simulated concentration-time curves were generated by Simcyp. The 99.998% geometric confidence intervals were calculated to serve as the success criteria when individual data were available as proposed by Abduljalil et al. (Abduljalil et al. 2014) (Equation 12).

$$\exp\left[\ln(\bar{x}) \pm 4.26\frac{\sigma}{\sqrt{N}}\right] \qquad \text{Equation 12}$$

The geometric confidence intervals were dependent on the coefficient of variance of observed data. All parent, metabolite and inhibitor concentrations were verified in healthy volunteers before they were simulated in morbidly obese patients pre- and post-RYGBS.

For the DDI simulations, the inhibited parameter ratios were calculated as the parameter under the inhibited condition divided by the parameter under the control condition for the fraction absorbed (fa), the fraction absorbed accounting for drug reabsorption following P-gp efflux

(fa,app), the fraction escaping intestinal first pass metabolism (Fg), the apparent oral clearance (CL/F), C_{max} and AUC.

3.3 Results

Verification of models in healthy volunteers and RYGB patients.

The PBPK models successfully simulated observed drug concentrations in healthy volunteers given a single intravenous bolus dose or intravenous infusion (Figure 3.3) or a single oral dose (Figure 3.4) of midazolam, acetaminophen, digoxin, verapamil and posaconazole. The pharmacokinetics of major metabolites, including 1'-hydroxymidazolam, acetaminophen-glucuronide, acetaminophen-sulfate, and norverapamil, were captured by linking to the parent drugs in the models (Figures 3.3a, 3.4a and 3.4b). Linking the modeling between a parent and a metabolite ensures more accurate prediction of metabolite kinetics. The models also successfully predicted the inhibited observed concentrations of midazolam and digoxin after multiple doses of verapamil or posaconazole in healthy volunteers (Figures 3.4c, 3.4d, and 3.4f). The simulations in healthy volunteers under control and inhibited conditions confirmed the validity of compound-related parameters.

After verification in healthy volunteers, simulations were performed morbidly obese patients. Population parameters (Table 3.1) were adjusted to emulate the post-operative conditions and verified using observed data from pre- and post-RYGBS patients. In both pre- and post-RYGBS simulations, the observed mean concentrations of all parents and major metabolites fell between the 5th and 95th percentile confidence intervals (Figure 3.5). Acetaminophen-glucuronide was consistently slightly overpredicted during the formation phase before its observed peak concentrations in healthy volunteers and in morbidly obese patients pre-

and post-RYGBS. Using in-house individual data (Chen K. 2020), the models were further verified in terms of pharmacokinetic parameter predictions. The quantitative comparison between model predictions and observed values is shown in Figure 3.6. The means of the observed parent pharmacokinetic parameters, including $AUC_{0\text{-last}}$, peak concentration (C_{max}), time to peak concentration (T_{max}), apparent oral clearance (CL/F), and apparent volume of distribution (V/F) were within their corresponding 99.998% geometric confidence intervals. The summary of the predicted mean and geometric confidence intervals, and the observed mean and variability are summarized in Table 3.6.

Comparison of pre- and post-RYGBS absorption and metabolism.

The predicted oral bioavailability (fa, Fg, Fh and F) of midazolam, acetaminophen, digoxin, verapamil, and posaconazole in healthy volunteers and in pre- and post-RYGBS patients were determined from the simulations (Table 3.7). The predicted fraction absorbed (fa) of midazolam, acetaminophen, digoxin, and verapamil (BCS Class I) were comparable (close to 100%) before and after RYGBS, whereas the predicted fraction absorbed of posaconazole (BCS Class II) decreased from 13% to 5% after RYGBS (Table 3.7). The predicted fraction absorbed of digoxin in morbidly obese patients (pre- and post-RYGBS) was 17% higher than in healthy subjects (fa = 82%). Modeling of the BCS Class I compounds suggested that the predicted pre-RYGBS absorption occurred during a wider absorption window from duodenum to ileum II, whereas the predicted post-RYGBS absorption was more rapid, and mainly occurred in jejunum II (Figures 3.7a-3.7d). For posaconazole, the predicted pre- and post-RYGBS absorption occurred throughout the entire length of intestine due to its low solubility, and the predicted absorption rate and the predicted extent of absorption decreased by more than half after the surgery (Figure 3.7e).

The predicted regional intestinal metabolism mirrored the predicted regional intestinal absorption (Figure 3.8). The predicted fraction escaping first pass intestinal metabolism (Fg) of midazolam increased from 64% to 71% due to decreased metabolism by intestinal CYP3A4/5 as a result of RYGBS (Table 3.7), but the increase in predicted Fg of acetaminophen and verapamil were negligible. Due to post-RYGBS upregulation of hepatic CYP3A4, the predicted fraction escaping first pass hepatic metabolism (Fh) of midazolam decreased from 66% to 60% and predicted fraction metabolized (f_m) by CYP3A4 increased from 82% to 87% (Figure 3.8a). Similarly, the predicted Fh of verapamil decreased from 29% to 25% and the predicted f_m increased from 41% to 50% (Figure 3.8d). Due to post-RYGBS downregulation of CYP2E1 and/or UGTs, the predicted Fh of acetaminophen increased from 83% to 85% and the predicted Fh of posaconazole increased from 90% to 92% (Table 3.7). For acetaminophen metabolism, the predicted f_m by UGTs and SULTs increased slightly from 48% to 53% and from 31% to 35%, respectively, whereas the predicted f_m by CYPs significantly decreased from 15% to 3% (Figure 3.8b). For posaconazole metabolism, the predicted f_m by hepatic or renal UGT1A4, the only pathway of metabolism, decreased slightly (Figure 3.8e). The fractions of parent drug excreted unchanged in the urine or bile were not substantially changed following RYGBS for all drugs.

Overall, the simulations suggest that BCS Class I drugs (e.g., midazolam, acetaminophen, digoxin, and verapamil) had comparable predicted oral bioavailability pre- and post-RYGBS because of the unchanged predicted fa and the counterbalancing effects of predicted Fg and predicted Fh. However, the predicted posaconazole oral bioavailability decreased from 12% to 5% primarily due to predicted decreased absorption (Table 3.7).

Comparison of DDIs with BCS Class I and Class II inhibitors.

Interactions via CYP3A. CYP3A DDIs in healthy controls, pre-RYGBS patients and post-RYGBS patients were simulated. For midazolam-verapamil interactions, the predicted inhibited peak midazolam concentrations were 177, 194, and 260 ng/mL, and the predicted inhibited midazolam exposures were 1410, 1100, and 1376 ng·hr/mL in healthy subjects, pre-RYGBS patients, and post-RYGBS patients, respectively (Figure 3.9a). The consequence of CYP3A inhibition were comparable pre- and post-RYGBS in terms of predicted fold-change in midazolam pharmacokinetic parameters. The predicted inhibited fold-change in peak concentration ratio between pre- and post-RYGBS decreased slightly after the surgery (1.8- vs. 1.7-fold). The predicted fold-change in AUC ratio increased slightly (2.9- vs. 3.1-fold for pre- and post-RYGBS, respectively, Figure 3.9a). Compared to the predicted inhibited fold-changes in peak concentration and AUC ratios in healthy subjects (2.4- and 4.6-fold), the predicted fold-changes were less pronounced in morbidly obese patients, suggesting less of an impact of CYP3A inhibition in morbidly obese patients than in healthy subjects.

For midazolam-posaconazole interactions, the predicted inhibited peak midazolam concentrations were 154, 173, and 209 ng/mL, and the predicted inhibited midazolam exposures were 902, 841, and 757 ng·hr/mL in healthy subjects, pre-RYGBS patients, and post-RYGBS patients, respectively (Figure 3.9b). The predicted effects of CYP3A inhibition were greater pre-RYGBS than post-RYGBS. The predicted inhibited fold-change in peak concentration ratio pre- and post-RYGBS decreased after the surgery (1.6- vs. 1.3-fold). The predicted inhibited fold-change in AUC ratio also decreased (2.0- vs. 1.6-fold for pre- and post-RYGBS, respectively, Figure 3.9b). Similar to results with midazolam-verapamil interactions, the predicted inhibited fold-changes in peak concentration and AUC ratios were greatest in healthy subjects (2.0- and

2.5-fold), which suggests a higher impact of verapamil inhibition in healthy subjects than in morbidly obese patients.

Interactions via P-gp. P-gp DDIs in healthy controls, pre-RYGBS patients and post-RYGBS patients were simulated. For digoxin-verapamil interactions, the predicted inhibited peak digoxin concentrations were 3.8, 3.8, and 4.7 ng/mL, and the predicted inhibited digoxin exposures were 23, 14, and 15 ng·hr/mL in healthy subjects, pre-RYGBS patients, and post-RYGBS patients, respectively (Figure 3.9c). The predicted effect of P-gp inhibition on digoxin pharmacokinetic parameters were comparable pre- and post-RYGBS. RYGBS did not have an effect on the predicted inhibited fold-change for peak concentration ratios (1.6-fold pre- and post-RYGBS) or AUC ratios (1.1-fold pre- and post-RYGBS, Figure 3.9c). Again, the predicted effects were more substantial in healthy subjects as evidenced by higher predicted inhibited fold-changes in peak concentrations and AUC ratios (2.0- and 1.5-fold, respectively). The simulations predicted no significant interactions between digoxin and posaconazole in healthy subjects and pre- and post-RYGBS patients (Figure 3.9d). The predicted fold-changes of the pharmacokinetic parameters in the DDI simulations are summarized in Table 3.8.

Sensitivity analysis.

A sensitivity analysis was performed by looking at the impact of varying intestinal and hepatic CYP3A4 abundance on the midazolam-verapamil DDIs and varying posaconazole solubility on midazolam-posaconazole DDIs. Intestinal CYP3A4 abundance (nmol/small intestine) and hepatic CYP3A4 abundance (pmol/mg protein) are key factors in determining midazolam bioavailability and exposure and were altered following RYGBS due to the anatomical bypass and CYP3A4 enzyme upregulation. Posaconazole solubility (mg/L) was

selected as gastric pH elevation due to RYGBS could play an important role in modulating the magnitude of CYP3A-mediated DDIs. The relationship between the predicted midazolam Fg and intestinal CYP3A4 abundance was identical in healthy subjects, pre-RYGBS patients and post-RYGBS patients (Figure 3.10a). In contrast, the predicted inhibited AUC ratio increased with intestinal CYP3A abundance in all three groups, but the predicted inhibited AUC ratio was consistently higher in healthy subjects (Figure 3.10b) compared to pre-RYGBS and post-RYGBS patients. The predicted inhibited midazolam oral clearance and predicted inhibited AUC ratio increased as hepatic CYP3A4 abundance increased. The predicted inhibited midazolam oral clearance was consistently highest in pre-RYGBS patients and the lowest in healthy subjects at various hepatic CYP3A4 abundances (Figure 3.10c). The predicted inhibited midazolam AUC ratios were less sensitive to changes in hepatic CYP3A4 abundance in morbidly obese patients and were indistinguishable between pre- and post-RYGBS at various hepatic CYP3A4 abundances (Figure 3.10d). Posaconazole fa and predicted inhibited midazolam AUC ratio increased with higher posaconazole solubility. The predicted relationship between posaconazole fa and solubility in pre-RYGBS patients and in healthy subjects overlapped, however higher solubility was required for post-RYGBS patients to reach the same degree of absorption (Figure 3.10e). Lastly, the predicted inhibited midazolam AUC ratio was more sensitive to posaconazole solubility in healthy subjects than in morbidly obese patients (Figure 3.10f).

3.4 Discussion

In the past decade, the use of *in silico* methods to model drug absorption and disposition in a mechanistic manner has improved the ability to predict the effects of patient demographics, disease, and drug-drug interactions, resulting in advances in personalized medicine and alleviating some of the burden of conducting clinical studies (Sager et al. 2015). Only recently has PBPK modeling been applied to understanding how gastric bypass procedures alter drug absorption and bioavailability (Darwich et al. 2012, Almukainzi M. 2014, Gesquiere et al. 2015). The post-operative changes in morbidly obese patients are multifactorial. By accounting for the combined effects of various physiological factors and drug characteristics, PBPK models have the advantage over traditional compartmental models in predicting necessary dose adjustments for DDIs. This study aims to simulate post-RYGBS absorption and disposition of substrates for Phase I and II enzymes and transporters, and to compare the impact of RYGBS on DDIs caused by low and high solubility drugs.

The PBPK models, equipped with ADAM absorption models and appropriate population parameters, successfully simulated clinically observed plasma concentrations and pharmacokinetic parameters of midazolam, acetaminophen, digoxin, verapamil, and posaconazole in healthy subjects, and pre- and post-RYGBS patients (Figures 3.3 and 3.4; Figures 3.5 and 3.6). The confidence in f_m predictions was increased by the inclusion of the metabolites. The plasma concentration vs. time profiles for 1'-hydroxymidazolam, acetaminophen-glucuronide, and acetaminophen-sulfate were successfully captured using linked metabolite models, demonstrating another layer of confidence in the simulated metabolism. Although the observed acetaminophen-glucuronide concentrations fell within the 5^{th} and 95^{th} confidence interval, the acetaminophen-glucuronide concentrations were consistently

overpredicted before reaching its peak concentration in both healthy subjects and morbidly obese patients (Figure 3.4a; Figures 3.5c and 3.5d). The overprediction could be due to a more rapid distribution of formed metabolites from the liver into systemic circulation than observed in the clinical studies.

Compared to healthy subjects, the predicted rates of absorption of highly soluble drugs (e.g., midazolam, acetaminophen, and verapamil) were increased in obese patients due to larger intestinal surface and greater splanchnic blood flow (Elbarbry 2015). As evidenced by higher predicted digoxin fa and predicted bioavailability in morbidly obese patients, a higher fraction of the digoxin dose can be absorbed and escape intestinal efflux by P-gp before being passed down to distal intestine (Table 3.7). The ADAM model highlighted the post-RYGBS changes in drug dissolution, cumulative absorption, and regional intestinal absorption and metabolism. For high solubility drugs, the predicted cumulative absorption reached 100% both pre- and post-RYGBS, but was more rapid after RYGBS, indicating RYGBS resulted in no change to the extent of absorption, but increased the rate of absorption. The predicted absorption window shifted to the distal jejunum and was shortened after the surgery, with most of the dose (> 80%) absorbed in jejunum II (Figures 3.7a-d). Following RYGBS, a higher drug concentration gradient across intestinal lumen may exist due to the drug being dissolved in a smaller volume (i.e., in significantly smaller stomach size post-RYGBS) that drives more rapid intestinal drug absorption. Additionally, the predicted increased absorption rate could be caused by intestinal hyperplasia, as well as increased intestinal leakiness, as a result of post-RYGBS intestinal adaptation (Savassi-Rocha et al. 2014, Cavin et al. 2016).

Although the predicted extent of absorption was unchanged, predicted intestinal and hepatic first pass metabolism were affected by the surgery. Following RYGBS, the predicted

intestinal first pass metabolism of CYP3A substrates that have significant intestinal extraction, such as midazolam, markedly decreased due to bypassing the proximal intestine, the region with the highest abundance of CYP3A4. The predicted patterns of regional intestinal metabolism were mirrored in the patterns of predicted regional intestinal absorption post-RYGBS (Figures 3.7 and 3.8). On the other hand, hepatic CYP3A4 was upregulated post-RYGBS, leading to an increase in the predicted hepatic first pass metabolism of substrates with significant hepatic extraction, such as midazolam and verapamil. As a result, the predicted increase in post-RYGBS Fg was offset by the predicted decrease in post-RYGBS Fh. Thus, the overall predicted bioavailability of midazolam and verapamil were comparable pre- and post-RYGBS (Table 3.7). Further work will need to explore whether absolute bioavailability is unchanged for other highly soluble CYP3A substrates post-RYGBS.

In contrast, for posaconazole, a drug with low solubility and minimal first pass metabolism, the predicted change in bioavailability was mainly governed by the predicted change in absorption. The predicted post-RYGBS cumulative absorption decreased by half and more than 90% of the dose was not absorbed (Figure 3.7e). The solubility of posaconazole is highly pH-dependent (Hens et al. 2017). Hence, the predicted elevated pH in the post-RYGBS gastrointestinal environment enhanced precipitation, decreasing the amount of dissolved posaconazole available to be absorbed. However, the impact of solubility is drug-specific; some BCS Class II drugs, such as fenofibrate, are unaffected by changes in pH. The solubility of fenofibrate is bile salt-dependent (Chen et al. 2009), thus its post-RYGBS solubility was not affected as the surgical procedure allows the bypassed duodenum to continue supplying bile acids (Gesquiere et al. 2016).

While the predicted fraction of highly soluble drugs entering systemic circulation was similar pre- and post-RYGBS, predicted hepatic drug metabolism was altered following RYGBS. Due to CYP3A4 upregulation post-RYGBS, the predicted contribution of hepatic CYP3A4 increased for midazolam and verapamil (Figures 3.8a and d), but was counteracted by a decrease in liver size with weight-loss, resulting in slightly decreased predicted systemic clearance. Major acetaminophen metabolizing enzymes were all markedly downregulated post-RYGBS, thus the post-RYGBS predicted acetaminophen exposure increased. However, the downregulation was more pronounced for CYP2E1 than for UGTs and SULTs, shunting the metabolism from CYP2E1 pathway to the UGT and SULT pathways (Figure 3.8b). Since acetaminophen hepatotoxicity is caused by a reactive intermediate metabolite formed by CYP2E1 (Yoon et al. 2016), the post-operative risk of toxicity may decrease given a predicted lower fraction of acetaminophen metabolized by CYPs. Alternatively, toxicity may increase if glutathione is depleted during the absorption phase where the acetaminophen peak concentrations are predicted to be much higher post-RYGBS compared to pre-RYGBS. For posaconazole disposition following RYGBS, the predicted fraction metabolized by UGT1A4 was unchanged (Figure 3.8e), but due to reduced levels of UGT1A4, the only contributor to posaconazole metabolism, and reduced liver weight, the predicted systemic clearance of posaconazole was decreased.

The consequences of CYP3A4-mediated DDIs with verapamil were comparable pre- and post-RYGBS in terms of predicted inhibited midazolam peak concentration and AUC ratios as there was little change in predicted inhibitor concentrations post-RYGBS (Figure 3.9a). Similarly, when P-gp was inhibited by verapamil, the predicted inhibited digoxin peak concentration and AUC ratios were comparable pre- and post-RYGBS (Figure 3.9c). In contrast,

the DDI interactions post-RYGBS markedly decreased with posaconazole, because posaconazole absorption was predicted to decrease as a result of reduced solubility (Figure 3.9b). Unfortunately, the comparison of BCS Class I and Class II compounds could not be made for P-gp inhibition, as posaconazole was a weak P-gp inhibitor in the simulations.

The predicted effects of DDIs were consistently higher in healthy subjects. Having 35% lower liver mass, healthy subjects were predicted to have lower clearance of verapamil and posaconazole, leading to higher object and precipitant drug exposures compared to morbidly obese patients. Nonetheless, predicted peak midazolam and digoxin concentrations were still higher in post-RYGBS patients (Figure 3.9). The predicted increased peak concentrations post-RYGBS for highly soluble, rapidly absorbed drugs may be especially concerning for drugs where peak concentrations are at the upper end of the therapeutic window. Although dose reductions may be required to avoid DDIs in all groups, different adjustments might be suitable for healthy, pre-RYGBS, and post-RYGBS conditions. Healthy subjects may need the largest reduction in dose of the object drug, but the post-RYGBS patients may require adjustments in doses and frequency (e.g., lower doses at increased intervals to reduce C_{max}).

Sensitivity analyses revealed the influence of intestinal and hepatic CYP3A4 abundance and posaconazole solubility on DDI magnitude. At the same intestinal CYP3A4 abundance, healthy subjects had the highest predicted inhibited midazolam AUC ratio as a consequence of having higher hepatic CYP3A4 abundance and higher verapamil exposure (Figure 3.10b). One would expect a higher predicted inhibited midazolam AUC ratio post-RYGBS than pre-RYGBS, since verapamil exposure slightly increased after the surgery. However, the pre-RYGBS and post-RYGBS predicted inhibited AUC ratios overlapped because the difference was offset by the post-RYGBS decrease in intestinal CYP3A4 abundance. Lastly, because post-RYGBS gastric

pH was elevated, the predicted absorption at the same intrinsic solubility was lower in the post-operative condition (Figure 3.10e). Due to predicted lower posaconazole clearance in healthy subjects, the predicted magnitude of CYP3A4 inhibition was considerably more sensitive to posaconazole solubility compared to obese individuals (Figure 3.10f).

There are several limitations to this study. Although the parameter inputs accounted for the major enzymes responsible for metabolism of these drugs and most abundant metabolites, the inclusion of less abundant metabolites or enzymes with a minor role may provide a more comprehensive picture of the disposition of the drug. There is limited information regarding the physiological differences resulting from obesity or RYGBS, such as gastrointestinal emptying rate, intestinal diameter, villi density, and epithelial tight junctions. It is likely that the impact of RYGBS on the pharmacokinetics of drugs will decrease over time with changes in stomach emptying time, hepatic enzyme regulation and intestinal adaptation that occurs ~6 months after RYGBS. Although we assumed that albumin was unchanged by RYGBS as suggested in the literature (Cheymol 1988, Ritz et al. 2009, Oliveira Cda et al. 2015, Antoniewicz et al. 2019), any changes in albumin would affect the fraction unbound of the drugs and have an impact on all subsequent modeling. In the scaling of total hepatic enzyme abundance, it is important to discern how much liver mass reduction comes from decreased hepatocyte count versus decreased fat accumulation. Also, the post-RYGBS changes in bile salt composition are critical for predicting drug dissolution and permeation for drugs with bile-acid dependent solubility (Mathavan et al. 2016, Gniado et al. 2018). Little is known about how intestinal CYP3A4 expression is altered due to obesity as hepatic and intestinal CYP3A4 expression are not correlated (von Richter et al. 2004), and the regional expression of UGTs and SULTs along the intestinal tract are unknown (Riches et al. 2009, Yang et al. 2017). At this time, different SULT isoforms and their hepatic

abundances are not available in Simcyp and we made assumptions based on results from our previous study. In situations where glucuronides and sulfates are actively transported or undergo enterohepatic circulation, transporters responsible for biliary efflux (Kock and Brouwer 2012) and renal secretion/reabsorption (Biber et al. 2014) should be included. Post-RYGBS changes in gut microbiome (Liou et al. 2013, Duboc et al. 2019) could also add complexity, as gut flora can not only metabolize drugs but also regulate regional and remote DMETs by microbial metabolites (Swanson 2015, Wilson and Nicholson 2017). The inclusion of these data, with a gut microbiome component, would permit more comprehensive, system pharmacology-based models to be developed (Thiele I. 2017). Many of these limitations stem from the lack of data from obese individuals or RYGBS patients to inform the Simcyp model. This study reviewed a limited number of drugs with liquid or immediate release formulations and used data from the maximal change at 3-month post-RYGBS. Additional PBPK modeling with robust supporting clinical data (e.g., for more commonly used dosage forms) should be done to continue to explore the impact of RYGBS and other bariatric surgeries on drug disposition and DDIs, and the persistence of drug disposition changes post-surgery.

In conclusion, the models provided a mechanistic framework to understand pre- and post-RYGBS pharmacokinetics. Taking post-RYGBS changes into account, the concentrations and pharmacokinetic parameters of midazolam, acetaminophen, digoxin, verapamil, and posaconazole were simulated successfully in morbidly obese patients undergoing RYGBS. The linked-metabolites, including 1’-hydroxymidazolam, acetaminophen-glucuronide, and acetaminophen-sulfate, were well predicted. The simulated DDI results indicate that the impact of RYGBS is dependent on the predicted inhibitor solubility. The predicted magnitude of the DDIs were similar pre- and post-RYGBS when studied with a highly soluble BCS Class I

inhibitor (i.e., verapamil), whereas the magnitude of the DDIs were greater pre-RYGBS than post-RYGBS when studied with a less soluble BCS Class II inhibitor (i.e., posaconazole). When DDIs exist, a smaller dose reduction, in terms of fold-change, is needed for morbidly obese patients compared to healthy subjects. However, due to significantly higher predicted peak concentrations, the dose and frequency of the object drug may need to be decreased in the post-RYGBS patient to minimize adverse effects of DDIs. The ADAM-PBPK model should be modified to incorporate new findings regarding enzyme expression and physiological changes following RYGBS.

3.5 Acknowledgments

This research was supported by American College of Clinical Pharmacy Research Institute Frontiers Research Award (L-NC) and the University of Washington School of Pharmacy DMTPR funding (YSL).

3.6 References

Abduljalil, K., T. Cain, H. Humphries and A. Rostami-Hodjegan (2014). "Deciding on success criteria for predictability of pharmacokinetic parameters from in vitro studies: an analysis based on in vivo observations." Drug Metab Dispos **42**(9): 1478-1484.

Abernethy, D. R., D. J. Greenblatt and T. W. Smith (1981). "Digoxin disposition in obesity: clinical pharmacokinetic investigation." Am Heart J **102**(4): 740-744.

Abernethy, D. R. and J. B. Schwartz (1988). "Verapamil pharmacodynamics and disposition in obese hypertensive patients." J Cardiovasc Pharmacol **11**(2): 209-215.

Albaugh, V. L., B. Banan, H. Ajouz, N. N. Abumrad and C. R. Flynn (2017). "Bile acids and bariatric surgery." Mol Aspects Med **56**: 75-89.

Almukainzi M., L. V., Löbenberg R. (2014). "Modelling the Absorption of Metformin with Patients Post Gastric Bypass Surgery." Journal of Diabetes and Metabolism **5**(3).

Antoniewicz, A., P. Kalinowski, K. J. Kotulecka, P. Kocon, R. Paluszkiewicz, P. Remiszewski and K. Zieniewicz (2019). "Nutritional Deficiencies in Patients after Roux-en-Y Gastric Bypass and Sleeve Gastrectomy during 12-Month Follow-Up." Obes Surg **29**(10): 3277-3284.

Arterburn, D. E. and A. P. Courcoulas (2014). "Bariatric surgery for obesity and metabolic conditions in adults." Bmj **349**: g3961.

Backman, J. T., K. T. Olkkola, K. Aranko, J. J. Himberg and P. J. Neuvonen (1994). "Dose of midazolam should be reduced during diltiazem and verapamil treatments." Br J Clin Pharmacol **37**(3): 221-225.

Benet, L. Z., F. Broccatelli and T. I. Oprea (2011). "BDDCS applied to over 900 drugs." Aaps j **13**(4): 519-547.

Biber, J., H. Murer, N. Mohebbi and C. A. Wagner (2014). "Renal handling of phosphate and sulfate." Compr Physiol **4**(2): 771-792.

Brill, M. J., A. van Rongen, E. P. van Dongen, B. van Ramshorst, E. J. Hazebroek, A. S. Darwich, A. Rostami-Hodjegan and C. A. Knibbe (2015). "The Pharmacokinetics of the CYP3A Substrate Midazolam in Morbidly Obese Patients Before and One Year After Bariatric Surgery." Pharm Res **32**(12): 3927-3936.

Cavin, J. B., A. Couvelard, R. Lebtahi, R. Ducroc, K. Arapis, E. Voitellier, F. Cluzeaud, L. Gillard, M. Hourseau, N. Mikail, L. Ribeiro-Parenti, N. Kapel, J. P. Marmuse, A. Bado and M. Le Gall (2016). "Differences in Alimentary Glucose Absorption and Intestinal Disposal of Blood Glucose After Roux-en-Y Gastric Bypass vs Sleeve Gastrectomy." Gastroenterology **150**(2): 454-464.e459.

Chan, L. N., Y. S. Lin, J. C. Tay-Sontheimer, D. Trawick, B. K. Oelschlager, D. R. Flum, K. K. Patton, D. D. Shen and J. R. Horn (2015). "Proximal Roux-en-Y gastric bypass alters drug absorption pattern but not systemic exposure of CYP3A4 and P-glycoprotein substrates." Pharmacotherapy **35**(4): 361-369.

Chen K., C. L., Senn T., Oelschlager B.K., Flum D.R., Shen D.D., Horn J.R., Lin Y.S. (2020). "The Impact of Proximal Roux-en-Y Gastric Bypass Surgery on Acetaminophen Absorption and Metabolism." Pharmacotherapy.

Chen, Y., Y. Lu, J. Chen, J. Lai, J. Sun, F. Hu and W. Wu (2009). "Enhanced bioavailability of the poorly water-soluble drug fenofibrate by using liposomes containing a bile salt." Int J Pharm **376**(1-2): 153-160.

Cheymol, G. (1988). "Drug pharmacokinetics in the obese." Fundam Clin Pharmacol **2**(3): 239-256.

Chiew, A., P. Day, C. Salonikas, D. Naidoo, A. Graudins and R. Thomas (2010). "The comparative pharmacokinetics of modified-release and immediate-release paracetamol in a simulated overdose model." Emerg Med Australas **22**(6): 548-555.

Courtney, R., A. Sansone, W. Smith, T. Marbury, P. Statkevich, M. Martinho, M. Laughlin and S. Swan (2005). "Posaconazole pharmacokinetics, safety, and tolerability in subjects with varying degrees of chronic renal disease." J Clin Pharmacol **45**(2): 185-192.

Cristofoletti, R., N. Patel and J. B. Dressman (2016). "Differences in Food Effects for 2 Weak Bases With Similar BCS Drug-Related Properties: What Is Happening in the Intestinal Lumen?" J Pharm Sci **105**(9): 2712-2722.

Darwich, A. S., D. Pade, B. J. Ammori, M. Jamei, D. M. Ashcroft and A. Rostami-Hodjegan (2012). "A mechanistic pharmacokinetic model to assess modified oral drug bioavailability post bariatric surgery in morbidly obese patients: interplay between CYP3A gut wall metabolism, permeability and dissolution." J Pharm Pharmacol **64**(7): 1008-1024.

Darwich, A. S., D. Pade, K. Rowland-Yeo, M. Jamei, A. Asberg, H. Christensen, D. M. Ashcroft and A. Rostami-Hodjegan (2013). "Evaluation of an In Silico PBPK Post-Bariatric Surgery Model through Simulating Oral Drug Bioavailability of Atorvastatin and Cyclosporine." CPT Pharmacometrics Syst Pharmacol **2**: e47.

Duboc, H., C. C. Nguyen, J. B. Cavin, L. Ribeiro-Parenti, A. C. Jarry, D. Rainteau, L. Humbert, B. Coffin, M. Le Gall, A. Bado and H. Sokol (2019). "Roux-en-Y Gastric-Bypass and sleeve gastrectomy induces specific shifts of the gut microbiota without altering the metabolism of bile acids in the intestinal lumen." Int J Obes (Lond) **43**(2): 428-431.

Elbarbry, F. (2015). "Oral Bioavailability in Special Populations." MOJ Bioequiv Availab. **1**(3): 49-52.

Gazzard, B. G., A. W. Ford-Hutchinson, M. J. Smith and R. Williams (1973). "The binding of paracetamol to plasma proteins of man and pig." J Pharm Pharmacol **25**(12): 964-967.

Gesquiere, I., A. S. Darwich, B. Van der Schueren, J. de Hoon, M. Lannoo, C. Matthys, A. Rostami, V. Foulon and P. Augustijns (2015). "Drug disposition and modelling before and after gastric bypass: immediate and controlled-release metoprolol formulations." Br J Clin Pharmacol **80**(5): 1021-1030.

Gesquiere, I., B. Hens, B. Van der Schueren, R. Mols, J. de Hoon, M. Lannoo, C. Matthys, V. Foulon and P. Augustijns (2016). "Drug disposition before and after gastric bypass: fenofibrate and posaconazole." Br J Clin Pharmacol **82**(5): 1325-1332.

Ghosal, A., N. Hapangama, Y. Yuan, J. Achanfuo-Yeboah, R. Iannucci, S. Chowdhury, K. Alton, J. E. Patrick and S. Zbaida (2004). "Identification of human UDP-glucuronosyltransferase enzyme(s) responsible for the glucuronidation of posaconazole (Noxafil)." Drug Metab Dispos **32**(2): 267-271.

Gniado, K., P. MacFhionnghaile, P. McArdle and A. Erxleben (2018). "The natural bile acid surfactant sodium taurocholate (NaTC) as a coformer in coamorphous systems: Enhanced physical stability and dissolution behavior of coamorphous drug-NaTc systems." Int J Pharm **535**(1-2): 132-139.

Hachon, L., X. Decleves, P. Faucher, C. Carette and C. Lloret-Linares (2017). "RYGB and Drug Disposition: How to Do Better? Analysis of Pharmacokinetic Studies and Recommendations for Clinical Practice." Obes Surg **27**(4): 1076-1090.

Hardwick, R. N., D. W. Ferreira, V. R. More, A. D. Lake, Z. Lu, J. E. Manautou, A. L. Slitt and N. J. Cherrington (2013). "Altered UDP-glucuronosyltransferase and sulfotransferase expression and function during progressive stages of human nonalcoholic fatty liver disease." Drug Metab Dispos **41**(3): 554-561.

Hartman, J. H., L. G. Letzig, D. W. Roberts, L. P. James, E. K. Fifer and G. P. Miller (2015). "Cooperativity in CYP2E1 metabolism of acetaminophen and styrene mixtures." Biochem Pharmacol **97**(3): 341-349.

Hausman, D. B., M. DiGirolamo, T. J. Bartness, G. J. Hausman and R. J. Martin (2001). "The biology of white adipocyte proliferation." Obes Rev **2**(4): 239-254.

Hens, B., S. M. Pathak, A. Mitra, N. Patel, B. Liu, S. Patel, M. Jamei, J. Brouwers, P. Augustijns and D. B. Turner (2017). "In Silico Modeling Approach for the Evaluation of Gastrointestinal Dissolution, Supersaturation, and Precipitation of Posaconazole." Mol Pharm **14**(12): 4321-4333.

Iisalo, E. (1977). "Clinical pharmacokinetics of digoxin." Clin Pharmacokinet **2**(1): 1-16.

Izukawa, T., M. Nakajima, R. Fujiwara, H. Yamanaka, T. Fukami, M. Takamiya, Y. Aoki, S. Ikushiro, T. Sakaki and T. Yokoi (2009). "Quantitative analysis of UDP-glucuronosyltransferase (UGT) 1A and UGT2B expression levels in human livers." Drug Metab Dispos **37**(8): 1759-1768.

Jamei M., Y. J., Turner D., Yeo K. R., Tucker G. T., Rostami-Hodjegan A. (2007). "A Novel Physiologically-based Mechanistic Model for Predicting Oral Drug Absorption: The Advanced Dissolution, Absorption, and Metabolism (ADAM) Model." from https://www.certara.com/posters/a-novel-physiologically-based-mechanistic-model-for-

predicting-oral-drug-absorption-the-advanced-dissolution-absorption-and-metabolism-adam-model-2/?ap=PBPK.

Jiang, S. Z., W. Lu, X. F. Zong, H. Y. Ruan and Y. Liu (2016). "Obesity and hypertension." Exp Ther Med **12**(4): 2395-2399.

Jiang, X. L., P. Zhao, J. S. Barrett, L. J. Lesko and S. Schmidt (2013). "Application of physiologically based pharmacokinetic modeling to predict acetaminophen metabolism and pharmacokinetics in children." CPT Pharmacometrics Syst Pharmacol **2**: e80.

Karimi, M., A. Kabir, M. Nejatifar and A. Pazouki (2018). "Trend of Changes in Serum Albumin and Its Relation with Sex, Age, and BMI Following Laparoscopic Mini-gastric Bypass Surgery in Morbid Obese Cases." Obes Surg **28**(3): 671-680.

Kelly, T., W. Yang, C. S. Chen, K. Reynolds and J. He (2008). "Global burden of obesity in 2005 and projections to 2030." Int J Obes (Lond) **32**(9): 1431-1437.

Kersemaekers, W. M., T. van Iersel, U. Nassander, E. O'Mara, H. Waskin, M. Caceres and M. L. van Iersel (2015). "Pharmacokinetics and safety study of posaconazole intravenous solution administered peripherally to healthy subjects." Antimicrob Agents Chemother **59**(2): 1246-1251.

Kock, K. and K. L. Brouwer (2012). "A perspective on efflux transport proteins in the liver." Clin Pharmacol Ther **92**(5): 599-612.

Krishna, G., L. Ma, M. Martinho and E. O'Mara (2012). "Single-dose phase I study to evaluate the pharmacokinetics of posaconazole in new tablet and capsule formulations relative to oral suspension." Antimicrob Agents Chemother **56**(8): 4196-4201.

Krishna, G., A. Moton, L. Ma, I. Savant, M. Martinho, M. Seiberling and J. McLeod (2009). "Effects of oral posaconazole on the pharmacokinetic properties of oral and intravenous

midazolam: a phase I, randomized, open-label, crossover study in healthy volunteers." Clin Ther **31**(2): 286-298.

Laine, J. E., S. Auriola, M. Pasanen and R. O. Juvonen (2009). "Acetaminophen bioactivation by human cytochrome P450 enzymes and animal microsomes." Xenobiotica **39**(1): 11-21.

Lempers, V. J., J. J. van den Heuvel, F. G. Russel, R. E. Aarnoutse, D. M. Burger, R. J. Bruggemann and J. B. Koenderink (2016). "Inhibitory Potential of Antifungal Drugs on ATP-Binding Cassette Transporters P-Glycoprotein, MRP1 to MRP5, BCRP, and BSEP." Antimicrob Agents Chemother **60**(6): 3372-3379.

Levitt, D. G. (2013). "Quantitation of small intestinal permeability during normal human drug absorption." BMC Pharmacol Toxicol **14**: 34.

Li, Y., U. Theuretzbacher, C. J. Clancy, M. H. Nguyen and H. Derendorf (2010). "Pharmacokinetic/pharmacodynamic profile of posaconazole." Clin Pharmacokinet **49**(6): 379-396.

Link, B., M. Haschke, N. Grignaschi, M. Bodmer, Y. Z. Aschmann, M. Wenk and S. Krahenbuhl (2008). "Pharmacokinetics of intravenous and oral midazolam in plasma and saliva in humans: usefulness of saliva as matrix for CYP3A phenotyping." Br J Clin Pharmacol **66**(4): 473-484.

Liou, A. P., M. Paziuk, J. M. Luevano, Jr., S. Machineni, P. J. Turnbaugh and L. M. Kaplan (2013). "Conserved shifts in the gut microbiota due to gastric bypass reduce host weight and adiposity." Sci Transl Med **5**(178): 178ra141.

Loftsson, T. and D. Hreinsdottir (2006). "Determination of aqueous solubility by heating and equilibration: a technical note." AAPS PharmSciTech **7**(1): E4.

Mathavan, S., N. Chen-Tan, F. Arfuso and H. Al-Salami (2016). "A comprehensive study of novel microcapsules incorporating gliclazide and a permeation enhancing bile acid: hypoglycemic effect in an animal model of Type-1 diabetes." Drug Deliv **23**(8): 2869-2880.

Milligan, T. P., H. C. Morris, P. M. Hammond and C. P. Price (1994). "Studies on paracetamol binding to serum proteins." Ann Clin Biochem **31 (Pt 5)**: 492-496.

Miras, A. D. and C. W. le Roux (2018). "Surgery: The new gold-standard - medical gastric bypass." Nat Rev Endocrinol **14**(5): 257-258.

Mokdad, A. H., J. S. Marks, D. F. Stroup and J. L. Gerberding (2004). "Actual causes of death in the United States, 2000." Jama **291**(10): 1238-1245.

Mutlib, A. E., T. C. Goosen, J. N. Bauman, J. A. Williams, S. Kulkarni and S. Kostrubsky (2006). "Kinetics of acetaminophen glucuronidation by UDP-glucuronosyltransferases 1A1, 1A6, 1A9 and 2B15. Potential implications in acetaminophen-induced hepatotoxicity." Chem Res Toxicol **19**(5): 701-709.

Nguyen, H. Q., E. Kimoto, E. Callegari and R. S. Obach (2016). "Mechanistic Modeling to Predict Midazolam Metabolite Exposure from In Vitro Data." Drug Metab Dispos **44**(5): 781-791.

Ohmori, J., S. Maeda, H. Higuchi, M. Ishii, Y. Arai, Y. Tomoyasu, A. Kohjitani, M. Shimada and T. Miyawaki (2011). "Propofol increases the rate of albumin-unbound free midazolam in serum albumin solution." J Anesth **25**(4): 618-620.

Oliveira Cda, S., B. T. Beserra, R. S. Cunha, A. G. Brito, R. C. de Miranda, L. A. Zeni, E. A. Nunes and E. B. Trindade (2015). "Impact of Roux-en-Y gastric bypass on lipid and inflammatory profiles." Rev Col Bras Cir **42**(5): 305-310.

Raffa, R. B., J. Pawasauskas, J. V. Pergolizzi, Jr., L. Lu, Y. Chen, S. Wu, B. Jarrett, R. Fain, L. Hill and K. Devarakonda (2018). "Pharmacokinetics of Oral and Intravenous Paracetamol (Acetaminophen) When Co-Administered with Intravenous Morphine in Healthy Adult Subjects." Clin Drug Investig **38**(3): 259-268.

Riches, Z., J. Bloomer, A. Patel, A. Nolan and M. Coughtrie (2009). "Assessment of cryopreserved human hepatocytes as a model system to investigate sulfation and glucuronidation and to evaluate inhibitors of drug conjugation." Xenobiotica **39**(5): 374-381.

Riches, Z., E. L. Stanley, J. C. Bloomer and M. W. Coughtrie (2009). "Quantitative evaluation of the expression and activity of five major sulfotransferases (SULTs) in human tissues: the SULT "pie"." Drug Metab Dispos **37**(11): 2255-2261.

Risstad, H., J. A. Kristinsson, M. W. Fagerland, C. W. le Roux, K. I. Birkeland, H. L. Gulseth, P. M. Thorsby, R. P. Vincent, M. Engstrom, T. Olbers and T. Mala (2017). "Bile acid profiles over 5 years after gastric bypass and duodenal switch: results from a randomized clinical trial." Surg Obes Relat Dis **13**(9): 1544-1553.

Ritz, P., G. Becouarn, O. Douay, A. Salle, P. Topart and V. Rohmer (2009). "Gastric bypass is not associated with protein malnutrition in morbidly obese patients." Obes Surg **19**(7): 840-844.

Rodin, S. M., B. F. Johnson, J. Wilson, P. Ritchie and J. Johnson (1988). "Comparative effects of verapamil and isradipine on steady-state digoxin kinetics." Clin Pharmacol Ther **43**(6): 668-672.

Sager, J. E., J. Yu, I. Ragueneau-Majlessi and N. Isoherranen (2015). "Physiologically Based Pharmacokinetic (PBPK) Modeling and Simulation Approaches: A Systematic Review of

Published Models, Applications, and Model Verification." Drug Metab Dispos **43**(11): 1823-1837.

Santostasi, G., M. Fantin, I. Maragno, R. M. Gaion, O. Basadonna and S. Dalla-Volta (1987). "Effects of amiodarone on oral and intravenous digoxin kinetics in healthy subjects." J Cardiovasc Pharmacol **9**(4): 385-390.

Savassi-Rocha, A. L., M. T. Diniz, E. G. Vilela, F. Diniz Mde, S. R. Sanches, A. S. da Cunha, L. Ferrari Mde, H. O. Torres, B. A. Maciente, G. S. Ataliba, P. M. Araujo, T. B. Guerra and I. K. Balbino (2014). "Changes in intestinal permeability after Roux-en-Y gastric bypass." Obes Surg **24**(2): 184-190.

Sawicki, W. (2002). "Pharmacokinetics of verapamil and norverapamil from controlled release floating pellets in humans." Eur J Pharm Biopharm **53**(1): 29-35.

Scheinfeld, N. S. (2004). "Obesity and dermatology." Clin Dermatol **22**(4): 303-309.

Seo, K. A., S. K. Bae, Y. K. Choi, C. S. Choi, K. H. Liu and J. G. Shin (2010). "Metabolism of 1'- and 4-hydroxymidazolam by glucuronide conjugation is largely mediated by UDP-glucuronosyltransferases 1A4, 2B4, and 2B7." Drug Metab Dispos **38**(11): 2007-2013.

Sugimoto, H., S. Matsumoto, M. Tachibana, S. Niwa, H. Hirabayashi, N. Amano and T. Moriwaki (2011). "Establishment of in vitro P-glycoprotein inhibition assay and its exclusion criteria to assess the risk of drug-drug interaction at the drug discovery stage." J Pharm Sci **100**(9): 4013-4023.

Swanson, H. I. (2015). "Drug Metabolism by the Host and Gut Microbiota: A Partnership or Rivalry?" Drug Metab Dispos **43**(10): 1499-1504.

Thiele I., C. C. M., Heinken A., Fleming R.M.T. (2017). "Quantitative systems pharmacology and the personalized drug–microbiota–diet axis." Current Opinion in Systems Biology **4**: 43-52.

Tillement, J. P., R. Zini, M. Lecomte and P. d'Athis (1980). "Binding of digitoxin, digoxin and gitoxin to human serum albumin." Eur J Drug Metab Pharmacokinet **5**(3): 129-134.

Ulldemolins, M., J. A. Roberts, J. Rello, D. L. Paterson and J. Lipman (2011). "The effects of hypoalbuminaemia on optimizing antibacterial dosing in critically ill patients." Clin Pharmacokinet **50**(2): 99-110.

Vaessen, S. F., M. M. van Lipzig, R. H. Pieters, C. A. Krul, H. M. Wortelboer and E. van de Steeg (2017). "Regional Expression Levels of Drug Transporters and Metabolizing Enzymes along the Pig and Human Intestinal Tract and Comparison with Caco-2 Cells." Drug Metab Dispos **45**(4): 353-360.

van Rongen, A., P. A. J. Valitalo, M. Y. M. Peeters, D. Boerma, F. W. Huisman, B. van Ramshorst, E. P. A. van Dongen, J. N. van den Anker and C. A. J. Knibbe (2016). "Morbidly Obese Patients Exhibit Increased CYP2E1-Mediated Oxidation of Acetaminophen." Clin Pharmacokinet **55**(7): 833-847.

von Richter, O., O. Burk, M. F. Fromm, K. P. Thon, M. Eichelbaum and K. T. Kivisto (2004). "Cytochrome P450 3A4 and P-glycoprotein expression in human small intestinal enterocytes and hepatocytes: a comparative analysis in paired tissue specimens." Clin Pharmacol Ther **75**(3): 172-183.

Vree, T. B., M. Shimoda, J. J. Driessen, P. J. Guelen, T. J. Janssen, E. F. Termond, R. van Dalen, J. C. Hafkenscheid and M. S. Dirksen (1989). "Decreased plasma albumin concentration

results in increased volume of distribution and decreased elimination of midazolam in intensive care patients." Clin Pharmacol Ther **46**(5): 537-544.

Wilson, I. D. and J. K. Nicholson (2017). "Gut microbiome interactions with drug metabolism, efficacy, and toxicity." Transl Res **179**: 204-222.

Yang, N., R. Sun, X. Liao, J. Aa and G. Wang (2017). "UDP-glucuronosyltransferases (UGTs) and their related metabolic cross-talk with internal homeostasis: A systematic review of UGT isoforms for precision medicine." Pharmacol Res **121**: 169-183.

Yoon, E., A. Babar, M. Choudhary, M. Kutner and N. Pyrsopoulos (2016). "Acetaminophen-Induced Hepatotoxicity: a Comprehensive Update." J Clin Transl Hepatol **4**(2): 131-142.

Zimmerman, E. I., J. L. Roberts, L. Li, D. Finkelstein, A. Gibson, A. S. Chaudhry, E. G. Schuetz, J. E. Rubnitz, H. Inaba and S. D. Baker (2012). "Ontogeny and sorafenib metabolism." Clin Cancer Res **18**(20): 5788-5795.

3.7 Figures and Tables

Table 3.1. Parameter inputs for a morbidly obese population pre- and post-RYGBS.

Parameters	Pre-RYGBS			Post-RYGBS		
Simcyp template						
Population	Morbidly obese			Morbidly obese		
Weight						
Total body weight (kg)	138[f]			114[f]		
BMI (kg/m^2)	51[d,f]			43[d,f]		
Liver weight (kg)	2.7[f]			2.4[d]		
Tissue composition						
Adipose volume scalar	1.32[f,i]			1.2[f,i]		
Liver volume scalar	1.25[a]			1.25[a]		
Liver enzyme abundances						
CYP3A4 (pmol/mg protein)	42.5[e]			65[a]		
CYP2E1 (pmol/mg protein)	140[f]			110[a]		
UGT1A1 (pmol/mg protein)	85[f]			55[f]		
UGT1A4 (pmol/mg protein)	93[f]			60[f]		
UGT1A9 (pmol/mg protein)	55[f]			35[f]		
UGT2B15 (pmol/mg protein)	69[f]			44[f]		
SULTs (pmol/mg protein) modeled as a user-UGT	0.01355[f,h]			0.009288[f,h]		
GI tract						
Initial stomach volume (mL)	50[a]			9.9[g]		
Stomach MRT (hr)	0.27[a]			0.1[g]		
Duodenum length linear multiplier	0.205[a]			0.001[b]		
CYP3A4 (nmol/small intestine)	66.2[a]			48.3[g]		
CYP3A5 (nmol/small intestine)	24.6[a]			18.0[g]		
ADAM model	Stomach[a]	Duodenum[a]	Jejunum I[a]	Stomach	Duodenum	Jejunum I
General						
Blood flow (Q_{villi} %)	--	8.8	24.2	--	0.001[b]	0.001[b]
Transit time (Total %)	--	4.6	17.3	--	0.001[b]	0.001[b]
CYP 3A (Total %)	--	13.76	27.24	--	0.001[b]	0.001[b]
S9PPI (Total %)	--	14.88	26.9	--	0.001[b]	0.001[b]
MPPI (Total %)	--	13.76	27.24	--	0.001[b]	0.001[b]
CPPI (Total %)	--	14.88	26.9	--	0.001[b]	0.001[b]
Luminal pH	1.5	6.4	6.5	6.5[g]	6.5[g]	6.5[g]
Luminal fluid velocity (m/s)	0.032	0.005	0.0013	10[c]	10[c]	10[c]
Luminal bile salts (mM)	0.29	3.31	2.3	0.0001[b]	0.0001[b]	0.0001[b]
GI morphology						
Villi channel depth (µm)	--	522.78	448.81	--	1[b]	1[b]
Villi channel width (µm)	--	28.03	22.44	--	1[b]	1[b]
Villi thickness (µm)	--	128.35	137.7	--	1[b]	1[b]
Fold expansion	--	1	1.97	--	1[b]	1[b]
Pore radius	--	8.6	8.6	--	1[b]	1[b]

ADAM: advanced dissolution, absorption and metabolism model; S9PPI: S9 protein per intestine; MPPI: microsomal protein per intestine; CPPI: cytosolic protein per intestine; -- = not applicable; [a] Simcyp default; [b] Simcyp minimum value; [c] Simcyp maximum value; [d] Simcyp predicted; [e] Brill et al., 2015 (Brill et al. 2015); [f] Calculated using Chen et al., 2020 (Chen K. 2020); [g] Darwich et al., 2013 (Darwich et al. 2013); [h] Hardwick et al., 2013 (Hardwick et al. 2013); [i] Hausman et al., 2001 (Hausman et al. 2001)

Table 3.2. Parameter inputs for acetaminophen, midazolam, and digoxin.

Parameters	Acetaminophen		Midazolam		Digoxin	
Physiochemical properties						
Molecular weight (g/mol)	151.2[f]		325.8[a]		780.94[a]	
LogP	0.51[f]		3.53[a]		1.26[a]	
Compound type	Monoprotic acid[f]		Ampholyte[a]		Neutral[a]	
pKa1	9.46[f]		10.95[a]		--	
pKa2	--		6.2[a]		--	
B/P	1.58[f]		0.603[a]		1.07[a]	
fu	0.82[f]		0.032[a]		0.71[a]	
Absorption	Pre-RYGBS	Post-RYGBS	Pre-RYGBS	Post-RYGBS	Pre-RYGBS	Post-RYGBS
Model	ADAM	ADAM	ADAM	ADAM	ADAM	ADAM
Permeability						
$P_{app, Caco-2}$ (10^{-6} cm/s)	64[n]	64[n]	213[a]	213[a]	12.7[a]	12.7[a]
Duodenum	Predicted[b]	0.0001[j]	Predicted[b]	0.0001[j]	0.5[a]	0.0001[j]
Jejunum I	Predicted[b]	0.0001[j]	Predicted[b]	0.0001[j]	4.67[a]	0.0001[j]
Jejunum II	Predicted[b]	Predicted[b]	Predicted[b]	Predicted[b]	4.67[a]	4.67[a]
Ileum I	Predicted[b]	Predicted[b]	Predicted[b]	Predicted[b]	4.67[a]	4.67[a]
Ileum II	Predicted[b]	Predicted[b]	Predicted[b]	Predicted[b]	3.67[a]	3.67[a]
Ileum III	Predicted[b]	Predicted[b]	Predicted[b]	Predicted[b]	2.67[a]	2.67[a]
Ileum IV	Predicted[b]	Predicted[b]	Predicted[b]	Predicted[b]	1.67[a]	1.67[a]
Colon	Predicted[b]	Predicted[b]	Predicted[b]	Predicted[b]	0.1[a]	0.1[a]
Formulation	Solution	Solution	Solution	Solution	Solid, immediate release	Solid, immediate release
Solubility (mg/mL)	--	--	--	--	0.986[k, p]	0.986[k, p]
Distribution	Pre-RYGBS	Post-RYGBS	Pre-RYGBS	Post-RYGBS	Pre-RYGBS	Post-RYGBS
Model	Full PBPK	Full PBPK	Full PBPK	Full PBPK	Full PBPK	Full PBPK
Tissue:plasma partition coefficients						
Adipose	Predicted[b]	Predicted[b]	Predicted[b]	Predicted[b]	5.4[e,l]	6.48[e,l]
Muscle	Predicted[b]	Predicted[b]	Predicted[b]	Predicted[b]	3.675[e,l]	4.41[e,l]
Other tissues	Predicted[b]	Predicted[b]	Predicted[b]	Predicted[b]	Predicted[b]	Predicted[b]
Kp scalar	1.2	1.2	0.35	0.3	0.5	0.6
Elimination						
fu_{mic}/fu_{inc}	1[a]		1[a]		1[a]	
fu_{gut}	1[a]		1[a]		1[a]	
CYP3A4 Vmax (pmol/min/pmol isoform)	0.3766[g]		5.23 (1'-OH pathway)[a]		--	

	Km (µmol/L)	130[g]	2.16 (1'-OH pathway)[a]	--
CYP3A4	Vmax (pmol/min/pmol isoform)	--	5.2 (4-OH pathway)[a]	--
	Km (µmol/L)	--	31.8 (4-OH pathway)[a]	--
CYP3A5	Vmax (pmol/min/pmol isoform)	--	19.7 (1'-OH pathway)[a]	--
	Km (µmol/L)	--	4.16 (1'-OH pathway)[a]	--
CYP3A5	Vmax (pmol/min/pmol isoform)	--	4.03 (4-OH pathway)[a]	--
	Km (µmol/L)	--	34.8 (4-OH pathway)[a]	--
CYP1A2	Vmax (pmol/min/pmol isoform)	0.4322[g]	--	--
	Km (µmol/L)	220[g]	--	--
CYP2C9	Vmax (pmol/min/pmol isoform)	0.08644[g]	--	--
	Km (µmol/L)	660[g]	--	--
CYP2C19	Vmax (pmol/min/pmol isoform)	1.143[g]	--	--
	Km (µmol/L)	2000[g]	--	--
CYP2D6	Vmax (pmol/min/pmol isoform)	0.432[g]	--	--
	Km (µmol/L)	440[g]	--	--
CYP2E1	Vmax (pmol/min/pmol isoform)	3.8[o]	--	--
	Km (µmol/L)	830[o]	--	--
UGT1A1	Vmax (pmol/min/mg protein)	6531[h]	--	--
	Km (µmol/L)	5500[h]	--	--
UGT1A4	Vmax (pmol/min/mg protein)	--	445[a]	--
	Km (µmol/L)	--	40.3[a]	--
UGT1A9	Vmax (pmol/min/mg protein)	10925[h]	--	--
	Km (µmol/L)	9200[h]	--	--
UGT2B15	Vmax (pmol/min/mg protein)	36417[h]	--	--
	Km (µmol/L)	23000[h]	--	--
SULTs	Vmax (pmol/min/mg protein)	958[i]	--	--
	Km (µmol/L)	300[i]	--	--
	Scalar liver, intestine, kidney	0.6[d], 0, 0	--	--
Typical CL_R (L/h)		--	--	7.5[m]
Additional Hep CL_{int} (µL/min/10^6)		--	--	0.37[a]

ADAM = advanced dissolution, absorption and metabolism; -- = not applicable; [a] Simcyp default; [b] Predicted by Simcyp; [d] Adjusted based on reported fm; [e] Simcyp default multiplied by scalar; [f] Jiang et al., 2013 (Jiang et al. 2013); [g] Laine et al., 2009 (Laine et al. 2009); [h] Mutlib et al., 2006 (Mutlib et al. 2006); [i] Riches et al., 2009 (Riches et al. 2009); [j] Darwich et al., 2013 (Darwich et al. 2013); [k] Benet et al. 2011 (Benet et al. 2011); [l] Abernethy et al. 1981 (Abernethy et al. 1981); [m] Adjusted as per apparent clearance in Chan et al. 2015 (Chan et al. 2015) and Simcyp predicted bioavailability; [n] Levitt et al., 2013 (Levitt 2013); [o] Hartman et al., 2015 (Hartman et al. 2015); [p] Loftsson et al., 2006 (Loftsson and Hreinsdottir 2006)

Table 3.3. Parameter inputs for acetaminophen-glucuronide, acetaminophen-sulfate and 1'-hydroxymidazolam.

Parameters	**Acetaminophen-Glucuronide** (linked to UGT pathway)		**Acetaminophen-Sulfate** (linked to SULT pathway)		**1'-hydroxymidazolam** (linked to CYP3Apathway)	
Physiochemical properties						
Molecular weight (g/mol)	327.2867[d]		231.226[d]		342[h]	
LogP	-0.68[e]		-1[e]		2.5[h]	
Compound type	Monoprotic acid[f]		Monoprotic acid[f]		Ampholyte[h]	
pKa1	3.17[f]		0[c] (-2.2[3])		13.6[h]	
pKa2	--		--		3.63[h]	
B/P	1[a]		1[a]		1[a]	
fu	0.996[b]		0.997[b]		0.15[h]	
Absorption						
	--		--		--	
Distribution	Pre-RYGBS	Post-RYGBS	Pre-RYGBS	Post-RYGBS	Pre-RYGBS	Post-RYGBS
Model	Minimal PBPK	Minimal PBPK	Minimal PBPK	Minimal PBPK	Full PBPK	Full PBPK
Kp	0.8	1.0	0.35	0.65	1.1	1.0
Elimination	Pre-RYGBS	Post-RYGBS	Pre-RYGBS	Post-RYGBS	Pre-RYGBS	Post-RYGBS
fu_{mic}	--	--	--	--	0.725[b]	0.725[b]
fu_{gut}	1[a]	1[a]	1[a]	1[a]	1[a]	1[a]
In vivo CL (L/h)	7.0[g]	7.0[g]	12.5[g]	11.5[g]	--	--
HLM CL_{int} (μL/min/mg protein)	--	--	--	--	227[j]	346.2[i]

-- = not applicable; [a] Simcyp default; [b] Predicted by Simcyp; [c] Simcyp minimum value; [d] DRUGBANK; [e] ALOGPS; [f] ChemAxon; [g] Estimated using predicted f_m and observed AUC_m from Chen et al., 2020 (Chen K. 2020); [h] Nguyen et al., 2016 (Nguyen et al. 2016); [i] Seo et al., 2010 (Seo et al. 2010); [j] Brill et al., 2015 (Brill et al. 2015)

Table 3.4. Parameter inputs for verapamil, norverapamil, and posaconzole.

Parameters		Verapamil		Norverapamil		Posaconazole	
Dosing regimen							
Pre-treatment		240 mg BID for 3 days		--		400 mg BID for 7 days	
Co-medication		20 mg MDZ or 0.5 mg DIG		--		20 mg MDZ or 0.5 mg DIG	
Class							
		BCS Class I[f]; antihypertensive		Verapamil metabolite		BCS Class II[f]; antifungal	
Interactions							
CYP3A4	Competitive inhibition	--		--		Ki (uM) = 0.38[h], fu_{mic} = 0.023[e]	
	Mechanism-based inhibition	K_{app} (uM) = 2.21[a]; k_{inact} (1/h) = 2[a]		K_{app} (uM) = 10.3[a]; k_{inact} (1/h) = 18[a]		--	
CYP3A5	Mechanism-based inhibition	K_{app} (uM) = 3.99[a]; k_{inact} (1/h) = 1.84[a]		K_{app} (uM) = 4.53[a]; k_{inact} (1/h) = 4.2[a]		--	
P-gp	Competitive inhibition	Ki (uM) = 0.16[a]		Ki (uM) = 0.04[a]		Ki (uM) = 0.675[i,n]	
Physiochemical properties[a]							
Molecular weight (g/mol)		454.6		440.575		700.78[g]	
LogP		4.46		4.66		4.6[g]	
Compound type		Monoprotic Base[g]		Monoprotic Base[g]		Diprotic Base[g]	
pKa1		8.78		10.29		3.6[j]	
pKa2		--		--		4.6[j]	
B/P		0.709		0.675		1.146[b]	
fu		0.09		0.083		0.02[k, p, q]	
Absorption		Pre-RYGBS	Post-RYGBS	Pre-RYGBS	Post-RYGBS	Pre-RYGBS	Post-RYGBS
Model		ADAM	ADAM	--	--	ADAM	ADAM
Permeability (10^{-4} cm/s)				--	--		
	$P_{app, Caco-2}$ (10^{-6} cm/s)	149.6[a]	149.6[a]	--	--	48[j]	48[j]
	Duodenum – Jejunum I	Predicted[b]	0.0001[c]	--	--	Predicted[b]	0.0001[c]
	Jejunum 2 – Ileum IV	Predicted[b]	Predicted[b]	--	--	Predicted[b]	Predicted[b]
	Colon	Predicted[b]	Predicted[b]	--	--	Predicted[b]	Predicted[b]
Formulation		Solid, immediate release	Solid, immediate release	--	--	Suspension	Suspension
	Solubility (mg/mL)	70[f]	70[f]	--	--	--	--
	Fraction of API Dissolved	--	--	--	--	70% (pH1.6)[j]	70% (pH1.6)[j]
	Intrinsic solubility (mg/mL)	--	--	--	--	0.00098[j, o]	0.00098[j, o]
	Solubility factor	--	--	--	--	71.35[j]	2.86l
	$logK_{m:w}$ neutral	--	--	--	--	4.52[j]	4.52[j]

$logK_{m:w}$ ion	--	--	--	--	1.0[j]	1.0[j]
Particle size (um)	--	--	--	--	10[j]	10[j]
Critical supersaturation ratio	--	--	--	--	2.9[j]	1l
Precipitation rate constant	--	--	--	--	50[e]	--
2nd precipitation rate constant	--	--	--	--	50e	200e
Particle h_{eff}	--	--	--	--	Hintz-Johnson	Hintz-Johnson
Distribution	**Pre-RYGBS**	**Post-RYGBS**	**Pre-RYGBS**	**Post-RYGBS**	**Pre-RYGBS**	**Post-RYGBS**
Model	Minimal PBPK	Minimal PBPK	Minimal PBPK	Minimal PBPK	Full PBPK	Full PBPK
Kp scalar	0.7	0.7	1	1	0.06	0.075
Elimination	**Norverapamil[a]**	**D-617[a]**	**D-620[a]**	**D-715[a]**		
CYP2C8 Vmax (pmol/min/pmol isoform)	221.2	218.9	38.5	113.2	--	--
Km (µmol/L)	140.5	156	68	59	--	--
CYP3A4 Vmax (pmol/min/pmol isoform)	154.3	174	46	--	--	--
Km (µmol/L)	122	99.5	90	--	--	--
CYP3A5 Vmax (pmol/min/pmol isoform)	169.3	117.7	18.8	--	--	--
Km (µmol/L)	87.5	73	19.5	--	--	--
UGT1A4 Vmax (pmol/min/pmol isoform)	--	--	--	--	16.9[m]	16.9[m]
Km (µmol/L)	--	--	--	--	15.9[m]	15.9[m]
fu_{mic}	--	--	--	--	0.012[d]	0.012[d]

-- = not applicable; [a] Simcyp default; [b] Predicted by Simcyp; [c] Simcyp minimum value; [d] Back-calculated from CL_{iv} (6.54 L/h); [e] Fitted by Simcyp using observed in vivo data; [f] MP BIOMEDICALS; [g] DRUGBANK; [h] Zimmerman et al., 2012 (Zimmerman et al. 2012); [i] Lempers et al., 2016 (Lempers et al. 2016); [j] Hens et al., 2017 (Hens et al. 2017); [k] Noxafil label; [l] Derived based on post-RYGBS gastric pH; [m] Ghosal et al., 2004 (Ghosal et al. 2004); [n] Sugimoto et al., 2011 (Sugimoto et al. 2011); [o] Cristofoletti et al., 2016 (Cristofoletti et al. 2016); [p] Courtney et al., 2005 (Courtney et al. 2005); [q] Ulldemolins et al., 2011 (Ulldemolins et al. 2011)

Table 3.5. Literature sources used in model verifications.

Population	Route	Concentrations	Source
healthy adults	single iv	midazolam and 1'-hydroxymidazolam	Link et al., 2008 (Link et al. 2008)
		acetaminophen	Raffa et al., 2018 (Raffa et al. 2018)
		digoxin	Santostasi et al., 1987 (Santostasi et al. 1987)
		verapamil	Abernethy et al., 1988 (Abernethy and Schwartz 1988)
		posaconazole	Kersemaekers et al., 2015 (Kersemaekers et al. 2015)
	single po	midazolam	Backman et al., 1994 (Backman et al. 1994)
		acetaminophen, -gluc, and -sulf	Chiew et al., 2010 (Chiew et al. 2010)
		digoxin	Rodin et al., 1988 (Rodin et al. 1988)
		verapamil and norverapamil	Sawicki et al., 2002 (Sawicki 2002)
		posaconazole	Krishna et al., 2012 (Krishna et al. 2012)
	multiple po perpetrator + single po object	verapamil and midazolam DDI	Backman et al., 1994 (Backman et al. 1994)
		verapamil and digoxin DDI	Rodin et al., 1988 (Rodin et al. 1988)
		posaconazole and midazolam DDI	Krishna et al., 2009 (Krishna et al. 2009)
pre-RYGBS patients	single po	midazolam and 1'-hydroxymidazolam	Chan et al., 2015 (Chan et al. 2015)
		acetaminophen, -gluc, and -sulf	Chen et al., 2020 (Chen K. 2020)
		digoxin	Chan et al., 2015 (Chan et al. 2015)
		verapamil	Abernethy et al., 1988 (Abernethy and Schwartz 1988)
		posaconazole	Gesquiere et al., 2016 (Gesquiere et al. 2016)
post-RYGBS patients	single po	midazolam and 1'-hydroxymidazolam	Chan et al., 2015 (Chan et al. 2015)
		acetaminophen, -gluc, and -sulf	Chen et al., 2020 (Chen K. 2020)
		digoxin	Chan et al., 2015 (Chan et al. 2015)
		posaconazole	Gesquiere et al., 2016 (Gesquiere et al. 2016)

Table 3.6. Summary of predicted and observed pharmacokinetic parameters for midazolam, acetaminophen, and digoxin.

		Pre-RYGBS		Post-RYGBS	
	PK parameters	Predicted mean [geoCI]	Observed mean (% CV)	Predicted mean [geoCI]	Observed mean (% CV)
Midazolam	V/F (L)	903 [620, 1315]	726 (31.3)	617 [379, 1005]	553 (37.4)
	CL/F (L/hr)	77.4 [31.4, 191]	79.7 (84.5)	66.9 [31.5, 142]	95.3 (60.6)
	$AUC_{0\text{-last}}$ (ng·hr/mL)	25.6 [14.3, 45.8]	24.4 (50.2)	30.4 [15.9, 57.8]	21.5 (50.6)
	C_{max} (ng/mL)	9.1 [4.7, 17.4]	10.7 (56.7)	14.4 [8.6, 24.0]	16.8 (39.6)
	T_{max} (hr)	0.6 [0.4, 1.0]	0.6 (36.8)	0.2 [0.2, 0.4]	0.3 (27.4)
1'-OH-Midazolam	$AUC_{0\text{-last}}$ (ng·hr/mL)	5.8 [3.1, 10.9]	6.3 (54.5)	5.1 [3.0, 8.8]	7.8 (42.2)
	C_{max} (ng/mL)	1.7 [0.9, 3.2]	3.1 (55.2)	2.0 [1.3, 3.1]	5.9 (34.6)
	T_{max} (hr)	0.6 [0.4, 1.0]	0.7 (42.0)	0.2 [0.2, 0.4]	0.3 (27.1)
Acetaminophen	V/F (L)	84.3 [56.7, 125]	99.8 (31.7)	63.9 [41.3, 98.7]	86.3 (33.2)
	CL/F (L/hr)	26.4 [19.1, 36.6]	30.0 (25.7)	19.9 [12.8, 31.0]	21.1 (33.7)
	$AUC_{0\text{-last}}$ (µg·hr/mL)	63.7 [44.8, 90.4]	51.9 (27.9)	83.7 [53.8, 130]	76.5 (33.7)
	C_{max} (µg/mL)	15.1 [9.6, 23.9]	18.7 (36.6)	32.2 [24.0, 43.2]	35.1 (22.0)
	T_{max} (hr)	0.8 [0.4, 1.6]	0.6 (58.7)	0.2 [0.1, 0.3]	0.2 (35.1)
Acetaminophen-glucuronide	$AUC_{0\text{-last}}$ (µg·hr/mL)	232 [158, 343]	200 (31.0)	262 [159, 433]	231 (38.5)
	C_{max} (µg/mL)	23.4 [17.2, 31.8]	25.4 (24.2)	26.3 [15.7, 44.0]	27.3 (39.6)
	T_{max} (hr)	3.3 [2.6, 4.3]	3.5 (19.9)	3.1 [2.6, 3.8]	3.6 (14.3)
Acetaminophen-sulfate	$AUC_{0\text{-last}}$ (µg·hr/mL)	55.6 [42.5, 72.6]	53.4 (21.1)	65.0 [44.5, 94.9]	65.4 (28.7)
	C_{max} (µg/mL)	8.7 [6.4, 11.8]	8.6 (24.1)	8.7 [5.8, 13.0]	8.7 (30.3)
	T_{max} (hr)	2.0 [1.2, 3.3]	2.1 (40.8)	2.5 [1.6, 3.8]	2.2 (32.0)
Digoxin	V/F (L)	719 [536, 964]	876 (24.2)	657 [428, 1007]	809 (32.6)
	CL/F (L/hr)	23.6 [16.2, 34.2]	20.4 (31.1)	20.8 [12.6, 34.3]	18.0 (38.4)
	$AUC_{0\text{-last}}$ (ng·hr/mL)	13.3 [10.1, 17.6]	13.3 (23.0)	14.6 [10.5, 20.2]	14.6 (24.7)
	C_{max} (ng/mL)	2.7 [1.7, 4.4]	3.1 (39.9)	3.3 [2.3, 4.7]	3.1 (26.2)
	T_{max} (hr)	0.7 [0.5, 1.0]	0.8 (34.8)	0.5 [0.3, 0.8]	0.5 (38.3)

For predicted values: geometric mean and 99.998% geometric confidence intervals (geoCI) given. For observed values: mean and percent coefficient of variation (CV%) given. V/F = apparent oral volume of distribution; CL/F = apparent oral clearance; $AUC_{0\text{-last}}$ = area under the concentration-time curve from 0 to last observed timepoint; C_{max} = peak concentration; T_{max} = time to reach peak concentration.

Table 3.7. Predicted oral bioavailability parameters for midazolam, acetaminophen, digoxin, verapamil, and posaconazole in a healthy population and in morbidly obese pre- and post-RYGBS patients.

Drug	Population	fa	Fg	Fh	F
Midazolam	healthy	0.99	0.65	0.56	0.36
	pre-RYGBS	1.00	0.64	0.66	0.42
	post-RYGBS	1.00	0.71	0.60	0.43
Acetaminophen	healthy	1.00	0.97	0.89	0.87
	pre-RYGBS	1.00	0.97	0.83	0.81
	post-RYGBS	1.00	0.98	0.85	0.83
Digoxin	healthy	0.82	1.00	0.97	0.80
	pre-RYGBS	0.99	1.00	0.96	0.95
	post-RYGBS	0.99	1.00	0.96	0.95
Verapamil	healthy	1.00	0.89	0.27	0.24
	pre-RYGBS	1.00	0.89	0.29	0.25
	post-RYGBS	1.00	0.90	0.25	0.23
Posaconazole	healthy	0.12	0.99	0.94	0.11
	pre-RYGBS	0.13	0.99	0.90	0.12
	post-RYGBS	0.05	0.99	0.92	0.05

Mean values of the parameter listed. F = overall bioavailability, fa = fraction absorbed, Fg = fraction escaping intestinal first pass metabolism, Fh = fraction escaping hepatic first pass metabolism.

Table 3.8. Predicted inhibited-to-control parameter ratios for midazolam and digoxin.

			Object drugs					
			Midazolam			Digoxin		
		Ratios	Healthy	Pre-RYGBS	Post-RYGBS	Healthy	Pre-RYGBS	Post-RYGBS
Inhibitors	Verapamil	fa	1.00	1.00	1.00	1.18	1.01	1.01
		fa,app	1.00	1.00	1.00	0.95	0.73	0.72
		Fg	1.32	1.31	1.16	1.00	1.00	1.00
		CL/F	0.22	0.34	0.33	0.65	0.91	0.90
		C_{max}	2.40	1.83	1.74	1.96	1.57	1.63
		AUC	4.60	2.85	3.09	1.51	1.10	1.10
	Posaconazole	fa	1.00	1.00	1.00	1.02	1.00	1.00
		fa,app	1.00	1.00	1.00	1.03	1.00	1.00
		Fg	1.34	1.28	1.14	1.00	1.00	1.00
		CL/F	0.47	0.53	0.66	0.95	0.99	0.99
		C_{max}	1.98	1.56	1.27	1.07	1.08	1.06
		AUC	2.50	1.98	1.58	1.04	1.01	1.01

Mean values of the parameter listed. fa = fraction absorbed; fa,app = fraction absorbed accounting for drug reabsorption following P-gp efflux; Fg = fraction escaping intestinal first pass metabolism; CL/F = apparent oral clearance; C_{max} = peak concentration; AUC = area under the concentration-time curve.

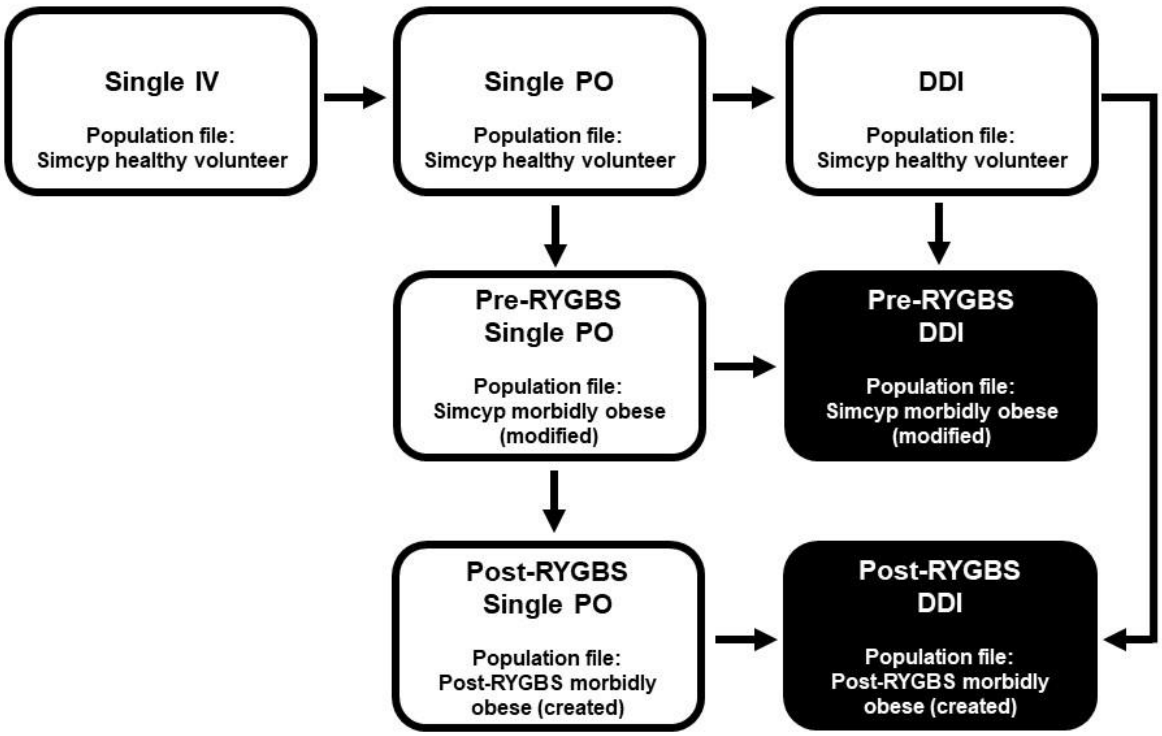

Figure 3.1. PBPK modeling workflow. White boxes represent verification steps and black boxes represent prediction steps. The population file used in each step is indicated.

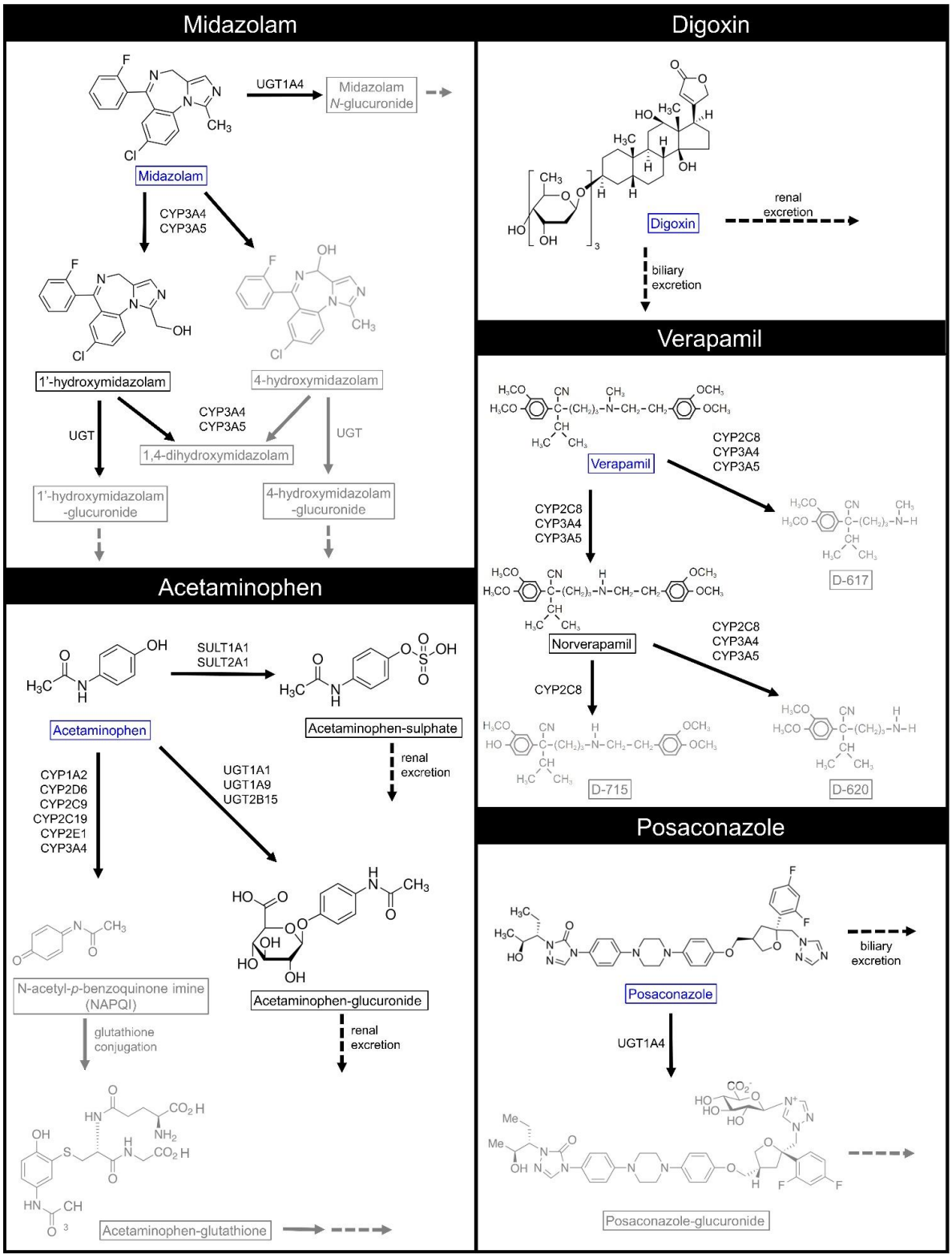

Figure 3.2. Metabolic scheme of object drugs and inhibitors. Metabolites and pathways in black were included in the PBPK modeling.

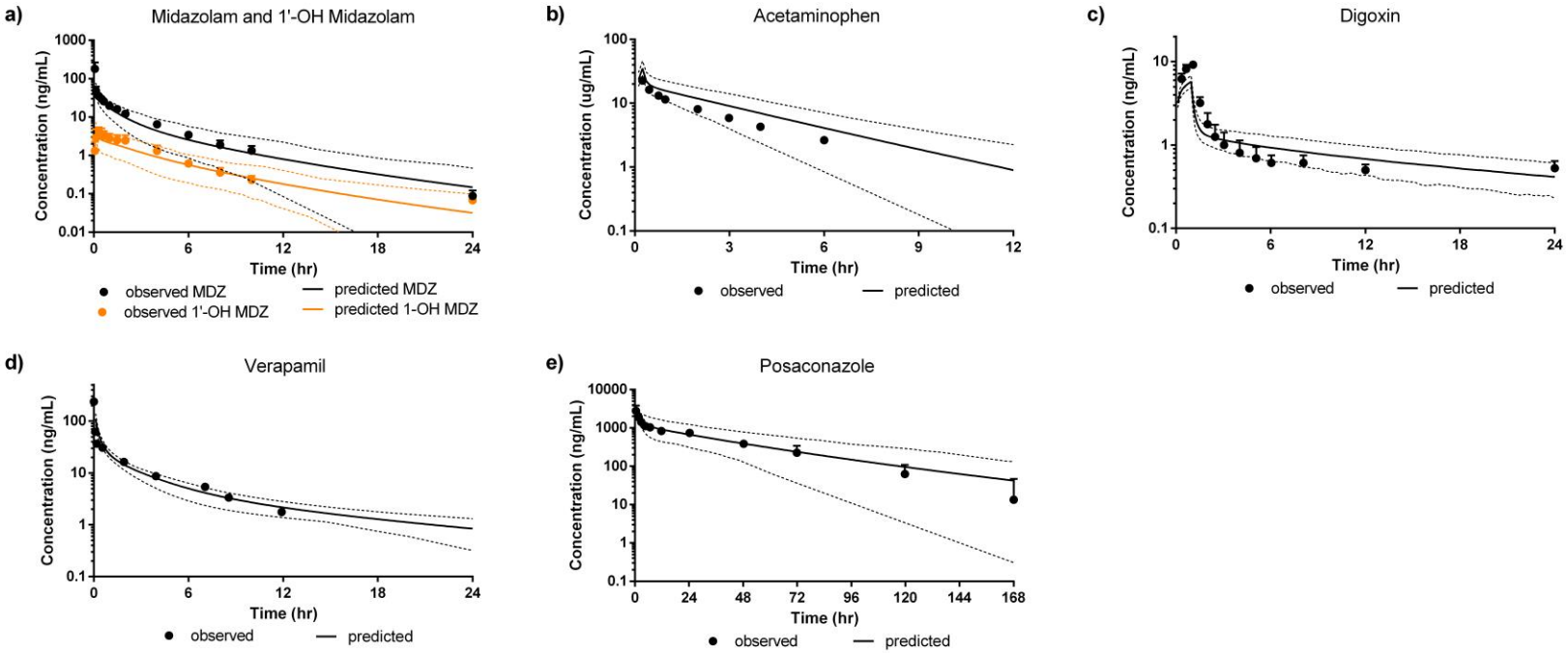

Figure 3.3. Observed and simulated plasma concentration vs. time profiles in heathy volunteers after a single intravenous bolus dose or infusion. Panels: a) midazolam and 1'-hydroxymidazolam (Link 2008); b) acetaminophen (Raffa 2018); c) digoxin (Santostasi 1987); d) verapamil (Darell 1988); e) posaconazole (Kersemaekers 2015). Shown: predicted concentration (solid curve); 5th and 95th confidence intervals (dashed curves); parent (black curves); linked metabolite (colored curves).

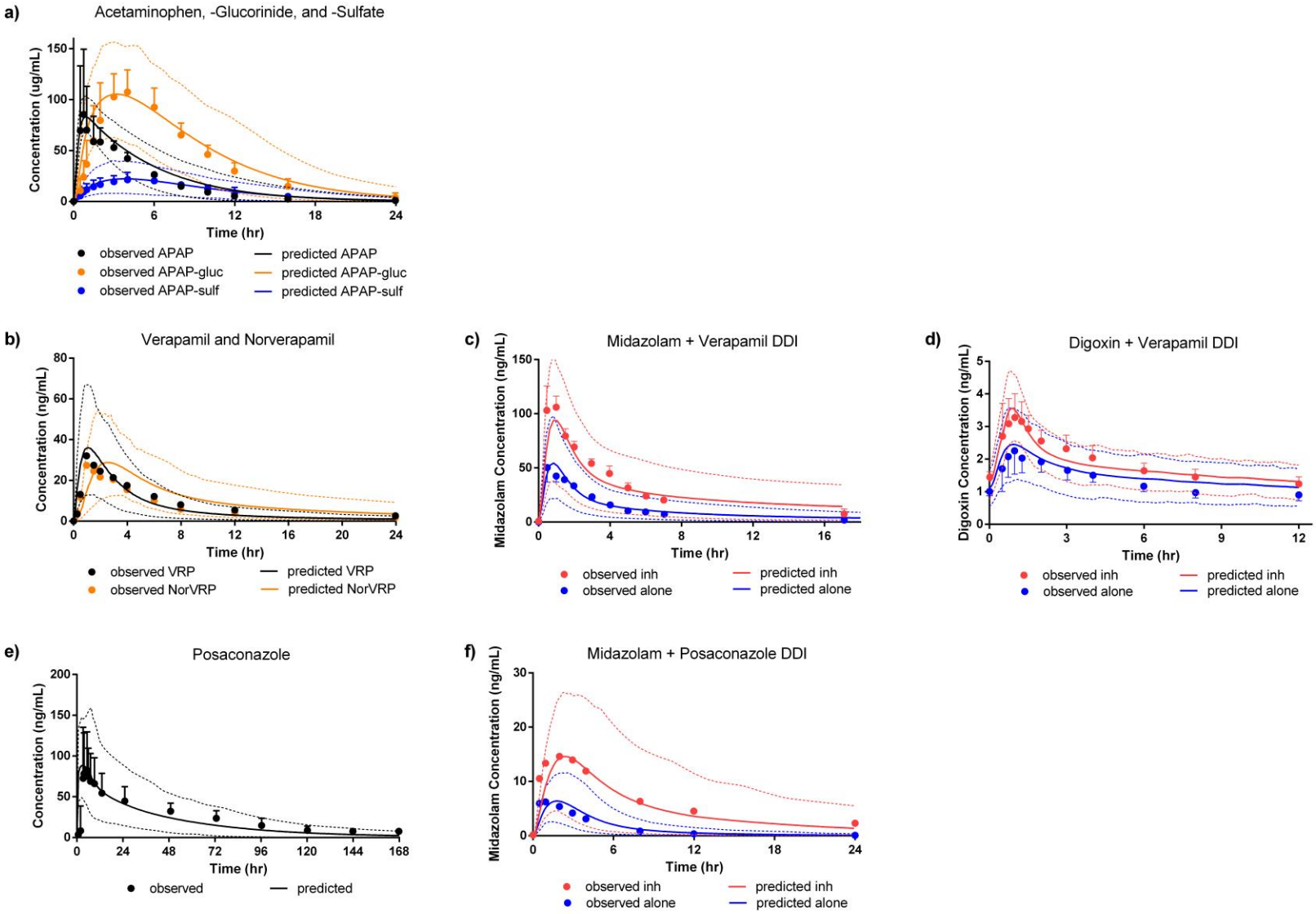

Figure 3.4. Observed and simulated plasma concentration vs. time profiles in heathy volunteers after a single oral dose with and

without inhibitor. Panels: a) acetaminophen (Chiew 2010); b) verapamil (Sawicki 2002); c) midazolam and verapamil (Backman 1994); d) digoxin and verapamil (Rodin 1988); e) posaconazole (Krishna 2012); f) midazolam and posaconazole (Krishna 2009). Shown: predicted concentration (solid curve); 5^{th} and 95^{th} confidence intervals (dashed curves). In a), b), and e), black curves represent parent drug and colored curves represent linked metabolites. In c), d), and f), blue curves represent the object drug concentrations under control conditions and red curves represent the object drug concentrations in the presence of inhibitor.

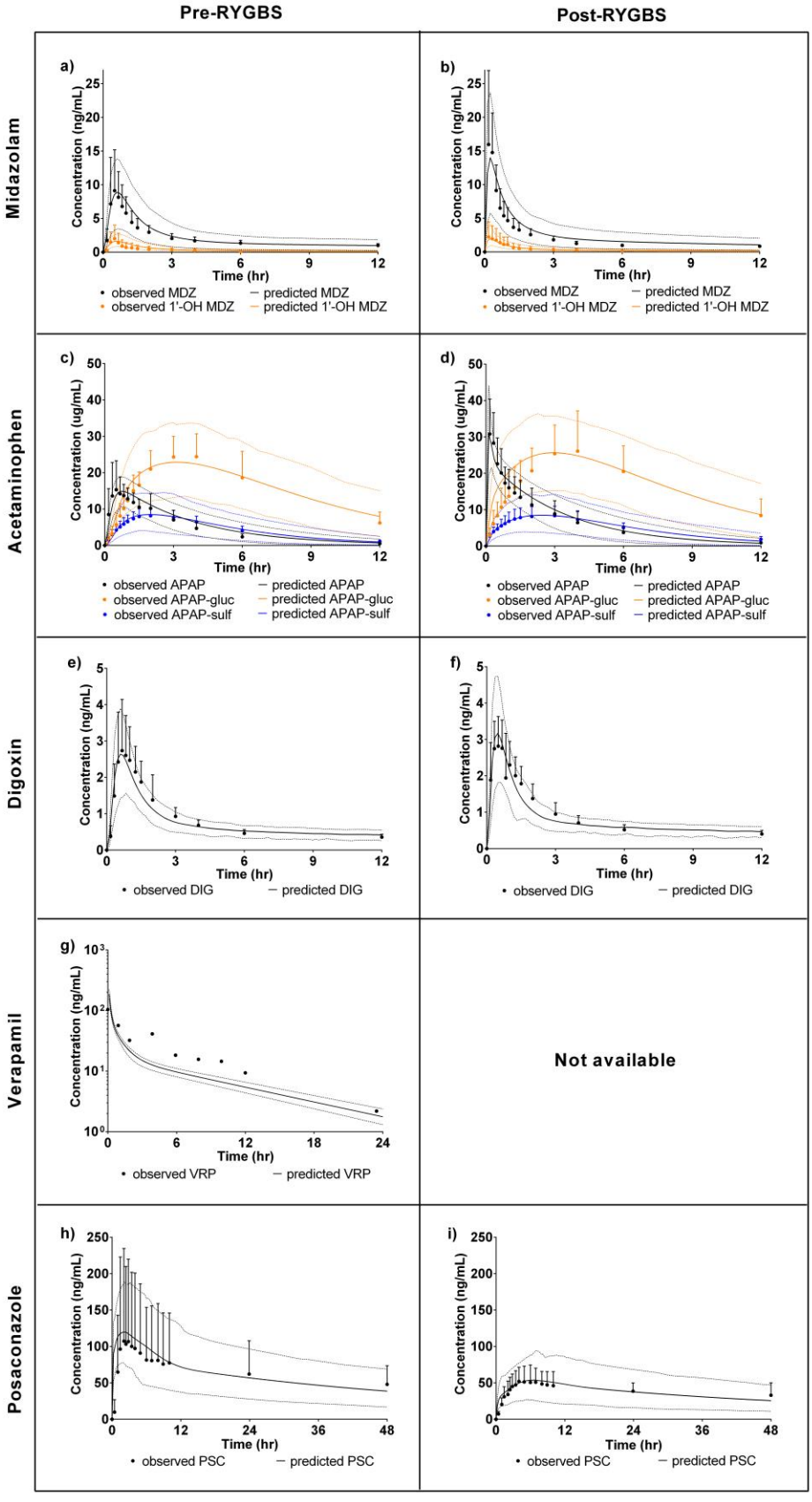
Pre-RYGBS
Post-RYGBS
Midazolam
Acetaminophen
Digoxin
Verapamil
Posaconazole
a)
b)
c)
d)
e)
f)
g)
h)
i)
Concentration (ng/mL)
Concentration (ug/mL)
Time (hr)
observed MDZ
predicted MDZ
observed 1'-OH MDZ
predicted 1'-OH MDZ
observed APAP
predicted APAP
observed APAP-gluc
predicted APAP-gluc
observed APAP-sulf
predicted APAP-sulf
observed DIG
predicted DIG
observed VRP
predicted VRP
observed PSC
predicted PSC
Not available

Figure 3.5. Simulated vs. observed plasma concentration-time profiles in morbidly obese patients before and after RYGBS. Shown: observed mean concentration (dot) and standard deviation (bar); predicted concentration (solid curve); 5^{th} and 95^{th} confidence intervals (dashed curves); parent (black curve); linked metabolite (colored curve). Panels: a-b) midazolam (Chan 2015); c-d) acetaminophen (Chen 2020); e-f) digoxin (Chan 2015); g) verapamil (Abernethy 1988); h-i) posaconazole (Gesquiere 2016).

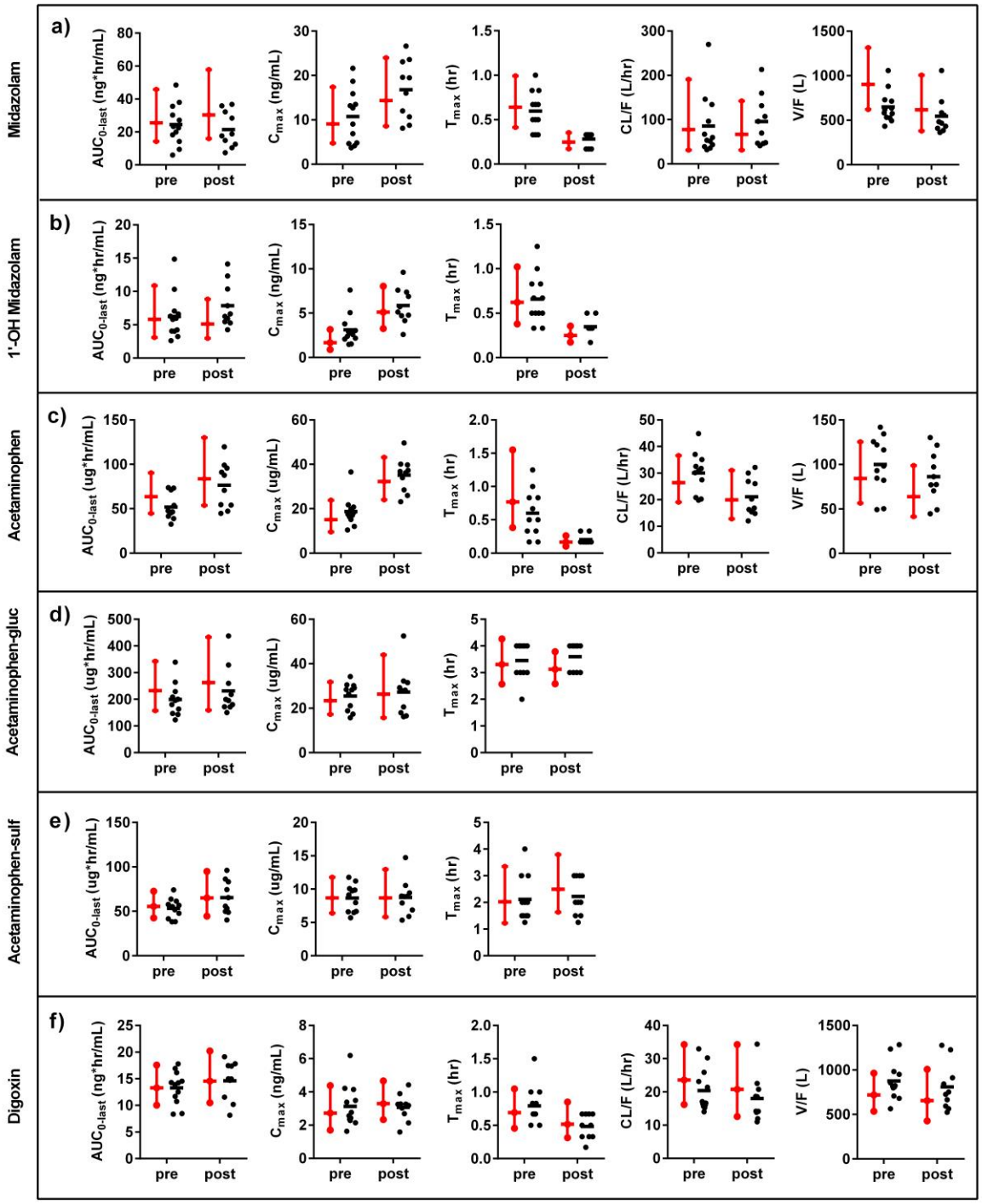

Figure 3.6. Simulated vs. observed pharmacokinetic parameters in morbidly obese patients using PBPK models with linked metabolites. Shown: 99.998% geometric confidence interval calculated using the equation by Abduljalil et al. (Abduljalil et al. 2014) (red); observed individual and mean values estimated using non-compartmental analysis (black). $AUC_{0\text{-last}}$ = area under the concentration-time curve from 0 to last observed timepoint, C_{max} = peak concentration,

T_{max} = time to peak concentration, CL/F = apparent oral clearance, and V/F = apparent volume of distribution. Panels: a) midazolam (Chan 2015); b) 1'-hydroxymidazolam (Chan 2015); c) acetaminophen (Chen 2020); d) acetaminophen-glucuronide (Chen 2020); e) acetaminophen-sulfate (Chen 2020); f) digoxin (Chan 2015).

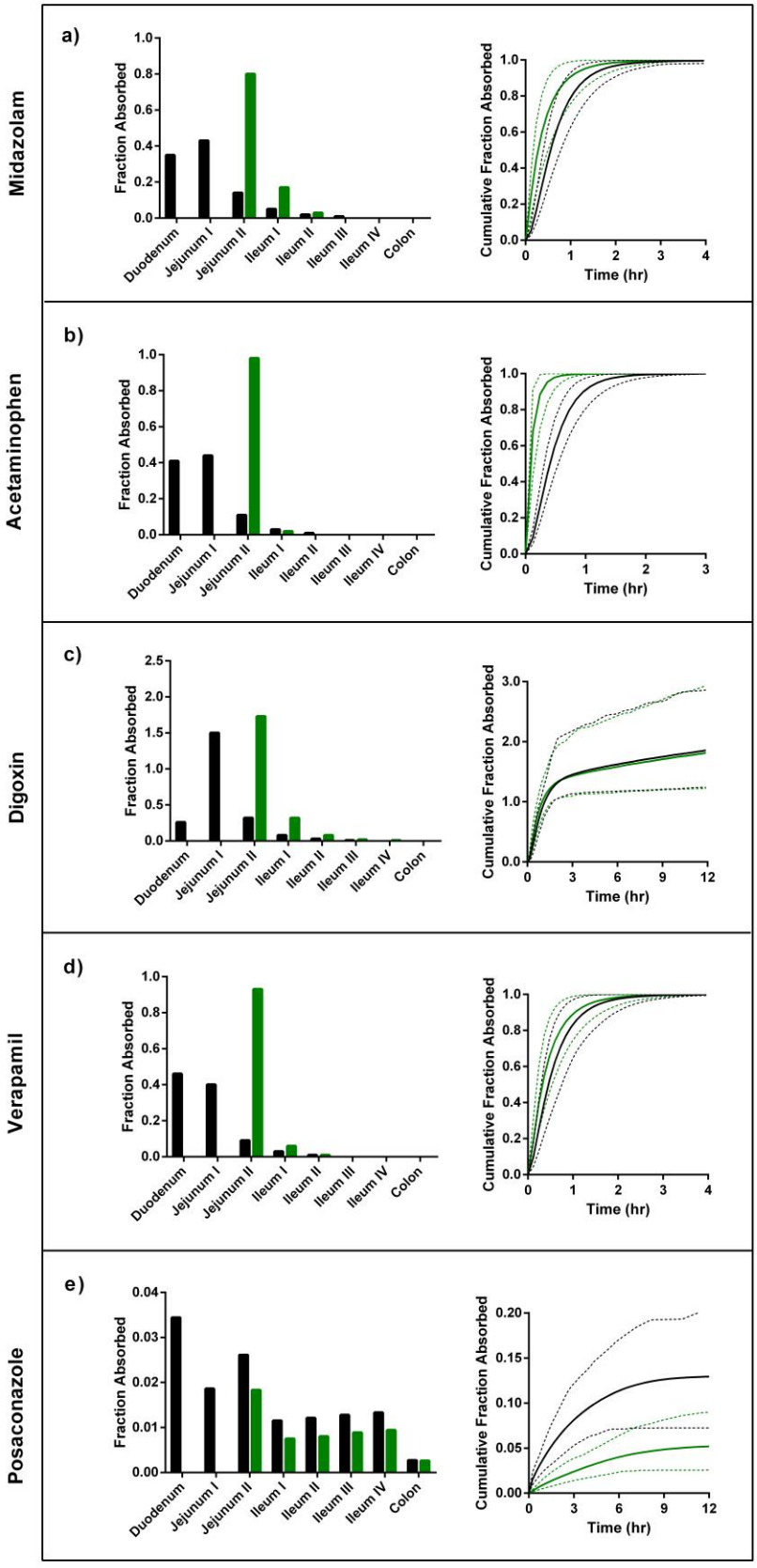
a)
Midazolam
Fraction Absorbed
Duodenum
Jejunum I
Jejunum II
Ileum I
Ileum II
Ileum III
Ileum IV
Colon
Cumulative Fraction Absorbed
Time (hr)
b)
Acetaminophen
c)
Digoxin
d)
Verapamil
e)
Posaconazole

Figure 3.7. Graphs of the regional intestinal absorption (bar graphs) and cumulative absorption over time (line graphs). Shown: pre-RYGBS patients (black); post-RYGBS patients (green); predicted cumulative absorption (solid curve); 5^{th} and 95^{th} confidence intervals (dashed curves). Panels: a) midazolam; b) acetaminophen; c) digoxin; d) verapamil; e) posaconazole.

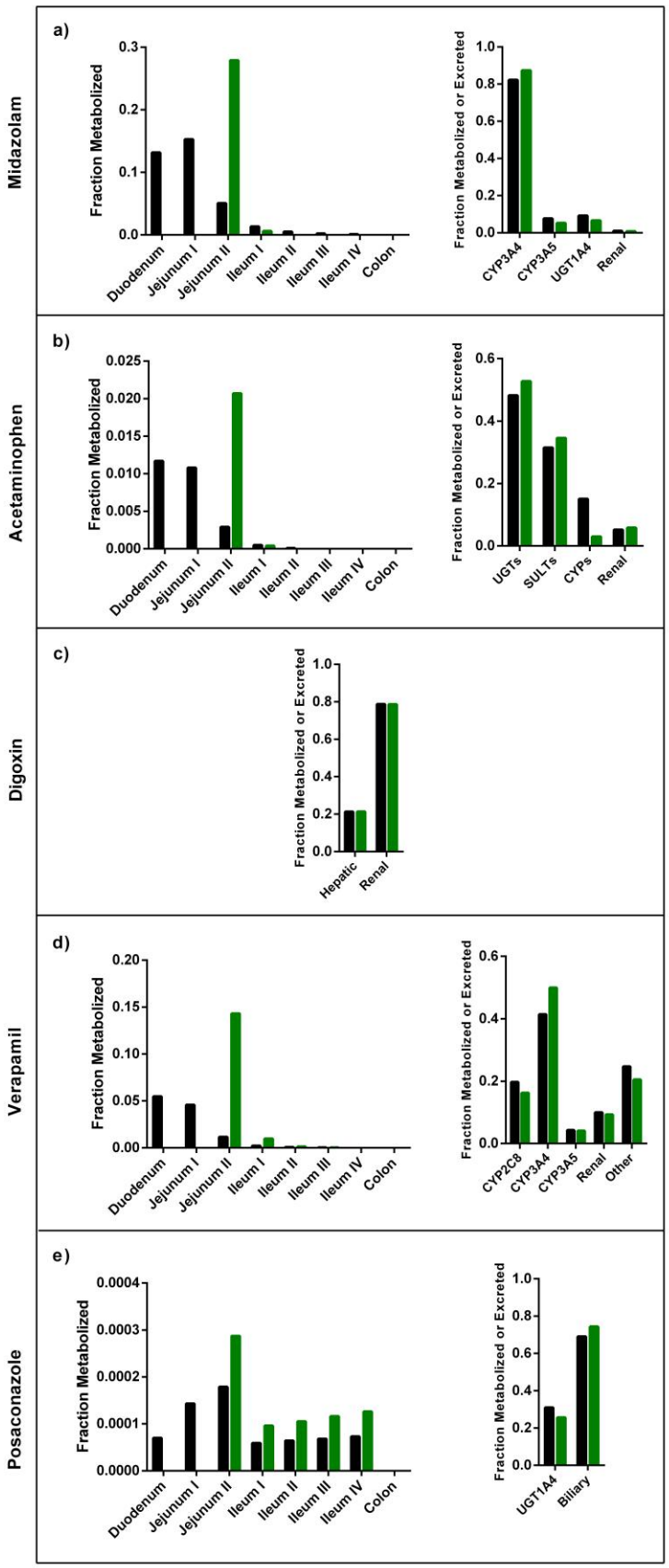
Midazolam
a)
Fraction Metabolized
0.3
0.2
0.1
0.0
Duodenum
Jejunum I
Jejunum II
Ileum I
Ileum II
Ileum III
Ileum IV
Colon
Fraction Metabolized or Excreted
1.0
0.8
0.6
0.4
0.2
0.0
CYP3A4
CYP3A5
UGT1A4
Renal
Acetaminophen
b)
Fraction Metabolized
0.025
0.020
0.015
0.010
0.005
0.000
Duodenum
Jejunum I
Jejunum II
Ileum I
Ileum II
Ileum III
Ileum IV
Colon
Fraction Metabolized or Excreted
0.6
0.4
0.2
0.0
UGTs
SULTs
CYPs
Renal
Digoxin
c)
Fraction Metabolized or Excreted
1.0
0.8
0.6
0.4
0.2
0.0
Hepatic
Renal
Verapamil
d)
Fraction Metabolized
0.20
0.15
0.10
0.05
0.00
Duodenum
Jejunum I
Jejunum II
Ileum I
Ileum II
Ileum III
Ileum IV
Colon
Fraction Metabolized or Excreted
0.6
0.4
0.2
0.0
CYP2C8
CYP3A4
CYP3A5
Renal
Other
Posaconazole
e)
Fraction Metabolized
0.0004
0.0003
0.0002
0.0001
0.0000
Duodenum
Jejunum I
Jejunum II
Ileum I
Ileum II
Ileum III
Ileum IV
Colon
Fraction Metabolized or Excreted
1.0
0.8
0.6
0.4
0.2
0.0
UGT1A4
Biliary

Figure 3.8. Graphs of regional intestinal metabolism, fraction metabolized per enzyme and fraction excreted unchanged. Shown: pre-RYGBS patients (black); post-RYGBS patients (green). Panels: a) midazolam; b) acetaminophen; c) digoxin; d) verapamil; e) posaconazole.

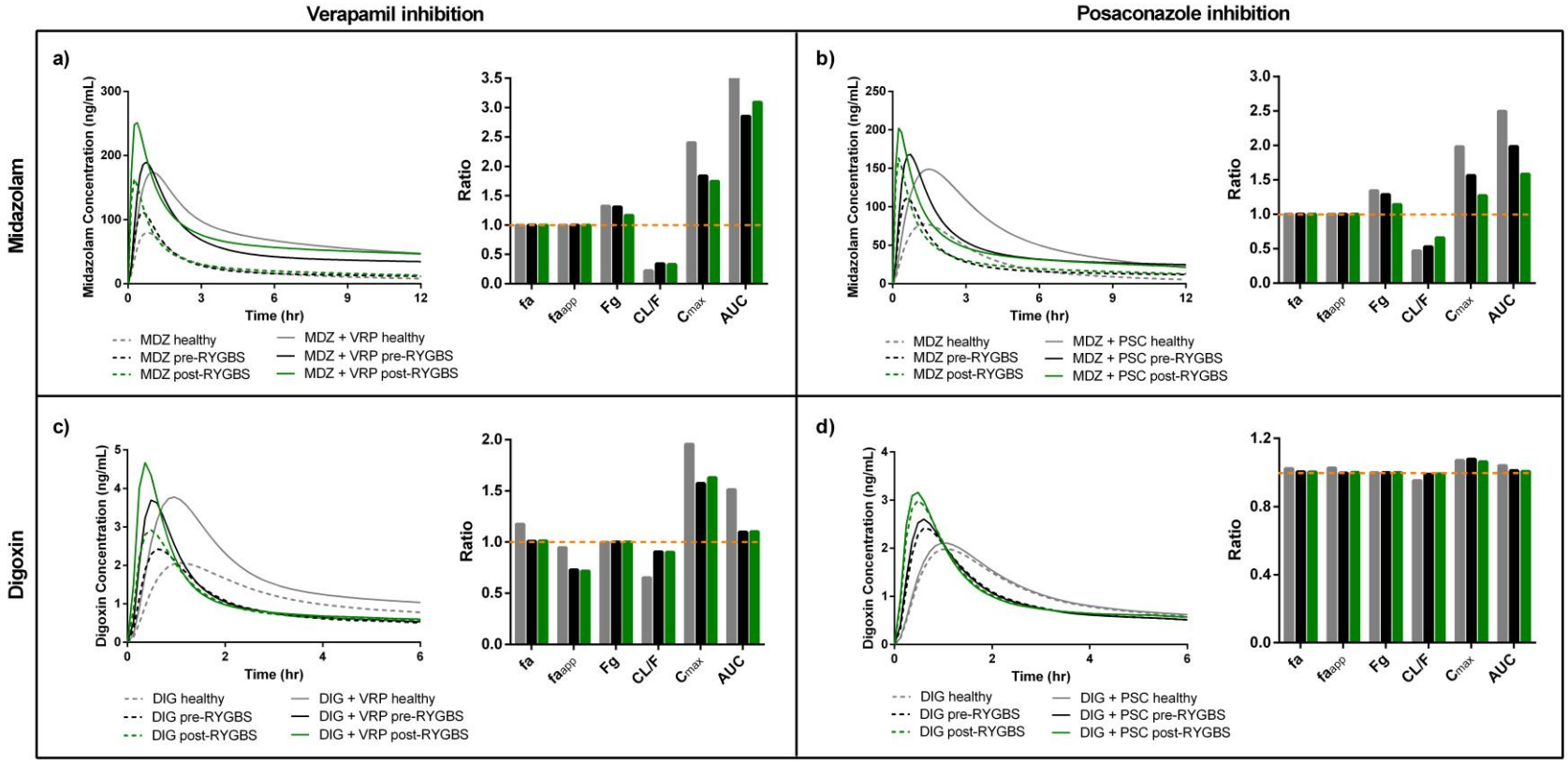

Figure 3.9. Predicted midazolam and digoxin concentrations with and without inhibition by verapamil or posaconazole and associated inhibited-to-control ratios. Panels: a) midazolam with verapamil; b) midazolam with posaconazole; c) digoxin with verapamil; d) digoxin with posaconazole. Shown: healthy subjects (gray); pre-RYGBS patients (black); post-RYGBS patients (green); predicted concentration (solid curves); 5th and 95th confidence intervals (dashed curves); ratio = 1 (orange dashed line). Inhibited-to-control parameter ratios: fa = fraction absorbed, fa,app = fraction absorbed accounting for drug reabsorption following P-gp efflux, Fg = fraction escaping first pass intestinal metabolism, CL/F = apparent oral clearance, C_{max} = peak concentration, AUC = area under the concentration-time curve.

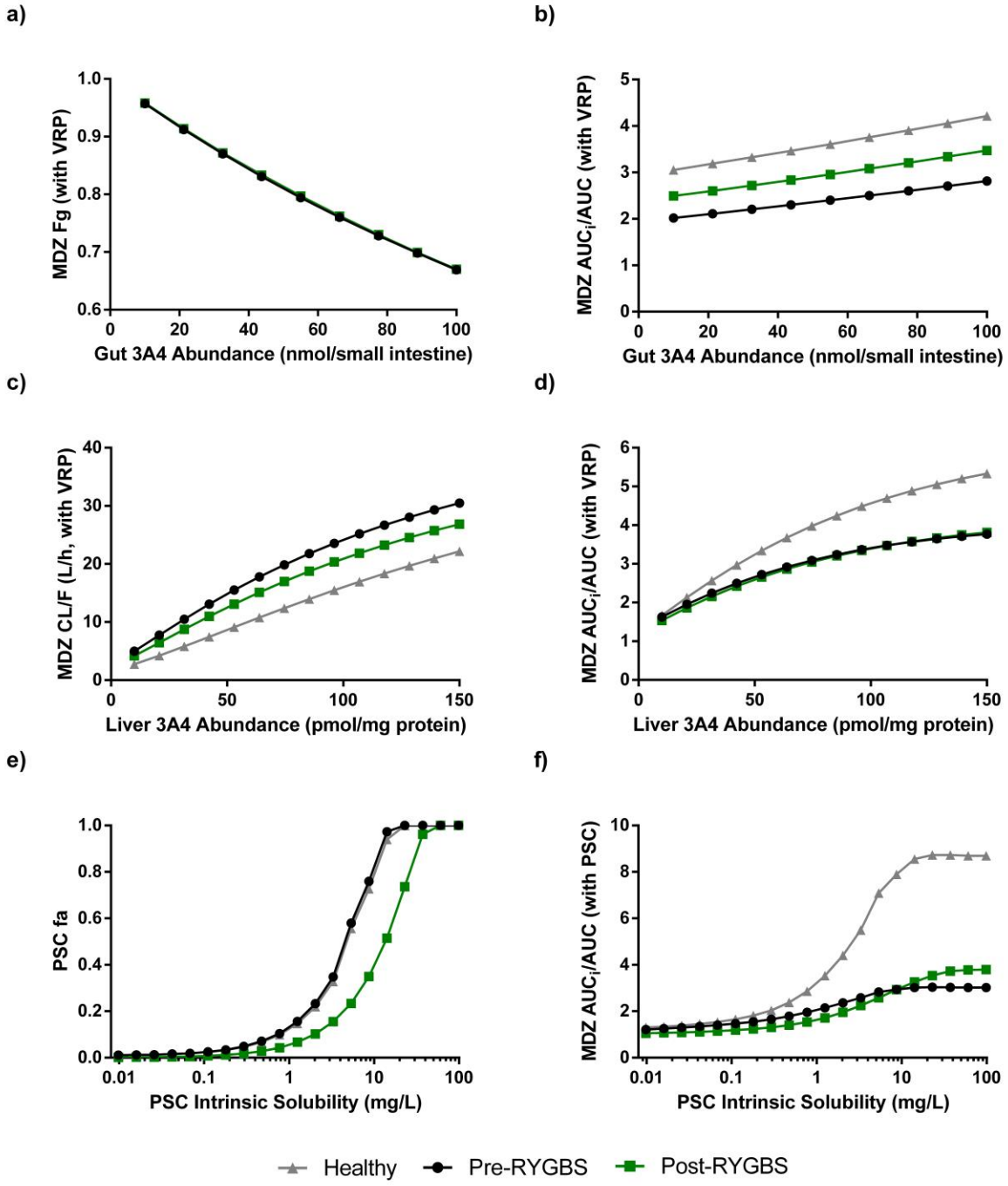

Figure 3.10. Sensitivity analysis of intestinal and hepatic CYP3A expression and posaconazole solubility on DDIs in healthy subjects (gray), pre-RYGBS patients (black), and post-RYGBS patients (green). Panels: a) midazolam fraction escaping first pass intestinal metabolism (Fg) vs. intestinal CYP3A4 abundance; b) inhibited midazolam AUC ratio vs. intestinal CYP3A4 abundance; c) apparent oral midazolam clearance vs. hepatic CYP3A4 abundance; d) inhibited

midazolam AUC ratio vs. hepatic CYP3A4 abundance; d) posaconazole fraction absorbed (fa) vs. posaconazole solubility; e) inhibited midazolam AUC ratio vs. posaconazole solubility.

CHAPTER 4

Identifying Kinetic Characteristics of a Potential Hepatic CYP3A Endogenous Biomarker

4.1 Introduction

The cost of clinical studies is a major contributor to the overall expense in development of a new chemical entity (NCE) (Morgan et al. 2011). Across the various therapeutic areas, the Phase 2 and Phase 3 clinical study costs are estimated at $7 million for cardiovascular indications, $11.5 million for dermatological indications, $19.6 for hematological indications, and $52.9 for anesthesia (Sertkaya et al. 2016). Apart from necessary clinical studies to determine the pharmacokinetics, efficacy and tolerability in humans, drug-drug interaction (DDI) studies may need to be conducted based on *in vitro* data. Typical DDI studies are conducted during late Phase 2 and Phase 3 stages (Kuhlmann 1994). The criteria, such as *in vitro* data suggesting that the NCE may be an enzyme inhibitor or cause induction of enzymes, are described in the guidance written by the US Food and Drug Administration and its international counterparts (Rekic et al. 2017). However, in one report, about 30% of the DDI study outcomes were falsely predicted based on *in vitro* data (15% false positive and 14% false negative), thereby causing tremendous loss in financial resources and time (3). Many studies have focused on addressing the discrepancy between *in vitro* predictions and *in vivo* outcomes resulting from inaccurate protein binding measurements, inconsistent IC50s for inhibition assessed using different probe substrates, and variability in expression systems or incubation conditions (3,4). Nonetheless, if the NCE has the potential to cause a DDI, clinically-relevant alternative screening methods conducted at an earlier stage of drug development, can reduce the number of full drug-drug interactions trials needed and lessen the financial burden for pharmaceutical companies.

For example, demonstrating that the NCE has no DDI risk as early as in First-in-Human clinical studies may avert the need for further dedicated DDI clinical trials. If the typical DDI

study relies on the use of a probe drugs or sensitive index substrates to detect a DDI, how can that be done in a First-in Human study? The use of endogenous biomarkers, which respond dynamically to *in vivo* enzyme or transporter activity, could be an alternative approach. This is not a new area of research as endogenous substrates of cytochrome P450 3A4 (CYP3A4), responsible for the breakdown of more than 50% of drugs undergoing metabolism (Paine et al. 2006, Achour et al. 2014), have been studied for decades. Urinary 6β-hydroxycortisol/cortisol was the first identified endogenous biomarker in the 1980s (Saenger et al. 1981, Ged et al. 1989). More recently, several other endogenous biomarkers for hepatic CYP3A4 have been proposed, including urinary 6β-hydroxy-cortisone/cortisone (with 6β-hydroxycortisol/cortisol), plasma 4β-hydroxycholesterol (4β-OHC), urinary 7β-hydroxy-dehydroepiandrosterone/dehydroepiandrosterone (7β-OH-hydroxy-DHEA/DHEA), and urinary 1β-hydroxydeoxycholic acid/deoxycholic acid (1β-OH-DCA/DCA) (Mariappan et al. 2017).

As briefly presented below, each of these endogenous biomarkers has limitations for assessing CYP3A4 activity. Diurnal variation of cortisol, the interconversion of cortisol with cortisone, and active renal secretion by organic anion transporter 3 (OAT3) lead to a high variability in the urinary 6β-hydroxy-cortisol/cortisol ratio and can confound its utility in assessing CYP3A4 activity (Chen et al. 2006, Peng et al. 2011, Imamura et al. 2014). While sensitive for assessing CYP3A4 induction, plasma 4β-hydroxycholesterol cannot detect short-term CYP3A4 inhibition due to its the long half-life (Shin et al. 2013, Kasichayanula et al. 2014, Mao et al. 2017). Although the urinary 7β-OH-DHEA/DHEA ratio was moderately correlated (r^2 = 0.407) with intravenous midazolam clearance under induced and inhibited conditions, the *in vitro* validation of 7β-OH-DHEA as a specific CYP3A4 substrate is lacking (Shin et al. 2013).

Finally, 1β-OH-DCA showed promising *in vitro* sensitivity and selectivity for CYP3A4 inhibition based on incubation studies, but clinical validation is needed (Hayes et al. 2016).

Although the need for CYP3A4 endogenous biomarkers is acknowledged, the kinetic characteristics required for a useful endogenous CYP3A4 biomarker remains obscure. A useful biomarker must be sensitive to short- and long-term changes in CYP3A4 activity, but also be selective for CYP3A4 activity. Sensitivity is affected by the half-lives of the parent and its metabolite, and the indices for quantifying the change in the endogenous biomarker, such as peak metabolite concentration changes and area under the curve (AUC). Selectivity is affected by the fraction metabolized by CYP3A4 as well as the fraction metabolized to the metabolite of interest. The CYP3A4 endogenous biomarker should reflect CYP3A4 induction, moderate competitive inhibition, strong competitive inhibition, and mechanism-based inhibition. This simulation study was conducted to explore the effects of altering metabolite half-life, the fraction metabolized by CYP3A4 and the fraction metabolized to the metabolite of interest on the utility of a hypothetical CYP3A4 endogenous biomarker under different DDI scenarios. The goal of this work was to provide a better understanding of the kinetic characteristics of a useful endogenous CYP3A4 biomarker for DDIs studies.

4.2 Methods

Model structure

The structure of the models describing changes in CYP3A4 activity, endogenous parent and metabolite concentrations following administration of an inducer, a competitive inhibitor, and a mechanism-based inhibitor are illustrated in Figure 4.1. We further divided competitive inhibition into moderate and strong competitive inhibition for comparison. In each DDI scenario, we explored the interplay between sensitivity and selectivity with the half-life of metabolite vs. the fraction metabolized to the metabolite of interest (k_m vs. $f_{m,metabolite}$) and the half-life of metabolite vs. the fraction metabolized by CYP3A4 (k_m vs. $f_{m,CYP3A4}$). The former depicts the situation where the parent can be cleared by a different pathway, whereas the latter depicts the situation where the metabolite can be formed by enzymes other than CYP3A4. In addition, formation and elimination rate-limited metabolite kinetics were compared in each scenario. Formation rate-limited and elimination rate-limited kinetics were simulated assuming metabolite half-lives 0.5-fold shorter and 2-fold longer than the parent half-life, respectively.

Initial values, constants, and variables

Equations describing the rate of change of each species in the models are summarized in Table I. The starting condition was assumed to be at steady-state, in which the baseline values of CYP3A4, the metabolite, and Enz (the enzyme metabolizing rifampin) were set to 1 or an appropriate value. For the parent, the baseline value and the zero-order formation rate constant ($K_{in,\ parent}$) were derived using steady-state conditions:

For k_m vs. $f_{m,metabolite}$ interplay,

$$\frac{d[Met]}{dt} = [CYP3A4] \cdot f_m \cdot k_p \cdot [Par] - k_m \cdot [Met] = 0$$

$$f_m \cdot k_p \cdot [Par] = k_m$$

$$[Par] = \frac{k_m}{f_m k_p}$$

$$\frac{d[Par]}{dt} = K_{in,parent} - [CYP3A4] \cdot f_m \cdot k_p \cdot [Par] - (1 - f_m) \cdot k_p \cdot [Par] = 0$$

$$K_{in,parent} = [Par] \cdot k_p$$

$$K_{in,parent} = \frac{k_m}{f_m}$$

For k_m vs. $f_{m,CYP3A4}$ interplay,

$$\frac{d[Met]}{dt} = [CYP3A4] \cdot f_m \cdot k_f \cdot [Par] + (1 - f_m) \cdot k_f \cdot [Par] - k_m \cdot [Met] = 0$$

$$k_f \cdot [Par] = k_m$$

$$[Par] = \frac{k_m}{k_f}$$

$$\frac{d[Par]}{dt} = K_{in,parent} - [CYP3A4] \cdot f_m \cdot k_f \cdot [Par] - (1 - f_m) \cdot k_f \cdot [Par] = 0$$

$$K_{in,parent} = [Par] \cdot k_f$$

$$K_{in,parent} = k_m$$

To test the DDIs, the precipitants are based on actual inducers and inhibitors listed as clinical index inducers or inhibitors by the FDA. The drug-associated constants were borrowed from rifampin (inducer), fluconazole (moderate competitive inhibitor), itraconazole (strong competitive inhibitor), and clarithromycin (mechanism-based inhibitor) provided in Simcyp (version 17, Certara, Princeton, NJ) or from literature values (Csajka et al. 2001, Abduljalil et al. 2009, Svensson et al. 2018). As used in DDI clinical studies, 600 mg rifampin was administered once daily for 7 days for CYP3A4 induction and 500 mg clarithromycin was administered twice

daily for 3 days for mechanism-based inhibition of CYP3A4. A single dose of 200 mg fluconazole or 200 mg itraconazole was simulated for strong and moderate competitive inhibition, respectively. The CYP3A4 half-life was assumed to be 29 hours (Ramsden et al. 2015). The metabolite half-life ($t_{1/2,m} = \ln 2/k_m$) was simulated from 1 to 168 hours by 1-hour increment. The parent half-life was either 0.5-, 1-, or 2-fold of the metabolite half-life to represent elimination rate-limited (0.5- and 1-fold) and formation rate-limited kinetics (2-fold). The values of f_m for $f_{m,metabolite}$ and $f_{m,CYP3A4}$ were 0.01, 0.25, 0.5, 0.75, and 1. All the constants and variable sample spaces in our simulations are summarized in Table 4.1.

Sensitivity index

The threshold for a DDI was defined as a cutoff value of a 20% change in the index (i.e., greater than or equal to 1.2 for an induced-to-baseline ratio or less than or equal to 0.8 for an inhibited-to-baseline ratio). Multiple sensitivity indices were explored. Theoretically, metabolite concentration (C_m) and metabolite-to-parent concentration ratio (C_m/C_p) sampled at their maximal values for induction and at their minimal values for inhibition, would be the most sensitive measures of DDIs. However, sampling at the maximal changes is only achievable in theoretical simulations as the timing would be difficult to predict in real life. Therefore, a practical version of C_m and C_m/C_p were sampled at the time of the precipitant drug's peak concentration (t_{max}) after a single dose or the last dose for multiple dosing of the precipitant. Alternatively, using the area under the concentration time curve (AUC) avoids the inconvenience in determining the exact timing for spot sampling. Thus, we also included metabolite AUC (AUC_m) and metabolite-to-parent AUC ratio (AUC_m/AUC_p) for practicality. The sampling time for AUC was from time = 0 to t_{max} plus four of the precipitant half-lives following a single dose and was from 0 to tau for the last dose in the multiple dosing scenario.

Simulation platform

All endogenous biomarker simulations were performed and visualized in R (version 3.6.0) using RxODE (package version 0.9.2) and ggplot2 (package version 3.3.0). Intravenous midazolam DDIs were simulated using Simcyp (Certara, version xx) with the built-in drug files for each of the DDI scenarios. The Simcyp physiological-based pharmacokinetic DDI models were previously validated (Ke et al. 2014, Almond et al. 2016, Chen et al. 2016, Cristofoletti et al. 2016, Marsousi et al. 2018). The control-to-induced and control-to-inhibited midazolam AUC ratios in healthy Caucasians were predicted for sensitivity comparisons.

4.3 Results

Induction

Multiple-dose induction simulations are shown in Figure 2. In the absence of other pathways or enzymes other than CYP3A4 in the formation of metabolite ($f_{m,metabolite}$ = 1 or $f_{m,CYP3A4}$ = 1), the fold-change in peak C_m was nearly constant as the metabolite half-life increased. However, the fold-change in peak C_m was progressively less sensitive (20% threshold colored in gray) under elimination-rate limited kinetics for the metabolite. When the metabolite half-life was longer than 72 hours, C_m at the precipitant t_{max} and AUC_m had similar fold-changes compared to peak C_m.

As $f_{m,metabolite}$ decreased, the fold-change in peak C_m was higher and declined as the metabolite half-life increased. As expected, when $f_{m,metabolite}$ was small, C_p was unchanged during CYP3A4 induction. In contrast, when $f_{m,metabolite}$ was large, C_p decreased during CYP3A4 induction, which resulted in increased ratios for max C_m/C_p, C_m/C_p at the precipitant t_{max} and AUC_m/AUC_p. A smaller $f_{m,metabolite}$ resulted in an inversion of the rank ordering of the fold-change relationships: peak C_m, C_m at the precipitant t_{max} and AUC_m were highest for the lowest $f_{m,metabolite}$, whereas max C_m/C_p, C_m/C_p at the precipitant t_{max} and AUC_m/AUC_p were highest when f_m = 1. C_m/C_p at the precipitant t_{max} and AUC_m/AUC_p were sensitive indices for induction regardless of $f_{m,metabolite}$ and metabolite half-life, but their fold-change upon induction decreased with decreasing $f_{m,metabolite}$ and increasing metabolite half-life. For formation rate-limited kinetics, C_m and AUC_m were useful in assessing induction even under high $f_{m,metabolite}$ conditions, if the metabolite half-life was longer than 36 hours. For elimination rate-limited kinetics, C_m and AUC_m were useful only when CYP3A4 metabolism was less than 75% of all of the clearance pathways.

When considering $f_{m,CYP3A4}$, as $f_{m,CYP3A4}$ decreased, the fold-change in peak C_m and AUC_m decreased because the formation of the metabolite was less dependent on the induced CYP3A4 pathway. C_m and AUC_m were only useful when $f_{m,CYP3A4}$ was higher than 25% and under formation rate-limited metabolite kinetics. The sensitivity was amplified by normalizing with C_p or AUC_p, particularly in situations where C_m and AUC_m were insensitive due to low $f_{m,CYP3A4}$ or elimination-rate limited kinetics. Peak C_m/C_p and AUC_m/AUC_p were sensitive indices of CYP3A4 induction across all metabolite half-life even when $f_{m,CYP3A4}$ dropped to 25%. The magnifying effect became negligible when $f_{m,CYP3A4}$ was set to 1% as C_p was nearly constant.

The peak C_m/C_p and AUC_m/AUC_p ratios showed an inverse U-shaped fold-change curve over metabolite half-life. Upon multiple dosing of the inducer, C_m increased in early doses due to increased formation, but declined at later doses as C_p continued to drop (when the elimination rate exceeded the rate of synthesis, shown in Figure 4.3). The decline in peak C_m/C_p and AUC_m/AUC_p ratios occurred earlier with shorter metabolite half-lives. In contrast, metabolites with a long half-life for a given $f_{m,metabolite}$ were less sensitive to induction as the accumulation of the metabolite to the new steady-state was dependent on the metabolite half-life. Therefore, the fold-change in peak C_m/C_p and AUC_m/AUC_p ratios was dampened at short and long metabolite half-lives. This phenomenon was most noticeable for formation rate-limited kinetics and when $f_{m,metabolite}$ or $f_{m,CYP3A4}$ was high.

Strong competitive inhibition

Simulations for single-dose strong competitive inhibition are shown in Figure 4.4. When $f_{m,metabolite}$ and $f_{m,CYP3A4}$ were set to 1.0, the theoretical trough C_m was able to detect CYP3A4 inhibition with a maximum half-life of 96 hours for a formation-rate limited metabolite and 72

hours for an elimination rate-limited metabolite. When normalized by C_p, the theoretical trough C_m/C_p index was sensitive enough to assess inhibition with a metabolite half-life up to 168 hours. However, sampling at the metabolite trough is not realistic due to difficulties in determining when the trough would occur. When sampled at the precipitant t_{max}, C_m and C_m/C_p were restricted to metabolites with a maximum half-life between 12 and 24 hours. The loss of sensitivity is likely a result of the precipitant t_{max} occurring at the early stage of metabolite decline.

AUC_m can be used as an index for strong inhibition, but only for formation-rate limited kinetics when the metabolite half-life was between 12 to 60 hours. To understand the cause of the valley-shaped fold-change curve vs. metabolite half-life, one must consider the full time course of the C_m curves. The C_m vs. time curves after administration of a strong inhibitor can be separated into four stages: decline, rebound, overshoot and recovery (illustrated in Figure 4.5). Metabolite concentrations declined as CYP3A was inhibited, but the trough C_m lagged behind the peak inhibitor concentration. As the inhibitor concentrations dropped, C_p increased above baseline levels, and C_m hit trough levels and rebounded. The higher C_p caused increased metabolite formation and higher C_m, surpassing the basal C_m levels, with a return to basal C_m levels dependent on the metabolite half-life. The decline and rebound contributed to the decrease in AUC_m but the overshoot and recovery offset the decrease. A short metabolite half-life temporally compressed the four stages, while a long metabolite half-life resulted in a prolongation of the stages. Sampling from time = 0 to four precipitant half-lives would include the recovery stage if the metabolite half-life was short and would omit parts of the decline, overshoot and rebound stages if the metabolite half-life was long. Both extremes of metabolite half-life suppressed the fold-change in AUC_m.

The best index for detecting single dose, strong competitive inhibition when a single metabolite was formed entirely by CYP3A4 ($f_{m,metabolite}$ =1 and $f_{m,CYP3A4}$ = 1) was AUC_m/AUC_p, considering both sensitivity and practicality. AUC_m/AUC_p was sensitive for metabolites with a half-life of up to 108 hours for a formation rate-limited metabolite and 168 hours for an elimination rate-limited metabolite. However, with decreases in $f_{m,metabolite}$ or $f_{m,CYP3A4}$, the utility of AUC_m/AUC_p decreased. As $f_{m,metabolite}$ or $f_{m,CYP3A4}$ decreased, more parent could be cleared through an uninhibited pathway or metabolite would be formed by an uninhibited enzyme, thereby reducing C_p. A decrease in $f_{m,CYP3A4}$ had a higher impact on AUC_m/AUC_p than a decrease in $f_{m,metabolite}$ and was more apparent moving from formation to elimination rate-limited kinetics. When $f_{m,metabolite}$ was 50%, the maximum of metabolite half-life was 90 hours for a formation rate-limited metabolite and 132 hours for an elimination rate-limited metabolite. When $f_{m,CYP3A4}$ was 50%, the maximum metabolite half-life was 36 hours for a formation rate-limited metabolite and 72 hours for an elimination rate-limited metabolite. AUC_m/AUC_p was insensitive when $f_{m,CYP3A4} \leq 25\%$ as the metabolite formation essentially became independent of CYP3A4 activity. In contrast, AUC_m was more sensitive at lower $f_{m,metabolite}$. When $f_{m,metabolite}$ was 1%, AUC_m could be used for metabolites with a half-life up to 72 hours. Because C_p was unaffected, C_m did not overshoot after rebounding following CYP3A4 inhibition, making the change in AUC_m more directly correlated with the change in CYP3A4 activity.

Moderate competitive inhibition

Simulations following a single dose of a moderate competitive inhibitor are shown in Figure 4.6. The trends were similar to the single dose of a strong competitive inhibition, but the magnitude of the fold-change in the various indices following inhibition were smaller. At 100% $f_{m,metabolite}$ and $f_{m,CYP3A4}$, the theoretical trough C_m could detect CYP3A4 inhibition with a

maximum half-life of 36 hours for formation rate-limited metabolite, but was insensitive at all metabolite half-lives for elimination rate-limited metabolites. Normalizing by C_p for the C_m/C_p ratio widened the formation and elimination rate-limited metabolite half-life windows to 84 hours and 108 hours, respectively. However, the sensitivity of practical indices for detecting CYP3A4 inhibition was restricted. C_m and C_m/C_p at the precipitant t_{max} may be impractical as a metabolite half-life of less than 12 hours was required and AUC_m lacked sensitivity at any metabolite half-life simulated. The AUC_m/AUC_p was sensitive for metabolites with half-lives less than 48 hours for a formation rate-limited metabolite and 96 hours for an elimination rate-limited metabolite.

Although AUC_m/AUC_p was the best option to detect moderate inhibition when a single metabolite was formed entirely by CYP3A4, the sensitivity of AUC_m/AUC_p decreased with decreasing $f_{m,CYP3A4}$ or $f_{m,metabolite}$. The AUC_m/AUC_p was insensitive at any metabolite half-life when $f_{m,CYP3A4}$ was less than 75%. When $f_{m,metabolite}$ was as low as 1%, AUC_m and AUC_m/AUC_p required a metabolite half-life of less than 24 hours, though in reality, any variability in $f_{m,metabolite}$ would result in no inhibition being detected as values were very close to the 0.8 threshold (i.e., estimated 0.75 fold-change).

Mechanism-based inhibition

The multiple dose, mechanism-based inhibition simulations are shown in Figure 4.7. The overall trend in the fold-change of the various indices resembled those following single-dose, strong competitive inhibition. However, the repeated dosing of the MBI decreased hepatic CYP3A4 levels and led to higher accumulation of the inhibitor due to auto-inhibition following each subsequent dose (Figure 4.8). The resulting C_m reduction from baseline to the last MBI dose was substantial, resulting in larger fold-changes than observed with competitive inhibition. Both

AUC_m and C_m manifested the "valley" fold-change pattern (seen with the four stages: decline, rebound, overshoot and recovery), which was only observed for AUC_m following strong competitive inhibition.

For $f_{m,metabolite} = 1$ or $f_{m,CYP3A4} = 1$, the theoretical trough C_m and minimum C_m/C_p were sensitive across almost all the metabolite half-lives, except for the trough C_m when the metabolite half-life was less than 4 hours for an elimination-rate limited metabolite. During each dosing interval for the MBI, a shorter metabolite half-life resulted in C_m that mirrored the precipitant drug concentration vs. time curve and a fast rebound and overshoot in C_m (Figure 4.8). For metabolites with long half-lives, no fluctuation was seen during the dosing interval for the MBI, although the rebound and overshoot occurred to varying degrees.

For formation rate-limited kinetics, the trough C_m and C_m/C_p at the precipitant t_{max} were sensitive for metabolites with half-lives up to 96 hours and 144 hours, respectively. AUC_m was sensitive for metabolites with a half-life up to 108 hours. For elimination rate-limited kinetics, the trough C_m, AUC_m and C_m/C_p at the precipitant t_{max} were sensitive for metabolites with half-lives up to 84 hours, 96 hours and 1 week, respectively. AUC_m/AUC_p was sensitive across the metabolite half-lives for either formation or elimination rate-limited metabolite kinetics. Both C_m/C_p and AUC_m/AUC_p were useful for mechanism-based inhibition assessment.

As $f_{m,metabolite}$ decreased, the sensitivity of trough C_m and AUC_m were not affected by metabolite half-life, but of the range of metabolite half-lives decreased for minimum C_m/C_p and AUC_m/AUC_p. At $f_{m,metabolite} = 1\%$, the minimum C_m/C_p and AUC_m/AUC_p were sensitive for metabolite half-lives up to 96 hours and 108 hours, respectively. When $f_{m,CYP3A4}$ was 50% for formation-rate limited kinetics and 25% for elimination-rate limited kinetics, C_m and AUC_m were not sensitive at most of the metabolite half-lives. At $f_{m,CYP3A4} = 50\%$, the ratios were more

sensitive with minimum C_m/C_p and AUC_m/AUC_p reflecting mechanism-based inhibition for metabolites with half-lives up to 60 hours and 72 hours, respectively for formation rate-limited kinetics and metabolite half-lives up to 120 hours and 132 hours, respectively for elimination rate-limited kinetics.

4.4 Discussion

This theoretical study investigates the kinetic characteristics of a useful CYP3A4 endogenous biomarker in different DDI scenarios and generalizes the sensitivity window in terms of metabolite half-life based on a 20%-change threshold. The dynamic approach used in our simulations better reflects time-dependent changes compared to a static approach and allows comparisons between theoretical vs. practical indices, and spot (C_m at the precipitant t_{max}) vs. continuous sampling (AUC_m). The variables (i.e., metabolite half-life, formation or elimination rate-limited kinetics, $f_{m,metabolite}$, and $f_{m,CYP3A4}$) created numerous scenarios and the overwhelming number of simulation results can be daunting. To facilitate selecting a CYP3A4 endogenous biomarker, the simulation results are summarized in Figure 4.9, by DDI scenario, kinetic characteristics, and the sensitive indices for given metabolite half-lives. As not all endogenous metabolites will have $f_{m,metabolite}$ and $f_{m,CYP3A4}$ = 100%, the lowest $f_{m,metabolite}$ and $f_{m,CYP3A4}$ detectable are included in the figure. For example, to detect competitive inhibition similar to that caused by a single dose of 200 mg itraconazole, a useful CYP3A4 endogenous biomarker that is formation-rate limited and has $f_{m,CYP3A4}$ as low as 50% needs to have a metabolite half-life of less than 36 hours and be quantified in the form of AUC_m/AUC_p. The figure provides a convenient way to guide the application of a biomarker.

The simulations confirm the usefulness and limitations of previously discovered CYP3A4 endogenous biomarkers. 4β-hydroxycholesterol, measured in plasma by spot sampling, is useful for induction assessment, but insensitive to competitive inhibition (Shin et al. 2013, Kasichayanula et al. 2014, Mao et al. 2017). 4β-hydroxycholesterol is formed mainly by CYP3A4 as a minor pathway of cholesterol metabolism (Mao et al. 2017). The half-lives of cholesterol and 4β-hydroxycholesterol are 72-120 hours and 60-64 hours, respectively (Bodin et

al. 2002, Daniels et al. 2009). According to the multiple dose simulations of induction, at 1% $f_{m,metabolite}$ and 100% $f_{m,CYP3A4}$, a formation-rate limited C_m is sensitive for metabolites with a half-life of up to 168 hours (Figure 2). For a metabolite with a 60 hours half-life, the simulations predicted a 3.75-fold increase in C_m at precipitant t_{max} after the last inducer dose. Shin et al. (2013) reported a 2.43-fold increase in 4β-hydroxycholesterol at steady-state after multiple dose administration of 600 mg rifampin once daily (n = 26) (Shin et al. 2013). Based on the single dose simulations of strong competitive inhibition, for 1% $f_{m,metabolite}$ and 100% $f_{m,CYP3A4}$, a metabolite half-life of less than 12 hours would be required for a sensitive C_m (Figure 3), explaining why Kasichayanula et al. (2014) observed a minimal decrease in 4β-hydroxycholesterol after a single 600 mg dose of ketoconazole (n = 34) (Kasichayanula et al. 2014). No change was observed in 4β-hydroxycholesterol even after four days of 400 mg ketoconazole given once daily (n = 24) (Lee et al. 2019). Although the half-life of 4β-hydroxycholesterol is too long for C_m to be sensitive, the simulations suggest that quantifying 4β-hydroxycholesterol AUC from time = 0 to four precipitant half-lives could detect strong competitive inhibition.

6β-hydroxycortisol/cortisol, another endogenous CYP3A4 biomarker, is measured in urine usually over 24 hours. The advantage of urinary sampling is convenience and non-invasiveness. Excreted parent and metabolite compounds accumulate in urine and the metabolite-to-parent urinary concentration ratio reflects plasma AUC_m/AUC_p with the assumption that the renal clearance of the parent and metabolite are equal. When the assumption is violated, it confounds the estimation of hepatic CYP3A4 activity. The half-lives of cortisol and 6β-hydroxycortisol are very short. The former is reported to be 1 hour in humans (Weitzman et al. 1971) and the latter is 1-2 hours in animals (no human data are available) (Lai et al. 1986). Based

on the simulations, at a metabolite half-life close to 1 hour, the fold-change of AUC_m/AUC_p becomes independent of $f_{m,metabolite}$ and metabolite kinetics. The $f_{m,CYP3A4}$ of cortisol hydroxylation is estimated to be 60% (Peng et al. 2011). At $f_{m,CYP3A4}$ = 60%, we predicted a steady-state AUC_m/AUC_p ~ 3.2-fold higher following CYP3A4 induction (Figure 2). Following 600 mg rifampin once daily, Shin et al. and Dutreix et al. reported a 1.48-fold (n = 24) and a 4-fold (n = 20) higher steady-state urinary 6β-hydroxycortisol/cortisol, respectively (Shin et al. 2013, Dutreix et al. 2014). The high variability in 6β-hydroxycortisol/cortisol could be due to diurnal variation, active renal transport, and interconversion between cortisol and cortisone (Galteau and Shamsa 2003, Imamura et al. 2014). As an example of CYP3A4 inhibition, Peng et al. studied the changes in 6β-hydroxycortisol and 6β-hydroxycortisone formation clearances (Peng et al. 2011). Instead of using the two sets of biomarkers separately, the authors suggested the using the combined formation clearances to avoid the complication of interconversion. Following a single dose of 200 mg itraconazole, the combined formation clearance decreased by 40% (Peng et al. 2011) compared to a predicted ~35% decrease in AUC_m/AUC_p using our models (Figure 3).

The urinary 7β-OH-DHEA/DHEA ratio was significantly changed following CYP3A4 inhibition as well as induction in a metabolomics study (Shin et al. 2013). DHEA, with a half-life of approximately 24 hours, is primarily metabolized to DHEA-sulfate (Legrain et al. 2000). 7β-OH-DHEA is a minor oxidative metabolite of DHEA (El Kihel 2012). Following 4 days of daily administration of 400 mg ketoconazole, a 0.34-fold change in 7β-OH-DHEA/DHEA was observed, corresponding to a $f_{m,CYP3A4}$ = 66% (Shin et al. 2013). Between an $f_{m,CYP3A4}$ of 50% to 75%, the induction simulations predicted a fold-change in AUC_m/AUC_p between 2.9 to 3.8, assuming that 7β-OH-DHEA and DHEA have similar half-lives. Shin et al. reported a 1.88-fold

increase in urinary 7β-OH-DHEA/DHEA after 10 days of multiple daily doses of 600 mg rifampin (n = 26) (Shin et al. 2013).

Urinary 1β-OH-DCA/DCA is the most recently proposed CYP3A biomarker. In HLMs, the complete inhibition of DCA hydroxylation using ketoconazole is suggestive of $f_{m,CYP3A}$ = 100% (Hayes et al. 2016). A rough estimate of $f_{m,metabolite}$ = 11% is based on the fraction the hydroxylated metabolite peak area to parent MS peak area by mass spectrometry. The terminal half-life of DCA is 15-23 minutes (Cowen et al. 1975). Compared to DCA, 1β-OH-DCA has a depletion rate at least 50% slower in HLMs, suggesting elimination-rate limited kinetics if the same renal clearance is assumed for the parent and the metabolite (Hayes et al. 2016). The predicted change in AUC_m/AUC_p following strong competitive inhibition and induction are approximately 0.5-fold and 4.5-fold, respectively. Based on a comparison between pooled control urine samples (n = 6) and a sample from single patient treated with carbamazepine, Hayes et al. (2016) reported a 7-fold higher 1β-OH-DCA/DCA for the induced patient (Hayes et al. 2016). Further clinical validation of 1β-OH-DCA/DCA, especially under inhibited conditions, is still needed.

Midazolam is the gold-standard sensitive index substrate to measure CYP3A4 activity in DDI trials. Predicted intravenous midazolam control-to-precipitant treatment AUC ratios were 1.7, 0.43, 0.70 and 0.37 following the administration of rifampin, itraconazole, fluconazole, and clarithromycin with dosing regimens simulated in this study. Endogenous biomarker simulations showed that detection of the same degree of change was possible by measuring AUC_m/AUC_p after multiple doses of rifampin or clarithromycin, whereas a single dose of itraconazole or fluconazole could only be detected under certain kinetic conditions (as shown in Figure 6). An

endogenous biomarker that could detect single dose inhibition would be of great value for early detection of CYP3A4 inhibition in First-in-Human studies.

One of the major limitations of this study is that the utility of endogenous biomarkers is restricted to hepatic CYP3A4 assessment. To our knowledge, there is no way to predict intestinal CYP3A4 activity based on endogenous biomarkers as hepatic and intestinal CYP3A4 are differentially regulated. Furthermore, there is a paucity of data to verify these predictions regarding the metabolic indices and half-life. Studies will need to be conducted to validate a range of endogenous biomarkers *in vivo* with various inhibitors and inducers and these predictions may need to be modified to account for additional considerations (i.e., changes in protein binding, induction or inhibition of multiple pathways, etc.) With endogenous biomarkers, there is likely to be a higher degree of inter- and intra-individual variability and additional work will need to be done to ascertain whether the synthesis rate of the parent, disease states, ontogeny, pregnancy, aging, or diet, among other factors, impact the utility of endogenous biomarkers to report on CYP3A4 activity. In addition, the contribution of other CYP3A isoforms (i.e., CYP3A5 or CYP3A7) to its metabolism would need to be determined for the endogenous biomarker. Finally, in these scenarios, only altered CYP3A4 activity under conditions of competitive inhibition, mechanism-based inhibition and induction were described. The utility of the theoretical endogenous biomarker to assess basal hepatic CYP3A4 activity is unknown.

In conclusion, we studied the impact of kinetic characteristics, including metabolite half-life, $f_{m,metabolite}$, and $f_{m,CYP3A4}$, on the utility of a hepatic CYP3A4 endogenous biomarker. Various sensitivity indices using spot and continuous sampling, as well as metabolite indices vs. metabolite-to-parent ratios were compared. The endogenous biomarker simulations helped to

understand the limitations of current proposed CYP3A4 biomarkers based on their kinetic characteristics and provided a guideline of the kinetic characteristics required for a sensitive endogenous biomarker given a DDI scenario. The simulation platform developed in this study is freely available in R and may be applicable to other hepatic drug metabolizing enzymes.

4.5 References

Abduljalil, K., M. Kinzig, J. Bulitta, S. Horkovics-Kovats, F. Sorgel, M. Rodamer and U. Fuhr (2009). "Modeling the autoinhibition of clarithromycin metabolism during repeated oral administration." Antimicrob Agents Chemother **53**(7): 2892-2901.

Achour, B., J. Barber and A. Rostami-Hodjegan (2014). "Expression of hepatic drug-metabolizing cytochrome p450 enzymes and their intercorrelations: a meta-analysis." Drug Metab Dispos **42**(8): 1349-1356.

Almond, L. M., S. Mukadam, I. Gardner, K. Okialda, S. Wong, O. Hatley, S. Tay, K. Rowland-Yeo, M. Jamei, A. Rostami-Hodjegan and J. R. Kenny (2016). "Prediction of Drug-Drug Interactions Arising from CYP3A induction Using a Physiologically Based Dynamic Model." Drug Metab Dispos **44**(6): 821-832.

Bodin, K., U. Andersson, E. Rystedt, E. Ellis, M. Norlin, I. Pikuleva, G. Eggertsen, I. Bjorkhem and U. Diczfalusy (2002). "Metabolism of 4 beta -hydroxycholesterol in humans." J Biol Chem **277**(35): 31534-31540.

Chen, Y., F. Ma, T. Lu, N. Budha, J. Y. Jin, J. R. Kenny, H. Wong, C. E. Hop and J. Mao (2016). "Development of a Physiologically Based Pharmacokinetic Model for Itraconazole Pharmacokinetics and Drug-Drug Interaction Prediction." Clin Pharmacokinet **55**(6): 735-749.

Chen, Y. C., S. K. Gotzkowsky, A. N. Nafziger, R. W. Kulawy, M. L. Rocci, Jr., J. S. Bertino, Jr. and A. D. Kashuba (2006). "Poor correlation between 6beta-hydroxycortisol:cortisol molar ratios and midazolam clearance as measure of hepatic CYP3A activity." Br J Clin Pharmacol **62**(2): 187-195.

Cowen, A. E., M. G. Korman, A. F. Hofmann and P. J. Thomas (1975). "Plasma disappearance of radioactivity after intravenous injection of labeled bile acids in man." Gastroenterology **68**(6): 1567-1573.

Cristofoletti, R., N. A. Charoo and J. B. Dressman (2016). "Exploratory Investigation of the Limiting Steps of Oral Absorption of Fluconazole and Ketoconazole in Children Using an In Silico Pediatric Absorption Model." J Pharm Sci **105**(9): 2794-2803.

Csajka, C., L. A. Decosterd, T. Buclin, J. L. Pagani, K. Fattinger, J. Bille and J. Biollaz (2001). "Population pharmacokinetics of fluconazole given for secondary prevention of oropharyngeal candidiasis in HIV-positive patients." Eur J Clin Pharmacol **57**(10): 723-727.

Daniels, T. F., K. M. Killinger, J. J. Michal, R. W. Wright, Jr. and Z. Jiang (2009). "Lipoproteins, cholesterol homeostasis and cardiac health." Int J Biol Sci **5**(5): 474-488.

Dutreix, C., S. Lorenzo and Y. Wang (2014). "Comparison of two endogenous biomarkers of CYP3A4 activity in a drug-drug interaction study between midostaurin and rifampicin." Eur J Clin Pharmacol **70**(8): 915-920.

El Kihel, L. (2012). "Oxidative metabolism of dehydroepiandrosterone (DHEA) and biologically active oxygenated metabolites of DHEA and epiandrosterone (EpiA)--recent reports." Steroids **77**(1-2): 10-26.

Galteau, M. M. and F. Shamsa (2003). "Urinary 6beta-hydroxycortisol: a validated test for evaluating drug induction or drug inhibition mediated through CYP3A in humans and in animals." Eur J Clin Pharmacol **59**(10): 713-733.

Ged, C., J. M. Rouillon, L. Pichard, J. Combalbert, N. Bressot, P. Bories, H. Michel, P. Beaune and P. Maurel (1989). "The increase in urinary excretion of 6 beta-hydroxycortisol as a

marker of human hepatic cytochrome P450IIIA induction." Br J Clin Pharmacol **28**(4): 373-387.

Hayes, M. A., X. Q. Li, G. Gronberg, U. Diczfalusy and T. B. Andersson (2016). "CYP3A Specifically Catalyzes 1beta-Hydroxylation of Deoxycholic Acid: Characterization and Enzymatic Synthesis of a Potential Novel Urinary Biomarker for CYP3A Activity." Drug Metab Dispos **44**(9): 1480-1489.

Imamura, Y., Y. Tsuruya, K. Damme, D. Heer, Y. Kumagai, K. Maeda, N. Murayama, N. Okudaira, A. Kurihara, T. Izumi, Y. Sugiyama and H. Kusuhara (2014). "6beta-Hydroxycortisol is an endogenous probe for evaluation of drug-drug interactions involving a multispecific renal organic anion transporter, OAT3/SLC22A8, in healthy subjects." Drug Metab Dispos **42**(4): 685-694.

Kasichayanula, S., D. W. Boulton, W. L. Luo, A. D. Rodrigues, Z. Yang, A. Goodenough, M. Lee, M. Jemal and F. LaCreta (2014). "Validation of 4beta-hydroxycholesterol and evaluation of other endogenous biomarkers for the assessment of CYP3A activity in healthy subjects." Br J Clin Pharmacol **78**(5): 1122-1134.

Ke, A. B., M. J. Zamek-Gliszczynski, J. W. Higgins and S. D. Hall (2014). "Itraconazole and clarithromycin as ketoconazole alternatives for clinical CYP3A inhibition studies." Clin Pharmacol Ther **95**(5): 473-476.

Kuhlmann, J. (1994). "Drug interaction studies during drug development: which, when, how?" Int J Clin Pharmacol Ther **32**(6): 305-311.

Lai, P. C., G. J. Mears and F. L. Lorscheider (1986). "Fetal-maternal transfer of [H3]-6 beta-hydroxycortisol in the pregnant ewe." Horm Metab Res **18**(8): 526-529.

Lee, J., S. H. Yoon, S. Yi, A. H. Kim, B. Kim, S. Lee, K. S. Yu, I. J. Jang and J. Y. Cho (2019). "Quantitative prediction of hepatic CYP3A activity using endogenous markers in healthy subjects after administration of CYP3A inhibitors or inducers." Drug Metab Pharmacokinet **34**(4): 247-252.

Legrain, S., C. Massien, N. Lahlou, M. Roger, B. Debuire, B. Diquet, G. Chatellier, M. Azizi, V. Faucounau, H. Porchet, F. Forette and E. E. Baulieu (2000). "Dehydroepiandrosterone replacement administration: pharmacokinetic and pharmacodynamic studies in healthy elderly subjects." J Clin Endocrinol Metab **85**(9): 3208-3217.

Mao, J., I. Martin, J. McLeod, G. Nolan, R. van Horn, M. Vourvahis and Y. S. Lin (2017). "Perspective: 4beta-hydroxycholesterol as an emerging endogenous biomarker of hepatic CYP3A." Drug Metab Rev **49**(1): 18-34.

Mariappan, T. T., H. Shen and P. Marathe (2017). "Endogenous Biomarkers to Assess Drug-Drug Interactions by Drug Transporters and Enzymes." Curr Drug Metab **18**(8): 757-768.

Marsousi, N., J. A. Desmeules, S. Rudaz and Y. Daali (2018). "Prediction of drug-drug interactions using physiologically-based pharmacokinetic models of CYP450 modulators included in Simcyp software." Biopharm Drug Dispos **39**(1): 3-17.

Morgan, S., P. Grootendorst, J. Lexchin, C. Cunningham and D. Greyson (2011). "The cost of drug development: a systematic review." Health Policy **100**(1): 4-17.

Paine, M. F., H. L. Hart, S. S. Ludington, R. L. Haining, A. E. Rettie and D. C. Zeldin (2006). "The human intestinal cytochrome P450 "pie"." Drug Metab Dispos **34**(5): 880-886.

Peng, C. C., I. Templeton, K. E. Thummel, C. Davis, K. L. Kunze and N. Isoherranen (2011). "Evaluation of 6beta-hydroxycortisol, 6beta-hydroxycortisone, and a combination of the

two as endogenous probes for inhibition of CYP3A4 in vivo." Clin Pharmacol Ther **89**(6): 888-895.

Ramsden, D., J. Zhou and D. J. Tweedie (2015). "Determination of a Degradation Constant for CYP3A4 by Direct Suppression of mRNA in a Novel Human Hepatocyte Model, HepatoPac." Drug Metab Dispos **43**(9): 1307-1315.

Rekic, D., K. S. Reynolds, P. Zhao, L. Zhang, K. Yoshida, M. Sachar, M. Piquette Miller, S. M. Huang and I. Zineh (2017). "Clinical Drug-Drug Interaction Evaluations to Inform Drug Use and Enable Drug Access." J Pharm Sci **106**(9): 2214-2218.

Saenger, P., E. Forster and J. Kream (1981). "6 beta-Hydroxycortisol: a noninvasive indicator of enzyme induction." J Clin Endocrinol Metab **52**(3): 381-384.

Sertkaya, A., H. H. Wong, A. Jessup and T. Beleche (2016). "Key cost drivers of pharmaceutical clinical trials in the United States." Clin Trials **13**(2): 117-126.

Shin, K. H., M. H. Choi, K. S. Lim, K. S. Yu, I. J. Jang and J. Y. Cho (2013). "Evaluation of endogenous metabolic markers of hepatic CYP3A activity using metabolic profiling and midazolam clearance." Clin Pharmacol Ther **94**(5): 601-609.

Svensson, R. J., R. E. Aarnoutse, A. H. Diacon, R. Dawson, S. H. Gillespie, M. J. Boeree and U. S. H. Simonsson (2018). "A Population Pharmacokinetic Model Incorporating Saturable Pharmacokinetics and Autoinduction for High Rifampicin Doses." Clin Pharmacol Ther **103**(4): 674-683.

Weitzman, E. D., D. Fukushima, C. Nogeire, H. Roffwarg, T. F. Gallagher and L. Hellman (1971). "Twenty-four hour pattern of the episodic secretion of cortisol in normal subjects." J Clin Endocrinol Metab **33**(1): 14-22.

4.6 Figures and Tables

Table 4.1. Model equations describing the rate of change of each species following administration of an inducer, a competitive inhibitor, or a mechanism-based inhibitor.

		Inducer/Inhibitor		Enz		CYP3A4		Parent		Metabolite	
		BL	$\frac{d[ind]}{dt}$ or $\frac{d[inh]}{dt}$	BL	$\frac{d[Enz]}{dt}$	BL	$\frac{d[CYP3A4]}{dt}$	BL	$\frac{d[Par]}{dt}$	BL	$\frac{d[Met]}{dt}$
Sensitivity (k_m) and Selectivity ($f_{m,metabolite}$) Interplay	Ind	0	$k_a \cdot \frac{Dose}{V_F} - k_e \cdot [Enz][Ind]$	1	$K_{in,Enz} \cdot \left(1 + \frac{E_{max,1} \cdot f_u \cdot [Ind]}{EC_{50,1} + f_u \cdot [Ind]}\right) - k_{o,Enz} \cdot [Enz]$	1	$K_{in,CYP3A4} \cdot \left(1 + \frac{E_{max,2} \cdot f_u \cdot [Ind]}{EC_{50,2} + f_u \cdot [Ind]}\right) - k_{O,CYP3A4} \cdot [CYP3A4]$	$\frac{k_m}{f_m k_p}$	$K_{in,parent} - [CYP3A4] \cdot f_m \cdot k_p \cdot [Par] - (1 - f_m) \cdot k_p \cdot [Par]$	1	$[CYP3A4] \cdot f_m \cdot k_p \cdot [Par] - k_m \cdot [Met]$
	CI	0	$k_a \cdot \frac{Dose}{V_F} - k_e \cdot [Inh]$	NA	NA	1	$K_{in,CYP3A4} - k_{O,CYP3A4} \cdot [CYP3A4]$	$\frac{k_m}{f_m k_p}$	$K_{in,parent} - \frac{[CYP3A4]}{1 + f_u \cdot [inh]/Ki} \cdot f_m \cdot k_p \cdot [Par] - (1 - f_m) \cdot k_p \cdot [Par]$	1	$\frac{[CYP3A4]}{1 + f_u \cdot [inh]/Ki} \cdot f_m \cdot k_p \cdot [Par] - k_m \cdot [Met]$
	MBI	0	$k_a \cdot \frac{Dose}{V_F} - k_e \cdot [CYP3A4] \cdot [Inh]$	NA	NA	1	$K_{in,CYP3A4} - \left(k_{O,CYP3A4} + \frac{k_{inact} \cdot f_u \cdot [inh]}{Ki + f_u \cdot [inh]}\right) \cdot [CYP3A4]$	$\frac{k_m}{f_m k_p}$	$K_{in,parent} - [CYP3A4] \cdot f_m \cdot k_p \cdot [Par] - (1 - f_m) \cdot k_p \cdot [Par]$	1	$[CYP3A4] \cdot f_m \cdot k_p \cdot [Par] - k_m \cdot [Met]$
Sensitivity (k_m) and Selectivity ($f_{m,CYP3A4}$) Interplay	Ind	0	$k_a \cdot \frac{Dose}{V_F} - k_e \cdot [Enz][Ind]$	1	$K_{in,Enz} \cdot \left(1 + \frac{E_{max,1} \cdot f_u \cdot [Ind]}{EC_{50,1} + f_u \cdot [Ind]}\right) - k_{o,Enz} \cdot [Enz]$	1	$K_{in,CYP3A4} \cdot \left(1 + \frac{E_{max,2} \cdot f_u \cdot [Ind]}{EC_{50,2} + f_u \cdot [Ind]}\right) - k_{O,CYP3A4} \cdot [CYP3A4]$	$\frac{k_m}{k_f}$	$K_{in,parent} - [CYP3A4] \cdot f_m \cdot k_f \cdot [Par] - (1 - f_m) \cdot k_f \cdot [Par]$	1	$[CYP3A4] \cdot f_m \cdot k_f \cdot [Par] + (1 - f_m) \cdot k_f \cdot [Par] - k_m \cdot [Met]$
	CI	0	$k_a \cdot \frac{Dose}{V_F} - k_e \cdot [Inh]$	NA	NA	1	$K_{in,CYP3A4} - k_{O,CYP3A4} \cdot [CYP3A4]$	$\frac{k_m}{k_f}$	$K_{in,parent} - \frac{[CYP3A4]}{1 + f_u \cdot [inh]/Ki} \cdot f_m \cdot k_f \cdot [Par] - (1 - f_m) \cdot k_f \cdot [Par]$	1	$\frac{[CYP3A4]}{1 + f_u \cdot [inh]/Ki} \cdot f_m \cdot k_f \cdot [Par] + (1 - f_m) \cdot k_f \cdot [Par] - k_m \cdot [Met]$
	MBI	0	$k_a \cdot \frac{Dose}{V_F} - k_e \cdot [CYP3A4] \cdot [Inh]$	NA	NA	1	$K_{in,CYP3A4} - \left(k_{O,CYP3A4} + \frac{k_{inact} \cdot f_u \cdot [inh]}{Ki + f_u \cdot [inh]}\right) \cdot [CYP3A4]$	$\frac{k_m}{k_f}$	$K_{in,parent} - [CYP3A4] \cdot f_m \cdot k_f \cdot [Par] - (1 - f_m) \cdot k_f \cdot [Par]$	1	$[CYP3A4] \cdot f_m \cdot k_f \cdot [Par] + (1 - f_m) \cdot k_f \cdot [Par] - k_m \cdot [Met]$

Ind = induction; CI = competitive inhibition; MBI = mechanism-based inhibition; BL = baseline values at steady-state; E_{max} = maximal induction capacity; EC_{50} = concentration to produce half of maximal induction (μM); Ki = concentration to product half of

maximal inhibition (μM); k_{inact} = inactivation rate of the enzyme (1/hr); k_a = first-order drug absorption rate constant (1/hr); k_e = first-order drug elimination rate constant (1/hr); V/F = apparent drug volume of distribution (L); f_u = fraction unbound of drugs in plasma; $K_{in,Enz}$ = zero-order Enz synthesis rate constant ([Enz]/hr); $k_{o,Enz}$ = first-order enz degradation rate constant (1/hr); $K_{in,CYP3A4}$ = zero-order CYP3A4 synthesis rate constant ([CYP3A4]/hr); $k_{o,CYP3A4}$ = first-order CYP3A4 degradation rate constant (1/hr); $K_{in,parent}$ = zero-order parent synthesis rate constant ([parent]/hr); k_p = first-order parent elimination rate constant; k_f = first-order metabolite formation rate constant (1/hr); k_m = first-order metabolite elimination rate constant (1/hr); f_m = fraction metabolized to metabolites or fraction metabolized by CYP3A4.

Table 4.2. A summary of doses, constants, and biomarker variable sample spaces specified in different simulation scenarios.

		Dose	Drug constants	Enzyme constants	Parent and metabolite variables
Sensitivity (k_m) and Selectivity ($f_{m,metabolite}$) Interplay	Ind	QD for 7 days	$E_{max,1}$ = 1.16[ϫ]; $EC_{50,1}$ = 0.00985[ϫ], $E_{max,2}$ = 15[§]; $EC_{50,2}$ = 0.32[§]; k_a = 1.77[ϫ]; k_e = 0.17[ϫ]; V/F = 87.2[ϫ]; f_u = 0.116[§]	$K_{in,Enz} = k_{o,Enz}$ k_{Enz} = 0.00603[ϫ] $K_{in,CYP3A4} = k_{o,CYP3A4}$ $k_{o,CYP3A4}$ = 0.024[Д]	$K_{in,parent} = \frac{k_m}{f_{m,metabolite}}$ (based on steady-state) $k_p = n \cdot k_m$ where n ∈{0.5, 1, 2} $f_{m,metabolite}$ ∈{0.01, 0.25, 0.5, 0.75, 1} $k_m = \frac{\ln 2}{t_{1/2,m}}$ where $t_{1/2,m}$ ∈{1, 2, … , 168}
	Strong CI	single	Ki = 0.0013[¥]; k_a = 0.6[¥]; k_e = 0.033[Θ]; V/F = 796[Θ]; f_u = 0.016[¥]	$K_{in,CYP3A4} = k_{o,CYP3A4}$ $k_{o,CYP3A4}$ = 0.024[Д]	same as above
	Moderate CI	single	Ki = 10.7[Φ]; k_a = 0.93[X]; k_e = 0.0231[Θ]; V/F = 48.3[Θ]; f_u = 0.89[Φ]	same as above	same as above
	MBI	BID for 3 days	k_{inact} = 2.13[ק]; Ki = 12[ק]; k_a = 2.42[ק]; k_e = 0.35[ε]; V/F = 172[ε]; f_u = 0.18[ק]	same as above	same as above
Sensitivity (k_m) and Selectivity ($f_{m,CYP3A4}$) Interplay	Ind	QD for 7 days	$E_{max,1}$ = 1.16[ϫ]; $EC_{50,1}$ = 0.00985[ϫ], $E_{max,2}$ = 15[§]; $EC_{50,2}$ = 0.32[§]; k_a = 1.77[ϫ]; k_e = 0.17[ϫ]; V/F = 87.2[ϫ]; f_u = 0.116[§]	$K_{in,Enz} = k_{o,Enz}$ k_{Enz} = 0.00603[ϫ] $K_{in,CYP3A4} = k_{o,CYP3A4}$ $k_{o,CYP3A4}$ = 0.024[Д]	$K_{in,parent} = k_m$ (based on steady-state) $k_f = n \cdot k_m$ where n ∈{0.5, 1, 2}12 $f_{m,CYP3A4}$ ∈{0.01, 0.25, 0.5, 0.75, 1} $k_m = \frac{\ln 2}{t_{1/2,m}}$ where $t_{1/2,m}$ ∈{1, 2, … , 168}
	Strong CI	single	Ki = 0.0013[¥]; k_a = 0.6[¥]; k_e = 0.033[Θ]; V/F = 796[Θ]; f_u = 0.016[¥]	$K_{in,CYP3A4} = k_{o,CYP3A4}$ $k_{o,CYP3A4}$ = 0.024[Д]	same as above
	Moderate CI	single	Ki = 10.7[Φ]; k_a = 0.93[X]; k_e = 0.0231[Θ]; V/F = 48.3[Θ]; f_u = 0.89[Φ]	same as above	same as above
	MBI	BID for 3 days	k_{inact} = 2.13[ק]; Ki = 12[ק]; k_a = 2.42[ק]; k_e = 0.35[ε]; V/F = 172[ε]; f_u = 0.18[ק]	same as above	same as above

Ind = induction; CI = competitive inhibition; MBI = mechanism-based inhibition; QD = once a day; BID = twice a day; $E_{max,1}$ = maximal enz induction capacity; $EC_{50,1}$ = concentration to produce half of maximal enz induction (μM); $E_{max,2}$ = maximal CYP3A4 induction capacity; $EC_{50,2}$ = concentration to produce half of maximal CYP3A4 induction (μM); Ki = concentration to product half of maximal inhibition (μM); k_{inact} = inactivation rate of the enzyme (1/hr); k_a = first-order drug absorption rate constant (1/hr); k_e = first-order drug elimination rate constant (1/hr); V/F = apparent drug volume of distribution (L); f_u = fraction unbound of drugs in plasma; $K_{in,Enz}$ = zero-order Enz synthesis rate constant ([Enz]/hr); $k_{o,Enz}$ = first-order enz degradation rate constant (1/hr); $K_{in,CYP3A4}$ = zero-order CYP3A4 synthesis rate constant ([CYP3A4]/hr); $k_{o,CYP3A4}$ = first-order CYP3A4 degradation rate constant (1/hr); $K_{in,parent}$ =

zero-order parent synthesis rate constant ([parent]/hr); k_p = first-order parent elimination rate constant; k_f = first-order metabolite formation rate constant (1/hr); k_m = first-order metabolite elimination rate constant (1/hr); $f_{m,metabolite}$ = fraction metabolized to metabolites; $f_{m,CYP3A4}$ = fraction metabolized by CYP3A4; $t_{1/2,m}$ = metabolite half-life (hr); [§]based on rifampin in Simcyp; [¥]based on itraconazole in Simcyp; [Φ]based on fluconazole in Simcyp; [ϡ]based on clarithromycin in Simcyp; [ϫ]Svensson 2018; [ϫ]Csajka 2001; [ε]Abduljalil 2009; [Θ]FDA label; [д]Ramsden 2015.

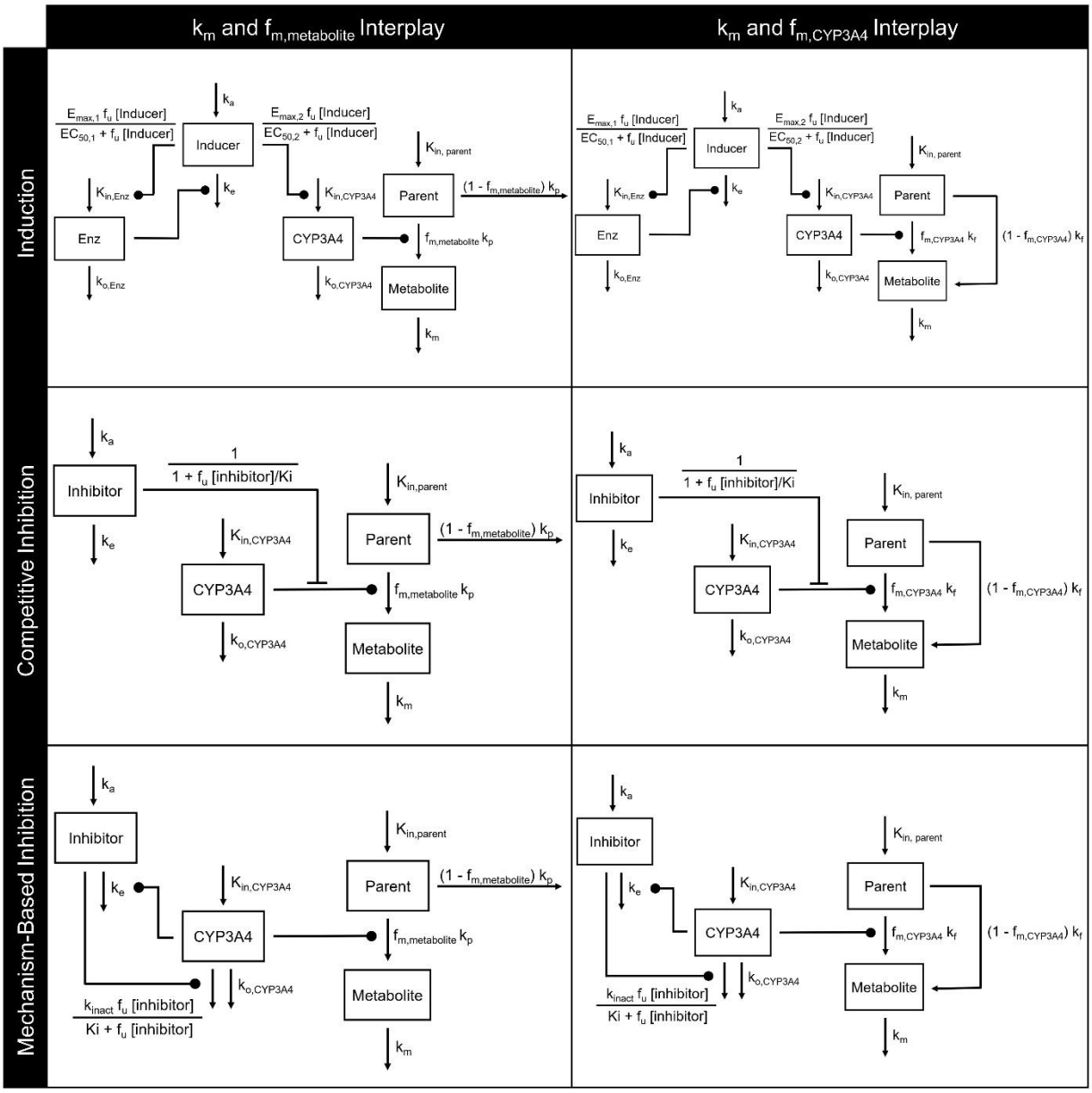

Figure 4.1. Models for induction, competitive inhibition, and mechanism-based inhibition. E_{max} = maximal induction capacity; EC_{50} = concentration to produce half of maximal induction (μM); Ki = concentration to product half of maximal inhibition (μM); k_{inact} = inactivation rate of the enzyme (1/hr); k_a = first-order drug absorption rate constant (1/hr); k_e = first-order drug elimination rate constant for the precipitant (1/hr); f_u = fraction unbound of precipitant in plasma; $K_{in,CYP3A4}$ = zero-order CYP3A4 synthesis rate constant ([CYP3A4]/hr); $k_{o,CYP3A4}$ = first-order

CYP3A4 degradation rate constant (1/hr); $K_{in,parent}$ = zero-order endogenous parent synthesis rate constant ([parent]/hr); k_p = first-order endogenous parent elimination rate constant; k_f = first-order endogenous metabolite formation rate constant (1/hr); k_m = first-order endogenous metabolite elimination rate constant (1/hr); $f_{m,metabolite}$ = fraction of the endogenous parent metabolized to the endogenous metabolite of interest; $f_{m,CYP3A4}$ = fraction of the endogenous parent metabolized by CYP3A4.

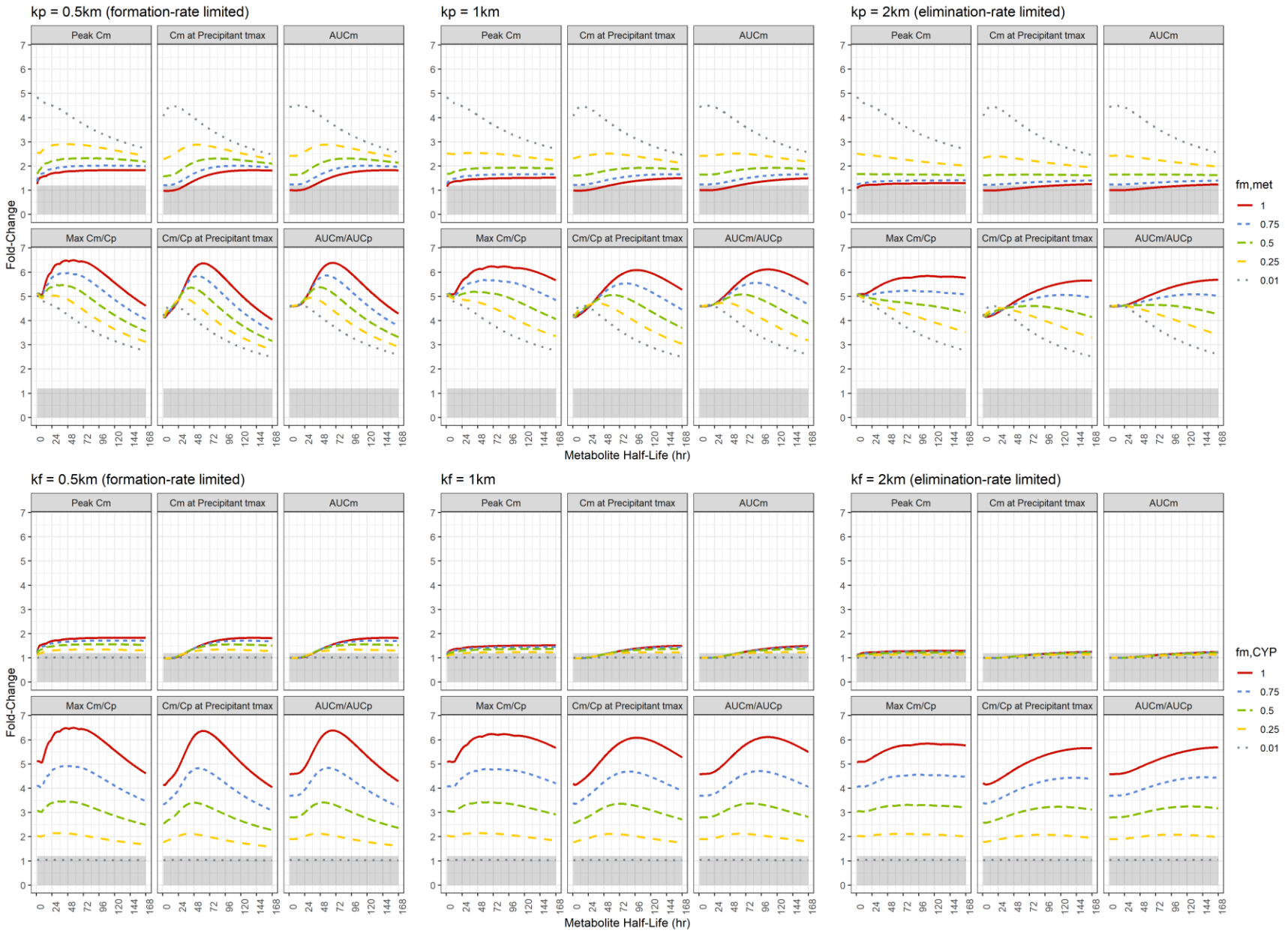
kp = 0.5km (formation-rate limited)
kp = 1km
kp = 2km (elimination-rate limited)
kf = 0.5km (formation-rate limited)
kf = 1km
kf = 2km (elimination-rate limited)
Peak Cm
Cm at Precipitant tmax
AUCm
Max Cm/Cp
Cm/Cp at Precipitant tmax
AUCm/AUCp
Fold-Change
Metabolite Half-Life (hr)
fm,met
fm,CYP
1
0.75
0.5
0.25
0.01

Figure 4.2. Simulations for CYP3A4 induction: fold-change of the sensitivity indices vs. metabolite half-life. Induction was simulated using 600 mg rifampin once a day dosed for 7 days. Abbreviations: Peak Cm = theoretical peak metabolite concentration; Cm at Precipitant tmax = metabolite concentration at the peak precipitant concentration; AUCm = metabolite area under the concentration-time curve; Max Cm/Cp = theoretical highest value of the metabolite-to-parent concentration ratio; Cm/Cp at Precipitant tmax = metabolite-to-parent concentration ratio at the peak precipitant concentration; AUCm/AUCp = metabolite-to-parent area under the concentration-time curve ratio.

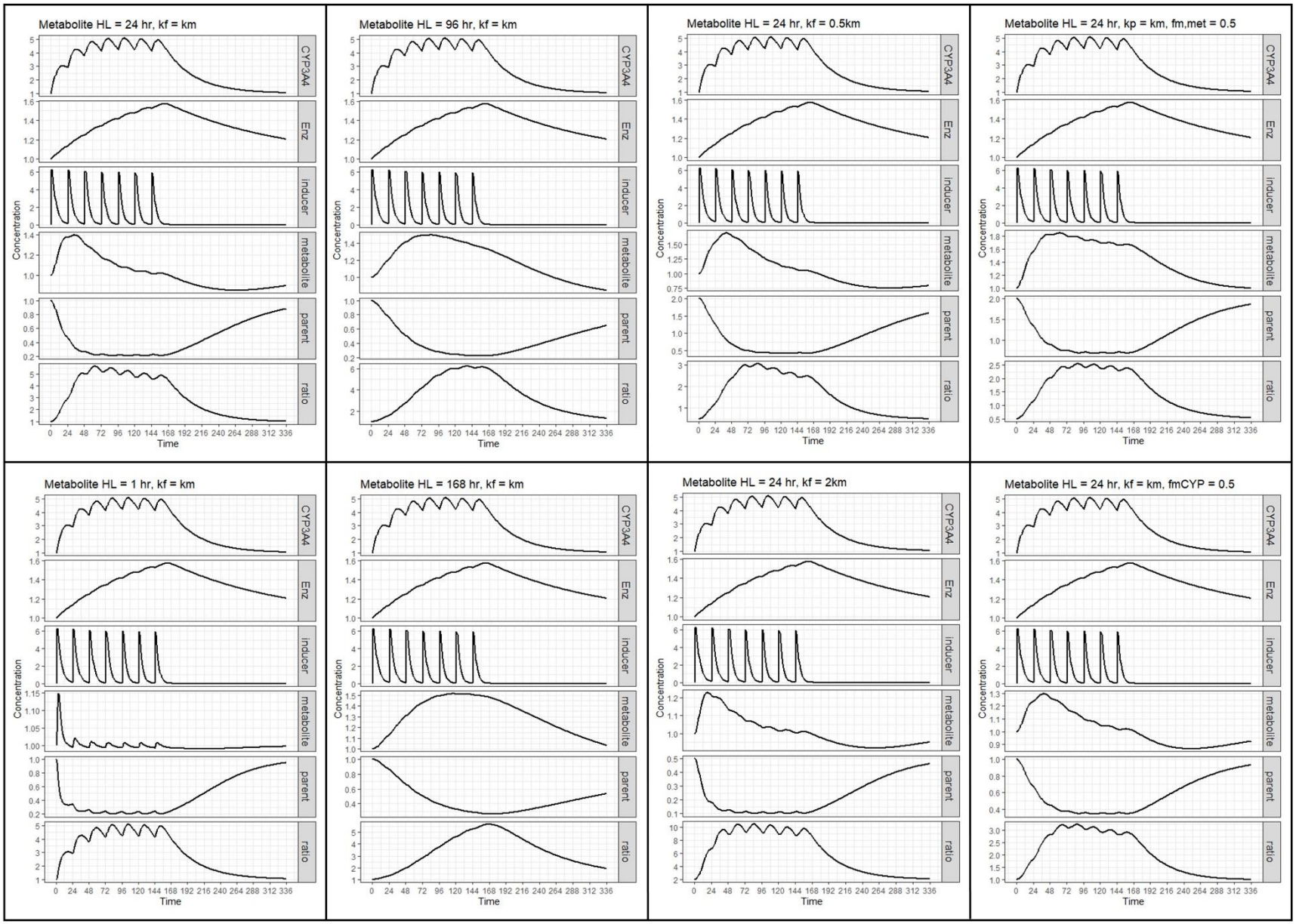
Metabolite HL = 24 hr, kf = km
Metabolite HL = 96 hr, kf = km
Metabolite HL = 24 hr, kf = 0.5km
Metabolite HL = 24 hr, kp = km, fm,met = 0.5
Metabolite HL = 1 hr, kf = km
Metabolite HL = 168 hr, kf = km
Metabolite HL = 24 hr, kf = 2km
Metabolite HL = 24 hr, kf = km, fmCYP = 0.5
CYP3A4
Enz
inducer
metabolite
parent
ratio
Concentration
Time
0 24 48 72 96 120 144 168 192 216 240 264 288 312 336

Figure 4.3. Examples of concentration-time profiles of simulated species following CYP3A4 induction. Enz = rifampin metabolizing enzyme; ratio = metabolite-to-parent concentration ratio.

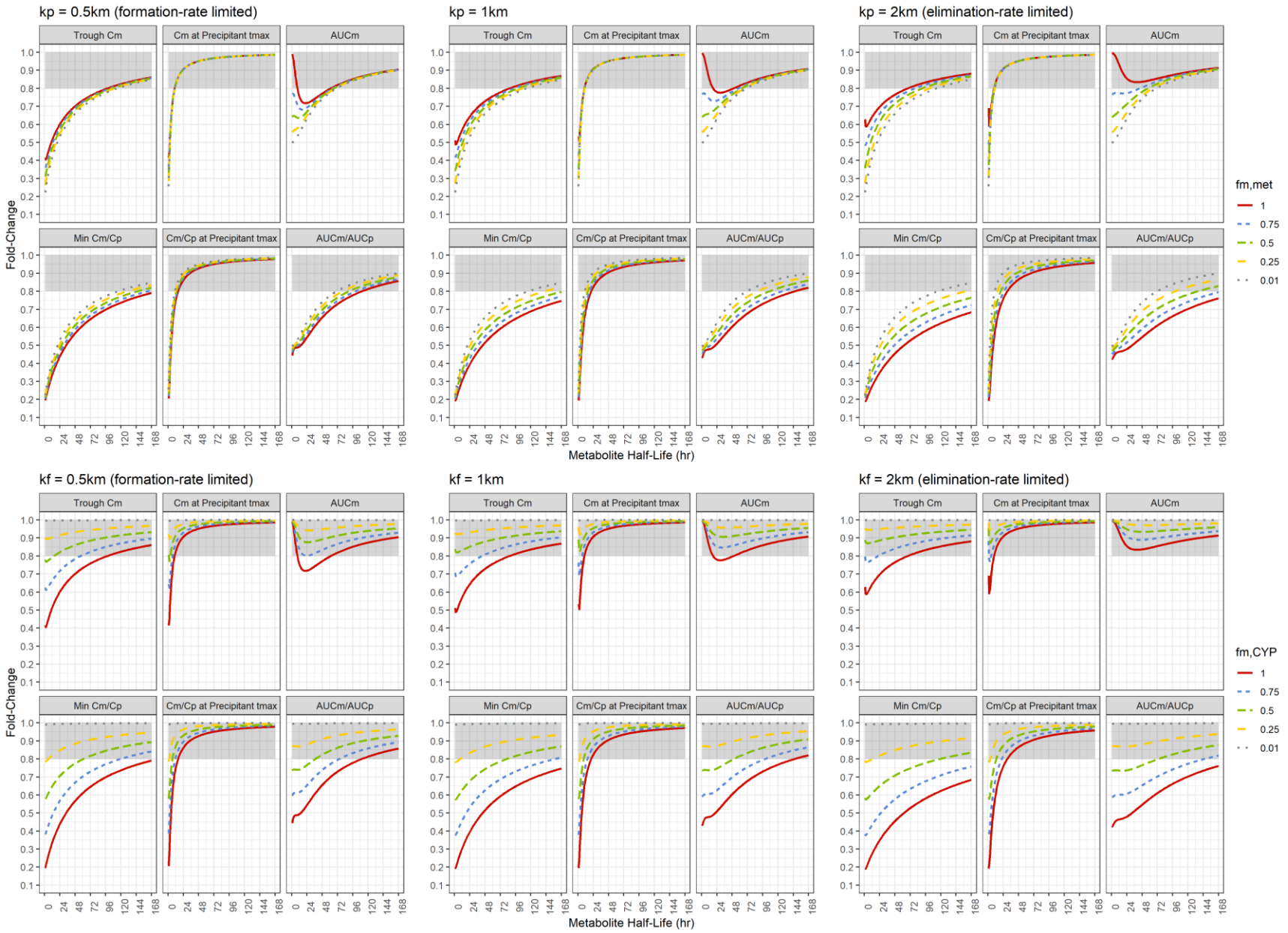
kp = 0.5km (formation-rate limited)
kp = 1km
kp = 2km (elimination-rate limited)
kf = 0.5km (formation-rate limited)
kf = 1km
kf = 2km (elimination-rate limited)
Trough Cm
Cm at Precipitant tmax
AUCm
Min Cm/Cp
Cm/Cp at Precipitant tmax
AUCm/AUCp
Fold-Change
Metabolite Half-Life (hr)
fm,met
fm,CYP
1
0.75
0.5
0.25
0.01

Figure 4.4. Simulations of strong competitive inhibition of CYP3A4: fold-change of the sensitivity indices vs. metabolite half-life. Strong competitive inhibition was simulated using a single dose of 200 mg itraconazole. Abbreviations: Trough Cm = theoretical trough metabolite concentration; Cm at Precipitant tmax = metabolite concentration at the peak precipitant concentration; AUCm = metabolite area under the concentration-time curve; Min Cm/Cp = theoretical lowest value of the metabolite-to-parent concentration ratio; Cm/Cp at Precipitant tmax = metabolite-to-parent concentration ratio at the peak precipitant concentration; AUCm/AUCp = metabolite-to-parent area under the concentration-time curve ratio.

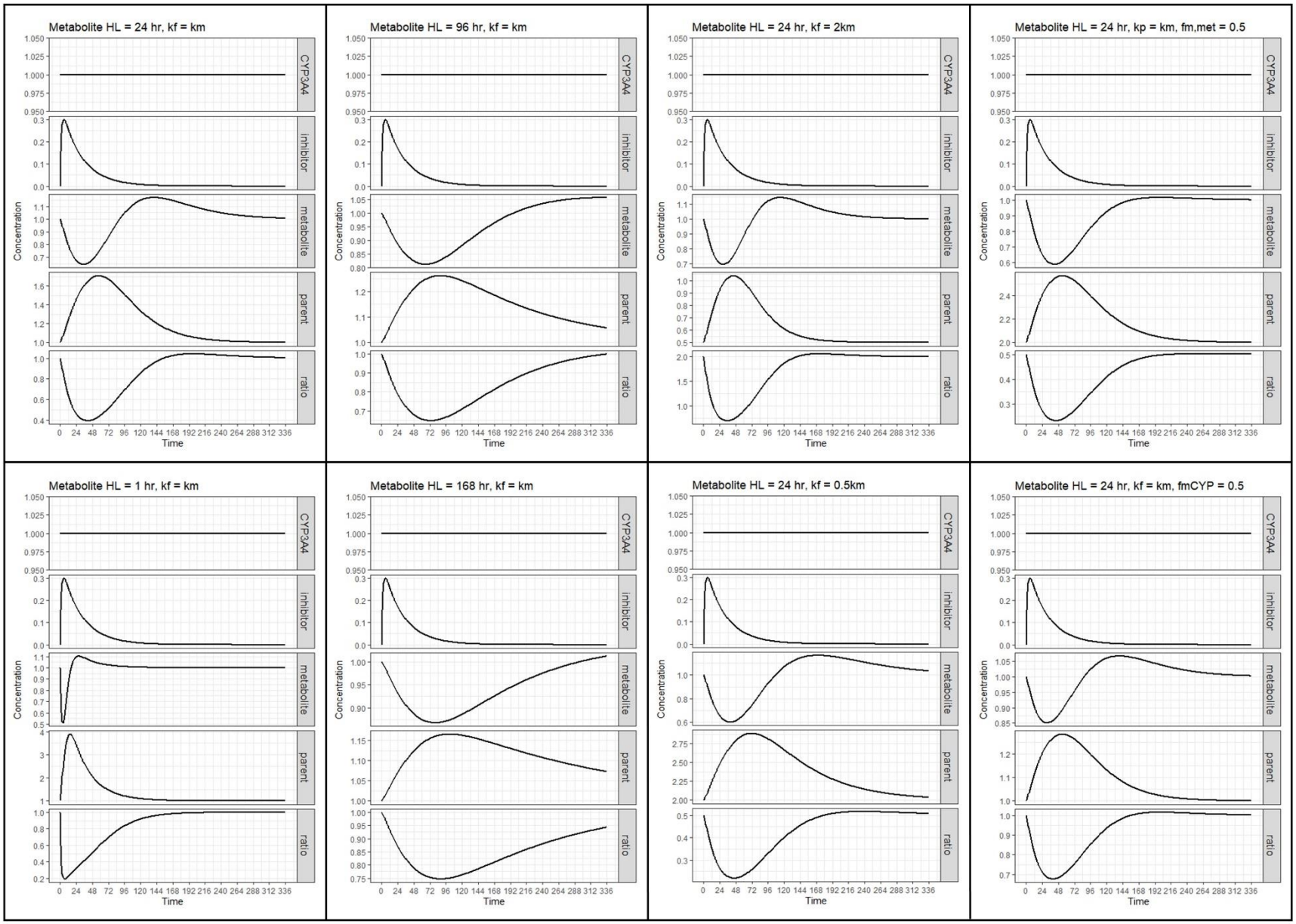
Metabolite HL = 24 hr, kf = km
Metabolite HL = 96 hr, kf = km
Metabolite HL = 24 hr, kf = 2km
Metabolite HL = 24 hr, kp = km, fm,met = 0.5
Metabolite HL = 1 hr, kf = km
Metabolite HL = 168 hr, kf = km
Metabolite HL = 24 hr, kf = 0.5km
Metabolite HL = 24 hr, kf = km, fmCYP = 0.5
CYP3A4
inhibitor
metabolite
parent
ratio
Concentration
Time

Figure 4.5 Examples of concentration-time profiles of simulated species following strong competitive inhibition. The ratio is the metabolite-to-parent concentration ratio.

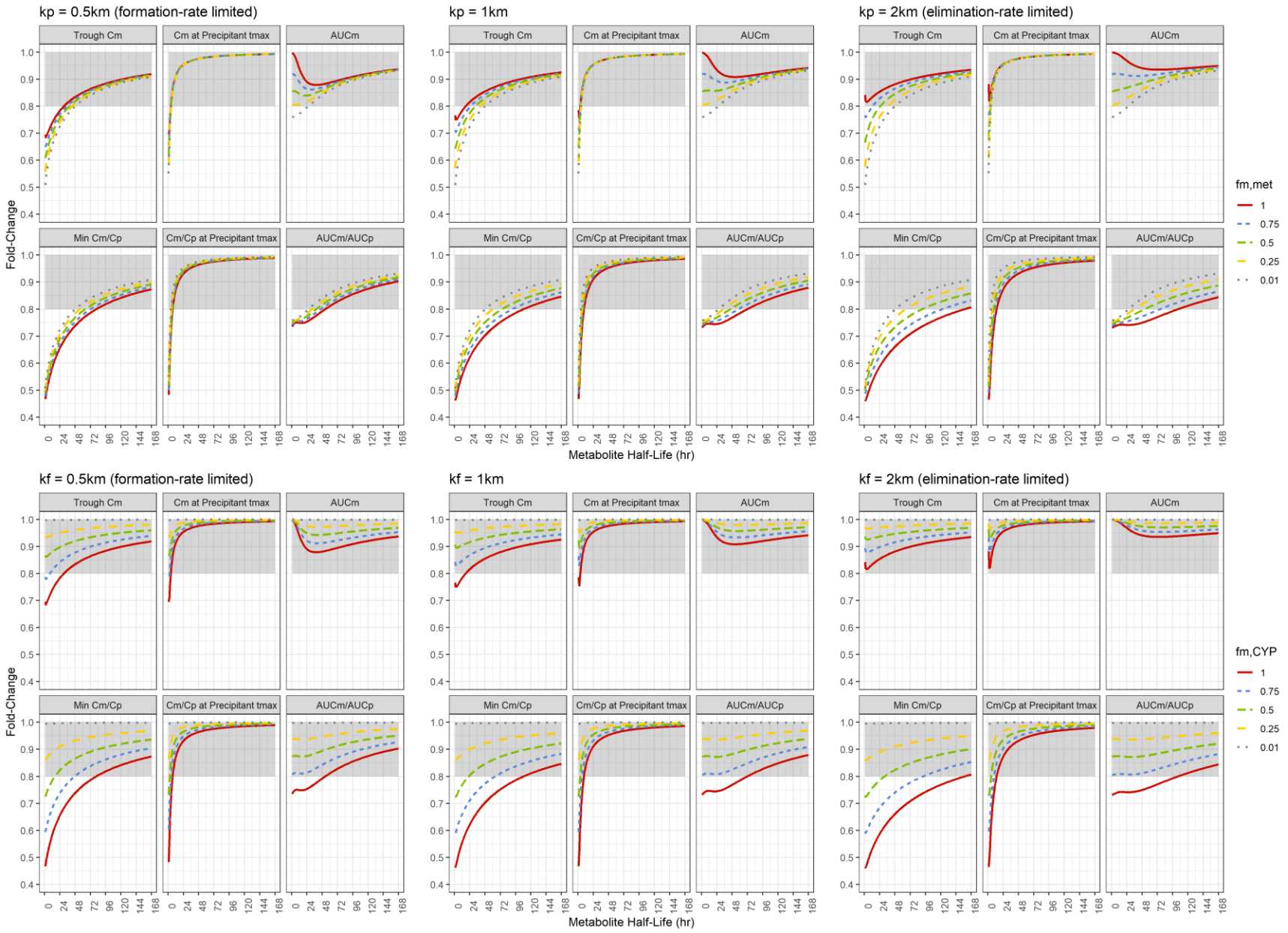
kp = 0.5km (formation-rate limited)
kp = 1km
kp = 2km (elimination-rate limited)
kf = 0.5km (formation-rate limited)
kf = 1km
kf = 2km (elimination-rate limited)
Trough Cm
Cm at Precipitant tmax
AUCm
Min Cm/Cp
Cm/Cp at Precipitant tmax
AUCm/AUCp
Fold-Change
Metabolite Half-Life (hr)
fm,met
fm,CYP
1
0.75
0.5
0.25
0.01

Figures 4.6. Simulations of moderate competitive inhibition of CYP3A4: fold-change of the sensitivity indices vs. metabolite half-life. Moderate competitive inhibition was simulated using a single dose of 200 mg fluconazole. Abbreviations: Trough Cm = theoretical trough metabolite concentration; Cm at Precipitant tmax = metabolite concentration at the peak precipitant concentration; AUCm = metabolite area under the concentration-time curve; Min Cm/Cp = theoretical lowest value of the metabolite-to-parent concentration ratio; Cm/Cp at Precipitant tmax = metabolite-to-parent concentration ratio at the peak precipitant concentration; AUCm/AUCp = metabolite-to-parent area under the concentration-time curve ratio.

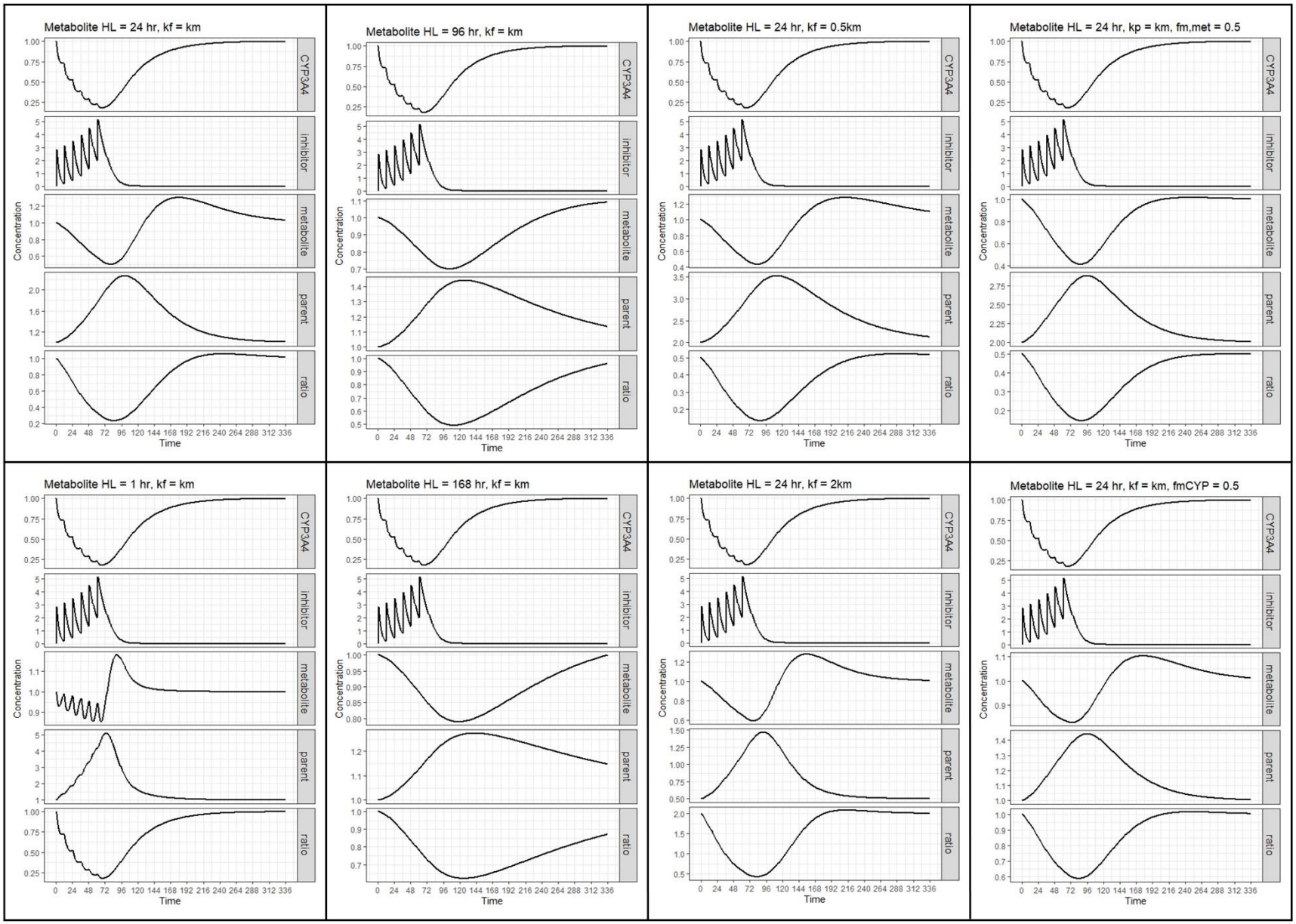
Metabolite HL = 24 hr, kf = km
Metabolite HL = 96 hr, kf = km
Metabolite HL = 24 hr, kf = 0.5km
Metabolite HL = 24 hr, kp = km, fm,met = 0.5
Metabolite HL = 1 hr, kf = km
Metabolite HL = 168 hr, kf = km
Metabolite HL = 24 hr, kf = 2km
Metabolite HL = 24 hr, kf = km, fmCYP = 0.5
CYP3A4
inhibitor
metabolite
parent
ratio
Concentration
Time

Figure 4.7. Examples of concentration-time profiles of simulated species following mechanism-based inhibition scenario. The ratio is the metabolite-to-parent concentration ratio.

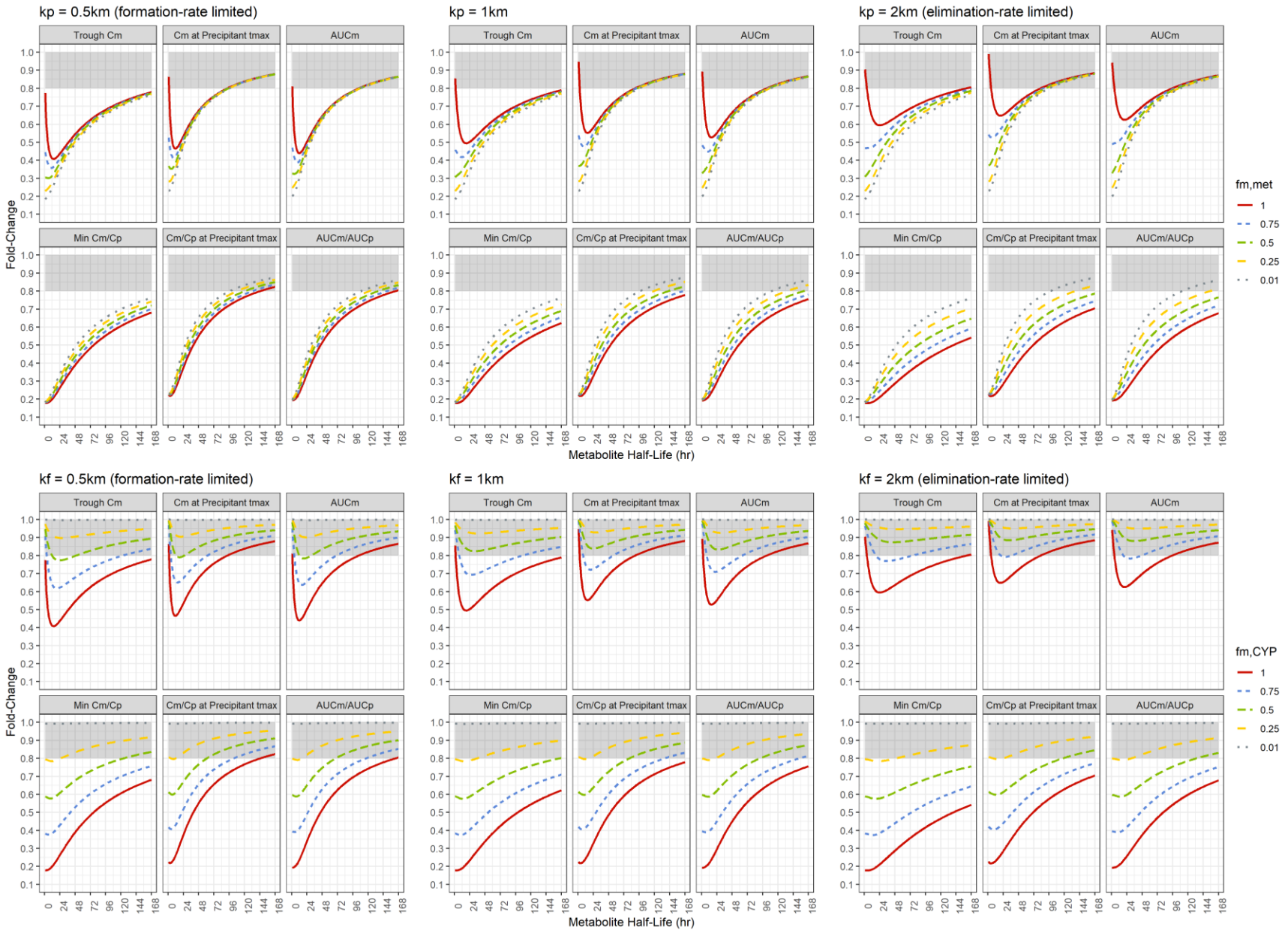
kp = 0.5km (formation-rate limited)
kp = 1km
kp = 2km (elimination-rate limited)
kf = 0.5km (formation-rate limited)
kf = 1km
kf = 2km (elimination-rate limited)
Trough Cm
Cm at Precipitant tmax
AUCm
Min Cm/Cp
Cm/Cp at Precipitant tmax
AUCm/AUCp
Fold-Change
Metabolite Half-Life (hr)
fm,met
fm,CYP
1
0.75
0.5
0.25
0.01

Figure 4.8. Simulations of mechanism-based inhibition of CYP3A4: of fold-change of the sensitivity indices vs. metabolite half-life. Mechanism-based inhibition was simulated using 500 mg clarithromycin twice a day for 3 days. Abbreviations: Trough Cm = theoretical trough metabolite concentration; Cm at Precipitant tmax = metabolite concentration at the peak precipitant concentration; AUCm = metabolite area under the concentration-time curve; Min Cm/Cp = theoretical lowest value of the metabolite-to-parent concentration ratio; Cm/Cp at Precipitant tmax = metabolite-to-parent concentration ratio at the peak precipitant concentration; AUCm/AUCp = metabolite-to-parent area under the concentration-time curve ratio.

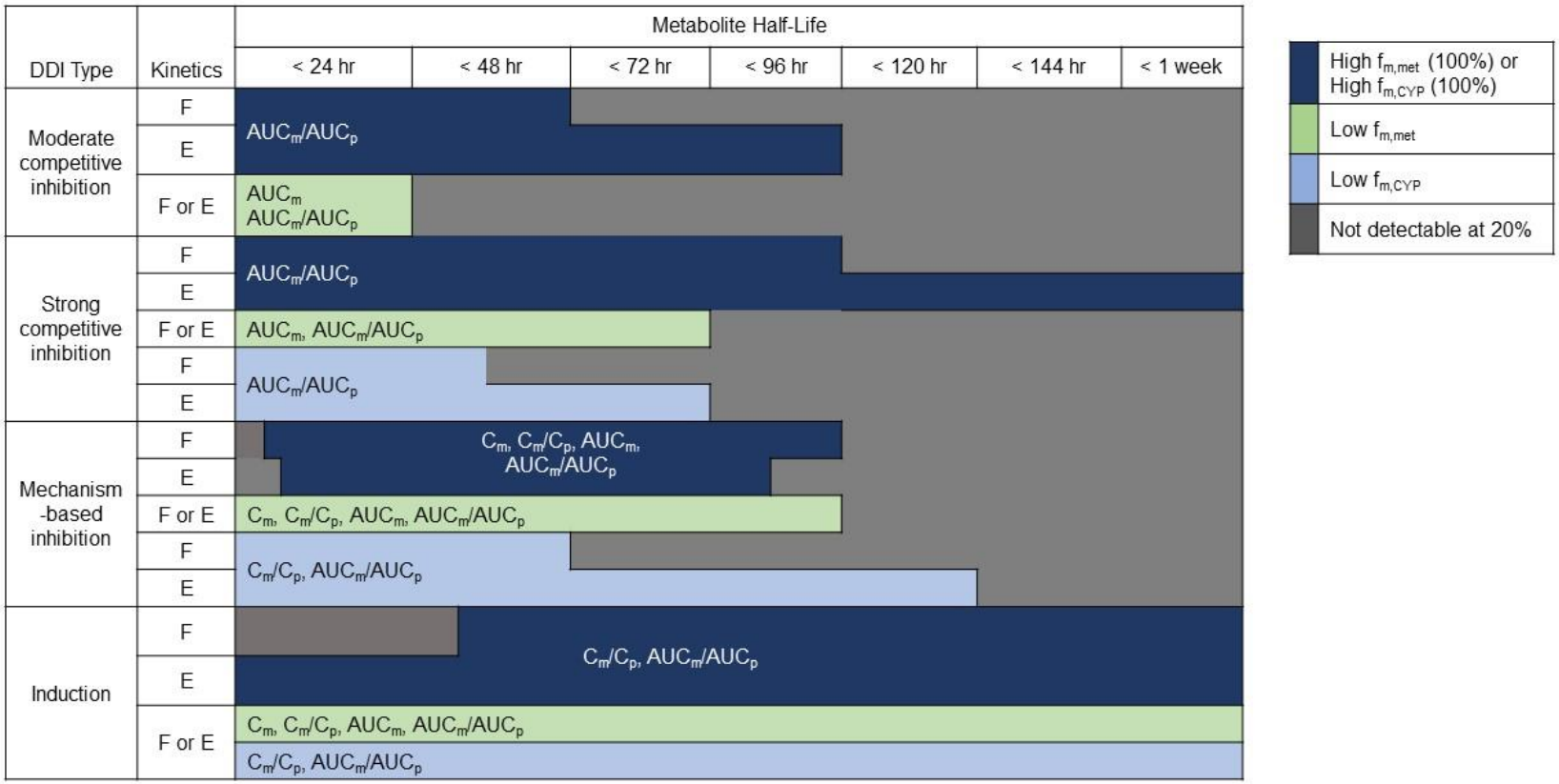

Figure 4.9. A summary of kinetic characteristics required for a sensitive endogenous CYP3A4 biomarker under different drug-drug interaction scenarios. Abbreviations: Cm = metabolite concentration at the peak precipitant concentration; AUCm = metabolite area

under the concentration-time curve; Cm/Cp = metabolite-to-parent concentration ratio at the peak precipitant concentration; AUCm/AUCp = metabolite-to-parent area under the concentration-time curve ratio.

CHAPTER 5

SUMMARY AND CONCLUSIONS

5.1 Conclusions

In the past decade, pharmacometrics has emerged as a powerful tool to model the pharmacokinetics of drugs in special populations, to predict drug-drug interactions (DDIs) *in silico*, and to conduct simulation studies to better understand drug disposition when performing clinical trials is not feasible. This dissertation focused on using pharmacometrics to understand drug disposition and predict drug interactions in morbidly obese individuals undergoing Roux-en-Y gastric bypass surgery (RYGBS) and to determine the kinetic characteristics of theoretical endogenous biomarkers that would permit the detection of competitive inhibition, mechanism-based inhibition and induction of hepatic CYP3A4.

RYGBS, a surgery that creates a smaller stomach pouch and reduces the length of small intestine, is one of the most common medical interventions for the treatment of obesity. The anatomical changes and resultant changes in drug metabolizing enzyme activity can substantially impact drug disposition and drug-drug interactions (DDIs). For DDI assessment, the use of endogenous biomarkers is an alternative approach to probe drug pharmacokinetic studies. Using endogenous biomarkers is attractive to drug developers and clinicians as they provide an opportunity for early detection of DDIs and non-invasive sampling. Novel endogenous CYP3A4 biomarkers are needed, but their required kinetics characteristics in a given DDI scenario remains obscure. This dissertation investigated how RYGBS affects drug absorption and intestinal and hepatic metabolism *in vivo* and *in silico* and summarized how different kinetic characteristics affect the utility of an endogenous biomarker for hepatic CYP3A4 through theoretical simulations.

In Chapter 2, we determined how RYGBS influences the absorption and metabolism of acetaminophen. Twelve morbidly obese patients received 1.5 g of liquid acetaminophen (APAP)

orally on three separate pharmacokinetic study days (i.e., pre-RYGBS baseline, 3-month, and 12-month post-RYGBS). Plasma was collected at pre-specified timepoints over 24 hours and the samples were analyzed using liquid chromatography-mass spectrometry for APAP, APAP-glucuronide (APAP-gluc), APAP-sulfate (APAP-sulf), APAP-cysteine (APAP-cys), and APAP-*N*-acetylcysteine (APAP-nac). Following RYGBS, peak APAP concentrations at the 3-month and 12-month visits increased by 2-fold compared to baseline ($p = 0.0039$ and $p = 0.0078$, respectively) and the median time to peak concentration decreased from 35 min to 10 min. In contrast, peak concentrations of APAP-gluc, APAP-sulf, APAP-cys, and APAP-nac were unchanged following RYGBS. The apparent oral clearance of APAP and the ratios of metabolite AUC-to-APAP AUC for all four metabolites decreased at 3-months and 12-months post-RYGBS compared to the presurgical baseline. In a simulation of expected steady-state plasma concentrations following multiple dosing of 650 mg APAP every 4 hours, post-RYGBS patients had higher peak-to-trough APAP concentrations (6.9-fold) compared to obese pre-RYGBS individuals (6.2-fold), and 1.7-fold higher APAP exposure. Following RYGBS, the rate and extent of APAP absorption increased and decreased formation of APAP-metabolites was observed, possibly due to down-regulation of Phase II and CYP2E1 enzymes.

In Chapter 3, our goal was to better understand the DDI potential of CYP3A and P-gp inhibitors in morbidly obese individuals pre- and post-RYGBS. Using physiologically-based pharmacokinetic (PBPK) modeling, we simulated the impact of RYGBS on the absorption and metabolism of midazolam, acetaminophen, digoxin, and their major metabolites. Secondly, we built PBPK models for verapamil and posaconazole to evaluate CYP3A- and P-gp-mediated DDIs pre- and post-RYGBS. We found that for highly soluble drugs, such as verapamil, bioavailability was comparable pre- and post-RYGBS. For verapamil inhibition, RYGBS did not

affect the fold-change of the inhibited AUC ratio or inhibited peak concentration ratio for either midazolam or digoxin. In contrast, the bioavailability of posaconazole, a poorly soluble drug, decreased from 12% to 5% from pre- to post-RYGBS. For posaconazole inhibition, the inhibited midazolam AUC increased by 2.0-fold pre-RYGBS, but only increased by 1.6-fold post-RYGBS. A similar trend was observed for pre- and post-RYGBS inhibited midazolam peak concentration ratios (2.0- and 1.6-fold, respectively). Absorption of highly soluble drugs was more rapid post-RYGBS, resulting in higher predicted midazolam peak concentrations, which was further increased following inhibition by verapamil or posaconazole. To reduce the risk of a drug-drug interaction in patients post-RYGBS, the dose or frequency of object drugs may need to be decreased when administered with highly soluble inhibitor drugs, especially if toxicities are associated with peak concentrations.

In Chapter 4, we used modeling to identify the kinetic characteristics of theoretical hepatic CYP3A4 biomarkers that would have the ability to detect induction, moderate competitive inhibition, strong competitive inhibition, and mechanism-based inhibition. We performed a simulation study to investigate how the sensitivity of a biomarker was affected by metabolite half-life, fraction of the endogenous parent that is metabolized to the metabolite of interest ($f_{m,metabolite}$), and fraction of the endogenous parent that is metabolized by CYP3A4 ($f_{m,CYP3A4}$). The metabolic indices (i.e., metabolite concentration (C_m), the metabolite-to-parent concentration ratio (C_m/C_p), the metabolite AUC (AUC_m), and the metabolite-to-parent AUC ratio (AUC_m/AUC_p)) were considered to be sensitive with at least a 20% change under the different DDI scenarios. To detect induction (i.e., 600 mg rifampin once daily for 7 days), C_m/C_p and AUC_m/AUC_p were sensitive indices for a hypothetical endogenous biomarker with a metabolite half-life of up to 1 week. To detect strong competitive inhibition (i.e., single 200 mg

dose of itraconazole), AUC_m/AUC_p was the only appropriate index for a hypothetical endogenous biomarker with a maximum metabolite half-life of 108 hours for a formation-rate limited metabolite and 168 hours for an elimination-rate limited metabolite. To detect moderate competitive inhibition (i.e., single 200 mg dose of fluconazole), AUC_m/AUC_p was the only appropriate index for a hypothetical endogenous biomarker with a maximum metabolite half-life of 48 hours for a formation-rate limited metabolite and 108 hours for an elimination-rate limited metabolite. To detect mechanism-based inhibition (i.e., 500 mg clarithromycin twice daily for 3 days), C_m/C_p and AUC_m/AUC_p were sensitive indices for a hypothetical endogenous biomarker with a maximum metabolite half-life of 144 hours for a formation-rate limited metabolite and 168 hours for an elimination-rate limited metabolite. The sensitivity of the hypothetical endogenous biomarker was reduced by decreasing $f_{m,metabolite}$ or $f_{m,CYP3A4}$. As $f_{m,metabolite}$ was decreased, the change in C_m and AUC_m increased, but the change in C_m/C_p and AUC_m/AUC_p decreased. As $f_{m,CYP3A4}$ was decreased, the change in C_m, C_m/C_p, AUC_m, and AUC_m/AUC_p decreased. These simulations provide a framework to better interpret the utility of published CYP3A4 endogenous biomarkers as well as providing useful characteristics of new endogenous CYP3A4 biomarkers. Furthermore, the biomarker simulation platform was developed using open-source software and is easily adaptable to other hepatic enzymes.

Finally, there are several future directions that can be taken to further the research presented in this dissertation. Given that the RYGBS PBPK model was built using existing *in vitro* and *in vivo* data, knowledge about changes in physiological parameters, such as hepatic fat content, gastric pH, post-surgical intestinal adaptation, and tissue-specific enzyme and transporter expression due to RYGBS would help refine the PBPK model. Although challenging to conduct, clinical studies should be conducted to verify the DDI outcomes that were predicted

using PBPK models developed for RYGBS patients. Moreover, the physiologic changes are likely to be time-dependent as patients recover from surgery, lose weight and either establish a new lifestyle or begin to regain weight. Thus, the window of maximum risk for DDIs may be dependent on individual-level factors. Second, not all drugs have liquid formulations and thus poorly soluble drugs, such as posaconazole, may need to be taken by patients post-RYGBS. The general recommendation to take poorly soluble drugs with food may be complicated in patients post-RYGBS as the amount of food that can be ingested is far different than in healthy individuals. Comparisons of drug disposition and DDIs for poorly soluble drugs in the fasted state versus the fed state in pre- and post-RYGBS patients would be informative. Third, the current RYGBS PBPK model can be adapted to other bariatric surgeries by emulating the surgical alterations of gastrointestinal anatomy in the ADAM model, though model training and verification may be challenging with the limited clinical pharmacokinetic data following other bariatric surgical procedures.

With respect to the biomarker simulation study, comparisons of the predicted changes have been verified with available clinical data for putative CYP3A4 endogenous biomarkers (e.g., urinary 6β-hydroxycortisol/cortisol, plasma 4β-hydroxycholesterol, urinary 7β-hydroxy-dehydroepiandrosterone/dehydroepiandrosterone, and urinary 1β-hydroxydeoxycholic acid/deoxycholic acid). However, additional work will need to be done to verify the predicted fold-changes under various dosing schemes (duration of treatment and different inhibitors or inducers). To improve the accuracy of the predicted changes, models can be developed incorporating changes in $f_{m,metabolite}$ and $f_{m,CYP3A4}$ due to induction or inhibition of other CYP pathways, substrates with more complex kinetics (i.e., circadian rhythm or enterohepatic recirculation) and comparison of endogenous CYP3A4 biomarkers against the other DDI index

substrates. In addition, using the simulation models, we can optimize the sampling time based on metabolite half-life to increase the sensitivity window.

Overall, this dissertation applied pharmacometrics to better understand the disposition of acetaminophen, midazolam and digoxin in patients undergoing RYGBS, provided predictions of CYP3A4 and P-gp DDIs that differ based on the solubility of the inhibitor and whether the patient is healthy, morbidly obese or post-RYGBS, and defined the kinetic characteristics of sensitive hypothetical endogenous CYP3A4 biomarkers to detect various DDIs.